HHS Public Access

Author manuscript

Chem Rev. Author manuscript; available in PMC 2017 January 11.

Published in final edited form as:

Chem Rev. 2015 October 14; 115(19): 10575–10636. doi:10.1021/acs.chemrev.5b00100.

Gold Nanoparticles for In Vitro Diagnostics

Wen Zhou[†,§], **Xia Gao**[†,§], **Dingbin Liu**[*,†], and **Xiaoyuan Chen**[‡,*]

[†]College of Chemistry, Research Center for Analytical Sciences, State Key Laboratory of Medicinal Chemical Biology, Tianjin Key Laboratory of Molecular Recognition and Biosensing, and Collaborative Innovation Center of Chemical Science and Engineering, Nankai University, 94 Weijin Road, Tianjin 300071, China

[‡]Laboratory of Molecular Imaging and Nanomedicine (LOMIN), National Institute of Biomedical Imaging and Bioengineering (NIBIB), National Institutes of Health (NIH), Bethesda, Maryland 20892, United States

Graphical abstract

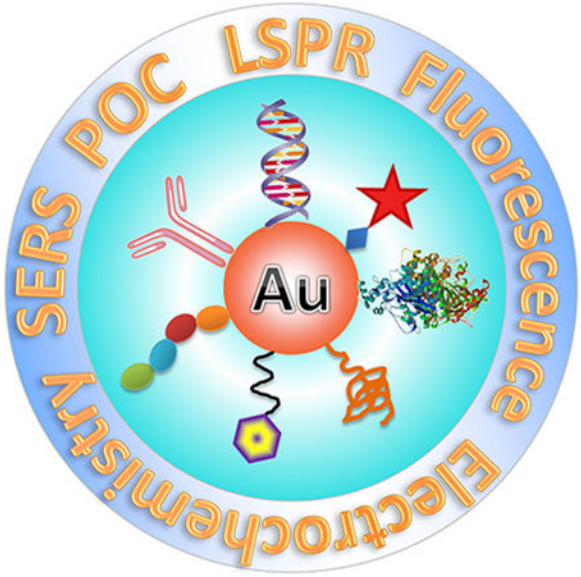

1. INTRODUCTION

1.1. Significance of IVDs in the Clinic

IVD test is a crucial component of clinical care that performs a diagnostic test on biological samples that have been taken from a living body, such as blood, urine, and tissue.[1] Such tests are usually performed to determine or confirm the presence of disease in an individual. “In vitro” literally means “within the glass”, which indicates that the test was historically

[*]Corresponding Authors: liudb@nankai.edu.cn. shawn.chen@nih.gov.

[§]**Author Contributions**

W.Z. and X.G. contributed equally to this work.

The authors declare no competing financial interest.

conducted in glass test tubes. In contrast, in vivo tests, literally “within the living”, are conducted within a whole, living organism including human body.[2] IVD tests have received much public attention because of their distinct features in the medical profession. First, IVD tests do not interact with the human body directly, making such diagnosis accessible without invasive surgeries and thus saving a great deal of suffering. Second, the procedures of IVDs are performed on samples rather than human body, avoiding the possible biological safety problems on patients that often take place in the in vivo diagnostics. Third, an IVD test can quickly provide valuable information on a patient’s healthcare conditions. On the basis of the information, physicians or patients are able to make a timely decision for patient care or treatment. Fourth, the application of IVDs enables early diagnosis and makes treatment of serious diseases easier. Generally, the cost of early testing is much lower than that of the later on extensive treatment. Last, IVDs play a particularly vital role in remote settings for managing outbreaks of acute infectious diseases, where effective but simple diagnostic systems are highly desirable. These features make IVDs unique and of great importance among medical technologies.

1.2. Currently Available IVD Tools

As to the currently available IVD systems in the clinic, diabetic glucose meters and pregnancy test strips are the two formats that most people are familiar with. Typically, IVD tests can be classified into three main types: (1) Clinical laboratory tests: Certain samples from patients are sent to these clinical laboratories. The tests are relatively complex and require advanced laboratory facilities and skilled operators. When completing the test, the results are reported back to the doctor who has requested the test. The obtained information may guide the doctor to make clinical decisions on which intervention is most appropriate for the patients’ healthcare. One example of this kind of IVD test is multiplexed detection of cancer biomarkers (such as prostate-specific antigen (PSA), carcinoembryonic antigen (CEA), and cancer antigen-125, etc.) using immunoassays.[3] (2) Near-patient tests: This kind of test does not rely on sophisticated instruments and can be easily performed on a simple platform by physicians or nurses. The results can be obtained quickly without resorting to complex analysis, which allows for making immediate clinical management decisions. An example for this test is urine test strips, which determine the presence of proteins, glucose, ketones, hemoglobin, bilirubin, urobilinogen, acetone, nitrite, leucocytes, pathogens, as well as pH variation and specific gravity.[4] (3) In-home tests: These tests are the most convenient IVD systems among various medical diagnostic devices. No specialist facilities or healthcare professionals are required for the tests and the subsequent data analysis. Usually, the users can deal with the information by themselves. The most familiar examples for in-home tests are diabetic glucose meters[5] and home pregnancy tests.[6] These two in-home testing systems have already become commonplace and played important roles in managing health conditions and providing critical health information.

Nevertheless, IVDs can make clinical diagnosis faster, easier, and less painful to patients. In recent years, attention is increasingly paid to the prevention and early intervention of diseases, which drives the development of IVDs with greater efficiency and sustainability. Although we have made much progress in biotechnology and relevant fields, only a few IVD systems have been successfully translated into clinic use. The major limitation of most

currently used IVD systems is their moderate detection sensitivity. For example, the current gold standard for prostate cancer biomarker detection is the enzyme-linked immunosorbent assay (ELISA), whose detection limit is about 0.1 ng/mL.[7] This value is generally higher than the concentrations of cancer biomarker in most serum samples especially at their early stages or after radical prostatectomy.[8] Therefore, ELISA usually allows detection only after biomarker levels have already reached critical threshold concentrations, at which point the disease has already advanced markedly. Improvement of detection sensitivity is the key of early diagnostics. Another limitation for most IVD systems is their complex test procedures, which inevitably depend on advanced equipment and skilled operators. The involvement of professionals may lead to a high diagnosis cost, which makes this kind of test unsuitable particularly in resource-poor settings. For instance, polymerase chain reaction (PCR)-based IVDs are extensively applied for nucleic acid detection with ultrahigh sensitivity. However, the detection process is complicated, requiring costly equipment and reagents such as primers and enzymes, and is thus not suitable for rapid diagnostics.[9] Additionally, most IVD platforms are not amenable for multiplexed detection of analytes. Because many symptoms can be caused by multiple agents, it is important to accurately identify the responsible agents simultaneously.[10] High-throughput IVD sensors for multiplexed detection would improve the diagnostic efficiency. Therefore, the development of simple but effective IVD tools is highly desirable for healthcare systems.

1.3. Overview of AuNP-Based IVDs

The increasing demand of IVDs with improved features is pushing the development of highly sensitive and convenient sensors. Thanks to the development of nanotechnology, tremendous progress has been made in the design of IVD tools using nanomaterials.[11] Nanomaterials hold unique physicochemical properties that offer desirable and unmatched characteristics for chemical and biological detection such as significant surface area to volume ratio, strong signal intensities, and finely tunable surface chemistries.[12] For example, due to their large surface areas, nanomaterials can load a variety of signal transducers (such as enzymes, DNAs, and organic dyes), allowing the detection of very low concentrations of analytes. Additionally, nanomaterials can be readily multifunctionalized by chemical methods, and thus multiparametric analysis can be simultaneously realized for real time and direct detection of multiple targets. Furthermore, the tunable surface chemistries endow nanomaterials with many versatile properties, which allow the detection of analytes with enhanced analytical performance especially in combination with miniaturized devices.[13] To date, many studies based on various nanomaterials, such as carbon nanotubes,[13a] silica nanowires,[13d] quantum dots (QDs),[1c] magnetic nanoparticles,[14] and AuNPs,[15] just to name a few, have aimed at creating high-sensitivity IVD systems for biomarkers. These systems can detect biomarkers at pico-, femto-, atto-, and even zeptomolar levels. The high sensitivity would open a new era of early diagnosis and better treatment of diseases.

Among the above-mentioned nanosensors, AuNP-based IVDs have drawn considerable research interest because of their distinct physical and optical properties, including localized surface plasmon resonance (LSPR), fluorescence resonance energy transfer (FRET), surface enhanced Raman scattering (SERS), nonlinear optical properties, and quantized charging effect.[16] These properties make AuNPs excellent scaffolds for the fabrication of biosensors

for a variety of targets.[17] For example, the plasmon resonance of AuNPs in the visible range can be employed to detect particle structures using dark-field microscopy. This powerful approach has been extended to detect targets such as DNA, mRNA, and proteins due to the strong local field enhancement of AuNPs.[18] Besides, AuNPs hold several advantages over other nanomaterials that make them particularly suitable for IVDs. First, the synthesis of AuNPs can be easily and reproducibly realized in common chemical laboratories.[19] Second, the surface modification of AuNPs is usually based on the formation of Au–S bonds, which is highly stable and provides diverse functionalization options.[20] Third, the size, shape, aggregation state, and surface properties of AuNPs can be finely tuned, which is highly important in creating chemical and biological sensors. For example, solutions containing monodispersed AuNPs display a ruby red color, while the presence of analytes can induce a binding event between the analytes and the ligands on the Au surfaces, thus leading to the formation of AuNP aggregates and a red-to-blue color change.[21] The aggregation process is associated with interparticle plasmon coupling that generates a significant absorption band shift in the visible region of the electromagnetic spectrum. Finally, the biosafety of AuNPs is thought to be better than many other nanomaterials, offering excellent biocompatibility when choosing appropriate size and surface coating.[16a,22] These unique attributes allow researchers to develop novel sensing platforms with enhanced analytical features. The past few years have witnessed a variety of AuNP-based IVD systems for electrochemical, SERS, fluorescent, and colorimetric assays of various analytes ranging from small organic molecules to proteins.

To date, although several reviews have been presented to introduce the synthesis and functionalization of AuNPs as well as their applications in biosensing and bioimaging, none of them has focused on an instructive, systematic, and complete review of the exciting advancement in the field of IVDs.[16d,f,17a,23] Thus, we present an authoritative review on the AuNP-based IVD systems in the recent 10 years to summarize and comment on their development and advances. Particularly, we restrict our discussions to the detection strategies rather than synthesis and surface modification, which have been summarized extensively in many reviews.[16f,17a,23a] The detection strategies will be mainly categorized by different signal transducers including LSPR, fluorescence, electrical, SERS, and their integration with point-of-care (POC) systems (Figure 1).

2. AuNP-BASED LSPR ASSAYS

LSPR is a spectroscopic technique based on the resonant oscillation of conduction electrons at interfaces of noble metal nanoparticles stimulated by incident light.[24] The resonance can be achieved when the frequency of incident photons matches the natural frequency of surface electrons oscillating against their attraction to the positive nuclei. As a result, strong electromagnetic fields will form on the surfaces of nanoparticles (Figure 2), along with the appearance of a distinctive absorption peak in the visible frequency range.[25] Because the electromagnetic wave polarizing the surface charges is on the boundary of nanoparticle surfaces and external medium such as air or water, the oscillations are very sensitive to the events taking place at the nanoparticle–medium interfaces. These events can be transformed into the shift of absorption band as well as a color change of the nanoparticle solutions.

LSPR can be influenced by the nanoparticle's size, shape, surface coating, and local environment.[26] The sensitivity to local environment can be employed to detect disease-related biomarkers such as proteins and oligonucleotides, etc.[27] Gold and silver nanoparticles are the most commonly used candidates for fabricating LSPR sensing strategies. For gold and silver nanoparticles, their plasmon absorption bands are generally located in the visible region, making them particularly suitable for many sensing applications. With a given external dielectric constant, silver nanoparticles (AgNPs) can generally provide higher detection sensitivity than AuNPs. For example, AgNPs were applied to detect extremely low concentrations of biomarkers such as streptavidin[28] and Alzheimer's disease.[11a,29] However, both the surface stability and the biosafety of AuNPs are much better than those of AgNPs.[24a,30] Because of this, a great number of AuNP-based LSPR assays have been reported in the past decade. On the basis of readout, there are two LSPR sensing strategies, including absorption band shift and colorimetric sensing. In general, the specific binding of analytes on AuNP surfaces can change the local dielectric environments of nanoparticles, leading to a dramatic LSPR peak shift. The shift distance is approximately in proportion to the amount of analytes added. The LSPR peak shift can be easily measured by a simple UV–visible spectrophotometer.[31] The other readout is colorimetric analysis, which is based on the analyte-induced aggregation or dispersion of AuNPs. The remarkable red shift of LSPR often causes a distinctive color change of the AuNP solutions from red to blue or purple, which can be seen by the naked eye.[20b,21a,c,32] Besides the aggregation-based colorimetric assays, the precise control of the shape and size of AuNPs was applied for signal amplification of colorimetric assays by labeling antibody with a specific enzyme such as glucose oxidase (GOx) and catalase. The detection limit can be as low as the attomolar level. Several reviews in the aspect of LSPR spectroscopy and its biosensing applications were reported, but those for IVD systems are rare.[24c,33] We herein put our attention on the recent advances in the development of AuNP-based IVD platforms categorized by LSPR shift and color change. The analytes of the AuNP-based assays mainly include small organic molecules,[21a,32b,34] nucleic acids,[17b,35] proteins,[36] and even cells (Table 1).[37]

2.1. LSPR Shift as Readout

LSPR shift as the readout for biomarker detection is advantageous over many other strategies because the detection is label free, avoiding the necessity of expensive instruments and long operation time. The typical procedure of the LSPR assays is to modify AuNPs with recognition elements, such as antibodies, biotin, DNA strands, polymers, etc. For example, AuNPs modified with specific antibodies can recognize their antigens via immunereaction, causing the local environment changes of the nanoparticles and resulting in a peak shift in the LSPR spectrum.[38] Demirci and his colleagues[39] presented a LSPR platform for HIV viral detection and quantification of multiple HIV subtypes from unprocessed whole blood. The virus-spiked blood samples enable a dramatic wavelength shift as compared to those without viruses. A standard curve was generated by performing a least-squares fit to the combined data of all HIV subtypes. The viral load can be quantitatively measured with the assistance of the standard curve. On the basis of a similar mechanism, a plethora of LSPR biosensors have been developed for nucleic acids, streptavidin, bacterial, and virus.[40] However, the lack of amplification procedure in these label-free assays inherently limits

their sensitivity. Diverse strategies have been reported to increase the refractive index sensitivity of nanoparticles to achieve improved sensitivity of LSPR shift-based probes. Preparation of metal nanoparticles with specific size and shape may improve the detection sensitivity because the refractive index sensitivity of nanoparticles is highly dependent on their structural geometry. Another effective approach to increase refractive index is based on molecular binding events that happen on the surfaces of nanoparticles, where the increase of the mass of the biomolecules is likely to induce an enhancement of LSPR shift.[41]

Because the local environment of AuNPs is highly sensitive to external stimulus, it is significant to fabricate high-quality substrate to load AuNPs, aiming at specific and selective detection as well as to minimize background signal noise. An ideal substrate should have sufficient durability for AuNPs immobilization and the subsequent chemical reactions. Lin et al.[42] reported a substrate bound Au nanostructure with uniform spacing. The AuNPs with an average nanoparticle size of 8 nm were partially embedded in a glass substrate, where a uniform interparticle gap of 11 nm was obtained. Single molecules of immunoglobulin G (IgG) were individually occupied at the space constraints to capture anti-IgG. When the binding events occurred, a distinct increase of absorbance and wavelength red shift was clearly observed. The phenomenon can be attributed to the increase of the local refractive index in the interstice regions. In addition, this platform exhibits excellent sensitivity to the analytes, affording a detection limit of 66.7 pM for IgG. This system was subsequently integrated with microfluidics, making this LSPR assay promising for high throughput and label free detection.[43] The thickness of the Au layer is essential to determine specific LSPR properties and thus is critical to the LSPR assay sensitivity. The Au thickness on substrate can be finely modulated by two steps: First, a staple mask is fixed on the top of the substrate to simultaneously fabricate different zones of AuNPs via a single vacuum evaporation process. Next, several cycles of Au evaporation are conducted to generate different nominative thicknesses of AuNPs.[44]

Another method to improve the detection sensitivity of LSPR assays is labeling the antibody with an enzyme.[36b,45] The commonly used enzyme is horseradish peroxidase (HRP), which catalyzes the localized formation of an insoluble precipitate in the presence of its substrate and hydrogen peroxide (H_2O_2). As indicated in Figure 3, the precipitates can deposit around the catalytic site to result in a dramatic LSPR shift. A measurable plasmon peak shift was observed with even only one or a few HRP per nanoparticle, reaching single molecular sensitivity when conjugating HRP with secondary antibody for the detection of clinically relevant antigens.[45]

The LSPR signals are highly related to the shape of AuNPs because the refractive index of nanoparticles is largely influenced by their structural geometry. Gold nanorods (AuNRs) are attractive optical transducers for label free detection because their LSPR is highly sensitive to the dielectric constant of the surrounding medium modulated by biological bindings.[46] To apply this system for immunodetection, antibodies are covalently conjugated onto AuNRs, and the specific binding of targets induces a distinct peak shift of the LSPR spectrum.[38b] The magnitude of peak red shift is linearly proportional to the concentration of the target. This strategy was successfully applied to detect cancer biomarkers[47] and hepatitis B surface antigen (HBsAg)[48] with high sensitivity. The absorption spectrum of AuNRs displays two

peaks corresponding to their transverse and longitudinal absorption bands, respectively. The longitudinal absorption band is more sensitive to changes in the dielectric constants of the surrounding medium around the nanoparticles than the transverse absorption band. More importantly, the longitudinal absorption band can be selectively tuned from the visible to the near-infrared (NIR) region as the length-to-width ratio of AuNRs increases.[49] This unique optical property offers the possibility to develop multiplexed LSPR biosensors through the combination of AuNRs with different longitudinal absorption bands. For example, a multiplexed LSPR assay was reported for simultaneous quantification of cardiac biomarkers myoglobin and cardiac troponin I in clinical samples. The multiplexed detection was realized by using two different AuNRs whose longitudinal plasmonic bands were 640 and 830 nm, respectively.[50] Furthermore, the sensitivity of the AuNR-based LSPR assay can be significantly enhanced by the conjugation of detection antibody (Ab2) with a magnetic nanoparticle.[51] The use of magnetic nanoparticles not only amplifies the LSPR shift of AuNRs, but also makes the detection convenient due to the fact that magnetic nanoparticles can separate and enrich analytes from complex solutions under an external magnet. The detection limit of the magnetic nanoparticle-mediated LSPR assays can be as low as the picomolar level, without the requirement of enzyme amplification or sophisticated instrumentation setups.

In addition to antibody-coated AuNRs, aptamer-immobilized AuNRs have attracted much research attention. An aptamer-antigen–antibody sandwich structure on AuNRs was obtained to enlarge the mass of the target of interest, thus leading to an enhanced LSPR shift.[36b,41a] The functionalization of aptamer on AuNRs brings two advantages. First, the activity of aptamer can be regenerated when the captured targets are washed away by concentrated salt solutions. Second, the aptamer layer on the substrates is much thinner than that using antibody, shortening the distance between the AuNR surface and the target molecules. As a consequence, high sensitivity of this LSPR sensor can be expected. In addition, further binding of secondary antibodies on captured targets can improve the detection sensitivity by generating a secondary red-shift of LSPR peak (λ_2). Several other LSPR sensors for immunodetection have been reported for the biomarkers and showed high sensitivity and simplicity when combined with other ease-of-use formats such as microfluidics, microtiter plate system, or optical fiber.[41b,52]

The AuNP dimers can provide enhanced detection sensitivity than individual AuNPs. For example, the recognition capability of protein A toward IgG was tested by human IgG modified AuNP dimers, which were stabilized with a conducting polymer.[53] AuNP dimers were applied to construct a homogeneous assay to detect very low concentrations of protein A. This phenomenon can be attributed to the fact that the sensitivity of the longitudinal LSPR of AuNP dimers to biomolecular binding is much higher than that of the transverse LSPR, which is similar to the case of AuNRs as mentioned above. Another important Au nanostructure is nanoplates, which provides a larger contact surface area than Au spheres or AuNRs and allows them to obtain a large red shift.[52b] The results showed that the LSPR peak of Au nanoplates red-shifted as large as 45 nm when they were incubated with 10 pg/mL of IgG. The detection limit of the LSPR assay for PSA was down to 1 pg/mL.

The size of nanoparticle also plays a decisive role in LSPR shift and shows a great effect on the sensitivity of LSPR sensors. Different sized AuNPs were immobilized on glass substrate for detecting MCF-7 and RPE-1 cells.[54] The results indicated that the large sized AuNPs have a longer electromagnetic field decay length, and they provide a broader linear range and a higher sensitivity than that of small sized AuNPs. For instance, the detection range for MCF-7 cells on 500 nm NPs is 8.56×10^3 to 1.09×10^6 cells/mL, while that on 60 nm AuNPs is 3.43×10^4 to 2.73×10^5 cells/mL. Additionally, larger sized AuNPs showed better capture efficiency of flatter cells than small sized AuNPs, thus displaying larger LSPR shifts.

Au-incorporated nanocomplexes are increasingly important structures for creating high sensitivity LSPR bioassays. These assays take advantage of the merits of the elements in the nanostructures. Taking the core–shell Ag@AuNPs as an example, the strong plasmon and refractive indexes of AgNPs were combined with the high chemical stability and low toxicity of AuNPs. By depositing the Ag@AuNPs on an indium tin oxide (ITO) substrate and subsequently conjugating with recognition elements such as biotin, various concentrations of streptavidin can be quantified in a linear detection range from 1 pM to 10 nM.[55]

The magnitude of wavelength shift in conventional LSPR assays is directly proportional to the concentration of analyte, which means a lower concentration of analyte induces less LSPR shift. This property makes these assays inappropriate for early detection of diseases where the clinical concentrations of the analytes are often too low to be detectable by this method. Recently, Stevens et al.[56] developed a new LSPR assay in which the signal is inversely proportional to the analyte concentration; that is, a lower concentration of analyte induces a larger LSPR shift. This LSPR assay is based on the growth of Ag crystals in the presence of Au nanostars, whose absorption band is in the NIR region (Figure 4). GOx was employed to catalyze the generation of H_2O_2, the amount of which can determine the rate of crystallization of Ag to favor either the nucleation of AgNPs in solutions or the epitaxial growth of Ag nanocrystals around the Au nanostars. A low concentration of GOx induces a small amount of H_2O_2, and the Ag crystallizes slowly to cover the surfaces of Au nanostars, leading to a marked blue-shift of the LSPR band of nanostars. At high GOx concentrations, a large amount of H_2O_2 is generated, which favors the formation of independent AgNPs in solutions and less Ag is deposited around the Au nanostars, yielding a diminished LSPR shift. This “inverse sensitivity” LSPR assay was applied to detect PSA in whole serum with a detection limit of 10^{-18} g/mL (4×10^{-20} M) and a broad linear detection range from 10^{-18} to 10^{-13} g/ mL. This strategy offers a great opportunity for developing LSPR assays to detect analytes, not limited to proteins, with ultrahigh detection sensitivity.

In addition to immunoassays, the LSPR shift-based sensors have been extended to monitor other biological binding events. Artificial polymer recognition materials are particularly attractive in the applications of bioanalysis and biomedicine. These polymer-based materials are more stable, easier to use, and much cheaper than biorecognition molecules especially in complex samples. Takeuchi and his colleagues[57] developed a versatile design of AuNPs, which were grafted with poly(2-methacryloyloxyethyl phosphorylcholine) (PMPC) as an artificial C-reactive protein (CRP) recognition layer (PMPC-*g*-AuNPs). When the specific

binding events occurred, a LSPR red-shift could be measurable even when the concentration of CRP was down to 50 ng/mL. This sensitivity is sufficient for use in clinical diagnostics of inflammation or infection. Another similar strategy is to functionalize the AuNP surface with synthetic oligosaccharides, which can be applied to detect toxins by using LSPR chips.[58] AuNP-based LSPR assays were also used to analyze specific carbohydrate–protein interactions, which play a critical role in some biological events such as cell adhesion and cell migration.[59] LSPR peak shifts of single AuNPs were measured for various binding constants of the biological interactions between receptors and ligands. The precise quantification of the carbohydrate–protein binding constants helps us assess various biological events and develop new diagnostic devices.

Undoubtedly, LSPR-based assays show great potential in the field of medical diagnostics as a simple, label-free, fast, sensitive, and quantitative method. Because this strategy is based on a simple optical extinction measurement, it is highly conceivable that portable devices such as microfluidics can be integrated with the LSPR assays for the development of IVD platforms.

2.2. AuNP-Based Colorimetric Assays

The simplicity of the colorimetric format points toward its use as a general method to detect a wide variety of analytes. Classically, enzyme cascade amplification strategy has been applied in colorimetric assays to detect the low level of biomolecules in real samples. These enzymes, such as GOx, catalase, HRP, and alkaline phosphatase (ALP), are covalently labeled onto a second antibody for immunoassays. The presence of detection analytes can cause the recognition of the enzyme-labeled antibody with the analyte through the antibody–antigen interactions, and the colorimetric signals can reflect the presence of analytes. In most cases, the intensity of the signal can quantify the concentration of the analytes. There are two main factors that influence the detection sensitivity of colorimetric immunoassays. One is enzyme activity; the other is extinction coefficient of the substrate of enzyme. Currently, most enzymes used in bioassays are macromolecular biological catalysts, whose catalytic activities are determined by their three-dimensional structures. Therefore, the maintenance of enzyme activity is a major task in the process of transportation, storage, and use. Recently, there has been the development of artificial enzymes with stable activity with aims to make the detection simple and cost-effective.[60] The substrates used in immunoassays can be catalytically converted into different molecules by the labeled enzymes to induce a color appearance. According to the Lambert–Beer law, the extinction coefficient of substrate is directly related to detection sensitivity. In general, substrates with higher extinction coefficients can provide higher detection sensitivity.

AuNPs are a perfect candidate for colorimetric assays because of their ultrahigh extinction coefficients (e.g., 2.7×10^8 M^{-1} cm^{-1} for 13 nm AuNPs), more than 1000 times higher than those of organic dyes.[61] This property allows the detection limit for AuNP-based colorimetric assays to be as low as the nanomolar level, much lower than the assays using organic molecules as substrates. AuNP-based colorimetric assay was pioneered by Mirkin and co-workers in 1997.[62] After that, an explosive development of colorimetric sensors has been reported for various species including nucleic acids, proteins, saccharides, ions, organic

molecules, pathogens, and even cells.[63] In this Review, these assays will be summarized into two categories: (1) AuNPs are directly used in the assays by forming cross-linking assembly without signal amplification; and (2) AuNPs replace conventional small organic molecules as substrates in enzyme-catalyzed reactions to provide high-sensitivity IVDs.

In the first category, targeted analytes trigger aggregation of AuNPs in a direct or indirect manner, resulting in a wavelength red shift in the visible region. A dramatic LSPR shift can be confirmed by a red-to-blue (or purple) color change of the bulk AuNP solutions, providing a simple platform for colorimetric detection. The readout of the assays can be collected by UV–vis spectroscopy or even the naked eye. DNA-meditated AuNP assembly was first demonstrated by Mirkin in 1996[64] and then applied for colorimetric detection of DNA.[62] The addition of the target DNA molecules induces the hybridization of two complementary DNA strands on AuNPs, leading to the formation of the cross-linked AuNP aggregates. A red-to-blue (or purple) color change was therefore observed (Figure 5). The dissociation of the AuNP aggregates can be realized upon elevating the incubation temperature above the melting temperature of the hybridized DNA. An interesting finding by the authors is that the melting transition is extremely sharp, offering excellent selectivity of fully complementary DNA targets over those with one or more mismatches.[65] On the basis of a similar strategy, biorecognition element modified AuNPs have been successfully employed as colorimetric reporters for glucose, dopamine, glutathione (GSH), adenosine triphosphate (ATP), K^+, etc.[16f] The controlled loss of surface ligands can also be applied to construct colorimetric bioassays. For example, single-stranded DNA (ssDNA) can bind onto citrate-coated AuNPs via DNA base–Au interactions to stabilize AuNPs. In contrast, double-stranded DNA (dsDNA) formed by the hybridization of ssDNA and its complementary sequence shows negligible affinity for citrate-AuNPs, most likely due to the very weak interactions between the hybridized DNA bases and Au. Therefore, addition of an appropriate concentration of salt (e.g., 300 mM NaCl) into the mixture of citrate-coated AuNPs and dsDNA may cause the aggregation of AuNPs, while those mixed with ssDNA remain monodispersed.[66] This non-cross-linking aggregation strategy was also applied to detect other biomolecules. A typical example is the detection of ATP with the aid of its aptamer.[67] The ATP aptamer was hybridized with its complementary oligonucleotide to form a dsDNA, which is unable to stabilize the unmodified AuNPs in high concentrations of salt solutions. In the presence of ATP, it interacts with its aptamer to release a random coil-like ssDNA, which can stabilize the AuNPs and prevent the salt-induced aggregation.

Because the dramatic LSPR shifts and its corresponding color changes rely on the formation of large AuNP aggregates, both cross-linked and non-cross-linked AuNP-based colorimetric assays directly for DNA detection show moderate sensitivity, generally at the nanomolar level. This sensitivity is insufficient for DNA biomarkers in most clinical samples where their concentrations generally range from attomolar to picomolar. To enhance detection sensitivity, enzyme-based amplification strategies were integrated in the AuNP-based colorimetric assays. Chan et al.[68] demonstrated such integration for diagnosis of infectious diseases by combing the DNAzyme-catalyzed amplification strategy with the linker-induced LSPR coupling of AuNPs. This strategy is based on the linker DNAs that can induce the aggregation of AuNPs, thus leading to a color change of the bulk solutions. As shown in Figure 6, in the presence of the DNA target, the initially inactive multi-component nucleic

acid enzyme (MNAzyme) is activated due to the binding of the target DNA with the MNAzyme. The active MNAzyme then recognizes its substrate, a linker DNA, and in turn catalyzes the cleavage of multiple linker DNAs. The degradation of linker DNAs allows the dispersion of AuNPs, and the color of the solutions remains red. If the target DNA is absent, the MNAzyme remains inactive and has no cleavage activity on the linker DNAs. Therefore, the linkers hybridize with their complementary strands coated on AuNPs and cause the aggregation of AuNPs along with a red-to-blue change in color. On the basis of the enzyme-catalyzed signal amplification, the detection limit of the AuNP-based colorimetric assay can be as low as 50 pM, much lower than those using direct AuNP assays. More importantly, this strategy was applied to detect several DNA targets for infectious diseases, including gonorrhea, syphilis bacteria, malaria parasite, and hepatitis B virus, in a multiplexed manner. This system shows great promise for IVDs because it does not rely on expensive instruments and reagents and complicated operation procedures.

Another strategy to further improve the detection sensitivity is to use the enzymatic ligation chain reaction (LCR) concept.[69] In the presence of ampligase, the target DNA acts as a template to hybridize with the capture sequences coated on AuNPs and guide the covalent ligation of the capture sequences to form DNA–AuNP assemblies. The denaturation of the solutions is able to release the target DNA and the ligated AuNPs. Repetition of the hybridization and ligation exponentially amplifies the number of ligated AuNPs, and eventually results in the color change of the bulk AuNPs solutions from red to purple. Because the ligated AuNPs can be exponentially formed with the thermal cycling, ultrahigh sensitivity (aM levels) can be achieved. However, there are at least three limitations to the LCR-based AuNPs assays. First, both the hybridization and the denaturation processes require precise control of temperature, and thus are not appropriate for rapid diagnostics. Second, the thermal cycles, especially the denaturation process, at high temperature tend to induce the detachment of capture sequences from Au surface, causing nonspecific aggregation of AuNPs. Third, the interactions between the enzymes and their ligation site are often restricted by the steric hindrance of DNA coated AuNPs, leading to low amplification efficiency. Recently, an enzyme free LCR-based AuNP colorimetric assay was reported and provided 50 zM sensitivity.[70] Click chemical ligation based on copper-free click chemistry was employed in this assay to replace enzymatic ligation. Some of the above issues were addressed by this method. However, the involvement of magnetic separation and many thermal cycles with precise control of temperature will inevitably impede the practical use in the clinic.

Besides the relatively low detection sensitivity, stability is another main issue that limits the wide applications of AuNP-based colorimetric assays. The biorecognition element modified AuNPs are often unstable in real samples such as serum, in which the high concentrations of salts induce the aggregation of AuNPs, thus generating nonspecific signals. In addition, the biothiols (e.g., cysteine and homocysteine) in real samples are likely to replace the biorecognition elements on Au surfaces, and decrease the recognition capability of the AuNP-based assays. It is worth noting that the aggregation process of AuNPs is dynamic, which means that the suspension of the aggregates is unstable in solutions. With the formation of large sized AuNP aggregates, the color of the solution changes from red to blue (or purple), and finally becomes colorless in a few hours to days, with the generation of

AuNP precipitate on the bottom of the container. The time-dependent color change makes this type of assay unreliable for accurate quantification of detection targets. To solve this issue, Guo et al.[71] provided an AuNP-based colorimetric assay with long-term stability, wide dynamic detection range, as well as high sensitivity. This assay was based on the oriented aggregation of asymmetrically functionalized AuNPs to form dimers, where the interparticle spacing was shorter than 1 nm. As shown in Figure 7, such a small gap in the dimeric AuNPs generally produces a larger peak shift and responds to an obvious red-to-blue color change. The asymmetrically PEGylated AuNP surfaces endow this assay extraordinary stability in complex samples, thus avoiding the appearance of false positive signals. This modification also prevents the formation of multimers and large aggregates. In comparison with conventional AuNP assays that require nanomolar levels of target DNA or more to induce the large LSPR shift, this oriented assay offers picomolar level sensitivity.

Proteins are vital biomacromolecules in living organisms with a variety of functions from catalyzing metabolic reactions to regulating cellular functions. The abnormal expression of proteins is often associated with diseases. Therefore, proteins serve as indicators in many diseases, and the accurate measurement of the proteins is significant in clinical diagnostics. AuNP-based colorimetric assays have been successfully used to detect proteins especially for proteases.[72] Proteases, such as thermolysin, thrombin, and lethal factor, function through selectively catalyzing the hydrolysis of their substrates at a specific site. The protease substrates are often peptides, which can form networks with AuNPs by a rational design, thereby inducing aggregation of AuNPs. The aggregates can be redispersed to individual AuNP by adding the target protease, which cleaves its substrates into proteolytic fragments, liberating single AuNPs from the cross-linked AuNP assemblies. As a result, the color of the solution turns red. A similar strategy has also been applied to determine the activity of phosphatase, inorganic pyrophosphatase, telomerase, and DNA methyltransferase/glycosylase, etc.[73]

The AuNP assembly can also be mediated by the products of protease-catalyzed hydrolysis.[74] For example, Liu et al.[75] designed an AuNP-based assay for acetylcholinesterase (AChE) and inhibitor screening. AChE is able to hydrolyze its substrate acetylthiocholine (ATC, an analogue of acetylcholine) to generate thiocholine, which is comprised of a thiol moiety and a positively charged group. The thiol group shows high affinity toward AuNP to induce a partial replacement of the fluorescent ligands such as rhodamine B from AuNP surfaces. At the same time, the positively charged tail groups interact with the negatively charged-ligand residues on AuNP surfaces, causing aggregation of AuNPs and the change of solution color. The partial removal of ligands provides two detection signals: fluorescence recovery and color change. This AuNP-based dual readout assay was employed to monitor the level of AChE in the cerebrospinal fluid (CSF) of transgenic mouse model for Alzheimer's disease and showed high detection sensitivity (0.1 mU/mL). This strategy was also used for AChE inhibitor screening and pesticide detection.[76] Using a similar principle, AuNPs were used to detect *Streptococcus pneumoniae* immunoglobulin A1 protease (IgA1P) based on the electrostatics-mediated AuNP assembly.[77] IgA1P catalyzes the proteolysis of human IgA1 to yield IgA1 Fc_{α} and positively charged lgA1 Fab_{α}. The negatively charged AuNPs selectively bind to the positively charged lgA1 Fab_{α} to produce a visual AuNPs aggregation. Similarly, cathepsin B

and its inhibitors were monitored by the controllable assembly of AuNPs, which can be visualized with the naked eye.[72b]

So far, the most well-known strategy for protein detection is immunoassay, which relies on the antigen–antibody interactions and various transducers such as fluorophores, radioisotopes, electrochemiluminescent tags, DNA barcodes, and enzymes. Among these signal transductions, ELISA allows sensitive detection of proteins by a color change, which can be seen by the naked eye and thus without resorting to sophisticated instruments. However, the moderate sensitivity of conventional ELISA limits its applications in early disease detection where the concentrations of protein biomarkers are generally very low. The high extinction coefficients of AuNPs enable them a perfect alternative of organic molecules, which serve as the substrates of the labeled enzymes in conventional ELISAs. The combination of immunoassays with AuNPs as readout is still challenging. Jiang et al.[78] developed an AuNP-based colorimetric immunoassay to detect proteins by means of the indirect detection of Cu^{2+}. To perform the detection, CuO NPs were first conjugated with secondary antibody. After conventional immunodetection procedures, the labeled CuO NPs were dissolved by diluted HCl to liberate Cu^{2+}, which can be detected by azide- and alkyne-modified AuNPs through click chemistry (Figure 8). The red-to-blue color change of AuNPs indicates the presence of Cu^{2+}, thus indirectly reflecting the amount of the sandwiched protein. This method was used to detect human HIV antibody in serum samples by the naked eye, making it especially suitable for clinical use in resource-poor settings. This strategy can also be realized by labeling secondary antibody with ALP.[79] ALP catalyzes the dephosphorylation of ascorbic acid-phosphate to produce ascorbic acid, which acts as a reducing agent to react with Cu^{2+} to generate Cu^{+}. The yielded Cu^{+} leads to the covalent ligation of azide and alkyne moieties coated on AuNPs, causing aggregation of AuNPs.

The color change upon aggregation of AuNPs has been increasingly utilized for colorimetric sensing of biomarkers. However, this principle often does not have high enough sensitivity due to the inherent lack of signal amplification strategy. To enhance detection sensitivity of this type of AuNP-based immunoassay, the AChE-induced aggregation of AuNPs and magnetic beads were integrated into the immunoassays to induce high signal amplification (Figure 9).[80] To do this, detection antibodies were conjugated with AChE, which catalyzes its substrate ATC to generate thiocholine, as aforementioned. Thiocholine can adsorb on the Au surfaces via Au–S bond and cause aggregation of the citrate-capped AuNPs due to the electrostatic interactions. This aggregation event can be transformed into a color change of the AuNP solutions from red to purple. In addition, magnetic beads can load a large number of AChE. After the normal immunoassay operation, a very small amount of analyte can thus be detected most likely due to the high density of AChE on magnetic beads where the AChE activity was still preserved. This enhanced colorimetric immunoassay was successfully applied for clinical detection of enterovirus 71 (EV71), the major causative agent of hand, foot, and mouth disease (HFMD), with ultrahigh detection sensitivity and specificity. This plasmonic immunoassay was further simplified and employed to detect *Treponema pallidum* antibodies.[81]

Undoubtedly, the employment of AuNPs can provide very high sensitivities with a simple readout. However, this system is unsuitable for quantitative detection because of the narrow

linear dynamic range, typically within 2 orders of magnitude. Additionally, unlike conventional ELISA, which can make use of stopping reagents to stabilize the detection signal, both color change and LSPR shift of AuNP-based assays are dynamic processes, making it difficult to create a convincing standard calibration curve for quantitative detection of targets. It is a daunting task to develop a quantitative AuNP-based colorimetric immunoassay. Liu and co-workers were inspired by conventional HRP-based ELISAs, where the solution changes from colorless to yellow color. They noted that the extinction coefficient of 5 nm AuNPs is much lower than those of larger sized AuNPs.[82] At a relatively low concentration (normally <10 nM), the solution containing 5 nm AuNPs appeared to be colorless, while at the same concentration, the solution containing larger sized AuNPs is usually red. Therefore, it is reasonable to construct a colorimetric immunoassay using 5 nm AuNPs as the substrate and GOx as the enzyme to conjugate with Ab2. GOx is able to catalyze glucose to generate H_2O_2, which reacts with $HAuCl_4$ to produce Au^0 to deposit on the surfaces of 5 nm AuNPs, causing the rapid growth of AuNPs. As a consequence, the colorless AuNP solution turned red quickly along with an appearance of an absorption band at around 530 nm in the visible region of the electromagnetic spectrum. The LSPR absorbance can be used as readout to quantitatively detect targets of interest. By virtue of this strategy, they obtained a wide linear dynamic range (4 orders of magnitude) and an extremely low detection limit (93 aM) for PSA. The capability of clinical detection was demonstrated by using real patient serum samples, showing great potential for IVDs in both resource-rich and resource-limited settings.

Another high-sensitivity immunoassay based on the controllable growth of AuNPs was reported by Stevens and coworkers;[83] they made use of catalase-labeled secondary antibody to create a so-called “plasmonic ELISA”. They found that H_2O_2 can react with the AuNP precursor ($HAuCl_4$) to form AuNPs. However, the aggregation state of AuNPs was largely determined by the concentration of H_2O_2. High concentration of H_2O_2 favors the formation of monodispersed spheric AuNPs, whose solution is typically red in color. Low concentration of H_2O_2 favors the formation of aggregated AuNPs, which appear blue in solution. In a sandwiched immunocomplex, catalase was labeled with a secondary antibody and consumed the added H_2O_2. Therefore, the concentration of the sandwiched analyte was linked to the H_2O_2-based growth of AuNPs. The blue and red colors can be readily differentiated by the naked eye, without need of expensive analytical tools or skilled labors. More importantly, the detection limits of this system can be as low as 10^{-18} g/mL for PSA and HIV-1 capsid antigen p24 in whole serum. Furthermore, the capability of this assay in detecting p24 in clinical samples was tested against the gold standard PCR test. This colorimetric method can detect HIV positive samples that were undetectable by PCR. If commercialized, this plasmonic ELISA may revolutionize the field of IVDs because of its high-sensitivity and simple readout.

Indeed, the AuNP-based plasmonic immunoassays have offered ultrahigh sensitivity for biomarkers of interest. They however face several challenges. First, the immunodetection requires several cycles of time-consuming incubation and rinse steps, like any ELISA. Second, activity of enzyme, the key of high sensitivity, needs to be well maintained in the process of transportation, storage, and use. To solve the problems, a possible way is to use recognition element-modified AuNPs for direct detection of analytes, where AuNPs act as

substrate and readout. However, unlike small molecule or DNA detection, the direct detection of proteins using antibody modified AuNPs is generally unrealistic because the interparticle spacing in the antibody-protein-AuNP networks is larger than the size of the particles. The basis of color change is that the interparticle spacing of the cross-linked AuNPs should be smaller than the diameter of the nanoparticles.[84] To break this barrier, Stevens and co-workers[85] used 60 nm AuNPs, whose surfaces were functionalized with short viral peptide epitope, to detect antiviral epitope antibodies. By adding the analytes, significant changes in the absorption band as well as colorimetric response were yielded, most likely due to the fact that the interparticle spacing of the particle networks was greatly reduced. This AuNP-based colorimetric assay allows direct detection of protein biomarkers in a single incubation step, avoiding the use of enzyme and tedious rinse procedures. The simple operation procedures of this assay enable it particularly suitable for IVD testing.

2.3. Outlook of AuNP-Based LSPR Assays

LSPR-based bioassays show great potential as IVD platforms because these methods are low-cost, fast, simple, and sometimes highly sensitive. Particularly, for the label-free LSPR shift-based assays, the LSPR response is dependent only on the refraction index change of the nanoparticles' surrounding environment, and the specificity is achieved through the molecular recognition involved. Therefore, there is no requirement of chemical modification of the analytes or their subsequent recognition elements. For the color change-based AuNP assays, there is no need of expensive analytical equipment to read the signal, which even can be seen by the naked eye alone, making it particularly suitable for IVD detection. However, several issues need to be addressed before the widespread applications of these AuNP-based LSPR assays in clinical diagnostics. First, AuNPs tend to aggregate in complex samples to generate false positive signals. In the past few years, a variety of ligands containing chemical groups such as ethylene glycol moieties, zwitterionic groups, and imidazole groups have been employed to resist the nonspecific aggregation of AuNPs. However, the functionalization of the stabilizing agents on AuNP surfaces is likely to affect or even prevent the analyte–receptor interactions. The development of appropriate stabilizing ligands or functionalization strategies to minimize the nonspecific signals remains a challenge. Second, the signals of the AuNP-based LSPR assays are based on a dynamic aggregation process, and there is no standardized procedure for data collection and analysis. Third, it is far insufficient to combine AuNP-based LSPR assays with portable devices such as microfluidic chips, most likely due to the difficulty in embedding the illumination systems into the small chips. Last, the synthesis and functionalization of AuNPs are performed under highly optimized conditions in research laboratories. The robust preparation of various AuNPs is of paramount importance for mass production of standardized products.

Future development of AuNP-based LSPR assays lies in designing biosensors with ultrahigh sensitivity and reliability, assuring the assays effective in complex biological samples as described above, further engineering user-friendly interfaces and incorporating with miniaturized devices. For example, to improve the sensitivity and simultaneously minimize the nonspecific nanoparticle aggregation, asymmetrically PEGylated AuNPs were employed as an effective platform for LSPR assays, where the PEG part functioned to maintain the stability of the AuNPs probes in complex samples, and the other part was utilized to

selectively form dimers without forming large aggregates upon target binding. This design enabled the LSPR assay with an improved long-term stability, a wide dynamic range of detection, and surprisingly high sensitivity.[71] Nevertheless, the unique characteristics of AuNP-based LSPR assays make them a perfect candidate for clinical diagnostics especially in combination with portable platforms.

3. AuNP-BASED FLUORESCENT ASSAYS

Fluorescence is known as a highly sensitive technique that can even offer single-molecule detection sensitivity. Fluorescent assay is an established and dominant optical technology that plays a vital role in biomedical diagnostics and biotechnology. However, many fluorescent assays are facing several challenges such as photostability and autofluorescence of biological samples.[86] In recent years, nanomaterial-based fluorescent assays have great potential to serve as alternatives to traditional fluorescent dye-based assays. These nanomaterials include semiconductor QDs,[87] fluorescent dye-doped silica nanoparticles,[88] upconverting lanthanide-doped nanoparticles,[89] carbon nanodots,[90] noble metallic nanoparticles,[91] and so on. Among these nanosensors, AuNP-based fluorescent assays have received much attention due to their excellent photostability and biocompatibility, facile surface tailorability, color tenability, high surface-to-volume ratios, and high emission rates.[92] In this section, we will introduce two types of AuNP-based fluorescent assays. One uses Au nanoclusters (AuNCs), which consist of 2–100 Au atoms. The other uses distance-dependent nanoparticle surface energy transfer (NSET) of organic dyes on the surface of AuNPs, offering activatable fluorescent assays.

3.1. AuNPs as Fluorophores

AuNC acts as a new type of fluorescent nanomaterial whose size is typically smaller than 2 nm. The fluorescent AuNCs offer unique optical features, which are dramatically different from AuNPs whose sizes are generally 3–100 nm composed of many hundreds to thousands of Au atoms.[93] In principle, when the size of AuNCs approaches the Fermi wavelength of electrons, molecule-like optical properties including discrete electronic states and size-dependent fluorescence can be observed. By virtue of one-photon excitation, two different emission wavelengths were found to be in the visible and the NIR region.[94] In Figure 10, the energy diagram for nanoclusters shows that the emission in the visible region is most likely associated with the Au core, while that in the NIR region is attributed to the interaction of the surface ligands with AuNCs. Therefore, both the size of the Au core and the polarity of the ligand have a direct effect on the emission efficiency. It was reported that the emission of fluorescent AuNCs can be gradually modulated from UV to NIR region depending on cluster size and composition.[24b] This feature is similar to that of semiconductor QDs whose emission property is also size-dependent. However, unlike QDs that are composed of toxic heavy metals, AuNCs show excellent biocompatibility, making them ideal replacements of QDs and organic dyes especially in combination with their strong photoluminescence, ultrasmall size, and photostability. The past few years have witnessed considerable efforts in the synthesis of AuNCs with high fluorescence quantum yields and applications in chemical and biological labeling and sensors. Several review papers have been dedicated to the synthesis, functionalization, and applications of AuNCs for fluorescent analysis of

environmental and biological samples.[95] Herein, we attempt to summarize several important applications of AuNCs as fluorophores in IVD assays.

The ligands used for the synthesis and stabilization of AuNCs are essential to determine the size and fluorescence intensity of AuNCs because they are prone to aggregate into large clusters. As reported, these ligands mainly include small thiol-based molecules, polymers, DNA oligonucleotides, peptides, and proteins.[96] A variety of bioassays were created by controlling the interactions between the AuNCs and their ligands. For example, Chang et al.[97] reported an AuNC-based fluorescent assay for the quantitative measurement of H_2O_2 using 11-mercaptoundecanoic acid (11-MUA) bound AuNCs based on fluorescence quenching. If H_2O_2 is present, the 11-MUA units capped on the Au surfaces via Au–S bonds tend to be oxidized to form organic disulfide products, causing the loss of ligands from Au surfaces and thus resulting in reduced fluorescence of the AuNCs. The authors demonstrated that the fluorescence quenching was attributed to the decreased density of 11-MUA ligands on the surface of the AuNCs rather than the aggregation of clusters. Furthermore, this fluorescent assay can be applied to detect glucose when combined with GOx, which is capable of catalyzing the generation of H_2O_2 in the presence of glucose.

Bovine serum albumin (BSA) stabilized AuNCs (BSA-AuNCs), which exhibit strong fluorescence emissions, have been used to detect various analytes.[98] Dong et al.[99] demonstrated that H_2O_2 is able to induce the degradation of AuNCs, which leads to the fluorescence quenching. This phenomenon was employed to detect H_2O_2 and glucose with very high sensitivity and selectivity. Qu et al.[100] reported a BSA-AuNC-based fluorescent assay for dopamine. Dopamine is able to attach onto AuNCs and leads to the reduced fluorescence intensity of BSA-AuNCs through a photoinduced electron transfer process. The detection limit for dopamine can be as low as 10 nM, much lower than many other previously reported nanoparticle-based assays.

Like small organic fluorophores, the formation of AuNC aggregates can lead to the fluorescence self-quenching phenomenon. For example, a NIR fluorescent assay using urease-stabilized AuNCs has been developed for the detection of urea in blood samples.[101] In the presence of urea, the AuNC embedded urease remains active as free urease and enables the catalytic reaction of urea to produce NH_4^+ and CO_2. The positive charge of NH_4^+ interacts with the negatively charged AuNCs and thus forms AuNC aggregates. As a consequence, the fluorescence of AuNCs is effectively quenched. The AuNC aggregation-based fluoroescence quenching was also applied to detect other biospecies like phosphate containing metabolites. GSH-bound AuNCs emit strong reddish fluorescence under illumination of UV light. However, the fluorescence of GSH-AuNCs was found to be highly quenched in the presence of Fe^{3+}, most likely due to the formation of Fe^{3+}-GSH-AuNC aggregates through the chelation between Fe^{3+} and GSH-AuNCs. The addition of phosphate containing metabolites, such as ATP and pyrophosphate, restored the fluorescence of AuNCs. This is because phosphate anions have high formation constants with Fe^{3+}, resulting in the release of Fe^{3+} and individual GSH-AuNCs from the Fe^{3+}-GSH-AuNC networks. Real samples such as cell lysate and human plasma were used to evaluate the capability of this assay in clinical settings.[102] A similar strategy was performed to detect protein kinase and screen its inhibitors.[103] This aggregation-based fluorescence quenching

phenomenon was applied to detect Concanavalin A (Con A) and *E. coli* when α-D-mannose-conjugated AuNCs (Man-AuNCs) were used as the fluorophores.[104] The Man-AuNCs were able to bind with the analytes through multivalent cooperative interactions between Man-AuNCs and Con A or the mannose receptors on *E. coli*.

The AuNC-based fluorescent bioassays were also extensively used in protein detection. Various recognition elements such as antibody, aptamer, biotin, and polymer have been functionalized onto surfaces of AuNCs to improve the selectivity of protein detection. Leblanc et al.[105] prepared fluorescent AuNCs using poly(amido amine) (PAMAM) dendrimers as stabilizing agents and made use of this fluorescent assay for human IgG detection. To realize the immunodetection, a polyclonal, goat-derived antihuman IgG antibody was electrostatically conjugated with the as-prepared AuNCs. As reported, the conjugation of antibody was unable to change the fluorescence of AuNCs. However, the introduction of human IgG antigen caused the decrease of fluorescence intensity, which was due to the formation of AuNC aggregates. It was reasoned that the polyclonal antibody has two binding sites for antigens, and two antigen molecules may bind to one molecule of antibody on AuNCs to induce the formation of cross-linking quenching complex, along with an aggregation process. The aggregation of AuNCs readily accounted for the decrease in fluorescence intensity. AuNC-based immunofluorescent assays have also been successfully explored to enhance the assay sensitivity by utilizing AuNCs as marker labeling tags.[106] To amplify the detection signal, porously structured $CaCO_3$ spheres were utilized to load AuNCs to form strongly fluorescent $CaCO_3$/ AuNCs hybrid composites. This nanosensor was employed to detect neuron specific enolase, a prognostic marker in neuronal injury as well as a cancer biomarker often used to monitor disease progression and management in small cell lung cancer. A detection limit of 2.0 pg mL^{-1} was achieved with a linear detection range from 5 pg mL^{-1} to 1.0 ng mL^{-1}. Similarly, boron nitride sheet was employed to load many AuNCs for the subsequent sandwich immunoassay.[107] The application of the AuNC-embedded nanocomposites allowed fluorescent detection of interleukin-6 (IL-6) with a limit of detection down to 0.03 ng mL^{-1}.

Proteases serve as a major class of enzymes in all organisms that are involved in digesting long protein chains into shorter fragments by catalyzing the hydrolysis of peptide bonds that link amino acid residues. The accurate measurement of proteases is of great importance to many biological processes. Wang et al. prepared a simple fluorescent probe for proteases based on the protein-protected AuNCs, whose fluorescence intensity was strong under normal conditions. The protein templates used for the synthesis of fluorescent AuNCs acted as a compact coating, preventing the AuNCs from direct contact with O_2 that was dissolved in the solution, and thus avoiding O_2-induced fluorescence quenching. The presence of proteases was able to degrade the protein shell on AuNCs, by which O_2 molecules can quickly access the AuNC cores and thus quench their fluorescence.[108] On the basis of a similar design, peptide-templated AuNCs were allowed to measure the protein post-translational modification (PTM) enzymes such as histone deacetylase 1 (HDAC 1) and protein kinase A (PKA).[109] As illustrated in Figure 11, the PTM enzyme is able to deacetylate its substrate peptides that were densely coated on the surfaces of AuNCs, altering the interactions between the peptides and the AuNC cores. Thus, the peptide layer became loose and O_2 molecules can be accessible to the surfaces of AuNC cores, causing

the fluorescence quenching by oxidizing them into nonfluorescent clusters. By virtue of this assay, subpicomolar detection limits are readily achieved for both enzymes. Similarly, GSH-bound AuNCs were employed for selective detection of liver disease biomarker GSH S-transferase (GST) and GST fusion proteins in cell lysates.[110] These strategies were extended to detect cystatin C, a significant cysteine protease inhibitor in human bodies that is mainly used as a biomarker of kidney function. Huang et al.[111] reported a simple, label-free, cost-effective, and immune-independent fluorescent probe for cystatin C by using BSA-protected AuNCs as the fluorophores. The high fluorescence of BSA-templated AuNCs can be effectively quenched by papain, a kind of cysteine protease capable of digesting the BSA layer. Because the activity of papain can be specifically inhibited by cystatin C, the concentration of cystatin C can thus be quantified by the restored fluorescence intensity of the AuNCs–papain mixture. This approach was used for sensitive and selective detection of papain and cystatin C in clinical samples.

3.2. AuNP-Based Activatable Fluorescent Assays

Over the past decades, activatable fluorescent probes have been designed to monitor the biological events in biochemical processes.[112] Typically, an activatable fluorescent probe is composed of two parts: a fluorophore that acts as the donor and a quencher that acts as the acceptor. When the two components are in close proximity, the fluorescence of the dye can be quenched by various energy transfer mechanisms. The classical mode of energy transfer is Förster resonance energy transfer (FRET), as first reported by Stryer and Haugland in 1967.[113] On the basis of the quantum physical model, FRET occurs via a dipole–dipole interaction, where an energetically excited fluorophore acts as a donor, and transfers its excitation energy to a nearby acceptor through a nonradiative energy transfer process. In addition, the energy transfer efficiency is highly dependent on the distance of the FRET pairs as well as the overlap of the absorbance spectrum of the donor and acceptor. It was reported that the energy transfer efficiency is inversely proportional to the sixth power of the distance between the donor and acceptor.[114] On the basis of this, effective FRET distance is estimated to be less than 10 nm. The FRET phenomenon provides a powerful tool in biological and chemical fields to measure the distances between molecules on a molecular scale, which is particularly useful for determining conformational changes of biomolecules and molecular interactions in biochemical process. However, FRET fails in monitoring many other biochemical events that occur across a distance greater than 10 nm.

NSET, nanoparticle surface energy transfer, can overcome the FRET distance-dependent energy transfer limit.[115] AuNPs have been demonstrated as a highly efficient energy acceptor most likely due to the continuous electron–hole pair excitations on their surfaces. Like FRET, when an acceptor AuNP and a donor fluorophore are brought into proximity, the energy of the fluorophore can be transferred to the AuNP surfaces via dipole–surface interactions. Because free conducting electrons are isotropically distributed in the dipole vectors of AuNPs, the conducting electrons can interact strongly with the oscillating dipole of the fluorophore. Therefore, the dipole–surface interactions in NEST are dipole–dipole in nature. The continuum of the electron–hole pair excitations on AuNP surfaces increases the possibility of the dipole–surface interactions, thus enhancing the energy transfer efficiency of NSET over FRET. As a consequence, the strong dipole–surface interactions enable the

NEST model widely applicable to AuNP-fluorophore studies across longer distance ranges as opposed to FRET. Several experimental observations indicate that the dipole–nanosurface energy transfer distances in NEST can be more than double those attainable using traditional dipole–dipole energy transfer-based FRET model. As shown in Figure 12, 1.4 nm sized AuNCs were conjugated with fluorescein and separated by a DNA strand, and energy transfer was observed when the distance was in the range of 5–25 nm.[116] In addition, when the distance is above 7 nm, NEST was found to have a higher energy transfer efficiency than FRET. The high fluorescence quenching abilities of AuNPs make them excellent candidates as substitutes for organic dye quenchers, to construct activatable probes for various bioanalytes ranging from small organic biomolecules to DNA, proteins, and pathogens.

To bring the AuNP-based activatable fluorescent assays into the real world, various fluorophores, for example, organic dyes, fluorescent proteins, QDs, metal nanoclusters, and water-soluble fluorescent polymers, were usually first immobilized on the surfaces of AuNPs by chemical binding or electrostatic interaction, leading to fluorescence quenching of the fluorophores. The target molecules then can bind selectively to the activatable probes and cause detachment of the fluorophores from the AuNP surfaces.[117] The restored fluorescence intensity is proportional to the concentration of the target of interest. In recent years, much attention has been paid to these highly fluorescent assays.

Biothiols play a central role in reversible redox reactions and cellular functions including detoxification and metabolism. Zhang and co-workers[118] developed an off–on fluorescent probe for biothiols using a Ru(II) polypyridyl complex-coated AuNP composite. The Ru(II) complex is known for its high fluorescence, high photostability, and outstanding two-photon properties. Upon loading of the Ru(II) complex onto surfaces of AuNPs via Au–N bonds, the fluorescence of Ru(II) complex was almost completely quenched by AuNPs (up to 99.8%). In the presence of biothiols, the Ru(II) complexes can be removed from the AuNP surface because the coordination capability of Au–S bond is stronger than that of the Au–N bond. As a result, the displacement reaction causes the turn-on fluorescence of Ru(II) complexes. The two-photon property of this probe allows the detection of biothiol levels in living cells and tissues at depths of 80–170 μm. Similarly, the highly soluble PEGylated pyrene was noncovalently adsorbed onto the surface of AuNPs to form a nonfluorescent nanocomposite. Biothiols such as cysteine can trigger the release of PEGylated pyrene from the AuNP surfaces; thus the restored fluorescence can be employed to detect cysteine with a detection limit of 11.4 nM, along with a linear range from 1.25×10^{-8} to 2.25×10^{-7} M.[119]

Glucose is an important carbohydrate in biology and is related to many physiological and pathological processes. It is highly desirable to accurately determine the level of glucose in biological samples such as blood and CSF. The conventional platforms for glucose detection are mainly dependent on the enzymatic reaction catalyzed by GOx. For these glucose assays, their detection sensitivities are insufficient in many cases where the concentrations of glucose are very low. Tang et al.[120] reported an AuNP-based FRET sensor for glucose based on a functionalized AuNP-QD assembly. The AuNPs were modified with thiolated β-cyclodextrins (β-SH-CDs), and QDs were conjugated with Con A. The specific recognition of β-SH-CDs and Con A induced the formation of AuNP-QD assemblies, resulting in the energy transfer from QD to AuNP indicated by a quenched fluorescence. The fluorescence

of QDs can be recovered in the presence of glucose due to its competition with β-SH-CDs for the binding sites of Con A. This FRET probe has a high sensitivity for glucose with a detection limit of 50 nM and an excellent selectivity for glucose over other species in clinical samples. Because the potential toxicity of QDs makes this assay unsuitable for use in living organisms, the authors improved the glucose assay by using apo-GOx (inactive form of GOx)-modified AuNPs as the FRET acceptor and fluorescein isothiocyanate (FITC)-conjugated dextran as the FRET donor.[121] As shown in Figure 13a, the apo-GOx on AuNP surfaces is able to interact with dextran labeled with FITC, leading to an efficient FRET from FITC to AuNPs, and thus no fluorescence can be observed in this nanocomposite. Glucose competes with dextran-FITC for the binding sites of apo-GOx and displaces the dextran-FITC segment from AuNP surfaces, resulting in the fluorescence recovery of FITC. This FRET assay shows good biocompatibility, selectivity, and sensitivity (5 nM) for quantitative analysis of glucose and imaging of glucose consumption in living cells.

The FRET mechanism has also been combined with the fluorescent AuNCs to create ratiometric fluorescent probes for small biomolecule detection. Boronic acid group is one of the most well-known recognition elements for glucose, and shows a widespread range of applications in biomolecular recognition. Boronic acid (or its derivatives) can react with molecules containing 1,2-diols or 1,3-diols through a reversible and covalent ester formation.[122] Mao et al.[123] took advantage of this property to construct an AuNC-based FRET assay for glucose in rat brain microdialysate. They first prepared a polymer containing boronic acid group that binds with Alizarin Red S (ARS, a fluorescent diol) and *N*-acryloxysuccinimide group that can be coupled with ovalbumin-protected AuNCs (Ova-AuNCs). Later, the fluorescent polymer was covalently coated onto AuNCs to achieve two emissions: one at 567 nm was derived from ARS, and the other at 610 nm was derived from AuNCs, respectively. As shown in Figure 13b, in the presence of glucose, the fluorescence intensity of the labeled-ARS decreased because of the removal of ARS from the polymer, while the fluorescence intensity of Ova-AuNCs emission peak at 610 nm showed negligible changes. This ratiometric fluorescent probe was successfully employed to monitor the amounts of glucose in the rat brain following the cerebral calm/ ischemia.

The functions of AuNCs similar to those of organic fluorophores have been integrated with FRET assays. Yan and co-workers[124] made use of cysteamine modified AuNPs (cyst-AuNPs) and trypsin stabilized gold nanoclusters (try-AuNCs) to detect heparin, a highly negatively charged polysaccharide playing a significant role in hemorrhage and thrombocytopenia during the surgery and the anticoagulant therapy. As shown in Figure 13c, the detection mechanism is based on the surface plasmon enhanced energy transfer between cyst-AuNPs and try-AuNCs. In the original state, try-AuNCs were attached onto surfaces of cyst-AuNPs through electrostatic interactions, leading to the significant decrease of fluorescence of the try-AuNCs. In the presence of heparin, the try-AuNCs were competitively removed from cyst-AuNP surfaces because of the extremely high affinity between heparin and cyst-AuNPs. The detachment of try-AuNCs caused the recovery of their fluorescence and a simultaneous formation of AuNP aggregates. This method was reported to detect heparin with a linear range of 0.1–4.0 μg mL^{-1} and a detection limit of

0.05 μg mL^{-1}. The FRET from AuNCs to AuNPs was also applied to detect platelet-derived growth factor AA (PDGF AA) molecules by Chang and colleagues (Figure 13d).[125]

Molecular beacon is one of the most well-known nucleic acid probes that can report the presence of specific nucleic acids in homogeneous solutions.[126] A typical molecular beacon is composed of a loop structure and a stem structure. The loop is complementary to the target nucleic acid and the stem is formed by two complementary arm sequences where a fluorophore and organic quencher are conjugated on either end of the sequences. Once the target nucleic acid is reached to hybridize with the looped sequence, the arm sequences are forced apart so that the fluorophore and quencher are separated and the fluorescence is recovered. AuNPs serve as ideal quenchers in molecular beacons due to their high quenching efficiency. Libchaber and co-workers[127] designed a molecular beacon using 1.4 nm AuNPs as the quenchers with respect to four fluorescent dyes including rhodamine 6G, fluorescein, Texas red, and Cy5. Their design was based on a hairpin structure where the fluorescence of the dyes was efficiently quenched by AuNPs. Upon the target binding, the loop was opened and the fluorescence of the dyes recovered because of the increased distance between the dyes and AuNPs. By employing AuNPs instead of the organic quencher (4-((40-(dimethylamino)-phenyl)azo)benzoic acid), 100-fold higher sensitivity was achieved, allowing one to detect single DNA mismatches. Later, Nie et al.[128] developed a new AuNP-based molecular beacon where a 2.5 nm AuNP served as both a nanoscaffold and a nanoquencher for fluorophore-tagged oligonucleotides. To realize the concept, a thiol group and a fluorescent dye were labeled on either end of the oligonucleotide, which was readily attached onto AuNP surfaces via Au–S bond to form a constrained arch-like structure (Figure 14a). The fluorescence of the dyes was completely quenched due to the close proximity of the dyes and AuNPs in the nanostructure. Once the oligonucleotide binds its target, the constrained confirmation opens because of the formation of the rigid double-stranded DNA. As a consequence, the arch-like configuration is lost and the fluorescent dye and AuNP are separated, restoring the fluorescence of the quenched dyes. Unlike conventional molecular beacons relying on a stem-and-loop structure, the AuNP-based FRET probes do not require a stem. However, the constrained arch-like confirmation essentially gave a quenching efficiency of almost 100% when the fluorophore approached AuNPs, meaning very low background noise, and thus offering higher sensitivity than conventional molecular beacons using organic quencher.

Activatable probes based on larger sized AuNPs have received a lot of research interest. As demonstrated by Fan and co-workers,[129] larger sized AuNPs show stronger SPR absorption over smaller particles; for example, 5–20 nm AuNPs absorb strongly at the 300–500 nm wavelength range, while the absorbance of 2 nm AuNPs at this range is hundreds of times less intense. The significant overlap between the absorption of larger sized AuNPs and fluorophore emission guarantees the high FRET efficiency, allowing a broad range of fluorophores to be efficiently quenched. In addition, larger sized AuNPs have greater surface areas to load a larger number of oligonucleotides as well as different oligonucleotides. On the basis of this hypothesis, Mirkin et al.[130] developed an activatable sensor for mRNA detection in living cells (Figure 14b). The so-called “nanoflare” sensor consisted of an AuNP core functionalized with oligonucleotides, which were hybridized with short dye-terminated fluorescent reporter sequences. The fluorescence was highly quenched because

of the high quenching ability of AuNPs. In the presence of the target mRNA, the recognition oligonucleotides hybridized with the complementary target sequence by forming longer and more stable duplexes, which caused the release of the fluorescent reporter sequences from the AuNPs and produced fluorescence signal like flares. The intensity of the restored fluorescence was closely correlated with the relative amount of the target. This system was then extended for simultaneous mRNA detection and regulation.[131] Later, the same group advanced this system for multiplexed detection of two different targets in living cells.[132] This “nanoflare” system has also been employed to directly quantify intracellular ATP levels by utilizing ATP aptamer-functionalized AuNPs.[133]

In some diseases like cancer, the progression of the disease is often associated with the expression of multiple mRNAs. Therefore, multiplexed detection of targets simultaneously is of great significance to improve the accuracy of disease diagnostics over single-target assays. Tang et al.[134] adapted an approach similar to Mirkin’s “nanoflare” to monitor the progression of tumor by detecting three different types of tumor-related mRNA targets. This FRET probe was composed of an AuNP core and a dense shell of recognition sequences, which were hybridized with three short dye-terminated reporter sequences. The recognition sequences were designed to selectively bind with three mRNA transcripts: c-myc mRNA, TK1 mRNA, and GalNAc-T mRNA. The probes were incubated with MCF-7 human breast cancer cells and MCF-10A normal human breast cells as well as HepG2 human liver cancer cells and HL-7702 normal liver cells. The results indicated that all three mRNAs in breast cancer cells were simultaneously determined by three fluorescence signals (green, yellow, and red), respectively, while no fluorescence signal was observed in healthy breast cells. Likewise, the three green, yellow, and red fluorescence signals were also observed in HepG2 human liver cancer cells. However, the red fluorescence signal was found to be strong in healthy liver cells, indicating the expression of GalNAc-T mRNA in healthy liver cells was also high. These results were further confirmed by RT-PCR, suggesting the capability of this multiplexed assay in distinguishing cancer cells from normal cells with negligible false positive results. To measure different levels of mRNA expressed in the cells, the nanoprobes were incubated with the drugs tamoxifen and β-estradiol, which inhibit or promote the expression of TK1, respectively.[135] The results indicated that the levels of tumor-related mRNA in living cells can be monitored by the multiplexed “nanoflare”, therefore showing its capability of evaluating the tumor progression. The same group advanced their work by providing a four-color “nanoflare” that can simultaneously detect and image four types of mRNAs in living cells (Figure 14c).[136] Most interestingly, these functional DNA-AuNP “nanoflares” not only possess the individual properties of both DNA and AuNPs but also show some new features including enhanced FRET efficiency, high resistance to enzymatic degradation, high cellular uptake, and low toxicity. These features make them particularly suitable for clinical diagnostics.

Besides the “nanoflare” FRET probes, hairpin structure has been employed to design multicolor molecular beacons. Fan et al.[137] reported such a FRET probe to detect three different tumor-suppressor genes. This probe consisted of a 15 nm AuNP core as the quencher, and three hairpin sequences labeled with fluorescein, Texas red, and Cy5, respectively, were bound to the AuNPs via Au–S bonds. The complementary targets were able to bind in the loop sequences and open the stem-loop structure like conventional

molecular beads. As a result, the dyes moved away from the AuNP surfaces, turning on the three fluorescence signals simultaneously. By virtue of different hairpin sequences on single particles, these molecular beacons hold great promise in multiplexed detection of single-base mismatched DNA targets. This approach was easily extended to detect adenosine, potassium, and cocaine simultaneously by using their aptamers as the hairpin sequences attached on the AuNP quenchers.[138]

MicroRNAs (MiRNAs), a class of small noncoding RNA molecules (18–25 nucleotides) found in plants, viruses, and mammals, have emerged as important clinical biomarkers that not only can signify the presence of relevant diseases but also can be employed to predict the disease progression.[139] Detection of miRNAs in clinical samples is challenging because of their short sequences, single base differences, and especially extremely low concentrations (normally <1 pM) in a wide dynamic range.[140] Over the past decades, many sensing strategies have been developed to detect miRNA.[141] Among these, AuNP-based activatable probes are ideal candidates because of their simplicity and high sensitivity. Cai and coworkers[142] developed a hairpin-structured probe using AuNP as quencher and FITC as reporter. The target miRNA can hybridize with the loop of the oligonucleotide, forcing it to open and leading to the recovery of the quenched fluorescence. This activatable probe provides a limit of detection of 0.01 pM (at a signal/noise of 3) with a linear range from 0.05 to 50 pM. Recently, enzymatic catalysis-based amplification method was successfully incorporated into AuNP-based activatable assays for absolute and direct miRNA quantification. Fiammengo et al.[143] designed such an assay by taking advantage of the specific property of duplex specific nuclease (DSN), which displays a strong preference for cleaving double-stranded DNA or DNA in DNA–RNA heteroduplexes and remains inactive to either ssDNA or single-/double-stranded RNA (Figure 15). To realize the concept, 5′-FAM-labeled oligonucleotides were first immobilized onto the passivation layer of PEGylated AuNPs via a heterobifunctional linker, and the fluorescence was highly quenched because of the vicinity of the fluorophores to the surfaces of AuNPs. The target miRNAs in standard solutions or clinical samples are capable of binding to the oligonucleotides on the AuNPs to form a double-stranded DNA–RNA heteroduplex, where the DNAs can be selectively and effectively hydrolyzed by the DSN enzyme while the target miRNAs are not degraded. The hydrolysis of the DNA probes leads to a gradual release of the fluorescence dyes from the AuNP surface, causing a persistent and dramatic increase of fluorescence in 2 h before reaching a plateau. Interestingly, the released target miRNAs can rehybridize to the DNA-AuNPs complexes for many times until the DNAs are completely degraded. The enzyme amplification approach allows one to quantify the absolute amount of target miRNAs in total RNA extracted from cultured cells with a method detection limit of 1×10^4 copies/ ng_{RNA} (or 100 copies/cell) in cancer cell lysates.

The rapid and efficient identification of abnormal expression of proteins in clinical samples is essentially critical to disease diagnosis. Most protein assays rely on antigen–antibody interactions, meaning that a specific antibody is inevitably required for the immunodetection. The FRET-based “chemical nose” strategy serves as a useful alternative to detect proteins of interest without the involvement of a specific antibody. Rotello et al.[144] developed a protein sensor using such a chemical nose strategy. This prototype sensor array was made up of an AuNP core and a fluorescent polymer monolayer. The AuNP core was

functionalized with a layer of thiolated ligands terminated in six cationic groups (Figure 16). The electrostatic interactions of the cationic AuNPs and the anionic fluorescent poly(*p*-phenyleneethynylene) (PPE) polymers result in fluorescence quenching of the polymers through a FRET process. The quenching efficiency can be modulated by choosing an appropriate cationic group, thus adjusting the binding ability of the fluorescent polymers with the AuNPs. Addition of protein analytes is able to competitively bind with the cationic AuNPs, thus displacing the fluorescent polymers from Au surface and the restored fluorescence can be observed. The different binding constants of various proteins to certain cationic AuNPs allow the chemical nose technology to be a fingerprint fluorescence response pattern for individual proteins characterized by linear discriminate analysis (LDA). This FRET-based chemical nose sensor has been successfully used to identify 52 unknown protein samples (including BSA, cytochrome c, lipase, subtilisin A, ALP, acid phosphatase, and β-galactosidase) with an accuracy of 94.2%. The same group extended the chemical nose sensors to identify 12 types of bacteria including both Gram-positive (e.g., *A. azurea*, *B. subtilis*) and Gram-negative (e.g., *E. coli*, *P. putida*) species in buffered solutions.[145] Furthermore, normal, cancerous, and metastatic cells were successfully differentiated by the AuNP-conjugated polymer systems.[146]

Rotello and co-workers improved their chemical nose systems by utilizing arrays of green fluorescent protein (GFP) instead of the PPE fluorophores.[147] GFP shows a similarly high binding constant to the cationic nanoparticles as do PPEs. However, GFP has defined size and molecular weight, which can prevent the nonspecific interactions with each other, thus significantly reducing aggregation. Therefore, unlike the above-described AuNP-conjugated polymer systems that can merely differentiate targets of interest in clean buffered solutions, the GFP-AuNP hybrid was able to discriminate specific proteins (like human serum albumin, IgG, transferrin, fibrinogen, and α-antitrypsin) in more biologically relevant samples, such as buffer and human serum with 100% and 97% accuracy, respectively. As the plasma/serum proteome contains tens of thousands of different proteins, it is of great significance to verify the practicability of any bioanalytical method in complex biological samples. Recently, Rotello et al. further advanced this GFP-AuNP conjugate sensor to profile chemotherapeutic mechanisms.[148] This sensor is composed of a benzyl head-group-terminated AuNP core and three different fluorescent proteins (EBFP2, EGFP, tdTomato). The drug-induced physicochemical changes on cancer cell surfaces can be “snified out” by the restored three-channel fluorescence. Different chemotherapeutic drugs can induce different changes of cell surfaces, thus generating different fluorescence response patterns. These fingerprint patterns were in turn used to identify the specific mechanisms of cell death induced by drugs. The fingerprint patterns were obtained by using a simple microplate, making this nanosensor applicable to high-throughput screening of unknown drugs that have not been commercially available yet.

Determination of the protease activity is vital to many physiological and pathological processes. Because of the unique properties of AuNPs, the AuNP-based FRET assays display several advantages over traditional fluorescent probes. It can be easily predicted that the FRET assays based on fluorescence quenching by AuNPs are designed exclusively for the enzymes that cleave their substrates. In principle, the fluorophore-labeled substrates are initially conjugated with AuNPs to turn off the fluorescence of the fluorophores. In the

presence of the target enzymes, the substrates are cleaved specifically, thus turning on the fluorescence. In one study, for example, Lee and coworkers[149] developed such a FRET assay to measure the activity of matrix metalloprotease (MMP) for both in vitro and in vivo tests. To minimize the signal background, a near-infrared fluorescence dye, Cy5.5, was labeled to the MMP substrate, and then anchored onto the surface of AuNPs. In the presence of MMP, the Cy5.5-labeled substrates were selectively degraded, releasing the Cy5.5 dyes from Au surfaces and thus restoring the near-infrared fluorescence. The AuNP-based FRET system can be applicable to other proteases by choosing an appropriate peptide substrate spacer. In addition, such simple protease-detection systems can be employed for high-throughput screening of drugs and early diagnosis of protease-relevant diseases.

The FRET assays based on organic fluorophores are usually limited by their insufficient quantum yield and photostability in clinical samples. To overcome these constraints, great efforts have been made in the past years to develop metallic or semiconducting nanostructures as a substitute of organic fluorophores. QDs are such a perfect candidate possessing many unique and advantageous optical properties, such as high brightness, robust photostability, and a large Stokes shift. The high quantum efficiency and photostability of QDs make them particularly useful for constructing AuNP-based FRET assays for protein detection.[150]

QDs were first introduced into AuNP-based FRET assays for protein detection in 2005 by Kim and co-workers.[151] They found that the fluorescence of QDs was significantly quenched by the AuNPs due to the specific biotin–streptavidin interactions. Avidin can competitively bind to the biotin-AuNPs and block the fluorescence quenching of QD by AuNPs. Later, this FRET assay was performed in a chip format where the QDs were immobilized onto a glass substrate.[152] By virtue of a variety of QDs with different emission profiles for each specific substrate peptide, multiplexed detection of three types of proteases (MMP-7, caspase-3, and thrombin) was achieved. Yet the analogous strategies have further been designed to measure the activity of many other enzymes.[153] When combining peptide-AuNP conjugates with FRET acceptor dye-labeled antibodies, the emission spectra of QDs can be finely adjusted, by which multiplexed detection of different classes of enzymes is likely. This concept was successfully demonstrated, for the first time, by Stevens and co-workers.[154] The multiplexed sensing system was allowed to simultaneously detect the protease activity of urokinase-type plasminogen activator at concentrations >0.9 nM and the kinase activity of human epidermal growth factor receptor 2 (HER2) at concentrations >7.5 nM. Both of the concentrations are clinically relevant for breast cancer prognosis, making this system useful for rapid disease diagnosis as well as high-throughput drug screening.

The AuNP-QD assembly system was also employed to detect pathogens like hepatitis B virus (HBV).[155] The AuNP-QD conjugates were easily formed through immunological interaction between the HBV surface antigen epitope coated on the AuNP acceptors and the Fab antibody decorated on the QD donors. The fluorescence of the QDs in the immuno-mediated 3D-oriented complex was greatly quenched due to the enhanced energy transfer from QDs to AuNPs. The HBV viral surface protein preS2 competitively displaces the epitope-carrying AuNPs bound on the Fab-carrying QD core, and thus disrupts the assembly of the AuNP-QD complex in a specific manner, causing the fluorescence restoring of QDs.

Similarly, a FRET assay based on graphene QDs and AuNPs was developed for pathogen detection by analyzing specific gene sequences of *Staphylococcus aureus*.[156]

The most well-known method for protein biomarker detection in clinical tests is ELISA format. However, the detection sensitivity of ELISA is insufficient in many clinical cases especially in their earlier stages or after treatment, where the concentrations of the biomarkers are generally very low. Fluorescent assays are widely used as high-sensitivity strategies in both in vitro detection and in vivo bioimaging. It is expectable to create fluorescence-based immunoassays with higher sensitivity than conventional ELISA. Typically, the fluorescent tags are labeled onto Ab2, and each Ab2 is usually allowed to conjugate with 3–5 fluorophores because higher conjugations may cause internal quenching between the dyes and influence the immunogenic activity of Ab2. AuNPs serve not only perfect fluorescence quenchers but also ideal carriers for loading many thousands of fluorophores per AuNP because of their very high surface area-to-volume ratios. The two features of AuNPs enable this type of platform for ultrasensitive detection of protein biomarkers. Liu et al.[157] developed an activatable probe to augment the detection sensitivity of fluorescent ELISA for serum protein biomarker PSA. In this study, Rhodamine B isothiocyanate (RBITC) was loaded onto AuNP to form RBITC-AuNP conjugates. In this state, the fluorescence of RBITC was completely quenched by AuNPs through the NSET mechanism. Because the RBITC-AuNP conjugates are positively charged, they are able to bind with the negatively charged Ab2 through electrostatic interactions, thus retaining their biological activity toward the target antigen PSA. With the typical immunoassay procedures, the Ab2-RBITC-AuNPs complexes were pulled down onto the surface to form a sandwich structure. By adding 1 mM of cysteamine, the loaded RBITC molecules were competitively displaced from AuNP surfaces, thus leading to a significant restoration of RBITC fluorescence (Figure 17a). The intensity of the recovered fluorescence is well associated with the concentration of PSA spiked in serum samples. The detection limit of the activatable probe for PSA was down to 0.032 pg/mL, 2–3 orders of magnitude lower than the conventional fluorescent immunoassays as well as the current HRP-based immunoassays (Figure 17b, c).

3.3. Outlook of AuNP-Based Fluorescent Assays

AuNP-based fluorescent assays such as AuNC-based assays and AuNP-based activatable assays have been summarized in this section (Table 2). Several enhanced features of the AuNP-based fluorescent assays, including high sensitivity, biocompatibility, ease of synthesis, and finely controlled sizes, make them attractive fluorescent probes for various biomedical applications. Despite the progress made in the past decade, AuNP-based fluorescent assays are still facing several challenges, which hamper the clinical translation of many of the technical advances into routine practice.

For AuNC-based fluorescent assays, the major challenge lies in the lack of uniform synthetic chemistry to prepare AuNCs in high yield. The quality of AuNCs directly determines the quantum yield, which, up to now, is still below 10%, much less than those of semiconductor QDs and organic dyes.[93b] Additionally, the crude products produced by current synthesis routes are often mixtures containing various sizes of clusters. The precise

control of the size and purity of AuNCs is critical for both fundamental studies and real applications. In addition, the accurate characterization of AuNCs is also a challenge. We still do not know how the gold atoms are connected to form clusters. Furthermore, the surface ligand is also a huge factor to influence the brightness of AuNCs. Jin et al.[96] found that the ligands with electron-rich atoms (e.g., N, O) or groups (e.g., –COOH, NH_2) can remarkably enhance the fluorescence of AuNCs. Because of the recent huge advances in the synthesis and characterization of AuNCs, we believe that it is feasible to obtain truly monodisperse AuNCs with precisely controlled nanoparticle size, without the need of tedious purification operations for various sizes of AuNCs. In addition, advanced tools such as X-ray crystallography will significantly help us understand the correlation of electronic properties of the AuNCs with their nanostructures, thus guiding scientists to develop AuNC-based fluorescent assay with enhanced analytical features.

For AuNP-based activatable assays, the NEST quenching mechanism is accepted as the model to explain the fluorescence quenching over a broad range of fluorophores on AuNPs in a large range of distances. However, it is still quite challenging to precisely control the distances between the fluorophores and large sized AuNPs because intrinsic SPR may interfere with fluorescence signals. Last, like other fluorescent assays, it still remains a major task to minimize the background signals of the AuNP-based fluorescent assays when bringing them into clinical use. This issue can be somewhat addressed by diminishing the nonspecific adsorption of AuNP sensors to biological samples and/or by using NIR dyes.

4. AuNP-BASED ELECTROCHEMICAL ASSAYS

Electrochemical biosensors are used for IVD testing because they are portable, simple, easy to use, cost-effective, and, in most cases, disposable. The electrochemical instruments used with the biosensors can be miniaturized to small pocket size devices, which make them applicable for IVD tests. Recently, nanomaterial-based electrochemical detection strategies offer new opportunities for highly sensitive biomarker detection.[158] Because of their excellent conductivity, high surface area, and catalytic properties, AuNPs are ideal platforms for electrochemical detection.[158a,159] The Au surface area is suitable for binding of biomolecules, and the metal facilitates direct and fast electron transfer that decreases the overpotentials of many electroanalytical reactions, thus maintaining the reversibility of redox reactions. In this section, we will summarize the use of AuNPs in electrochemical sensing for IVD testing (Table 3).

4.1. AuNPs as Electron Wires

Electron transfer in proteins, especially enzymes, generally occurs through metal centers or tunneling events. Yet efficient electrical communication between proteins and electrodes is often largely insulated by the surrounding globular protein structures. Promoting the electron transfer process between a redox protein and an electrode is important for developing biosensor devices and advancing their applications. AuNP-based electrodes acting as “electron wires” can facilitate electron transfer between redox proteins and bulk electrode materials, thus avoiding the use of redox mediators. Moreover, adsorption of biomolecules onto AuNP surfaces can preserve their bioactivity using biocompatible AuNPs. For example,

improved electrical contacting of flavoenzymes, apo-GOx, with the electrode support was achieved by incorporating the cofactor flavin adenine dinucleotide (FAD) functionalized AuNPs into the reconstituted apo-GOx molecules and integrating with a conductive film (Figure 18).[160] AuNPs acted as an electron relay or "electrical nanoplug" for the alignment of the enzyme and for the electrical wiring of its redox-active center. Incorporation of AuNPs in the reconstituted enzyme greatly increased its maximum turnover rate, and the value was 7 times higher than the electron-transfer rate constant of native GOx with O_2 as electron acceptor. This concept was further used to demonstrate the electrical contacting of pyrroloquinoline quinone (PQQ)-dependent enzymes by the reconstitution of apo-glucose dehydrogenase (apo-GDH) on the PQQ-functionalized AuNPs assembled on an Au electrode surface.[161]

Similarly, the reconstituted enzyme revealed direct electrical contact with the electrode surface, and the bioelectrocatalytic oxidation of glucose occurred with a turnover rate of 11 800 s^{-1}. In addition to the reconstituted methods, native GOx was also covalently connected to Au electrode surface by an AuNP monolayer[162] or by a layer-by-layer covalent attachment process[163] to construct multilayer films of GOx/AuNP to improve the electron transfer between analytes and electrode surfaces. Moreover, application of AuNPs as an "electron wire" was further extended from only monolayers of the "wired" enzyme electrodes to cross-linked three-dimensional AuNP/enzyme composites by coelectropolymerization of thioaniline-functionalized metallic AuNPs and thioaniline-modified enzymes on electrode surfaces.[164] The electro-synthesized bis-aniline-cross-linked enzyme/AuNPs composites allow efficient electrical contact with the electrode surface, resulting in an effective bioelectrocatalytic oxidation of glucose. Particularly, the O_2-insensitive GDH/AuNPs composite electrode was employed as an anode in a membraneless glucose/O_2 biofuel cell.[164a] To bypass the complex chemical synthesis and reconstitution of native enzymes around modified cofactors, a protein-engineering approach was demonstrated to bind glucose/galactose receptors (GGR) that sense glucose on the surface of AuNPs.[165] The alanine in GGR was replaced by cysteine at the N-terminal position to provide a thiol group for linking the protein molecules to the Au surface. The challenge in the development of these AuNP-based "wired" enzyme electrodes is how to overcome the long electron-tunneling distance between the redox-active cofactor of enzymes and electrodes. Atanassov and Banta reported a successful site-specific modification of GOx with AuNPs via another protein engineering approach.[166] The native cysteine in GOx was mutated to valine to prevent the attachment of AuNPs to the native free thiol, and then site-directed mutagenesis was applied to create additional single mutations to add cysteine side chains at strategic locations at distances from the FAD cofactor ranging from 13.8 to 28.5 Å. The result showed that only the H447C mutant with the shortest distance between the newly introduced cysteine group and the FAD center exhibited direct electron transfer activity.

In the development of electrochemical immunosensing strategies, stability or activity of the immobilized biocomponents and signal amplification of the immunoconjugates are two key factors. The latter has been achieved by using enzymes to label immunocomponents on the transducer surfaces. As one of the widely used enzyme labels, HRP has been utilized to produce the electrochemically active species for amperometric immunoassay. To avoid the use of substrates, a reagentless immunosensor was prepared in a hydrophilic, nontoxic, and

conductive colloidal AuNP/titania sol–gel composite membrane encapsulated with HRP-labeled hCG antibody to detect hCG in serum samples.[167] The presence of AuNPs in the sol–gel matrix played a role similar to that on a conducting wire, which decreased the electron transfer impedance, leading to a direct electrochemical behavior of the immobilized HRP. Similar strategies based on AuNP/chitosan composites were used to promote the electron transfer process between HRP and electrode to detect CEA[168] and H_2O_2.[169] A biocompatible film containing colloidal AuNPs and chitosan was used to encapsulate P450 enzymes and CYP2B6 on an electrode to study its electrochemistry and electrocatalysis to the common clinically used drugs.[170] The Au-chitosan composite provided a favorable bioenvironment for enzyme immobilization and accelerated the direct electron transfer between the immobilized enzyme and electrode. Another electrochemical immunosensor array was prepared by immobilizing HRP-labeled antibody modified AuNPs in biopolymer/sol–gel modified screen-printed carbon electrodes (Figure 19). In the presence of AuNPs, the HRP showed direct electrochemical responses, and the formation of immunocomplexes led to a decrease in the electrochemical signals due to the increased spatial blocking and impedance. This method could simultaneously detect carbohydrate antigens 153, 125, 199, and CEA.[171]

A series of biochemical and physiological processes in a living cell involve electron generation and transfer. Therefore, numerous studies have focused on electric behavior and characters of living cells using electrochemical methods. For example, strategies for immobilizing cells on electrode surface and accelerating electron transfer between electrode and the immobilized cells were proposed by Ju's group to study the electrochemical behavior of cells.[172] AuNPs were used to retain the activity of immobilized living cells and promote electron transfer between electroactive centers of cells and electrode, which resulted in a well-defined anodic peak of guanine. HIV-1 protease (HIV-1 PR), an aspartic protease that functions to cleave the nascent polyproteins synthesized during the viral replication cycle, has attracted much attention. Picomolar-level electrochemical detection of human HIV-1 PR was achieved by using ferrocene (Fc)-pepstatin conjugate self-assembled on thiolated single walled carbon nanotubes/gold nanoparticles (SWCNT/AuNP) surfaces on Au electrode.[173] The synergistic effect of AuNPs and SWCNT facilitates electron transfer between the redox Fc-pepstatin conjugate and the substrate. Thus, the resistance ohmic contacts of these composites were obviously decreased, and a more sensitive sensor was obtained than sensors only modified with AuNPs. This idea was further extended to construct a highly sensitive screening assay for detecting HIV-1 PR and subsequently evaluating its corresponding inhibitors at picomolar levels based on electrochemical impedance spectroscopy (EIS) methods (Figure 20).[174]

As another member of the carbon material family, graphene also has been widely applied due to the unique physical and chemical properties, such as high surface area, excellent conductivity, and ease of functionalization. Fu et al. constructed a novel reagentless and mediatorless electrochemical aptamer-based sensor (aptasensor) for PDGF detection based on the direct electrochemistry of GOx with poly-(diallyldimethylammonium chloride) (PDDA)-protected graphene-AuNPs composite assembled on glassy carbon electrode (GCE).[175] The cooperation of graphene and AuNPs not only assists direct electron transfer between active sites of GOx and electrode but also provides a favorable microenvironment

for immobilizing enzymes. A similar graphene-AuNPs nanocomposite was synthesized by Liu and co-workers and successfully used as a matrix for GOx immobilization in glucose sensing.[176]

4.2. AuNPs as Electrodes

Electrochemical detection methods combined with nanostructured sensor surfaces offer potentially low-cost, high-throughput solutions for IVD tests. Particularly, AuNP-modified electrodes have attracted great attention due to the excellent properties of AuNP, such as low cytotoxicity and high affinity with a wide range of enzymes and biomolecules containing thiol or amine groups. Thus, AuNPs have been involved in various electrode fabrications as a part of electrode substrate, signal transduction probe, or nanolabel. For example, by covalently attaching AuNPs to the surface of a carbon fiber microdisk electrode, an AuNP-network microelectrode sensor was developed for amperometric detection of dopamine secretion from single PC12 cells.[177] As compared to the existing carbon fiber microelectrodes, this probe showed comparable or even better performance in terms of kinetic peak parameters and prolonged storage stability. Fan et al. demonstrated that a new type of electrochemical DNA sensor with highly specific hybridization of target DNA occurred at the Au nanoelectrode surface.[178] Moreover, the interactions between an anticancer drug daunomycin and cancer cell membrane components have been studied using an aptamer probe immobilized on conducting polymer-AuNP composite substrates in Shim's group.[179] Merkoçi et al. developed another electrocatalytic platform/sensor for specific identification of tumor cells (Figure 21).[180] In their system, molecules on cell surfaces were recognized by antibodies conjugated with AuNPs with catalytic hydrogen reduction used for cell detection. AuNP as electrode substrate was also applied to construct electrochemical immunosensors for thrombin,[181] P-glycoprotein on cell membrane,[182] human IgG,[183] and antipeanut antibodies.[184]

In addition, commercially available AuNP electrodes were employed as substrates to fabricate a three-mode electrochemical sensor for detection and quantitation of ultralow levels of miRNA in a wide dynamic range (Figure 22).[185] MiRNAs are an emerging class of biomarkers that are frequently deregulated in cancer cells and have shown great promise for cancer classification and prognosis. Signal amplification strategies based on AuNPs have drawn much attention to the development of ultrasensitive assays for miRNAs.[186] Liu et al. presented a label-free and sensitive electrochemical sensor for miRNA detection with a triple signal amplification by combining 3-aminophenylboronic acid (APBA)-biotin-AuNPs, SA-ALP, and the *p*-aminophenol (pAP) redox cycling reaction together. A detection limit of 3 fM was ultimately achieved.[186a] The recently developed DNA-AuNP biobarcode assay provided PCR-like sensitivity for nucleic acid and protein targets without the need of enzymatic amplification. Xing et al. described electrochemiluminescence (ECL) determinations of telomerase[187] and DNA[188] based on the biobarcode amplification strategy. A signal amplification ECL method based on AuNP was also demonstrated to detect BSA and IgG.[189]

Biomarker levels in serum, for example, can detect and monitor diseases such as cancer. Conventional methods for biomarker detection such as ELISA often involve complicated

instrumentation, limited sensitivity, and time-consuming operation procedures. Thus, there is a real need for simple, rapid, sensitive, and inexpensive methods for biomarker measurements in IVD fields. AuNPs offer enhanced electron transfer efficiency and biocompatible interfaces to retain the activity of the adsorbed biomolecules. Therefore, AuNP electrodes were intensely investigated to measure protein biomarkers with sandwich-type formats. A HRP-labeled osteoproteogerin (OPG) immunosensor was fabricated by covalently immobilizing anti-OPG on the surface of AuNPs deposited onto conducting polymers. The immunosensor gave a detection limit of 2.0 pg/mL.[190] Furthermore, specific antibodies were immobilized onto AuNP-modified pyrolytic graphite (PG) disks[191] and inkjet-printed AuNP electrodes[192] to detect human cancer biomarker IL-6 in serum. The detection was based on sandwich immunoassays using multiple HRP labels conjugated to a secondary antibody, providing clinically relevant detection limits of 10 pg/mL (with the PG disks assay) and 20 pg/mL (with the inkjet-printed AuNPs assay), respectively. To further improve detection sensitivity, an electrochemical immunosensor of PSA was constructed using magnetic beads coated by 7500 HRP labels along with detection antibodies[15] (Ab2) per particle as the tags, and densely packed AuNP-modified PG electrodes as substrates. The sandwich structure was illustrated in Figure 23.[193] The detection limit can be as low as 0.5 pg mL^{-1} in 10 μL of undiluted serum, which is near or below the normal levels of most cancer biomarkers in human serum. The PSA determination in cell lysates and human serum of cancer patients gave excellent correlations with standard ELISA assays.[193] Recently, another nanostructured sandwich immunosensor for attomolar detection of interleukin-8 (IL-8) using massively labeled superparamagnetic particles was reported.[194] The sensor electrode was coated with a dense film of GSH-AuNPs with attached primary antibodies to capture human IL-8 from the sample. When coupled to superparamagnetic beads massively loaded with about 500 000 HRP labels and secondary antibodies, an ultralow detection limit and very high sensitivity were achieved in sandwich immunoassays for IL-8 in serum. Moreover, a microfluidic technique was introduced to construct a microfluidic electrochemical sandwich immunoassay with HRP label for ultrasensitive and simultaneous detection of two or more cancer protein biomarkers in serum.[195] An ultra-sensitive electrochemical microfluidic assay optimized to measure a panel of four protein biomarkers was reported.[195a] The protein panel was validated for accurate oral cancer diagnostics. An unprecedented ultralow detection in a 5–50 fg mL^{-1} range was achieved for simultaneous measurements of proteins IL-6, IL-8, vascular endothelial growth factor (VEGF), and VEGF-C in diluted serum.

For sandwich-type immunoassays, both signal amplification and noise reduction are crucial for obtaining high sensitivity in clinical immunoassays. Much attention has been focused on signal amplification by using an enzyme label, like HRP. It has been demonstrated that colloidal Au label when involved in an immunoassay can be sensitively detected by anodic stripping voltammetry (ASV) at a disposable screen-printed electrode (SPE) after oxidative release of Au^{3+} ions. The method was evaluated for a noncompetitive heterogeneous immunoassay of IgG and a detection limit of 3 pM was determined, which is competitive with colorimetric ELISA or immunoassays based on fluorescent europium chelate labels.[196] By using AuNP labels and silver enhancement, an electrochemical metalloimmunoassay has been presented by Velev and Kaler for IgG detection based on the direct electric

conductivity readout.[197] Moreover, Shen and co-workers demonstrated a strategy based on the precipitation of silver on colloidal gold labels, which, after silver metal dissolution in an acidic solution, was indirectly determined by ASV at a GCE. This method was also evaluated for an immunoassay of IgG as a model with a detection limit of 6 pM.[198] Later, a polymer-membrane-based potentiometric method for protein detection was developed utilizing AuNP labels and silver enhancement. In particular, a silver ion-selective electrode (ISE) was used as an effective transducer for sandwich immunoassays by a direct potentiometry without any ion accumulation involved in analogous ASV measurements of nanoparticle tags.[199] By direct adsorption of IgG on 10 nm AuNPs to form an IgG-nanocatalyst conjugate, Yang et al. fabricated an ultrasensitive and simple sandwich-type heterogeneous electrochemical immunosensor for IgG determination, and the detection limit was further reduced to 1 fg/mL.[158a] Double-codified gold nanolabels consisting of AuNPs conjugated with HRP-labeled IgG antibodies for enhanced immunoanalysis based on either a spectrophotometric or an electrochemical method were developed. The detection limits for this double-codified nanoparticle-based assay were 52 (spectrophotometric) and 260 pg (electrochemical) of human IgG/mL, respectively, much lower than those typically achieved by ELISA tests.[200] Thionine-doped magnetic AuNPs modified with HRP-anti-CEA were assembled on AuNP-modified carbon fiber microelectrode to form a double-codified nanolabel, which was used for electrochemical detection of CEA. The electrochemical signal is efficiently amplified both by magnetic bionanosphere labels and by the bound HRP toward the catalytic reduction of H_2O_2.[201] Similar strategies were also demonstrated to detect CEA[202] and human lung cancer-associated antigen α-enolase (ENO1)[203] by using HRP-encapsulated nanogold hollow microspheres as labels (Figure 24).

The scope of the sensitive AuNP label-based electrochemical detection was further extended to analysis of DNA hybridization, proteins, etc. Velev and Kaler have shown how to create an array of biosensors by in situ assembly of colloidal particles onto micropatterned electrodes.[197] Sequence-selective DNA detection has become increasingly important as scientists unravel the genetic basis of disease and use this new information to improve medical diagnosis and treatment. Mirkin and Letsinger described a method for analyzing combinatorial DNA arrays using oligonucleotide-modified AuNP probes and a conventional flatbed scanner.[204] This work was further extended to an electrical DNA array in which the binding of oligonucleotides-functionalized AuNP label and the subsequent silver enhancement led to direct measurable conductivity changes. As shown in Figure 25, concentrations of target DNA as low as 500 fM with a point mutation selectivity factor of ~100 000:1 were successfully detected.[205] Recently, Nilsson et al. described another electrical sensor that uses rolling circle amplification (RCA) of DNA to stretch across the gap between two electrodes. By adding target DNA sequences, the RCA products were able to interact with AuNP seeds and accelerate the silver enhancement to generate an electrically conductive nanowire, thus producing electrical conductivity signals.[206] Different forms of electrochemical methods with AuNP labels were also developed for DNA or enzyme detection. For example, Wang et al. have introduced a chronopotentiometric method with a nanoparticle-based protocol to detect DNA hybridization with a magnetically induced solid-state electrochemical stripping detection signals.[207] Another chronocoulometric DNA sensor was fabricated in Fan's group for sequence-specific detection of the femtomolar level of

DNA.[208] The strategy was based on the effects of AuNPs-mediated amplification and nanoscale control of DNA assembly at electrodes. In addition, Limoges[209] and Surareungchai[210] made use of the voltammetry method ASV to indirectly determine the solubilized Au^{3+} ions releasing from the AuNP label to analyze specific DNA sequences. Another voltammetry method of Differential pulse voltammetry was used to detect protein phosphorylation[211] and human serum albumin in clinical samples.[212]

4.3. AuNP-Incorporated Composite Electrode Matrixes

The incorporation of nanomaterials into composite electrode matrixes presents another approach to develop electrochemical biosensors with low background currents and improved electrocatalytic activity, electron conduction path, and stability. It is predictable that the incorporation of AuNPs into nanocomposites could promote electron transfer kinetics and will likely result in improved sensing characteristics. For example, AuNPs conjugated with CNT provide excellent electrocatalytic ability, enabling electrochemical biosensors for detection of α-fetoprotein (AFP),[213] CEA,[214] and cholesterol.[215] A strategy based on the unique characteristics of Azure I/multiwalled carbon nanotube (Azure I/MWNT) composite membranes and AuNPs was developed to construct a highly sensitive amperometric immunosensor for AFP. HRP instead of BSA was employed to block sites against nonspecific binding and amplify the signal of the antigen–antibody reaction with a detection limit of 0.04 ng mL^{-1}.[213a] Another approach for fabrication of reagentless immunosensor for CEA was demonstrated by immobilizing Prussian blue nanoparticles on a three-dimensional structured membrane of AuNP-doped chitosan-MWNT homogeneous composite. The electrodeposition of AuNPs on the surface of the composite can be used to immobilize antibody biomolecules and avoid the leakage of Prussian blue nanoparticles.[214a] Lee et al. also presented a novel amperometric biosensor for cholesterol detection based on the immobilization of cholesterol oxidase (ChOx) onto MWNT-AuNP composite covered with a layer of chitosanionic liquid network. The synergistic influence of MWNT, AuNP, chitosan, and ionic liquids contributes to the excellent performance of the biosensor with good sensitivity, low response time, repeatability, and long-term stability.[215]

Graphene, a single layer of carbon atoms in a two-dimensional honeycomb lattice, has potential applications in the electrical detection of biological species due to its unique physical properties. As compared to CNTs as a support for electrochemical biosensors, graphene possesses very small thickness, good thermal conductivity, mechanical strength, and larger surface area. Therefore, graphene is a very promising candidate as a new carbonaceous support, and the integration of graphene with AuNPs is beneficial to develop highly sensitive electrochemical sensors for proteins,[216] amino acids,[217] and DNA.[218] For example, Chen et al. reported on the fabrication and characterization of a specific IgG detection biosensor using thermally reduced graphene oxide (TRGO) sheets decorated with AuNP-antibody conjugates. This immunosensor avoids nonspecific protein immobilization on graphene/TRGO and provides a stable binding for probe proteins on the robust AuNPs.[216a] Wang and co-workers provided an electrochemical sensor to distinguish enantiomers of vasopressin by using a designed split aptamer as a new chiral selector and graphene-mesoporous silica-AuNP hybrids (GSGHs) as electrochemical sensing platform. The introduction of GSGHs can enrich a number of aptamers, which effectively reduces the

detection limit of vasopressin.[216b] Li et al. described an aptasensor for detection of L-histidine based on the switching structure of aptamer and AuNP-graphene nanosheet composite. The proposed sensing protocol exhibits excellent sensitivity and reasonable selectivity for its target molecules.[217] Yang and coworkers demonstrated an electrochemical DNA biosensor based on graphene-three-dimensional nanostructure gold nanocomposite-modified GCE for detection of survivin gene. A “sandwich-type” detection strategy was employed, and the detection limit was as low as 3.4 fM.[218]

Dendritic nanostructures are highly branched polymers showing unique properties, including structural homogeneity, integrity, and ease of functionalization. Encapsulating conducting nanomaterials such as AuNPs into the interior of the dendrimer can increase the conductivity of the dendrimer by accelerating the electron transfer process. Combining the properties of AuNPs and the surface reactivity of dendrimers for immobilizing a large amount of antibodies and mediators makes them an excellent immunosensor platform. For example, a chronoamperometric immunosensor for lung cancer biomarker Annexin II and MUC5AC detection was developed by covalently binding hydrazine and antibodies to the AuNP-doped dendrimers, which was then attached to a conducting polymer layer on AuNP/GCE surface. The use of dendrimer increased the sensitivity of the sensor by several folds.[219] Also, a highly sensitive electrochemical immunosensor was developed for CEA detection by means of dendrimer/AuNP as a sensor platform and MWNT-supported multiple bienzymes as labels. As indicated in Figure 26, the encapsulation of AuNPs in the interior of the dendrimer increased the conductivity of the sensor probe, thus accelerating the electron transfer reaction as well as the immunosensor’s response.[220] In addition, PAMAM and poly(propyleneimine) (PPI) dendrimers combined with AuNPs have been fabricated to detect glucose,[221] AFP,[222] and DNA.[223] Salimi et al. constructed an electrochemical immunosensing platform based on PAMAM-AuNP for the detection of AFP by sequentially immobilizing ethyleneamine viologen molecule as redox marker and AFP antibody as recognition element.[222] An electrochemical DNA nanobiosensor was also prepared by immobilization of probe DNA on electrodeposited dendrimer PPI doped with AuNP as platform on GCE.[223]

Another biopolymer chitosan has been used by several groups to serve as an immobilization matrix due to its biocompatibility and high mechanical strength. Using this approach, amperometric biosensors have been fabricated to measure drug sensitivity[224] and detect protein biomarkers.[225] A novel in situ interfacing of AuNPs with a chitosan hydrogel was achieved by one-step electrochemical deposition of tetrachloroauric(III) acid and chitosan on Au electrodes. With AChE as a model enzyme, rapid amperometric sensing of the pesticides malathion and monocrotophos was achieved with a detection limit of 1 ng mL^{-1}.[224] Another experimental methodology based on chitosan-branched Fc and AuNPs was developed to design a label-free immunosensor for the sensitive detection of HBsAg. The controllable electrodeposition of chitosan-branched Fc formed a three-dimensional robust film for the assembly of AuNPs and further immobilization of hepatitis B surface antibody.[225a] AuNPs combined with nafion and gelatin or polyvinyl butyral as matrixes were also developed by Yuan and his co-workers to construct electrochemical immunosensors for HBsAg determination.[226]

In addition to the above-mentioned carbon nanomaterials and polymers, Fc,[227] silica,[228] magnetic particles,[229] and dyes[230] were also used to fabricate AuNP-based composite electrode matrixes to construct electrochemical sensors for DNA, miRNA, and protein biomarkers. For example, Zhou et al. developed enhanced voltammetric assays for detecting DNA,[227a] p53,[227b] and miRNA[227c] based on Fc-capped AuNP/streptavidin conjugates. For the determination of miRNA, a biotinylated miRNA with the same sequence as that of target was introduced into samples of interest and allowed to compete with the target to combine with the oligonucleotide probe preimmobilized onto electrodes. Voltammetric quantification of the miRNA target was accomplished after complexation of the biotin-miRNA with Fc-capped AuNP/streptavidin conjugates. The Fc oxidation current was inversely proportional to the concentration of target miRNA, and the low detection levels allowed direct quantification of miRNA-182.[227c] The highly enhanced ECL from a hybrid gold/silica/QD nanostructure was reported by Zhang's group, and successfully applied to develop an ultrasensitive ECL immunosensor for the detection of CEA.[228] Yang et al. developed an electrochemical immunosensor for CEA detection by self-assembled nanogold coatings on magnetic core/shell particles. The limit of detection (1 pg/mL) is approximately 500 times more sensitive than that of the traditional ELISA methods.[229] Meanwhile, Yuan et al. reported a series of reagentless and label-free amperometric immunosensors with enhanced analytical features. These electrochemical sensors were employed to detect protein biomarkers like CEA, HBsAg, and AFP by integrating AuNPs with various nanocomposites containing matrixes such as thionine,[230a,b] toluidine blue,[230c,d] cysteine,[230e] BSA,[230f] porous organic material,[230g] and tris(2,2′-bipyridyl) cobalt(III)-BSA.[230h]

4.4. Outlook of AuNP-Based Electrochemical Assays

Over the past decades, intensive research effort has been made to design electrochemical biosensors capable of providing better analytical characteristics in terms of sensitivity, selectivity, reliability, ease of fabrication, and low cost. AuNPs were employed to be an ideal substrate to immobilize biomolecules without reducing their biological activity as well as an efficient conducting matrix with electrocatalytic ability, both of which make them a powerful tool to construct robust and sensitive biosensors for IVD tests. Despite the rapid development in this field, the ultimate goal of achieving long-term, accurate, and continuous target monitoring in patients has not yet been reached. For example, a major challenge for electrochemical biomarker sensors is the reliable, simultaneous detection of multiple biomarkers in complex biological samples. The past decade has witnessed great progress in developing various detection devices, especially those coupled with microfluidics.[231] These platforms may soon enable accurate detection of panels of biomarkers of interest in various clinical samples. It is not surprising that the detection results of any nanosensor are sensitive to the size, shape, composition of nanomaterials, or bioconjugation efficiency during the preparation of tags. Therefore, it is critical to keep the physiochemical properties of nanomaterials consistent in Different batches. To realize this, huge effort is still required to standardize the quality of the nanomaterials. To date, only a few kinds of nanomaterials can be prepared in Different laboratories with simple procedures and high reproducibility. Such a well-known example is AuNPs, which have been commercially available, and the size of AuNPs can be custom-tailored. More impressively, the commercial AuNPs are usually stabilized with citrates, which bind on AuNP surfaces through weak chemical bonds and can

be easily replaced from the AuNP surfaces by thiolate molecules. Also, much attention should be paid to the nonspecific adsorption issues of electrochemical immunoassays, which generally govern the detection limit of the assays. Last, the rapid development of these electrochemical assays should ultimately help physicians make timely clinical decisions and reduce the healthcare costs and patient stress. It is likely to realize the long-sought goal by allowing electrochemical assays to be conducted on inexpensive platforms such as papers to form paper-based electrochemical systems.

5. AuNP-BASED SERS ASSAYS

Because of the development of nanoscience and technology, SERS, surface-enhanced Raman spectroscopy, has made tremendous progress, and its applications have been expanded to diverse fields ranging from chemical sensing, materials science, biomedical studies, to art and forensic science. The Raman spectrum provides unique chemical and structural information for a specific species, but the sensitivity of the normal Raman detection is insufficient in most cases because of the relatively low cross section of inelastically scattered Raman photons. The magnitude of Raman cross sections can be greatly enhanced when the Raman-active molecules are placed on or near a roughened noble metal surfaces.[232] A wide variety of plasmonic nanoparticles or rough metal substrates have been found to enhance SERS signals by factors up to 10^{14}.[233] In particular, as compared to cadmium-containing QDs and other toxic or immunogenic nanoparticles, AuNPs have been considered as a good candidate in biomedical applications because of their long-term stability, good biocompatibility, easily controllable size distribution, and high homogeneity. Moreover, AuNPs can efficiently scatter visible light and do not blink or photobleach, which are able to amplify the Raman scattering efficiencies of the adsorbed species, achieving spectroscopic determination of the species even at the single-molecule level under ambient conditions.[234]

5.1. AuNP-Based Heterogeneous SERS Assays

Among the various applications of SERS spectroscopy, biochemical detection for IVDs has drawn considerable research attention because of its high sensitivity and finger-printing capabilities. Such enhanced properties were obtained as a result of the exploitation of silver or gold colloids served as the substrates of SERS. In general, AgNP-based substrates show strong SERS signals. However, AgNPs have some limitations mainly including ease of surface oxidation and biological toxicity, which hamper their wide applications especially in biological systems.[235] In contrast, AuNPs have been demonstrated as an ideal alternative because they are biocompatible, stable, and versatile for surface functionalization. As a result, SERS active substrates can be used for heterogeneous SERS assays by assembling AuNPs onto a solid surface to construct plasmonic sensors.

So far, it is accessible to obtain AuNPs of various sizes and shapes and even Different compositions to tune their SPR to maximize the SERS enhancement. The AuNP-based SERS assays have been widely applied to determine chemical or biological species, such as pH, small molecules, DNAs, proteins, bacteria, cells, etc.[235b] For example, Halas et al.[236] reported that the reproducibility of SERS spectra of thiolated ssDNA and dsDNA oligomers

bound to Au nanoshell-based SERS substrates can be dramatically increased with highly controllable electromagnetic enhancement. The high quality and reproducible DNA spectra may provide an opportunity for label-free DNA detection based on SERS. Ren et al.[237] prepared a homogeneous SERS substrate by chemical adsorption of iodide on the AuNP-assembled ITO substrates followed by electrochemical oxidation of the adsorbed iodide. This SERS substrate was used to study the plasma membrane of Chinese hamster lung fibroblasts cells with mapping technique. Yu and co-workers made use of Different sized AuNPs to construct heterogeneous SERS assays for the determination of human IgG,[238] thrombin,[239] and bacterial biomarker dipicolinic acid.[240] For example, they described a novel and efficient SERS assay for thrombin using 56 nm sized AuNPs to create the substrates. SERS signals with the concentrations of thrombin in the range of 0–1 μM were measured, and the linear range and detection limit were 0.1–10 nM and 20 pM, respectively.[239] Ziegler et al.[241] reported the SERS spectra of whole human blood, blood plasma, and red blood cells on AuNP-SiO_2 substrates. Dinish et al.[242] developed SERS for pH sensing using a Raman reporter, arene chromium tricarbonyl linked aminothiophenol ($Cr\text{-}(CO)_3$-ATP), which was bound to a nanoroughened planar substrates coated with AuNPs. Reinhard's group described a series of engineered substrates for SERS with noble metal nanoparticle cluster arrays (NCAs) and AuNRs to fabricate detectors for bacterial pathogens,[243] bacterial cells,[244] and breast cancer cells.[245] For example, they benchmarked NCAs with unpatterned two-dimensional AuNP substrates and regular gold nanodisc arrays. They found that NCAs offered a good compromise between signal enhancement and substrate reproducibility, which outperformed the other substrates in SERS measurements of bacteria (Figure 27).

Recently, DNA origami based on the assembly of AuNP dimers has been described for SERS.[246] Thacker et al. made use of self-assembly technique for accurate positioning of 40 nm AuNP dimers with sub-5 nm gaps on a 40 × 45 nm^2 DNA origami platform (Figure 28). The innovative design leads to strong plasmonic coupling between two 40 nm AuNPs reproducibly, which was used to demonstrate SERS measurements of both an external analyte and ssDNA oligonucleotide attached to the nanoparticles. In addition, other materials such as graphene[247] and mesoporous silica[248] have been combined with AuNPs to construct SERS active substrates. Song et al.[247] developed such a SERS-active substrate based on AuNP-decorated chemical vapor deposition growth of graphene and used it for multiplexed detection of DNA. Because of the combination of AuNPs and graphene, the Raman signals of dyes were dramatically enhanced by this substrate, and a detection limit as low as 10 pM was obtained. Moreover, SERS active substrates composed of Different shaped AuNPs including boot-shaped gold nanoparticles,[249] gold nanoflowers,[250] and gold nanoplates[251] have also been investigated for SERS-based biodetection.

Because the size, shape, and architecture of metallic nanostructures are highly related to their surface plasmons, it is likely to create a nanostructure with maximal local electromagnetic fields. Among various nanostructures, the controllable gap between metallic nanoparticles is particularly interesting because of the rich plasmonic properties in the gap caused by the coupling of the localized surface plasmon of the metallic nanoparticles. Abajo et al.[252] reported a zeptomole SERS assay based on the optical hot spots formed in the gaps between nanostar tips and the planar Au surface. Recently, Mahajan et al.[253] demonstrated

that a single gold nanosphere on a metal film junction is capable of detecting a single molecule with SERS. They showed the ability of this configuration to detect a variety of biomolecules, such as adenine and oxytocin. Kim et al.[254] reported a biomolecule detection method using an Au nanowire-nanoparticles configuration. The Raman signal was strongly enhanced at the hot spots between nanowire and NPs, which were produced by the self-assembly of biotinylated AuNPs on a biotinylated Au nanowire through avidin. Tian and co-workers[234c] reported a so-called shell-isolated nanoparticle-enhanced Raman spectroscopy (SHINERS), where the Raman signal amplification was provided by AuNPs coated with an ultrathin silica or alumina shell (Figure 29). To carry out the SERS detection, a monolayer of such core–shell nanoparticles was spread over a smooth substrate like “smart dust”. High-quality Raman spectra were obtained for various molecules in the gap of these nanoparticles. SHINERS was employed for in situ detection of cell wall proteins and pesticide residues on citrus fruits.

A series of heterogeneous SERS immunoassays based on AuNPs have been developed for biological species. These SERS assays rely on the immobilization of capture antibodies on a surface for capturing the target antigens, which subsequently bind with the Ab2-labeled Raman tags to form sandwiched structures. Porter and co-workers[255] developed SERS tags based on the coadsorption of reporter molecules and targeting ligands onto the surface of AuNPs. Later, the same group improved the detection capability of this format using chemical linkage.[256] In the new strategy, the AuNPs were coated with thiolate-containing reporter molecules that have a terminal succinimide group, which can react with the amines of antibodies to form an amide linkage. Sandwich-type heterogeneous immunoassays combined with the extrinsic Raman labels (ERLs) were demonstrated to detect PSA,[256] viral pathogens,[257] rabbit IgG,[258] and human IgG.[259] Another labeling design based on mixed monolayer on AuNPs was introduced by Lipert et al.[260] The mixed monolayer-based ERLs were employed in IgG assays and a simple diagnostic test for the potential pancreatic cancer marker MUC4 (Figure 30). Another unique, sensitive, and photobleaching-resistant SERS-based immunoassay utilizing AuNPs was described by Chang et al.[261] The immunogold nanoparticle (IgG-AuNP) was manufactured by chemisorption of antibody IgG on AuNP, followed by introducing 5,5′-dithiobis(2-nitrobenzoic acid) (DTNB) as the Raman-active reporter molecule to the surface of the IgG-AuNPs. This SERS-based immunoassay was applied to detect protein A, a specific surface antigen of *Staphylococcus aureus*. Choo et al.[262] created a SERS imaging-based immunoassay technique by means of a gold-patterned microarray chip and hollow gold nanospheres (HGNs). The HGNs were coated by Raman reporter molecules and antibodies to sandwich the specific antigens on the surfaces of gold patterned wells, followed by SERS mapping. Furthermore, Cui’s group developed a series of SERS-based immunoassays for antigen detection.[263] They exploited the concept of the optical encoding approach, SERS-fluorescence joint spectral encoding method, for multiplexed detection of antigens with dual readouts.[263c]

The SERS signals can also be amplified by using plasmonic bimetallic nanoparticles, exemplified by silver staining on AuNP labels. Mirkin and co-workers designed Raman dye-functionalized AuNPs probes with specific biological affinities.[264] These probes were treated with silver enhancement solutions for multiplexed detection of protein–small molecule interactions and protein–protein interactions. Bai et al.[265] demonstrated a method

based on 4-mercaptobenzoic acid (4-MBA)-labeling of immunogold nanoparticles with the silver staining enhancement for the quantitative detection of hepatitis B virus surface antigen with a detection limit of 0.5 μg mL^{-1}. Ren et al.[266] presented a seed growth method to prepare Ag/Au core–shell nanoparticles, which were then labeled with monoclonal antibodies and SERS probes for analysis of mouse IgG. Hu et al.[267] reported that Au/Ag core–shell nanoparticles were covered with a carbon shell to form triplex Au/Ag/C core–shell nanostructures. In this hybridized nanostructure, Au/Ag core–shell nanoparticle was loaded with Raman reporters for optical enhancement, and carbon shell was used for protection and conjugation of antibodies. The synergic effects of the multicomponent nanoparticles endow these SERS assays enhanced properties in comparison to those using single component alone.

In addition to immunoassays, sandwich SERS assays based on AuNP-incorporated nanostructures are also important for DNA detection. Multiplexed SERS detection of oligonucleotide targets has been performed by Mirkin et al.[268] In their format, AuNPs probes labeled with oligonucleotides and Raman-active dyes were captured by DNA targets on an underlying chip. The subsequent silver coating on AuNPs can promote the SERS signals of the dye-labeled particles. By using a Raman tag as a narrow-band spectroscopic fingerprint, a large number of highly sensitive and selective SERS assays can be designed for DNA targets with multiplexing and ratioing capabilities. Kim's group[269] reported an Au particle-on-wire system, allowing multiplexed detection of targeting DNAs in a quantitative manner with a detection limit of 10 pM (Figure 31). Irudayaraj et al.[270] applied a SERS-based detection system with nonfluorescent Raman tags to detect the alternative splice junctions of breast cancer susceptibility gene 1 (BRAC1). To do this, ssDNA and nonfluorescent Raman tags were separately tethered onto AuNPs, and the detection sensitivity can be up to 1 fM. A similar SERS assay was applied for monitoring multiplex and quantitative gene expression in cancer cells without an amplification procedure.[271] To further detect very low concentrations of DNA targets, some amplification strategies have been integrated into the SERS assays. Yu et al.[272] described a subattomolar SERS assay based on multilayer metal–molecule–metal nanojunctions. This strategy relies on a two-step amplification procedure. The targeting DNA was first applied to facilitate the immobilization of AuNP probes, which were then linked with other AuNP probes through the hybridization of the two complementary AuNP probes. As a result, the distance between the Raman tags on AuNP probes was drastically shortened, thus generating a great number of "hot spots" on Au substrates. With the aid of amplification strategy, this enhanced SERS assay was allowed to detect HIV-1 DNA sequences at concentrations down to 10^{-19} M. In addition, Zhang et al.[273] described another amplification strategy for DNA detection. By the combination of abundantly repeated sequences of RCA products with AuNP and Rox-modified detection probes, the SERS signal was amplified and the detection limit of 10 pM can be achieved.

AuNP-incorporated nanocomposites were also employed as SERS tags for creating aptamer biosensors. Wu et al.[274] presented a reagent-free ATP biosensor using ATP aptamer and SERS. In the SERS probe, gold nanostar@Raman label@ SiO_2 core–shell nanoparticles were fabricated where the Raman reporter molecules were sandwiched between the gold nanostar core and the silica shell. The detection limit for ATP was determined to be 12.4

pM, much lower than those from many other methods. Dong et al. and Hu et al.[275] separately developed SERS aptasensors for thrombin detection by means of AuNP-based Raman tags and promoted core–shell nanoparticles Raman tags, respectively. SERS aptasensors based on AuNPs labeled with aptamers and Raman reporters have opened a new era for bioanalysis with high sensitivity and selectivity.

5.2. AuNP-Based Homogeneous SERS Assays

In heterogeneous SERS assays, both the sandwich immunoassay and the sandwich DNA hybridization assay are performed on a solid substrate. Although this strategy has been successfully applied to the detection of various analysts, the time-consuming and complicated preparation of the SERS tags has limited its widespread applications. Recently, researches have revealed that the SERS signals can be controlled by modulating the electromagnetic field enhancement in interparticle plasmon coupling. This has offered a new strategy to design SERS-based homogeneous assays through the controlled assembly of metallic nanoparticles in solutions. For example, by utilizing the excellent adsorption property of metal–organic frameworks (MOFs), a AuNP-embedded MOF structure was applied to preconcentrate analytes of interest in close proximity to the electromagnetic fields at AuNP surfaces, thus offering strong SERS signals for highly sensitive detection of a variety of analytes.[276] Another strategy was based on the hydrolysis of the enzyme substrate 5-bromo-4-chloro-3-indolyl phosphate (BCIP) to form Raman-active indigo dyes, which were subsequently adsorbed onto the surface of AuNPs to produce strong Raman signals.[277] This approach was applied to detect ALP with a detection limit of 4 fM. Ogaidi et al.[278] developed a SERS biosensor for label-free detection of glucose using GOx enzyme-coated gold nanostar@silica core–shell nanoparticles. The intermediate product H_2O_2 produced during the enzyme catalytic reaction near the Au nanostar@silica nanoparticles can generate a strong SERS signal. Furthermore, the simple mixing of the whole bacterial cells with AuNP SERS tags allows characterization of bacterial cells, because homogeneous colloidal nanoparticles can provide much more interaction points with bacterial cell wall than heterogeneous surfaces.[279]

In nanoparticle-based SERS assays, Raman scattering intensity of a molecule at the “hot spot”, often located at the junctions and interstices in the interacting metal nanostructures such as dimers or aggregates, can be several orders of magnitude higher than that on the surface of single nanoparticles. Thus, the aggregates of colloidal AuNPs are very popular nanostructures in SERS with wide applications ranging from single molecule Raman spectroscopy to ultrasensitive imaging in live cells. For instance, AuNP aggregates have been used to construct SERS-based homogeneous assays for measurement of small molecules, DNA, cancer cells, etc. Kneipp et al.[280] fabricated these nanoaggregates with a SERS enhancement factor on the order of 10^9. Zhang et al.[281] developed a single base extension reaction-based SERS for DNA methylation assay. The single base extension reaction took place between AuNP-modified capture probes and cyanine 5-deoxyribonucleoside triphosphate (Cy5-dGTP). The strong SERS signal was produced by further adding AuNPs to enhance the local electromagnetic field in the AuNP aggregates. Besides, the addition of AuNPs in the last step of the detection procedure was allowed to create nanoaggregates to amplify the SERS signal. By means of this strategy, Zhang et al.[282]

and Yang et al.[283] have, respectively, demonstrated that the SERS assays can detect the femtomolar level of specific biomolecules and single-cell level of human cancer cells.

On the other hand, small nanoparticle aggregates can also be prepared by introduction of aggregation-inducing agents, such as dyes, peptides, salts, or targets, to be probed. A Raman tag called nanoagregate-embedded beads (NAEBs) was developed by Chau and his co-workers.[284] NAEBs are dye-induced, silica-coated aggregates consisting of a small number of AuNPs. These small AuNP aggregates can produce enhanced SERS signals for the recognition and targeted detection of pathogenic microorganism, such as *Staphylococcus aureus* cells.[284b] Causa et al.[285] reported that by adjusting the ratio of the number of peptide molecules to AuNPs, single AuNP to submicrometer AuNP aggregates can be created. The aggregated particles have been used for SERS detection of adenine. Chu et al.[286] developed a homogeneous SERS biosensor for the detection of DNA by utilizing the Difference in adsorption property of ssDNA and dsDNA on AuNPs, which leads to Different capability of protecting AuNPs against salt-induced aggregation. In addition, target-induced aggregation due to the interaction between antibodies and antigens or DNA hybridization has been used to fabricate SERS “turn on” detection methods. For example, the immunoreaction between antigen and antibody-modified AuNP tags induces aggregation of AuNPs, thus causing significant enhancement of SERS signals.[287] To provide rapid and accurate detection of DNA markers, an alternative SERS-based probe was designed by Irudayaraj’s group[288] by covalently attaching both DNA probing sequence and nonfluorescent Raman tags to the surface of AuNPs. The target DNA is complementary to the probing DNA sequence and can bring AuNPs together to produce enhanced SERS signals. The same group also presented thrombin-induced gold nanorod–nanoparticle junctions to detect thrombin at subnanomolar concentrations in diluted human blood serum.[289] By developing indirect sandwich-type assays in which one target DNA sequence can recognize two AuNP probes,[290] SERS signals could be modulated or controlled by long-range plasmonic interactions (Figure 32). The as-formed SERS beacons showed excellent sequence specificity and were able to discriminate single-base mismatches. Hwang[291] described a similar strategy to detect glucose and uric acid using $Au@SiO_2$ core/shell nanoparticle assemblage based on the glucose and uric acid-induced nanoparticle aggregate.

SERS-based “turn off” strategies, as a result of the target-induced protection of AuNPs against aggregation, have also been studied by several groups. Stevens et al.[292] demonstrated a route to enable the SERS detection of disease-specific enzymes using self-assembled nanoaggregates of peptide-AuNP conjugates. In the presence of the target enzyme, the peptides were degraded into small fragments, thus converting the state of the AuNP tags from aggregation to dispersion. Consequently, a clear decrease of SERS signal was observed. Similarly, the telomeric elongation-governed SERS effect was applied to detect telomerase by controlling the aggregation extent of the AuNP SERS tags.

In SERS, it is now well understood that the plasmonic coupling effect at the nanometre gap junction between particles can induce enormous electromagnetic enhancement that allows SERS signal to be detected with single-molecule sensitivity. However, it still faces a problem to prepare nanostructures with high reproducibility, as particle structure and interparticle spacing can markedly affect Raman signals. To obtain high-quality Au

nanostructures with as many “hot spots” as possible, quite a few strategies have been developed. Nam et al. prepared AuNP heterodimers by controlling the number of tethering DNA molecules on the AuNP surfaces followed by magnetic separation method.[293] These DNA-tethered AuNP heterodimers were allowed to sandwich a single Raman-active Cy3 dye molecule only in the gap of the dimers. With thickness-controlled growth of Ag shell on the surface of the dimeric AuNPs, gap-tailorable Au/Ag core–shell nanodumbbells (GSNDs) with structurally reproducible dimetric AuNP tags were obtained. Later, the same group[294] found that DNA on AuNPs can facilitate the formation of well-defined gold nanobridged nanogap particles (Au-NNP), which can generate highly stable and reproducible SERS signals. As shown in Figure 33, the uniform and hollow gap (~1 nm) between the gold core and gold shell can be precisely loaded with a quantifiable amount of Raman dyes whose SERS signals showed a linear dependence on probe concentration with a detection limit of 10 fM. Irudayaraj et al.[295] reported that the extraction of LSPR spectra from SERS signals can be applied to measure the interparticle distance from Raman enhancement data. The developed methodology was applied to calculate the interparticle distance between nanoparticle dimers from SERS signals and to detect and quantify DNA at the single-molecule level. Importantly, this approach has the advantage of clearly Differentiating dimers from nonspecific aggregation.

SERS-based homogeneous immunoassay using antibody-conjugated AuNPs has drawn great attention because of its rapid and sensitive sensing capability. The combination of magnetic and optical properties of nanoparticles into a single platform was employed for rapid immunomagnetic separation (IMS) and detection. For example, Choo et al.[296] created a SERS-based immunoassay technique using HGNs and magnetic beads. The HGNs were conjugated with polyclonal antibodies and Raman reporter molecules, while magnetic beads were conjugated with monoclonal antibodies. When they were incubated with CEA antigens, sandwich immunocomplexes were formed to generate SERS signals with reduced time and simplified procedures. Similar SERS methods have used to detect protein biomarkers, such as IgG, AFP, CEA, and BLV antigen gp51.[297] The combination of magnetic beads and AuNPs was also extended to aptamer-based SERS biosensors. For instance, Johnson et al.[298] described a paramagnetic nanoparticle assay for SERS detection of DNA oligonucleotides derived from the West Nile virus genome. The approach was based on the target-induced hybridization of complementary oligonucleotide probes on the surface of magnetic beads and Raman reporter tag-conjugated AuNPs. Tamer et al.[299] presented a homogeneous detection method for sensing staphylococcal enterotoxin B (SEB). In this assay, peptide ligand-functionalized core–shell-structured iron–gold magnetic particles were used as scavengers to capture SEB molecules, and the resulted sandwich assays were tested by AuNRs that acted as SERS probes. Other aptamer-based SERS homogeneous assays were also employed to measure telomerase activity[300] and cocaine.[301]

Identification of cancer cells has great value in predicting the invasiveness and metastatic potential of tumors. Circulating tumor cells (CTC) are a hallmark of invasive cancer cells, which are responsible for the development of metastasis. It is imperative to develop effective approaches for the detection and quantification of CTCs. Sha et al.,[302] for the first time, developed a homogeneous SERS-based assay for CTCs by taking advantage of magnetic beads and AuNP-based SERS tags (Figure 34). In this format, the SERS-active AuNPs were

encapsulated in a silica coat, whose surface was conjugated with HER2 antibodies. Magnetic beads were conjugated with anti-EpCAM antibody molecules to capture CTCs from human whole blood. The ligand–receptor interactions enable the specific binding of magnetic beads and SERS tags on CTC, allowing rapid detection of CTCs with a detection limit of 50 CTCs per mL of whole blood. Later, Nie et al. reported a SERS-based method to directly measure targeted CTCs in the presence of white blood cells. The AuNP-based SERS tags were conjugated with EGF peptide as a targeting ligand to identify CTCs in the peripheral blood of 19 patients suffering from squamous cell carcinoma of the head and neck, with a detection range of 1–720 CTCs per mL of whole blood.[303]

5.3. AuNP-Based Cellular SERS Assays

Raman scattering spectra can give molecular vibrational information on scattering objects, which therefore provide structural and environmental information on the targets in biological samples without any labeling. However, it remains a challenge for live-cell imaging using Raman microscopy alone because of the weak Raman signals. AuNP-based SERS can significantly improve the signals and has the potential to be applied in molecular imaging of living samples with nanometer-scale resolution. SERS is thought to be a powerful tool for cell detection and imaging because of its several advantages over traditional detection methods. First, the Raman signals do not suffer from rapid photobleaching and autofluorescence in biological samples as do fluorescent assays. Second, SERS can detect living cells or tissues noninvasively by using NIR excitation with low laser power. Third, the sensitivity of SERS can be as high as single-molecule level, which makes it possible to detect cancer cells even in the early stages of the disease.

For in situ cancer cell detection, Different antibody-conjugated AuNP SERS tags have been used for targeting and imaging specific cancer markers expressed on the surface membrane of cancer cells. For example, Choo et al. developed both antibody-conjugated HGNs and antibody-conjugated AuNRs for SERS imaging of HER2-overexpressing MCF7 cells.[304] Chang et al. presented a series of SERS nanotags consisting of AuNPs and Raman reporter molecules for cancer detection.[305] They prepared a lipoic acid-containing NIR-active tricarbocyanine library (CyNAMLA) and tested their SERS properties after chemisorption on AuNP surfaces. Among the NIR active dyes, CyNAMLA-381 exhibited strong SERS intensity and was further applied as an ultrasensitive SERS probe for in vivo cancer imaging.[305b] Irudayaraj and co-workers presented DNA-AuNP reversible networks grown on cell surface marker sites.[306] The SERS tags were used to determine cell surface markers, CD44 and CD24, in three breast cancer cell lines for sensing a $CD44^{+}/CD24^{-}$ subpopulation of breast cancer stem cells. This network nanostructure is capable of detecting a single target on the membrane of a living cell. Ray et al. synthesized “gold nano-popcorn” for targeted SERS sensing and photothermal therapy of human cancer cells.[307] In the presence of LNCaP human prostate cancer cells, the multi-functional popcorn-shaped AuNPs interacted with the cancer cells, providing a significant enhancement of the Raman signal intensity (2.5×10^{9}). As a result, the detection limit by this strategy can be as low as 50 human prostate cancer cells in PBS. Those popcorn-shaped AuNPs were also employed to detect multidrug-resistant bacteria as well as HIV DNA with high sensitivity.[308]

Recently, AuNP-based intracellular imaging by SERS has gained interest because this optical tool can provide high temporal and spatial resolution, which allows one to observe the native chemicals inside living cells and monitor the nanoscale dynamics of cellular organization. Kneipp's et al.[309] employed 60 nm sized AuNPs as the SERS active substrates to measure the native chemical constituents of the cells. Strong Raman signals can be observed especially when larger AuNP aggregates were formed inside the cells. The same group then proposed another SERS probe by using indocyanine green-modified AuNPs. This probe provided molecular structural information from the local biological environment around the particles.[310] By measuring the SERS spectra from endosomes in living individual cells, they observed enhanced Raman signals. As shown in Figure 35, the SERS enhancement was most likely attributed to the formation of Au nanoaggregates when the SERS tags were exposed to the changing endosomal environment. The size increase in morphology was confirmed by complementary TEM studies.[311] Later, they developed an intracellular SERS assay to reveal the specific interactions of silver and gold nanoparticles with hemoglobin and red blood cell components.[312] In addition, some other intracellular SERS assays based on AuNPs have been reported to detect cell organelles and monitor intracellular events. Hu et al.[313] reported a SERS assay to probe an original SERS signal from the living cell nucleus. The AuNPs were functionalized with nuclear localization signal peptide to selectively locate at the cell nuclei of HeLa cells and deliver the spatially localized chemical information. Tamiya and co-workers[314] employed AuNP-based SERS to noninvasively monitor the Differentiation of mouse embryonic stem cells, including undifferentiated single cells, embryoid bodies, and terminally Differentiated cardiomyocytes, without affecting cell viability or proliferation.

Dynamic SERS imaging of intracellular events was possible by slit-scanning Raman microscopy. By utilizing this advanced platform, the position and SERS spectra around AuNPs were simultaneously determined inside living cells with high spatial and temporal resolution. They also employed the AuNP-based SERS sensor to monitor the interactions of the particles with the cell membrane and the entry into the cell.[315] Cellular transport pathways then were monitored with the use of the endocytosed AuNPs, providing molecular maps of organelle transport and lysosomal accumulation.[316]

Intracellular pH plays a critical role in the function of cells. However, the dynamic imaging of pH variations inside living cells is still difficult. The pH-dependent SERS spectra of 4-MBA[317] or 2,5-dimercaptobenzoic acid (2,5-DMBA),[318] adsorbed on Au nanoaggregates, Au nanoshells, or Au nanoparticle silica nanopeapods, were used to create pH sensors for monitoring changes in local pH in living cells. For instance, Kneipp et al. made use of 4-MBA-functionalized Au nanoaggregates to image a wide range of pH values in live NIH/3T3 cells from pH 6.8 to 5.4. This SERS pH sensor was further extended to two-photon excitation using surface-enhanced hyper-Raman scattering (SEHRS) of 4-MBA on Au nanoaggregates, which exhibits a spectral signature capable of measuring pH values between 8 and 2.[317a] Lawson et al. described a pH-sensitive disulfide reporter molecule named 2,5-DMBA, which can attach onto AuNPs to induce a controlled aggregation of AuNPs without the addition of salts. The SERS pH sensor exhibited excellent pH resolution at and below a pH of 7, with the ability to quantify accurately pH values well below 5.5.[318] To enhance the SERS signals, Joo et al. reported a subnanometer gap-separated linear chain AuNP silica

nanotube peapod (SNTP), which was fabricated by self-assembly.[319] The TEM images indicated that numerous nanogap junctions with distances of roughly 1 nm were formed between the AuNPs. Intracellular pH values were examined after the endocytosis of 4-MBA-coated AuNP-embedded SNTPs in mammalian cells, offering more reliability and reproducibility of pH measurements than the usage of AuNPs alone.

SERS sensor was also applied to monitor the intracellular drug release and delivery after cellular internalization of the drug molecules. Particularly, AuNP-based drug delivery systems were combined with SERS tags to provide effective platforms for real-time monitoring of the therapeutic responses, thus enhancing the efficacy of treatment. Lee and co-workers reported a label-free confocal Raman spectroscopy to monitor the GSH-triggered release of anticancer drug thiopurine molecules from AuNPs inside living cells.[320] Tang et al. reported a NIR-SERS technique using AuNPs to probe the intracellular chemical information in single osteosarcoma cell with high spatial resolution.[321] El-Sayed et al. presented plasmonic-tunable Raman/fluorescence imaging spectroscopy, to track the release and delivery of doxorubicin (DOX) from AuNP carriers in real time at a single living cell level.[322] As shown in Figure 36, the anticancer drug DOX was conjugated to the surface of AuNPs via a pH-sensitive hydrazone linkage, resulting in enhanced SERS signal of DOX and quenched fluorescence. When the DOX-AuNPs are internalized by cells and enter the acidic lysosomes, the hydrazone bond breaks to release the DOX from AuNPs, thus greatly reducing its SERS signal, with a recovered fluorescence. This SERS-based imaging technique has the potential to be applied in studying dynamic processes of drug release in living cells as well as cellular response to therapeutics.

It remains a challenge for SERS imaging of living cells with high temporal and spatial resolution. The key to address this issue is improving signal-to-noise ratio, which can be realized either by making Au nanostructures with strong electromagnetic enhancement, by which SERS signals can be greatly increased, or by reducing the background noise of SERS sensor in biological samples, by which the SERS signals can be also enhanced indirectly.

Flower-like AuNPs have strong SERS enhancement performance due to the rich “hot spots” on their surfaces.[323] The facile preparation of Au nanoflowers (AuNFs) and their application in live cell imaging were reported by Xu and co-workers.[324] Raman reporter molecules and folic acid were capped onto AuNFs as the SERS tags to offer strong Raman signal in the living cells, with a high signal-to-noise ratio. Lee et al.[325] reported a facile, size-tunable synthesis method for AuNFs with high yield and good monodispersity. The as-prepared AuNFs were developed into Raman-active tags by packaging RhB@ AuNFs with denatured BSA molecules and showed much stronger SERS intensity than the spherical AuNPs. The capability of Raman imaging in living cells was demonstrated by using the RAW264.7 macrophage cell line.

Another advanced Au nanostructure, Au/Ag core–shell bimetallic nanoparticle, has also been prepared by making full use of the respective advantages of both Au and Ag nanoparticles to enhance SERS signals. For example, Choo et al.[326] prepared such Au/Ag core–shell nanoparticles labeled with secondary antibodies (Figure 37). These SERS tags were used for biomedical SERS imaging of HEK293 cells expressing PLCγ1 cancer

markers. In addition, this assay was able to differentiate cancerous cells from noncancerous cells. Cai et al. prepared a SERS-active aptamer–Ag–Au bimetallic nanostructure for specific detection and photothermal therapy of MCF-7 cells.[327] This SERS imaging was achieved on the basis of the specific interactions between S2.2 aptamer and MUC1 mucin overexpressed on the surface of MCF-7 cells.

In addition to Au/Ag core–shell nanostructures, the core–shell metallic nanoparticles with nanogaps have also been developed.[328] To fabricate this Au core–shell nanostructure, Duan et al. first prepared an amphiphilic block copolymer, which contains a Raman dye-tagged hydrophobic block and a hydrophilic block carrying redox-active phenol pedant groups. As shown in Figure 38, the AuNP-templated self-assembly of the amphiphilic block copolymers and the subsequently localized reduction of Au led to the formation of the core–shell nanogapped AuNPs, where Raman dyes were embedded into the gap of the nanostructure. The width of the nanogap can be tailored by controlling the thickness of polymer shell. They found that the sub-2 nm interior gap displayed the highest SERS enhancement. These core–shell nanogapped AuNPs were functionalized with a S2.2 aptamer for MUC-1 targeting. Singamaneni et al. designed a simple bilayered Raman-intense gold nanostructure where Raman reporters were trapped in the “hot spots” between the core and shell of the nanostructure.[329] The bilayered structure functions not only as a promoter to significantly enhance the electromagnetic field, but also as a protector to improve the stability of the Raman dyes by shielding them from unwanted desorption and degradation in complex biological samples. These SERS tags allowed for high resolution imaging of SKBR-3 cells using 785 and 633 nm laser as the excitation source.

In addition to the use of new nanostructures with strong SERS signals, the strategy of reducing background noise in biological samples is another important means to enhance the SERS signals. A method of obtaining a high-resolution Raman image is the development of advanced bioimaging technology and detection system. For example, Fujita et al. presented a protocol for constructing a Raman microscope equipped with both a slit-scanning excitation and detection system and a laser steering and nanoparticle-tracking system.[330] In addition, the employment of proper Raman dyes may also reduce background noise. For example, Kneipp et al. developed a robust and sensitive SERS label for imaging the native constituents of the cell. In these SERS tags, Rose Bengal or Crystal Violet was attached onto AuNPs as Raman reporter molecules exhibiting specific Raman signatures out of biological samples.[331] Porphyrin was also employed as a Raman reporter molecule by Zheng and co-workers, to allow cellular imaging with strong and specific Raman signals.[332]

Recently, Raman dyes with strong signals in the cellular Raman-silent region (approximately 1800–2800 cm^{-1}) showed great promise for cell imaging with negligible background noise. Olivo et al. prepared an organometallic-nanoparticle conjugate biotag by functionalizing AuNPs with osmium carbonyl clusters, $Os_3(CO)_{10}(\mu\text{-}H)_2$, where the Raman signal of the CO stretching vibrations appears in the mid-IR (1800–2200 cm^{-1}).[333] The inherently weak CO signal can be significantly enhanced by AuNPs, thus providing interference-free SERS signals for cellular imaging. To demonstrate their high sensitivity and spatial resolution in live cell imaging, the SERS tags were labeled with appropriate binding ligands, such as anti-EGFR, for cell targeting. The results undoubtedly showed that the CO stretching vibration

Raman signal can be well distinguished from other biomolecular vibrational modes in the cell. Another series of small chemical groups, like alkyne, nitrile, azide, and deuterium, are expected to show Raman scattering in the cellular silent region as well.[334] Among these groups, alkyne has clear advantages over the other three candidates in terms of high signal intensity, narrow line width, and suitable wavenumber of the signal. By combining AuNP-based SERS and a biorthogonal Raman reporter, the glycans on the membrane of living cells were measured.[334b] To effectively amplify the SERS signals, 4-mercaptophenylboronic acid (4-MPBA) was functionalized on AuNPs to preferentially recognize sialic acids due to the fact that the phenylboronic acid moiety can react with 1,2- or 1,3-diols of sugars to form boronate esters. As a result, the biorthogonal Raman reporter in the sialylated glycans was located in close proximity to the AuNPs, thus inducing strong Raman signals (Figure 39). This technology was applied to measure the targeting glycans on various cell surfaces such as HeLa cells and CHO cells, where a SERS peak can be unambiguously observed at about 2100 cm^{-1}. In contrast, no SERS peak was seen in the control cells treated with the same biorthogonal Raman reporter.

To improve the stability, biocompatibility, and optical properties of SERS tags, the surfaces of metallic nanoparticles are generally covered with a layer of polymers or silica, in which the Raman reporter molecules are covalently embedded. For example, Bishnoi et al. synthesized two Raman-active PEG molecules, one linear and the other branched, to fabricate SERS tags with high stability in cell culture media.[335] These SERS tags can provide semiquantitative information for tracking the particle localization in mouse macrophage and human breast cancer cells. Haisch et al.[336] reported Au/silica core–shell SERS tags with high stability in different environments such as extreme pH values, high ion strength, or in organic solvent. This SERS tag was functionalized with anti-*Salmonella* antibody for cell imaging. Choo's group[337] prepared AuNP SERS tags encapsulated with two layers of silica (Figure 40), where fluorescent dyes were loaded into the outer silica shell to offer a SERS-fluorescence dual modal nanoprobe (DMNP). CD24 and CD44 antibodies were then, respectively, labeled onto two different types of DMNPs to prove their capability of targeting imaging in MDA-MB-231 breast cancer cells where markers CD24 and CD44 are coexpressed. Cui et al.[338] reported a dual-mode probe based on mesoporous silica-coated AuNRs (MS-AuNRs), where Raman reporter molecules were coated onto AuNRs to generate strong SERS signals and fluorescent dyes were encapsulated into MS as the generator of fluorescence. The outer surfaces of MS-AuNRs were conjugated with folic acids as a targeting ligand to detect the HeLa cells overexpressing folate receptors. The same group provided another switchable dual-mode image probe based on silica-coated Au aggregates and water-soluble CdTe QDs.[339] In this probe, SERS and fluorescence signals can be separately generated and switched by changing the wavelength of the excitation light. Similar multimodal imaging methods was also reported by Ren's group using Au@organosilica multifunctional nanoparticles.[340]

5.4. Outlook of AuNP-Based SERS Assays

We herein summarized the AuNP-based SERS assays for sensing various analytes ranging from small biomolecules to cells (Table 4). The use of AuNPs can significantly improve the sensitivity of Raman detection up to the single-molecule level, which is of great value in the

field of biomedical diagnostics. Despite the great progress that has been made, AuNP-based SERS assays are still facing several challenges. First, it is difficult to prepare SERS-active nanostructures with structural reproducibility and narrowly distributed high enhancement factor values. This point is critical when promoting this format in clinical use, as particle structure and interparticle distance can markedly affect Raman signals. To accomplish this, it is desirable to reproducibly synthesize probes with a uniform 1 nm gap, and to control the hot spots and the uniformity of SERS enhancement in the nanostructures. Aside from DNA or polymer-guided formation of a 1 nm gap between the Au core–shell nanostructures, as described in this section, inorganic nanolayers with tunable thickness may serve as a promising candidate for creating uniform ultrasmall nanogaps. Silica shell is such an inorganic nanolayer that can be prepared on an AuNP core to form Au@SiNPs, where the thickness of silica shell can be readily modulated. Silica shell is also thought to be an ideal substrate for the subsequent Au deposition. Therefore, the further Au coating on the obtained Au@SiNPs may produce a nanogap-controllable Au nanostructure. Second, the currently developed SERS tags are unable to quantify the SERS signals particularly in complex biological samples. Third, it remains challenging to prepare SERS tags with ultrahigh sensitivity and stability, combined with a wide and reliable dynamic detection range. Future efforts should be devoted to develop SESR assays with enhanced analytical features such as high signal enhancement, reproducible and uniform signal response, stable half-life, and ease of preparation and use.

6. AuNP-BASED POINT-OF-CARE ASSAYS

POC biochemical assays are characteristic of portability and automatization, and the analysis of the readout results does not require a skilled technician. Therefore, these formats are promising tools for rapid diagnosis and on-site assessment of diseases particularly in resource-limited settings. In this section, the AuNP-based POC assays are mainly classified into paper-based assays and biobarcode assays, both of which have been brought into the detection of various analytes (Table 5).

6.1. AuNP-Based Paper Assays

The microfluidic chip system based on paper has attracted a lot of attention. The pioneering work using paper as a substrate in microfluidic assays was reported by Whitesides and co-workers in 2007.[341] This cost-effective microfluidic paper analysis device (μPAD) was employed to detect protein and glucose.[342] Later, paper-based assays were extended to disease diagnosis, environmental monitoring, and analysis of food and beverage contamination.[343] On the basis of the readout model, paper-based assays are mainly classified into colorimetric assays and electrochemical assays.

AuNP-based colorimetric paper assays offer high sensitivity and simplicity. Furthermore, the bleached papers provide higher contrast background than other substrates for colorimetric detection. It is worth pointing out that most POC assays visualized by the naked eye give a “yes or no” diagnosis result rather than quantitative analysis. With the rapid development of mobile phone and related software, the color signals on the paper can be transformed into digital information, which largely makes quantitative measurements of paper-based assays

feasible.[344] This format has the potential to be widely used as a simple telemedicine especially in resource-poor settings.[342] Because the colors of AuNP solutions are highly dependent on the interparticle spacing of AuNPs, detection targets are able to specifically mediate the interparticle spacing, thus causing the color change of the AuNP solutions. This detection mechanism can be transferred onto papers. Both hydrophobic and hydrophilic paper substrates are suitable for biosensing, without pretreatment of the paper and avoiding complex fabrication processes. Li and co-workers developed such an AuNP-based colorimetric bioassay on paper for sensing DNase I and adenosine. To do this, DNA cross-linked AuNPs aggregates were first spotted on the paper; upon addition of target analytes solution, the AuNP aggregates were dissociated into dispersed AuNPs, leading to an intense red color on paper within 1 min (Figure 41).[345] Paper-based ELISAs (P-ELISAs) have been demonstrated as effective tools for protein detection.[346] Murdock et al.[347] reported an AuNP-based P-ELISA format for IgG and neuropeptide Y by the naked eye. To further enhance the signal intensity, silver staining was performed on AuNPs conjugated with antibodies, and the color showed a concentration-dependent response to protein targets. To avoid specialized instrumentation and complex analysis, Windows- and Android-based mobile platforms were integrated with the detection for automated image analysis and quantification of protein concentrations.[348] In addition to protein detection, the AuNP-based paper assays were also designed for rapid diagnosis of tuberculosis, one of the most serious infectious diseases over the world. The combination of the colorimetric AuNPs probes on paper with the geolocation metadata of test images enables this diagnostics strategy fast and cheap for tuberculosis diagnostics at point-of-need.

The most well-known electrochemical assay for POC testing might be the commercial home-use glucose measurement systems, which are currently produced on an astonishing scale, approaching 10^{10}/year.[33a] Paper-based electrochemical assay is an important detection strategy due to its small size, low cost, portability, high sensitivity, and selectivity when choosing proper detection potential and electrode materials. In addition, very low electrical power requirement of the platforms makes them particularly useful for on-site measurements.[349] Typically, wax printer is used to produce collapsible microfluidic μPADs, which are combined with screen printed electrodes. Because AuNPs can improve the electronic transmission rate and increase the surface areas of the substrate, the AuNP-modified papers are usually employed as a working electrode in microfluidic paper-based electrochemical devices (μPEDs). For example, Lu et al.[350] reported an electrochemical DNA sensor based on the AuNPs/graphene-modified screen-printed working paper electrode in a three-dimensional folding paper. This paper bioassay allows one to detect DNA in human serum with a detection limit of 0.2 aM. Ge et al.[351] developed an AuNP-modified paper working electrode through electropolymerization of molecular imprinted polymer. Because of the enhanced specific surface area and conductivity of the AuNP layer, D-glutamic acid, a biomarker of neurotransmitter associated with brain damage, was detected in a linear range from 1.2 to 125 nM. The AuNP-assembled paper working electrodes were allowed to electrochemically detect many other biomolecules such as glucose, ATP, PSA, CEA, AFP, and DNA, etc.[352] These examples indicate that paper-based electrochemical assays have great potential for rapid diagnostics of diseases especially when the detection procedures are further simplified.

The lateral-flow assay (LFA) is a commercially available POC diagnostic format that usually works on polymer papers. LFA plays vital roles in various biomedical diagnostics, such as off-the-counter pregnancy tests, screening for infectious diseases and drugs of abuse, and for measurement of protein biomarkers in blood.[353] A LFA test strip is typically composed of a nitrocellulose membrane, sample pad, conjugate pad, absorbent pad, and backing pad (Figure 42). Capturing molecules, for example, antibodies or nucleic acid fragments, are immobilized onto the membranes to form test and control lines.[354] When the assay is performed, a small volume of sample is first applied to the sample pad. The flow of sample taking place in the membrane results in the dispersion of the antibody- or nucleic acid-labeled AuNPs, which specifically bind to the analyte in the sample to form analyte-decorated AuNP labels. The resulted AuNPs labels are then captured by the immobilized antibodies or nucleic acid fragments to form test and control lines, which can be quickly observed by the naked eye, without the need of any advanced instrument. Despite its strengths as a POC device, the detection sensitivity of LFA is still less than those of the gold standard diagnostic assays such as ELISA and PCR.

To improve sensitivity, various strategies have been integrated with the LFA platforms, mainly including enzyme-based and silver (or gold)-based signal enhancement. These strategies can improve detection sensitivity by 2 orders of magnitude. For example, Mao et al.[355] reported a strategy to enhance the detection sensitivity by taking advantage of a HRP-catalyzed reaction. The insoluble red products of the reaction can deposit on the AuNP surfaces to intensify the red lines, thus lowering the detection limit for DNA from 0.5 nM to 50 pM. They subsequently optimized the conjugation of HRP and detection procedures. The improved LFA assay based on the HRP-AuNP dual labels significantly lowered the detection limit by 1000 times and was capable of detecting 0.01 pM target DNA.[356] The same principle was used to detect miRNA in biological samples.[357] The on-site enlargement of AuNPs by gold or silver deposition is an effective strategy to improve detection because of the increased size and corresponding optical extinction. Li et al.[358] demonstrated that the addition of 1% $HAuCl_4$ and 10 mM NH_2OH-HCl (v/v, 1:5) into the LFA strips can induce the formation of Au clusters around the immobilized AuNPs, thus increasing the detection sensitivity by 10–100-fold.

AuNP aggregates have also been employed to improve the sensitivity of LFAs by subsequent introduction of functionalized AuNPs. In general, the detection limit can be lowered from several fold to dozens of fold, most likely due to the increased optical extinction of larger sized of Au clusters. Choi et al.[359] used two AuNP-antibody conjugates for signal amplification, in which the first AuNP-antibody conjugate was allowed to bind with an analyte for the purpose of the sandwich assay performed in a typical LFA system. The immobilized first AuNP conjugate was then designed to bind with the second AuNP conjugates. Under an optimal condition (10 and 40 nm for the first and second AuNP, respectively), the detection limit of troponin I can be as low as 0.01 ng/mL, which was 100-fold more sensitive than the conventional LFAs. The oligonucleotide-linked AuNP aggregates can be employed as an effective strategy for signal amplification in LFAs. Hu et al.[360] demonstrated this concept by using a nucleic acid sequence of HIV-1 as a model analyte, and observed that the detection limit of the enhanced LFA assay was 0.1 nM, 2.5-fold signal amplification. This signal amplification strategy was also employed for rapid and

sensitive immunoassay of histone methylation.[361] In this enhanced LFA, one part of AuNP was dual labeled with both Ab2 and an oligonucleotide (c-DNA) to perform the immunoassay on the test strip; the other part of AuNP was functionalized with the complementary strands of c-DNA for the subsequent hybridization between c-DNA and AuNP-DNA probes. As shown in Figure 43, the formation of the DNA-AuNPs cross-linking networks enhances the red bands on both test and control lines, thus indirectly improving the sensitivity of colorimetric LFAs. Other strategies for improving detection sensitivity of LFAs include the fabrication of two-dimensional paper network LFA, the use of thermal contrast, as well as the combination with the RT-PCR preamplification process.[362]

6.2. AuNP-Based Biobarcode Assays

AuNP-based biobarcode assay was first developed by Mirkin and co-workers to detect PSA with extraordinary sensitivity.[363] In this strategy, targeting antibody-modified magnetic microparticles were employed to capture PSA. As shown in Figure 44, AuNPs were functionalized with both target capture antibodies and double-stranded barcode DNAs. In the presence of target PSA, the magnetic microparticles and AuNPs formed sandwich structures, which were magnetically separated from the solution. Thermal dehybridization was conducted to release the single-stranded free barcode DNAs from the barcode DNAs on AuNPs. The free ssDNAs were measured by PCR amplification to determine the presence of the target PSA. Because one protein binding event was transformed into the strong PCR amplification signals induced by a large number of barcode DNAs, the detection limit of this assay was as low as 3 aM. To eliminate the PCR step, larger sized AuNPs were employed to load a larger absolute amount of barcode DNAs. By integrating with silver amplification, a high sensitivity assay was still possible. This approach was further employed to detect PSA in the serum of prostate cancer patients who have undergone radical prostatectomy.[364] The sensitivity of the assay is around 300 times higher than conventional immunoassays clinically used. The AuNP-based biobarcode assay has been applied to detect other specific protein targets for disease diagnostics. For example, this assay was used to measure the concentration of amyloid-β-derived diffusible ligands (ADDLs), a potential soluble pathogenic Alzheimer's disease marker in the cerebrospinal CSF.[365] The biobarcode assay is a semiquantitative approach for ADDLs in CSF that provides a detection range of 3 orders of magnitude, with a limit of detection at around 100 aM, much lower than the clinically relevant concentrations (<1 pM). The biobarcode assay was also employed to detect human telomerase activity with as few as 10 HeLa cells.[366] Mirkin et al.[367] also demonstrated that the biobarcode assay can be utilized for multiplexed detection of proteins at low-femtomolar concentrations.

The same principle of the AuNP-based biobarcode assay was also employed to detect target DNA. The DNA biobarcode assay was designed by replacing the antibodies on magnetic microparticles and AuNPs in the protein detection system with specific ssDNAs.[368] When the target DNA hybridizes with the complementary ssDNA sequences on magnetic microparticles and biobarcoded AuNPs, sandwich structures are formed and the unreacted biobarcoded AuNPs are easily removed by magnetic separation. With thermal dehybridization, the biobarcode DNAs are released from the sandwich assemblies, which are then analyzed by a scanometric method with a detection limit of 500 zM. This sensitivity is

comparable to many PCR-based assays. To realize multiplexed detection of DNA targets of interest, both the magnetic microparticles and the AuNPs probes were loaded with barcode DNA sequences specific to a given target.[369] This assay was employed to detect four DNA targets simultaneously with high selectivity at midfemtomolar concentrations.

To reduce the detection time of the assay and eliminate the use of barcode sorting, some other analytical methods such as fluorescence,[370] color change,[371] electrochemistry,[372] and gel electrophoresis[373] have been integrated with the biobarcode assays. Mirkin et al.[370a] demonstrated that fluorophores can be conjugated with the DNA barcodes, many thousands of which were loaded on a polystyrene microparticle probe. Thermal dehybridization was carried out to release the fluorophore-labeled barcode ssDNAs, whose intensity was employed to quantify the amount of target. The fluorescence-based biobarcode amplification method can detect PSA in the range from 300 aM to 3 pM. Additionally, the released barcode DNA can also be measured by an AuNP-based colorimetric assay through a barcode DNA-directed AuNP assembly process.[371a] The formation of AuNP assembly induces a red-to-purple color change, which can be visualized by the naked eye. The colorimetric biobarcode method allows the detection of cytokines down to 30 aM. This sensitivity is ~3 orders of magnitude higher than conventional nonenzymatic cytokine detection assays. Recently, Nam and co-workers[373] improved the readout methods by using a conventional gel electrophoresis platform and potassium cyanide chemistry. This biobarcode gel assay was employed to detect miRNA in cancer cells at attomolar levels without any enzymatic amplification strategy.

6.3. Outlook of AuNP-Based POC Assays

Over the past decade, a number of innovative POC assays have been presented in both academic research and commercial products. The representative examples are the well-established glucose and pregnancy POC tests. Those POC assays are changing the situation of human health, diagnosis, and therapy. An ideal POC assay should have the following properties: rapid diagnostics, ease of use, low cost, and reliability. Because of their unique properties, AuNPs may serve as an ideal candidate for creating POC platforms. For example, the high optical extinction coefficient of AuNPs makes high-sensitivity colorimetric detection possible in a POC platform. The high sensitivity means that the assays are promising for use in early diagnosis and monitoring the disease progression after treatment. The diversity of surface functionalization of AuNPs directly boosts the development of various signal amplification strategies. The advanced POC assays have been demonstrated in the research setting for ultrasensitive detection of targets of interest. However, only very few of them are commercially launched in the market, most likely due to the above-mentioned challenges. In addition, because the POC tests are often self-administered by the patients themselves, it is essential to further improve the reliability of the POC platforms. The sampling procedures and readout analysis are required to be standardized and familiarized by the users. The rapid development of advanced fabrication technologies, such as microelectro-mechanical system (MEMS), can be coupled with the basic principles of analytical chemistry to provide high-performance POC devices for disease diagnostics.[374]

7. CONCLUDING REMARKS

Diagnostic procedures are fundamental for disease management and treatment, and therefore the development of effective diagnostic tools is of great importance. IVDs show great value in different economic settings. In developed areas, IVD tools are typically used in bedside diagnostic tests, in-home tests, and bioemergency response. In resource-poor settings, IVD tools are mainly used in clinical laboratories or isolated village health service providers. There is still a long way before the extensive application of IVD tools to offer effective diagnostic capability. These requirements include the following: (1) High sensitivity. For many diseases such as cancer, metabolic diseases, infectious diseases, and cardiovascular diseases, the biomarker levels at the early stages of the diseases are generally below the critical threshold concentrations, at which point the biomarkers are often undetectable by means of current platforms. The high-sensitivity sensors make it possible for early diagnosis of the diseases as well as monitoring recurrence of the diseases after treatment. (2) Low-cost and sufficient simplicity. To meet the demands of personalized clinical diagnostics especially in developing countries, the IVD platforms should be cost-effective and easy to use. (3) Portability. A portable IVD device should not rely on sophisticated instruments and skilled technicians, making diagnostics faster and easier. In recent years, some of the requirements have been met because of the cross-disciplinary integration among physics, chemistry, biology, electrical engineering, and micromanufacturing technology. It is foreseeable that more IVD platforms will become available in the future market.

Undoubtedly, the rapid development of nanotechnology provides significant improvement in IVD systems. Among the nanomaterials, AuNPs have received considerable research interest due to its virtues, including unique enhanced electromagnetic field, ease of synthesis and functionalization, and excellent biocompatibility and stability. The unique physicochemical properties of AuNPs provide various specific signal transducers (like LSPR and SERS) and amplification strategies (like electrochemical signal and fluorescence enhancement), both of which can be harnessed to create IVD assays with appropriate clinical features.

Although much exciting progress in AuNP-based IVD systems has been successfully made, they are still facing several challenges. First, the combination of fundamental research with new technologies is insufficient. For example, a variety of AuNP-based assays show unsurpassed sensitivity and multiplexing capabilities; however, these characteristics have not been demonstrated in portable devices like microfluidics.[353b,375] Low-cost substrates such as papers and polymers are also impressive if they are coupled with AuNP sensors. To produce simple IVD platforms that are robust in settings outside of the lab and toward POC devices, manufacturing skill is further needed for the design and fabrication of the whole systems. Second, the reproducibility of IVD platforms has to be demonstrated using clinical samples before they are formally used in the clinic. The core of the IVD platforms is the AuNP probes. As discussed in this Review, variation of the probes in size, shape, composition, or surface coating could lead to significant variation in detection results. The current nanoprobes have been prepared under highly optimized conditions in laboratories, and their mass production with high reproducibility remains a great challenge. To bring the AuNP-based IVD assays into real clinical applications, it is highly desirable to prepare extremely reproducible AuNP probes to achieve reproducible detection signals. It is critical

to simplify the procedures of synthesis and functionalization of probes to minimize the variation in different batches. Third, most IVD assays were prepared in academic laboratories. Many bench researchers may not really know the clinical demand; thus many platforms are unrealistic for clinical translation. Therefore, future advances in creating reliable IVD platforms should involve close collaborations between scientists, engineers, and clinicians. Only their combination work could drive more IVD assays forward from laboratory bench to bedside.

Acknowledgments

We acknowledge the support from the National Natural Science Foundation of China (Grants 21475066 and 81401463), the Fundamental Research Funds for Central Universities (China), and the Intramural Research Program (IRP) of the National Institute of Biomedical Imaging and Bioengineering, National Institutes of Health.

Biographies

Wen Zhou obtained her M.Sc. in Analytical Chemistry from Jiangnan University under the guidance of Prof. Zhiguo Gu. She is currently pursuing her Ph.D. in the College of Chemistry at Nankai University under the supervision of Dr. Dingbin Liu. Her research interests focus on developing biosensors based on gold nanoparticles for cancer diagnosis and imaging.

Xia Gao received her Ph.D. in Applied Chemistry from the South China University of Technology in 2014. Before that, she was supported by a four-year joint training program at the Lab of Analytical Chemistry for Living Biosystems, Institute of Chemistry, Chinese Academy of Sciences (CAS), under the supervision of Prof. Lanqun Mao and Prof. Jianshan Ye. She is currently a postdoctoral fellow in Dr. Dingbin Liu's group at Nankai University. Her research involves in the design and fabrication of gold-related nanostructures for cell detection and Raman imaging.

Dingbin Liu is a tenure-track professor in the College of Chemistry at Nankai University. He is also a principal investigator at the State Key Laboratory of Medicinal Chemical Biology and the Collaborative Innovation Center of Chemical Science and Engineering (Tianjin). He received his B.S. in 2006 from Lanzhou University and his Ph.D. in 2012 from the National Center for Nanoscience and Technology, China (NCNST), under the supervision of Prof. Xingyu Jiang. He began his independent career at Nankai University in 2014 after a short postdoctoral training at the National Institutes of Health (NIH) under the support of an NRC NIH/NIST Joint Postdoctoral Associateship. His research interests include the design, preparation, and applications of advanced plasmonic nanoprobes in biodiagnostics and bioimaging.

Xiaoyuan Chen received his B.S. in 1993 and his M.S. in 1996 from Nanjing University, China. He then moved to the United States and obtained his Ph.D. in chemistry from the University of Idaho in 1999. After two quick postdocs at Syracuse University and Washington University in St. Louis, he joined the University of Southern California as an Assistant Professor of Radiology. He then moved to Stanford University in 2004. He was promoted to Associate Professor in 2008, and in the summer of 2009 he joined the intramural research program of the National Institute of Biomedical Imaging and Bioengineering (NIBIB), at the National Institutes of Health, as a Senior Investigator and Chief of the Laboratory of Molecular Imaging and Nanomedicine (LOMIN). Dr. Chen has published over 450 papers, 4 books, and numerous book chapters. He is the founding editor of the journal *Theranostics*, and sits on the editorial board of over 10 peer-reviewed journals.

ABBREVIATIONS

Ab2	detection antibody
AChE	acetylcholinesterase
ADDLs	amyloid-β-derived diffusible ligands
AFP	α-fetoprotein

AgNPs	silver nanoparticles
ALP	alkaline phosphatase
apo-GDH	apo-glucose dehydrogenase
ARS	Alizarin Red S
ASV	anodic stripping voltammetry
ATC	acetylthiocholine
ATP	adenosine triphosphate
AuNCs	gold nanoclusters
AuNFs	gold nanoflowers
AuNPs	gold nanoparticles
AuNRs	gold nanorods
Au-NNP	gold nanobridged nanogap particles
BCIP	5-bromo-4-chloro-3-indolyl phosphate
BSA	bovine serum albumin
CEA	carcinoembryonic antigen
ChOx	cholesterol oxidase
CNT	carbon nanotubes
Con A	concanavalin A
CRP	C-reactive protein
CSF	cerebrospinal fluid
CTC	circulating tumor cells
cyst-AuNPs	cysteamine modified AuNPs
try-AuNCs	trypsin stabilized gold nanoclusters
CyNAMLA	lipoic acid-containing NIR-active tricarbocyanine library
2,5-DMBA	2,5-dimercaptobenzoic acid
DMNP	dual modal nanoprobe
DOX	doxorubicin
dsDNA	double-stranded DNA
DSN	duplex specific nuclease

DTNB	5,5′-dithiobis (2-nitrobenzoic acid)
ECL	electrochemiluminescence
EIS	electrochemical impedance spectroscopy
ELISA	enzyme-linked immunosorbent assay
ENO1	α-Enolase
EV71	enterovirus 71
FRET	Förster resonance energy transfer
ERLs	extrinsic Raman labels
FAD	flavin adenine dinucleotide
Fc	ferrocene
FITC	fluorescein isothiocyanate
GCE	glassy carbon electrode
GGR	glucose/galactose receptors
GOx	glucose oxidase
GSGHs	graphene-mesoporous silica–AuNP hybrids
GSH	glutathione
GST	S-transferase
H_2O_2	hydrogen peroxide
HBsAg	hepatitis B surface antigen
HER2	human epidermal growth factor receptor 2
HGNs	hollow gold nanospheres
HIV-1 PR	HIV-1 protease
HRP	horseradish peroxidase
IgA1P	immunoglobulin A1 protease
IgG	immunoglobulin G
IL	interleukin
ITO	indium tin oxide
IVDs	in vitro diagnostics
LCR	ligation chain reaction

LDA	linear discriminate analysis
LFA	lateral-flow assay
LSPR	localized surface plasmon resonance
4-MBA	4-mercaptobenzoic acid
MEMS	microelectro-mechanical system
MMP	matrix metalloprotease
MNAzyme	multicomponent nucleic acid enzyme
MOFs	metal–organic frameworks
MS-AuNRs	mesoporous silica-coated AuNRs
11-MUA	11-mercaptoundecanoic acid
MWNT	multiwalled carbon nanotube
NAEBs	nanoagregate-embedded beads
NCAs	nanoparticle cluster arrays
NSET	nanoparticle surface energy transfer
Ova-AuNCs	ovalbumin-protected AuNCs
OPG	osteoproteogerin
***μ*PAD**	microfluidic paper analysis device
***μ*PEDs**	microfluidic paper-based electrochemical devices
PCR	polymerase chain reaction
PDDA	poly(diallyldimethylammonium chloride)
PDGF	platelet-derived growth factor
PG	pyrolytic graphite
MPBA	4-mercaptophenylboronic acid
PMPC	poly(2-methacryloyloxyethyl phosphorylcholine)
POC	point-of-care
PPE	poly(*p*-phenyleneethynylene)
PPI	poly(propyleneimine)
PSA	prostate-specific antigen
PTM	post-translational modification

QDs	quantum dots
RBITC	rhodamine B isothiocyanate
RCA	rolling circle amplification
SERS	surface-enhanced Raman spectroscopy
SHINERS	shell-isolated nanoparticle-enhanced Raman spectroscopy
SPE	screen-printed electrode
SPR	surface plasmon resonance
ssDNA	single-stranded DNA
SWCNT	single walled carbon nanotubes
VEGF	vascular endothelial growth factor
HDAC 1	histone deacetylase 1
PKA	protein kinase A
β-SH-CDs	β-cyclodextrins

References

1. (a) Jin Z, Hildebrandt N. Semiconductor Quantum Dots for *in Vitro* Diagnostics and Cellular Imaging. Trends Biotechnol. 2012; 30:394–403. [PubMed: 22608980] (b) Turner APF, Chen BN, Piletsky SA. In Vitro Diagnostics in Diabetes: Meeting the Challenge. Clin Chem. 1999; 45:1596–1601. [PubMed: 10471674] (c) Xing Y, Rao J. Quantum Dot Bioconjugates for in Vitro Diagnostics & in Vivo Imaging. Cancer Biomarkers. 2008; 4:307–319. [PubMed: 19126959]
2. (a) Golman K, in't Zandt R, Lerche M, Pehrson R, Ardenkjaer-Larsen JH. Metabolic Imaging by Hyperpolarized C-13 Magnetic Resonance Imaging for *in Vivo* Tumor Diagnosis. Cancer Res. 2006; 66:10855–10860. [PubMed: 17108122] (b) Michalet X, Pinaud FF, Bentolila LA, Tsay JM, Doose S, Li JJ, Sundaresan G, Wu AM, Gambhir SS, Weiss S. Quantum Dots for Live Cells, in Vivo Imaging, and Diagnostics. Science. 2005; 307:538–544. [PubMed: 15681376]
3. (a) Fradet Y. Biomarkers in Prostate Cancer Diagnosis and Prognosis: Beyond Prostate-Specific Antigen. Curr Opin Urol. 2009; 19:243–246. [PubMed: 19325493] (b) Luo LY, Katsaros D, Scorilas A, Fracchioli S, Bellino R, van Gramberen M, de Bruijn H, Henrik A, Stenman UH, Massobrio M, van der Zee AGJ, Vergote I, Diamandis EP. The Serum Concentration of Human Kallikrein 10 Represents a Novel Biomarker for Ovarian Cancer Diagnosis and Prognosis. Cancer Res. 2003; 63:807–811. [PubMed: 12591730] (c) Patz EF Jr, Campa MJ, Gottlin EB, Kusmartseva I, Guan XR, Herndon JE II. Panel of Serum Biomarkers for the Diagnosis of Lung Cancer. J Clin Oncol. 2007; 25:5578–5583. [PubMed: 18065730] (d) Sardana G, Dowell B, Diamandis EP. Emerging Biomarkers for the Diagnosis and Prognosis of Prostate Cancer. Clin Chem. 2008; 54:1951–1960. [PubMed: 18927246] (e) Winter JM, Yeo CJ, Brody JR. Diagnostic, Prognostic, and Predictive Biomarkers in Pancreatic Cancer. J Surg Oncol. 2013; 107:15–22. [PubMed: 22729569]
4. (a) Kouri T, Malminiemi O, Penders J, Pelkonen V, Vuotari L, Delanghe J. Limits of Preservation of Samples for Urine Strip Tests and Particle Counting. Clin Chem Lab Med. 2008; 46:703–713. [PubMed: 18839472] (b) Peter JG, Theron G, Dheda K. Can Point-of-Care Urine Lam Strip Testing for Tuberculosis Add Value to Clinical Decision Making in Hospitalised HIV-Infected Persons? PLoS One. 2013; 8:e54875. [PubMed: 23390504]
5. (a) Scott MG, Bruns DE, Boyd JC, Sacks DB. Tight Glucose Control in the Intensive Care Unit: Are Glucose Meters up to the Task? Clin Chem. 2009; 55:18–20. [PubMed: 19028817] (b) Xiang Y, Lu

Y. Using Personal Glucose Meters and Functional DNA Sensors to Quantify a Variety of Analytical Targets. Nat Chem. 2011; 3:697–703. [PubMed: 21860458]

6. (a) Blum J, Shochet T, Lynd K, Lichtenberg ES, Fischer D, Arnesen M, Winikoff B, Blumenthal PD. Can at-Home Semi-Quantitative Pregnancy Tests Serve as a Replacement for Clinical Follow-up of Medical Abortion? A Us Study. Contraception. 2012; 86:757–762. [PubMed: 22895097] (b) Butler SA, Khanlian SA, Cole LA. Detection of Early Pregnancy Forms of Human Chorionic Gonadotropin by Home Pregnancy Test Devices. Clin Chem. 2001; 47:2131–2136. [PubMed: 11719477]
7. (a) Giljohann DA, Mirkin CA. Drivers of Biodiagnostic Development. Nature. 2009; 462:461–464. [PubMed: 19940916] (b) Rissin DM, Kan CW, Campbell TG, Howes SC, Fournier DR, Song L, Piech T, Patel PP, Chang L, Rivnak AJ, Ferrell EP, Randall JD, Provuncher GK, Walt DR, Duffy DC. Single-Molecule Enzyme-Linked Immunosorbent Assay Detects Serum Proteins at Subfemtomolar Concentrations. Nat Biotechnol. 2010; 28:595–599. [PubMed: 20495550]
8. (a) Barletta JM, Edelman DC, Constantine NT. Lowering the Detection Limits of HIV-1 Viral Load Using Real-Time Immuno-PCR for HIV-1 P24 Antigen. Am J Clin Pathol. 2004; 122:20–27. [PubMed: 15272526] (b) Galasko D. Biomarkers for Alzheimer's Disease - Clinical Needs and Application. J Alzheimers Dis. 2005; 8:339–346. [PubMed: 16556965]
9. (a) Kubista M, Andrade JM, Bengtsson M, Forootan A, Jonak J, Lind K, Sindelka R, Sjoback R, Sjogreen B, Strombom L, Stahlberg A, Zori CN. The Real-Time Polymerase Chain Reaction. Mol Asp Med. 2006; 27:95–125.(b) Ye J, Coulouris G, Zaretskaya I, Cutcutache I, Rozen S, Madden TL. Primer-Blast: A Tool to Design Target-Specific Primers for Polymerase Chain Reaction. BMC Bioinformatics. 2012; 13:134. [PubMed: 22708584]
10. (a) Dunbar SA. Applications of Luminex (R) Xmap (Tm) Technology for Rapid, High-Throughput Multiplexed Nucleic Acid Detection. Clin Chim Acta. 2006; 363:71–82. [PubMed: 16102740] (b) Laxman B, Morris DS, Yu J, Siddiqui J, Cao J, Mehra R, Lonigro RJ, Tsodikov A, Wei JT, Tomlins SA, Chinnaiyan AM. A First-Generation Multiplex Biomarker Analysis of Urine for the Early Detection of Prostate Cancer. Cancer Res. 2008; 68:645–649. [PubMed: 18245462] (c) Zheng GF, Patolsky F, Cui Y, Wang WU, Lieber CM. Multiplexed Electrical Detection of Cancer Markers with Nanowire Sensor Arrays. Nat Biotechnol. 2005; 23:1294–1301. [PubMed: 16170313]
11. (a) Haes AJ, Chang L, Klein WL, Van Duyne RP. Detection of a Biomarker for Alzheimer's Disease from Synthetic and Clinical Samples Using a Nanoscale Optical Biosensor. J Am Chem Soc. 2005; 127:2264–2271. [PubMed: 15713105] (b) Liu X, Dai Q, Austin L, Coutts J, Knowles G, Zou J, Chen H, Huo Q. A One-Step Homogeneous Immunoassay for Cancer Biomarker Detection Using Gold Nanoparticle Probes Coupled with Dynamic Light Scattering. J Am Chem Soc. 2008; 130:2780–2782. [PubMed: 18257576] (c) Myung S, Solanki A, Kim C, Park J, Kim KS, Lee KB. Graphene-Encapsulated Nanoparticle-Based Biosensor for the Selective Detection of Cancer Biomarkers. Adv Mater. 2011; 23:2221–2225. [PubMed: 21469221] (d) Zhang J, Lang HP, Huber F, Bietsch A, Grange W, Certa U, McKendry R, Guentgerodt HJ, Hegner M, Gerber C. Rapid and Label-Free Nanomechanical Detection of Biomarker Transcripts in Human RNA. Nat Nanotechnol. 2006; 1:214–220. [PubMed: 18654189]
12. (a) Konvalina G, Haick H. Sensors for Breath Testing: From Nanomaterials to Comprehensive Disease Detection. Acc Chem Res. 2014; 47:66–76. [PubMed: 23926883] (b) Ray PC, Khan SA, Singh AK, Senapati D, Fan Z. Nanomaterials for Targeted Detection and Photothermal Killing of Bacteria. Chem Soc Rev. 2012; 41:3193–3209. [PubMed: 22331210] (c) Zhang L, Fang M. Nanomaterials in Pollution Trace Detection and Environmental Improvement. Nano Today. 2010; 5:128–142.(d) Zhang Y, Guo Y, Xianyu Y, Chen W, Zhao Y, Jiang X. Nanomaterials for Ultrasensitive Protein Detection. Adv Mater. 2013; 25:3802–3819. [PubMed: 23740753]
13. (a) Esser B, Schnorr JM, Swager TM. Selective Detection of Ethylene Gas Using Carbon Nanotube-Based Devices: Utility in Determination of Fruit Ripeness. Angew Chem, Int Ed. 2012; 51:5752–5756.(b) Hwang KS, Lee SM, Kim SK, Lee JH, Kim TS. Micro- and Nanocantilever Devices and Systems for Biomolecule Detection. Annu Rev Anal Chem. 2009; 2:77–98.(c) Luo CX, Fu Q, Li H, Xu LP, Sun MH, Ouyang Q, Chen Y, Ji H. Pdms Microfludic Device for Optical Detection of Protein Immunoassay Using Gold Nanoparticles. Lab Chip. 2005; 5:726–729. [PubMed: 15970965] (d) Patolsky F, Zheng G, Lieber CM. Fabrication of Silicon Nanowire

Devices for Ultrasensitive, Label-Free, Real-Time Detection of Biological and Chemical Species. Nat Protoc. 2006; 1:1711–1724. [PubMed: 17487154]

14. El-Boubbou K, Gruden C, Huang X. Magnetic Glyco-Nanoparticles: A Unique Tool for Rapid Pathogen Detection, Decontamination, and Strain Differentiation. J Am Chem Soc. 2007; 129:13392–13393. [PubMed: 17929928]
15. Ambrosi A, Airo F, Merkoci A. Enhanced Gold Nanoparticle Based ELISA for a Breast Cancer Biomarker. Anal Chem. 2010; 82:1151–1156. [PubMed: 20043655]
16. (a) Boisselier E, Astruc D. Gold Nanoparticles in Nanomedicine: Preparations, Imaging, Diagnostics, Therapies and Toxicity. Chem Soc Rev. 2009; 38:1759–1782. [PubMed: 19587967] (b) Eustis S, El-Sayed MA. Why Gold Nanoparticles Are More Precious Than Pretty Gold: Noble Metal Surface Plasmon Resonance and Its Enhancement of the Radiative and Nonradiative Properties of Nanocrystals of Different Shapes. Chem Soc Rev. 2006; 35:209–217. [PubMed: 16505915] (c) Ghosh SK, Pal T. Interparticle Coupling Effect on the Surface Plasmon Resonance of Gold Nanoparticles: From Theory to Applications. Chem Rev. 2007; 107:4797–4862. [PubMed: 17999554] (d) Giljohann DA, Seferos DS, Daniel WL, Massich MD, Patel PC, Mirkin CA. Gold Nanoparticles for Biology and Medicine. Angew Chem, Int Ed. 2010; 49:3280–3294.(e) Grzelczak M, Perez-Juste J, Mulvaney P, Liz-Marzan LM. Shape Control in Gold Nanoparticle Synthesis. Chem Soc Rev. 2008; 37:1783–1791. [PubMed: 18762828] (f) Saha K, Agasti SS, Kim C, Li X, Rotello VM. Gold Nanoparticles in Chemical and Biological Sensing. Chem Rev. 2012; 112:2739–2779. [PubMed: 22295941]
17. (a) Wilson R. The Use of Gold Nanoparticles in Diagnostics and Detection. Chem Soc Rev. 2008; 37:2028–2045. [PubMed: 18762845] (b) Xia F, Zuo X, Yang R, Xiao Y, Kang D, Vallee-Belisle A, Gong X, Yuen JD, Hsu BBY, Heeger AJ, Plaxco KW. Colorimetric Detection of DNA, Small Molecules, Proteins, and Ions Using Unmodified Gold Nanoparticles and Conjugated Polyelectrolytes. Proc Natl Acad Sci USA. 2010; 107:10837–10841. [PubMed: 20534499] (c) Zhou Y, Wang S, Zhang K, Jiang X. Visual Detection of Copper(II) by Azide- and Alkyne-Functionalized Gold Nanoparticles Using Click Chemistry. Angew Chem, Int Ed. 2008; 47:7454–7456.
18. (a) Lee YK, Kim S, Oh JW, Nam JM. Massively Parallel and Highly Quantitative Single-Particle Analysis on Interactions between Nanoparticles on Supported Lipid Bilayer. J Am Chem Soc. 2014; 136:4081–4088. [PubMed: 24521296] (b) Yang YH, Nam JM. Single Nanoparticle Tracking-Based Detection of Membrane Receptor-Ligand Interactions. Anal Chem. 2009; 81:2564–2568. [PubMed: 19228043] (c) Raschke G, Kowarik S, Franzl T, Sonnichsen C, Klar TA, Feldmann J, Nichtl A, Kurzinger K. Biomolecular Recognition Based on Single Gold Nanoparticle Light Scattering. Nano Lett. 2003; 3:935–938.(d) Lee K, Cui Y, Lee LP, Irudayaraj J. Quantitative Imaging of Single mRNA Splice Variants in Living Cells. Nat Nanotechnol. 2014; 9:474–480. [PubMed: 24747838]
19. (a) Han J, Liu Y, Guo R. Facile Synthesis of Highly Stable Gold Nanoparticles and Their Unexpected Excellent Catalytic Activity for Suzuki-Miyaura Cross-Coupling Reaction in Water. J Am Chem Soc. 2009; 131:2060–2061. [PubMed: 19170490] (b) Perrault SD, Chan WCW. Synthesis and Surface Modification of Highly Monodispersed, Spherical Gold Nanoparticles of 50–200 nm. J Am Chem Soc. 2009; 131:17042–17043. [PubMed: 19891442]
20. (a) Liu D, Chen W, Sun K, Deng K, Zhang W, Wang Z, Jiang X. Resettable, Multi-Readout Logic Gates Based on Controllably Reversible Aggregation of Gold Nanoparticles. Angew Chem, Int Ed. 2011; 50:4103–4107.(b) Liu D, Qu W, Chen W, Zhang W, Wang Z, Jiang X. Highly Sensitive, Colorimetric Detection of Mercury(II) in Aqueous Media by Quaternary Ammonium Group-Capped Gold Nanoparticles at Room Temperature. Anal Chem. 2010; 82:9606–9610. [PubMed: 21069969]
21. (a) Ai K, Liu Y, Lu L. Hydrogen-Bonding Recognition-Induced Color Change of Gold Nanoparticles for Visual Detection of Melamine in Raw Milk and Infant Formula. J Am Chem Soc. 2009; 131:9496–9497. [PubMed: 19537721] (b) Jiang Y, Zhao H, Zhu N, Lin Y, Yu P, Mao L. A Simple Assay for Direct Colorimetric Visualization of Trinitrotoluene at Picomolar Levels Using Gold Nanoparticles. Angew Chem, Int Ed. 2008; 47:8601–8604.(c) Lee JS, Han MS, Mirkin CA. Colorimetric Detection of Mercuric Ion (Hg^{2+}) in Aqueous Media Using DNA-Functionalized Gold Nanoparticles. Angew Chem, Int Ed. 2007; 46:4093–4096.

22. (a) Khlebtsov N, Dykman L. Biodistribution and Toxicity of Engineered Gold Nanoparticles: A Review of *in Vitro* and *in Vivo* Studies. Chem Soc Rev. 2011; 40:1647–1671. [PubMed: 21082078] (b) Murphy CJ, Gole AM, Stone JW, Sisco PN, Alkilany AM, Goldsmith EC, Baxter SC. Gold Nanoparticles in Biology: Beyond Toxicity to Cellular Imaging. Acc Chem Res. 2008; 41:1721–1730. [PubMed: 18712884]

23. (a) Daniel MC, Astruc D. Gold Nanoparticles: Assembly, Supramolecular Chemistry, Quantum-Size-Related Properties, and Applications toward Biology, Catalysis, and Nanotechnology. Chem Rev. 2004; 104:293–346. [PubMed: 14719978] (b) Huang X, Jain PK, El-Sayed IH, El-Sayed MA. Gold Nanoparticles: Interesting Optical Properties and Recent Applications in Cancer Diagnostic and Therapy. Nanomedicine. 2007; 2:681–693. [PubMed: 17976030] (c) Baptista P, Pereira E, Eaton P, Doria G, Miranda A, Gomes I, Quaresma P, Franco R. Gold Nanoparticles for the Development of Clinical Diagnosis Methods. Anal Bioanal Chem. 2008; 391:943–950. [PubMed: 18157524] (d) Liu D, Wang Z, Jiang X. Gold Nanoparticles for the Colorimetric and Fluorescent Detection of Ions and Small Organic Molecules. Nanoscale. 2011; 3:1421–1433. [PubMed: 21359318]

24. (a) Hutter E, Fendler JH. Exploitation of Localized Surface Plasmon Resonance. Adv Mater. 2004; 16:1685–1706.(b) Jain PK, Huang X, El-Sayed IH, El-Sayed MA. Noble Metals on the Nanoscale: Optical and Photothermal Properties and Some Applications in Imaging, Sensing, Biology, and Medicine. Acc Chem Res. 2008; 41:1578–1586. [PubMed: 18447366] (c) Anker JN, Hall WP, Lyandres O, Shah NC, Zhao J, Van Duyne RP. Biosensing with Plasmonic Nanosensors. Nat Mater. 2008; 7:442–453. [PubMed: 18497851]

25. Kelly KL, Coronado E, Zhao LL, Schatz GC. The Optical Properties of Metal Nanoparticles: The Influence of Size, Shape, and Dielectric Environment. J Phys Chem B. 2003; 107:668–677.

26. (a) Burda C, Chen XB, Narayanan R, El-Sayed MA. Chemistry and Properties of Nanocrystals of Different Shapes. Chem Rev. 2005; 105:1025–1102. [PubMed: 15826010] (b) Underwood SMP. Effect of the Solution Refractive Index on the Color of Gold Colloids. Langmuir. 1994; 10:3427–3430.(c) Lee KS, El-Sayed MA. Gold and Silver Nanoparticles in Sensing and Imaging: Sensitivity of Plasmon Response to Size, Shape, and Metal Composition. J Phys Chem B. 2006; 110:19220–19225. [PubMed: 17004772] (d) Zoric I, Zach M, Kasemo B, Langhammer C. Gold, Platinum, and Aluminum Nanodisk Plasmons: Material Independence, Subradiance, and Damping Mechanisms. ACS Nano. 2011; 5:2535–2546. [PubMed: 21438568] (e) PM. Surface Plasmon Spectroscopy of Nanosized Metal Particles. Langmuir. 1996; 12:788–800.

27. Brolo AG. Plasmonics for Future Biosensors. Nat Photonics. 2012; 6:709–713.

28. Haes AJ, Van Duyne RP. A Nanoscale Optical Blosensor: Sensitivity and Selectivity of an Approach Based on the Localized Surface Plasmon Resonance Spectroscopy of Triangular Silver Nanoparticles. J Am Chem Soc. 2002; 124:10596–10604. [PubMed: 12197762]

29. Haes AJ, Hall WP, Chang L, Klein WL, Van Duyne RP. A Localized Surface Plasmon Resonance Biosensor: First Steps toward an Assay for Alzheimer's Disease. Nano Lett. 2004; 4:1029–1034.

30. Haes AJ, Zou SL, Schatz GC, Van Duyne RP. A Nanoscale Optical Biosensor: The Long Range Distance Dependence of the Localized Surface Plasmon Resonance of Noble Metal Nanoparticles. J Phys Chem B. 2004; 108:109–116.

31. (a) Petryayeva E, Krull UJ. Localized Surface Plasmon Resonance: Nanostructures, Bioassays and Biosensing-a Review. Anal Chim Acta. 2011; 706:8–24. [PubMed: 21995909] (b) Szunerits S, Boukherroub R. Sensing Using Localised Surface Plasmon Resonance Sensors. Chem Commun. 2012; 48:8999–9010.

32. (a) Storhoff JJ, Elghanian R, Mucic RC, Mirkin CA, Letsinger RL. One-Pot Colorimetric Differentiation of Polynucleotides with Single Base Imperfections Using Gold Nanoparticle Probes. J Am Chem Soc. 1998; 120:1959–1964.(b) Jiang Y, Zhao H, Lin Y, Zhu N, Ma Y, Mao L. Colorimetric Detection of Glucose in Rat Brain Using Gold Nanoparticles. Angew Chem, Int Ed. 2010; 49:4800–4804.(c) Wang Z, Lee JH, Lu Y. Label-Free Colorimetric Detection of Lead Ions with a Nanomolar Detection Limit and Tunable Dynamic Range by Using Gold Nanoparticles and Dnazyme. Adv Mater. 2008; 20:3263–3267.

33. (a) Tokel O, Inci F, Demirci U. Advances in Plasmonic Technologies for Point of Care Applications. Chem Rev. 2014; 114:5728–5752. [PubMed: 24745365] (b) Willets KA, Van Duyne RP. Localized Surface Plasmon Resonance Spectroscopy and Sensing. Annu Rev Phys Chem.

2007; 58:267–297. [PubMed: 17067281] (c) Howes P, Rana S, Stevens M. Plasmonic Nanomaterials for Biodiagnostics. Chem Soc Rev. 2014; 43:3835–3853. [PubMed: 24323079]

34. Zhao W, Chiuman W, Lam JCF, McManus SA, Chen W, Cui Y, Pelton R, Brook MA, Li Y. DNA Aptamer Folding on Gold Nanoparticles: From Colloid Chemistry to Biosensors. J Am Chem Soc. 2008; 130:3610–3618. [PubMed: 18293985]
35. (a) Li H, Rothberg L. Colorimetric Detection of DNA Sequences Based on Electrostatic Interactions with Unmodified Gold Nanoparticles. Proc Natl Acad Sci USA. 2004; 101:14036–14039. [PubMed: 15381774] (b) Zheng X, Liu Q, Jing C, Li Y, Li D, Luo W, Wen Y, He Y, Huang Q, Long YT, Fan C. Catalytic Gold Nanoparticles for Nanoplasmonic Detection of DNA Hybridization. Angew Chem, Int Ed. 2011; 50:11994–11998.(c) Liu P, Yang X, Sun S, Wang Q, Wang K, Huang J, Liu J, He L. Enzyme-Free Colorimetric Detection of DNA by Using Gold Nanoparticles and Hybridization Chain Reaction Amplification. Anal Chem. 2013; 85:7689–7695. [PubMed: 23895103]
36. (a) Chen CK, Huang CC, Chang HT. Label-Free Colorimetric Detection of Picomolar Thrombin in Blood Plasma Using a Gold Nanoparticle-Based Assay. Biosens Bioelectron. 2010; 25:1922–1927. [PubMed: 20129774] (b) Li Y, Lee HJ, Corn RM. Detection of Protein Biomarkers Using RNA Aptamer Microarrays and Enzymatically Amplified Surface Plasmon Resonance Imaging. Anal Chem. 2007; 79:1082–1088. [PubMed: 17263339]
37. Liu F, Wong MMK, Chiu SK, Lin H, Ho JC, Pang SW. Effects of Nanoparticle Size and Cell Type on High Sensitivity Cell Detection Using a Localized Surface Plasmon Resonance Biosensor. Biosens Bioelectron. 2014; 55:141–148. [PubMed: 24373953]
38. (a) Endo T, Kerman K, Nagatani N, Hiepa HM, Kim DK, Yonezawa Y, Nakano K, Tamiya E. Multiple Label-Free Detection of Antigen-Antibody Reaction Using Localized Surface Plasmon Resonance-Based Core-Shell Structured Nanoparticle Layer Nanochip. Anal Chem. 2006; 78:6465–6475. [PubMed: 16970322] (b) Mayer KM, Lee S, Liao H, Rostro BC, Fuentes A, Scully PT, Nehl CL, Hafner JH. A Label-Free Immunoassay Based Upon Localized Surface Plasmon Resonance of Gold Nanorods. ACS Nano. 2008; 2:687–692. [PubMed: 19206599] (c) Jeong HH, Erdene N, Park JH, Jeong DH, Lee HY, Lee SK. Real-Time Label-Free Immunoassay of Interferon-Gamma and Prostate-Specific Antigen Using a Fiber-Optic Localized Surface Plasmon Resonance Sensor. Biosens Bioelectron. 2013; 39:346–351. [PubMed: 22951530] (d) Englebienne P. Use of Colloidal Gold Surface Plasmon Resonance Peak Shift to Infer Affinity Constants from the Interactions between Protein Antigens and Antibodies Specific for Single or Multiple Epitopes. Analyst. 1998; 123:1599–1603. [PubMed: 9830172]
39. Inci F, Tokel O, Wang S, Gurkan UA, Tasoglu S, Kuritzkes DR, Demirci U. Nanoplasmonic Quantitative Detection of Intact Viruses from Unprocessed Whole Blood. ACS Nano. 2013; 7:4733–4745. [PubMed: 23688050]
40. Mayer KM, Hafner JH. Localized Surface Plasmon Resonance Sensors. Chem Rev. 2011; 111:3828–3857. [PubMed: 21648956]
41. (a) Guo L, Kim DH. LSPR Biomolecular Assay with High Sensitivity Induced by Aptamer-Antigen-Antibody Sandwich Complex. Biosens Bioelectron. 2012; 31:567–570. [PubMed: 22099957] (b) Yamamichi J, Ojima T, Iida M, Yurugi K, Imamura T, Ashihara E, Kimura S, Maekawa T. Surface Chemical Approach to Single-Step Measurement of Antibody in Human Serum Using Localized Surface Plasmon Resonance Biosensor on Microtiter Plate System. Anal Bioanal Chem. 2014; 406:4527–4533. [PubMed: 24770806]
42. Hsu CY, Huang JW, Lin KJ. High Sensitivity and Selectivity of Human Antibody Attachment at the Interstices between Substrate-Bound Gold Nanoparticles. Chem Commun. 2011; 47:872–874.
43. Zhang Y, Tang Y, Hsieh YH, Hsu CY, Xi J, Lin KJ, Jiang X. Towards a High-Throughput Label-Free Detection System Combining Localized-Surface Plasmon Resonance and Microfluidics. Lab Chip. 2012; 12:3012–3015. [PubMed: 22772076]
44. Jia K, Bijeon JL, Adam PM, Ionescu RE. Sensitive Localized Surface Plasmon Resonance Multiplexing Protocols. Anal Chem. 2012; 84:8020–8027. [PubMed: 22894648]
45. Chen S, Svedendahl M, Van Duyne RP, Kall M. Plasmon-Enhanced Colorimetric ELISA with Single Molecule Sensitivity. Nano Lett. 2011; 11:1826–1830. [PubMed: 21428275]
46. Li C, Wu C, Zheng J, Lai J, Zhang C, Zhao Y. LSPR Sensing of Molecular Biothiols Based on Noncoupled Gold Nanorods. Langmuir. 2010; 26:9130–9135. [PubMed: 20426452]

47. (a) Truong PL, Cao C, Park S, Kim M, Sim SJ. A New Method for Non-Labeling Attomolar Detection of Diseases Based on an Individual Gold Nanorod Immunosensor. Lab Chip. 2011; 11:2591–2597. [PubMed: 21670836] (b) Phuoc Long T, Kim BW, Sim SJ. Rational Aspect Ratio and Suitable Antibody Coverage of Gold Nanorod for Ultra-Sensitive Detection of a Cancer Biomarker. Lab Chip. 2012; 12:1102–1109. [PubMed: 22298159]

48. Wang X, Li Y, Wang H, Fu Q, Peng J, Wang Y, Du J, Zhou Y, Zhan L. Gold Nanorod-Based Localized Surface Plasmon Resonance Biosensor for Sensitive Detection of Hepatitis B Virus in Buffer, Blood Serum and Plasma. Biosens Bioelectron. 2010; 26:404–410. [PubMed: 20729056]

49. (a) Huang X, Neretina S, El-Sayed MA. Gold Nanorods: From Synthesis and Properties to Biological and Biomedical Applications. Adv Mater. 2009; 21:4880–4910. [PubMed: 25378252] (b) Perez-Juste J, Pastoriza-Santos I, Liz-Marzan LM, Mulvaney P. Gold Nanorods: Synthesis, Characterization and Applications. Coord Chem Rev. 2005; 249:1870–1901.

50. Tang L, Casas J. Quantification of Cardiac Biomarkers Using Label-Free and Multiplexed Gold Nanorod Bioprobes for Myocardial Infarction Diagnosis. Biosens Bioelectron. 2014; 61:70–75. [PubMed: 24858675]

51. Tang L, Casas J, Venkataramasubramani M. Magnetic Nanoparticle Mediated Enhancement of Localized Surface Plasmon Resonance for Ultrasensitive Bioanalytical Assay in Human Blood Plasma. Anal Chem. 2013; 85:1431–1439. [PubMed: 23267460]

52. (a) Hall WP, Ngatia SN, Van Duyne RP. LSPR Biosensor Signal Enhancement Using Nanoparticle-Antibody Conjugates. J Phys Chem C. 2011; 115:1410–1414.(b) Beeram SR, Zamborini FP. Purification of Gold Nanoplates Grown Directly on Surfaces for Enhanced Localized Surface Plasmon Resonance Biosensing. ACS Nano. 2010; 4:3633–3646. [PubMed: 20575510] (c) Jeong HH, Erdene N, Park JH, Jeong DH, Lee HY, Lee SK. Real-Time Label-Free Immunoassay of Interferon-Gamma and Prostate-Specific Antigen Using a Fiber-Optic Localized Surface Plasmon Resonance Sensor. Biosens Bioelectron. 2013; 39:346–351. [PubMed: 22951530]

53. Cheng Y, Wang M, Borghs G, Chen H. Gold Nanoparticle Dimers for Plasmon Sensing. Langmuir. 2011; 27:7884–7891. [PubMed: 21574606]

54. Liu F, Wong MMK, Chiu SK, Lin H, Ho JC, Pang SW. Effects of Nanoparticle Size and Cell Type on High Sensitivity Cell Detection Using a Localized Surface Plasmon Resonance Biosensor. Biosens Bioelectron. 2014; 55:141–148. [PubMed: 24373953]

55. Dong P, Lin Y, Deng J, Di J. Ultrathin Gold-Shell Coated Silver Nanoparticles onto a Glass Platform for Improvement of Plasmonic Sensors. ACS Appl Mater Interfaces. 2013; 5:2392–2399. [PubMed: 23477284]

56. Rodríguez-Lorenzo L, de la Rica R, Álvarez-Puebla RA, Liz-Marzán LM, Stevens MM. Plasmonic Nanosensors with Inverse Sensitivity by Means of Enzyme-Guided Crystal Growth. Nat Mater. 2012; 11:604–607. [PubMed: 22635043]

57. Kitayama Y, Takeuchi T. Localized Surface Plasmon Resonance Nanosensing of C-Reactive Protein with Poly(2-Methacryloyloxyethyl Phosphorylcholine)-Grafted Gold Nanoparticles Prepared by Surface-Initiated Atom Transfer Radical Polymerization. Anal Chem. 2014; 86:5587–5594. [PubMed: 24830565]

58. Nagatsuka T, Uzawa H, Sato K, Kondo S, Izumi M, Yokoyama K, Ohsawa I, Seto Y, Neri P, Mori H, Nishida Y, Saito M, Tamiya E. Localized Surface Plasmon Resonance Detection of Biological Toxins Using Cell Surface Oligosaccharides on Glyco Chips. ACS Appl Mater Interfaces. 2013; 5:4173–4180. [PubMed: 23668627]

59. Liu X, Zhang Q, Tu Y, Zhao W, Gai H. Single Gold Nanoparticle Localized Surface Plasmon Resonance Spectral Imaging for Quantifying Binding Constant of Carbohydrate-Protein Interaction. Anal Chem. 2013; 85:11851–11857. [PubMed: 24266418]

60. Wei H, Wang E. Nanomaterials with Enzyme-Like Characteristics (Nanozymes): Next-Generation Artificial Enzymes. Chem Soc Rev. 2013; 42:6060–6093. [PubMed: 23740388]

61. Liu X, Atwater M, Wang J, Huo Q. Extinction Coefficient of Gold Nanoparticles with Different Sizes and Different Capping Ligands. Colloids Surf, B. 2007; 58:3–7.

62. Elghanian R, Storhoff JJ, Mucic RC, Letsinger RL, Mirkin CA. Selective Colorimetric Detection of Polynucleotides Based on the Distance-Dependent Optical Properties of Gold Nanoparticles. Science. 1997; 277:1078–1081. [PubMed: 9262471]

63. Rosi NL, Mirkin CA. Nanostructures in Biodiagnostics. Chem Rev. 2005; 105:1547–1562. [PubMed: 15826019]
64. Mirkin CA, Letsinger RL, Mucic RC, Storhoff JJ. A DNA-Based Method for Rationally Assembling Nanoparticles into Macroscopic Materials. Nature. 1996; 382:607–609. [PubMed: 8757129]
65. Wu S, Liang PP, Yu HX, Xu XW, Liu Y, Lou XH, Xiao Y. Amplified Single Base-Pair Mismatch Detection Via Aggregation of Exonuclease-Sheared Gold Nanoparticles. Anal Chem. 2014; 86:3461–3467. [PubMed: 24611947]
66. Li HX, Rothberg LJ. Label-Free Colorimetric Detection of Specific Sequences in Genomic DNA Amplified by the Polymerase Chain Reaction. J Am Chem Soc. 2004; 126:10958–10961. [PubMed: 15339181]
67. Wang J, Wang L, Liu X, Liang Z, Song S, Li W, Li G, Fan C. A Gold Nanoparticle-Based Aptamer Target Binding Readout for ATP Assay. Adv Mater. 2007; 19:3943–3946.
68. Zagorovsky K, Chan WCW. A Plasmonic Dnazyme Strategy for Point-of-Care Genetic Detection of Infectious Pathogens. Angew Chem, Int Ed. 2013; 52:3168–3171.
69. (a) Shen W, Deng H, Gao Z. Gold Nanoparticle-Enabled Real-Time Ligation Chain Reaction for Ultrasensitive Detection of DNA. J Am Chem Soc. 2012; 134:14678–14681. [PubMed: 22924646] (b) Shen W, Deng H, Teo AKL, Gao Z. Colorimetric Detection of Single-Nucleotide Polymorphisms with a Real-Time PCR-Like Sensitivity. Chem Commun. 2012; 48:10225–10227.
70. Kato D, Oishi M. Ultrasensitive Detection of DNA and RNA Based on Enzyme-Free Click Chemical Ligation Chain Reaction on Dispersed Gold Nanoparticles. ACS Nano. 2014; 8:9988–9997. [PubMed: 25256209]
71. Guo L, Xu Y, Ferhan AR, Chen G, Kim DH. Oriented Gold Nanoparticle Aggregation for Colorimetric Sensors with Surprisingly High Analytical Figures of Merit. J Am Chem Soc. 2013; 135:12338–12345. [PubMed: 23927761]
72. (a) Laromaine A, Koh L, Murugesan M, Ulijn RV, Stevens MM. Protease-Triggered Dispersion of Nanoparticle Assemblies. J Am Chem Soc. 2007; 129:4156–4157. [PubMed: 17358069] (b) Kim CJ, Lee DI, Kim C, Lee K, Lee CH, Ahn IS. Gold Nanoparticles-Based Colorimetric Assay for Cathepsin B Activity and the Efficiency of Its Inhibitors. Anal Chem. 2014; 86:3825–3833. [PubMed: 24673125] (c) Guarise C, Pasquato L, De Filippis V, Scrimin P. Gold Nanoparticles-Based Protease Assay. Proc Natl Acad Sci USA. 2006; 103:3978–3982. [PubMed: 16537471]
73. (a) Choi Y, Ho NH, Tung CH. Sensing Phosphatase Activity by Using Gold Nanoparticles. Angew Chem, Int Ed. 2007; 46:707–709.(b) Deng J, Jiang Q, Wang Y, Yang L, Yu P, Mao L. Real-Time Colorimetric Assay of Inorganic Pyrophosphatase Activity Based on Reversibly Competitive Coordination of Cu^{2+} between Cysteine and Pyrophosphate Ion. Anal Chem. 2013; 85:9409–9415. [PubMed: 24016028] (c) Sharon E, Golub E, Niazov-Elkan A, Balogh D, Willner I. Analysis of Telomerase by the Telomeric Hemin/G-Quadruplex-Controlled Aggregation of Au Nanoparticles in the Presence of Cysteine. Anal Chem. 2014; 86:3153–3158. [PubMed: 24502233] (d) Wu Z, Wu ZK, Tang H, Tang LJ, Jiang JH. Activity-Based DNA-Gold Nanoparticle Probe as Colorimetric Biosensor for DNA Methyl-transferase/Glycosylase Assay. Anal Chem. 2013; 85:4376–4383. [PubMed: 23544713] (e) de la Rica R, Aili D, Stevens MM. Enzyme-Responsive Nanoparticles for Drug Release and Diagnostics. Adv Drug Delivery Rev. 2012; 64:967–978.
74. Wang M, Gu X, Zhang G, Zhang D, Zhu D. Continuous Colorimetric Assay for Acetylcholinesterase and Inhibitor Screening with Gold Nanoparticles. Langmuir. 2009; 25:2504–2507. [PubMed: 19154124]
75. Liu D, Chen W, Tian Y, He S, Zheng W, Sun J, Wang Z, Jiang X. A Highly Sensitive Gold-Nanoparticle-Based Assay for Acetylcholinesterase in Cerebrospinal Fluid of Transgenic Mice with Alzheimer's Disease. Adv Healthcare Mater. 2012; 1:90–95.
76. Liu D, Chen W, Wei J, Li X, Wang Z, Jiang X. A Highly Sensitive, Dual-Readout Assay Based on Gold Nanoparticles for Organophosphorus and Carbamate Pesticides. Anal Chem. 2012; 84:4185–4191. [PubMed: 22475016]
77. Garner AL, Fullagar JL, Day JA, Cohen SM, Janda KD. Development of a High-Throughput Screen and Its Use in the Discovery Ofstreptococcus Pneumoniaeimmunoglobulin A1 Protease Inhibitors. J Am Chem Soc. 2013; 135:10014–10017. [PubMed: 23808771]

78. Qu W, Liu Y, Liu D, Wang Z, Jiang X. Copper-Mediated Amplification Allows Readout of Immunoassays by the Naked Eye. Angew Chem, Int Ed. 2011; 50:3442–3445.

79. Xianyu Y, Wang Z, Jiang X. A Plasmonic Nanosensor for Immunoassay Via Enzyme-Triggered Click Chemistry. ACS Nano. 2014; 8:12741–12747. [PubMed: 25423357]

80. Liu D, Wang Z, Jin A, Huang X, Sun X, Wang F, Yan Q, Ge S, Xia N, Niu G, Liu G, Walker ARH, Chen X. Acetylcholinesterase-Catalyzed Hydrolysis Allows Ultrasensitive Detection of Pathogens with the Naked Eye. Angew Chem, Int Ed. 2013; 52:14065–14069.

81. Nie XM, Huang R, Dong CX, Tang LJ, Gui R, Jiang JH. Plasmonic ELISA for the Ultrasensitive Detection of Treponema Pallidum. Biosens Bioelectron. 2014; 58:314–319. [PubMed: 24662060]

82. Liu D, Yang J, Wang H-F, Wang Z, Huang X, Wang Z, Niu G, Hight Walker AR, Chen X. Glucose Oxidase-Catalyzed Growth of Gold Nanoparticles Enables Quantitative Detection of Attomolar Cancer Biomarkers. Anal Chem. 2014; 86:5800–5806. [PubMed: 24896231]

83. de la Rica R, Stevens MM. Plasmonic ELISA for the Ultrasensitive Detection of Disease Biomarkers with the Naked Eye. Nat Nanotechnol. 2012; 7:821–824. [PubMed: 23103935]

84. Aili D, Stevens MM. Bioresponsive Peptide-Inorganic Hybrid Nanomaterials. Chem Soc Rev. 2010; 39:3358–3370. [PubMed: 20596582]

85. Andresen H, Mager M, Grießner M, Charchar P, Todorova N, Bell N, Theocharidis G, Bertazzo S, Yarovsky I, Stevens MM. Single-Step Homogeneous Immunoassays Utilizing Epitope-Tagged Gold Nanoparticles: On the Mechanism, Feasibility, and Limitations. Chem Mater. 2014; 26:4696–4704.

86. (a) Aitken CE, Marshall RA, Puglisi JD. An Oxygen Scavenging System for Improvement of Dye Stability in Single-Molecule Fluorescence Experiments. Biophys J. 2008; 94:1826–1835. [PubMed: 17921203] (b) Randolph JB, Waggoner AS. Stability, Specificity and Fluorescence Brightness of Multiply-Labeled Fluorescent DNA Probes. Nucleic Acids Res. 1997; 25:2923–2929. [PubMed: 9207044]

87. (a) Gao XH, Cui YY, Levenson RM, Chung LWK, Nie SM. *In Vivo* Cancer Targeting and Imaging with Semiconductor Quantum Dots. Nat Biotechnol. 2004; 22:969–976. [PubMed: 15258594] (b) Wu XY, Liu HJ, Liu JQ, Haley KN, Treadway JA, Larson JP, Ge NF, Peale F, Bruchez MP. Immunofluorescent Labeling of Cancer Marker Her2 and Other Cellular Targets with Semiconductor Quantum Dots. Nat Biotechnol. 2003; 21:41–46. [PubMed: 12459735]

88. (a) Lee JE, Lee N, Kim T, Kim J, Hyeon T. Multifunctional Mesoporous Silica Nanocomposite Nanoparticles for Theranostic Applications. Acc Chem Res. 2011; 44:893–902. [PubMed: 21848274] (b) Zhao XJ, Bagwe RP, Tan WH. Development of Organic-Dye-Doped Silica Nanoparticles in a Reverse Microemulsion. Adv Mater. 2004; 16:173–176.

89. (a) Gnach A, Bednarkiewicz A. Lanthanide-Doped up-Converting Nanoparticles: Merits and Challenges. Nano Today. 2012; 7:532–563.(b) Guo H, Sun S. Lanthanide-Doped Upconverting Phosphors for Bioassay and Therapy. Nanoscale. 2012; 4:6692–6706. [PubMed: 23001049]

90. (a) Baker SN, Baker GA. Luminescent Carbon Nanodots: Emergent Nanolights. Angew Chem, Int Ed. 2010; 49:6726–6744.(b) Qu S, Wang X, Lu Q, Liu X, Wang L. A Biocompatible Fluorescent Ink Based on Water-Soluble Luminescent Carbon Nanodots. Angew Chem, Int Ed. 2012; 51:12215–12218.

91. (a) Huang CC, Yang Z, Lee KH, Chang HT. Synthesis of Highly Fluorescent Gold Nanoparticles for Sensing Mercury(II). Angew Chem, Int Ed. 2007; 46:6824–6828.(b) Diez I, Ras RHA. Fluorescent Silver Nanoclusters. Nanoscale. 2011; 3:1963–1970. [PubMed: 21409225] (c) Peyser LA, Vinson AE, Bartko AP, Dickson RM. Photoactivated Fluorescence from Individual Silver Nanoclusters. Science. 2001; 291:103–106. [PubMed: 11141556]

92. (a) Wu X, He X, Wang K, Xie C, Zhou B, Qing Z. Ultrasmall Near-Infrared Gold Nanoclusters for Tumor Fluorescence Imaging in Vivo. Nanoscale. 2010; 2:2244–2249. [PubMed: 20835443] (b) Dulkeith E, Morteani AC, Niedereichholz T, Klar TA, Feldmann J, Levi SA, van Veggel F, Reinhoudt DN, Moller M, Gittins DI. Fluorescence Quenching of Dye Molecules near Gold Nanoparticles: Radiative and Nonradiative Effects. Phys Rev Lett. 2002; 89:203002. [PubMed: 12443474]

93. (a) Qian H, Zhu M, Wu Z, Jin R. Quantum Sized Gold Nanoclusters with Atomic Precision. Acc Chem Res. 2012; 45:1470–1479. [PubMed: 22720781] (b) Jin R. Quantum Sized, Thiolate-Protected Gold Nanoclusters. Nanoscale. 2010; 2:343–362. [PubMed: 20644816]

94. (a) Yau SH, Varnavski O, Goodson T III. An Ultrafast Look at Au Nanoclusters. Acc Chem Res. 2013; 46:1506–1516. [PubMed: 23651457] (b) Yau SH, Varnavski O, Gilbertson JD, Chandler B, Ramakrishna G, Goodson T III. Ultrafast Optical Study of Small Gold Monolayer Protected Clusters: A Closer Look at Emission. J Phys Chem C. 2010; 114:15979–15985.

95. (a) Chen LY, Wang CW, Yuan Z, Chang HT. Fluorescent Gold Nanoclusters: Recent Advances in Sensing and Imaging. Anal Chem. 2015; 87:216–229. [PubMed: 25275676] (b) Luo Z, Zheng K, Xie J. Engineering Ultrasmall Water-Soluble Gold and Silver Nanoclusters for Biomedical Applications. Chem Commun. 2014; 50:5143–5155.(c) Zhang L, Wang E. Metal Nanoclusters: New Fluorescent Probes for Sensors and Bioimaging. Nano Today. 2014; 9:132–157.

96. Wu Z, Jin R. On the Ligand's Role in the Fluorescence of Gold Nanoclusters. Nano Lett. 2010; 10:2568–2573. [PubMed: 20550101]

97. Shiang Y-C, Huang C-C, Chang H-T. Gold Nanodot-Based Luminescent Sensor for the Detection of Hydrogen Peroxide and Glucose. Chem Commun. 2009:3437–3439.

98. (a) Xie J, Zheng Y, Ying JY. Protein-Directed Synthesis of Highly Fluorescent Gold Nanoclusters. J Am Chem Soc. 2009; 131:888–889. [PubMed: 19123810] (b) Wen X, Yu P, Toh YR, Tang J. Structure-Correlated Dual Fluorescent Bands in BSA-Protected Au-25 Nanoclusters. J Phys Chem C. 2012; 116:11830–11836.

99. Jin L, Shang L, Guo S, Fang Y, Wen D, Wang L, Yin J, Dong S. Biomolecule-Stabilized Au Nanoclusters as a Fluorescence Probe for Sensitive Detection of Glucose. Biosens Bioelectron. 2011; 26:1965–1969. [PubMed: 20970316]

100. Tao Y, Lin Y, Ren J, Qu X. A Dual Fluorometric and Colorimetric Sensor for Dopamine Based on BSA-Stabilized Au Nanoclusters. Biosens Bioelectron. 2013; 42:41–46. [PubMed: 23202328]

101. Nair LV, Philips DS, Jayasree RS, Ajayaghosh A. A Near-Infrared Fluorescent Nanosensor (AuC@Urease) for the Selective Detection of Blood Urea. Small. 2013; 9:2673–2677. [PubMed: 23447125]

102. Li PH, Lin JY, Chen CT, Ciou WR, Chan PH, Luo L, Hsu HY, Diau EWG, Chen YC. Using Gold Nanoclusters as Selective Luminescent Probes for Phosphate-Containing Metabolites. Anal Chem. 2012; 84:5484–5488. [PubMed: 22762258]

103. Song W, Wang Y, Liang RP, Zhang L, Qiu JD. Label-Free Fluorescence Assay for Protein Kinase Based on Peptide Biomineralized Gold Nanoclusters as Signal Sensing Probe. Biosens Bioelectron. 2015; 64:234–240. [PubMed: 25222326]

104. Huang CC, Chen CT, Shiang YC, Lin ZH, Chang HT. Synthesis of Fluorescent Carbohydrate-Protected Au Nanodots for Detection of Concanavalin a and Escherichia Coli. Anal Chem. 2009; 81:875–882. [PubMed: 19119843]

105. Triulzi RC, Micic M, Giordani S, Serry M, Chiou W-A, Leblanc RM. Immunoasssay Based on the Antibody-Conjugated Pamam-Dendrimer? Gold Quantum Dot Complex. Chem Commun. 2006:5068–5070.

106. Peng J, Feng LN, Zhang K, Li XH, Jiang LP, Zhu JJ. Calcium Carbonate-Gold Nanocluster Hybrid Spheres: Synthesis and Versatile Application in Immunoassays. Chem—Eur J. 2012; 18:5261–5268. [PubMed: 22422592]

107. Yang GH, Shi JJ, Wang S, Xiong WW, Jiang LP, Burda C, Zhu JJ. Fabrication of a Boron Nitride-Gold Nanocluster Composite and Its Versatile Application for Immunoassays. Chem Commun. 2013; 49:10757–10759.

108. Wang Y, Wang Y, Zhou F, Kim P, Xia Y. Protein-Protected Au Clusters as a New Class of Nanoscale Biosensor for Label-Free Fluorescence Detection of Proteases. Small. 2012; 8:3769–3773. [PubMed: 22969016]

109. Wen Q, Gu Y, Tang LJ, Yu RQ, Jiang JH. Peptide-Templated Gold Nanocluster Beacon as a Sensitive, Label-Free Sensor for Protein Post-Translational Modification Enzymes. Anal Chem. 2013; 85:11681–11685. [PubMed: 24274625]

110. Chen CT, Chen WJ, Liu CZ, Chang LY, Chen YC. Glutathione-Bound Gold Nanoclusters for Selective-Binding and Detection of Glutathione S-Transferase-Fusion Proteins from Cell Lysates. Chem Commun. 2009:7515–7517.

111. Lin H, Li L, Lei C, Xu X, Nie Z, Guo M, Huang Y, Yao S. Immune-Independent and Label-Free Fluorescent Assay for Cystatin C Detection Based on Protein-Stabilized Au Nanoclusters. Biosens Bioelectron. 2013; 41:256–261. [PubMed: 23017686]

112. Swierczewska M, Lee S, Chen X. The Design and Application of Fluorophore-Gold Nanoparticle Activatable Probes. Phys Chem Chem Phys. 2011; 13:9929–9941. [PubMed: 21380462]

113. Stryer L, Haugland RP. Energy Transfer: A Spectroscopic Ruler. Proc Natl Acad Sci USA. 1967; 58:719–726. [PubMed: 5233469]

114. Stryer L. Fluorescence Energy Transfer as a Spectroscopic Ruler. Annu Rev Biochem. 1978; 47:819–846. [PubMed: 354506]

115. Ray PC, Fan Z, Crouch RA, Sinha SS, Pramanik A. Nanoscopic Optical Rulers Beyond the FRET Distance Limit: Fundamentals and Applications. Chem Soc Rev. 2014; 43:6370–6404. [PubMed: 24902784]

116. Yun CS, Javier A, Jennings T, Fisher M, Hira S, Peterson S, Hopkins B, Reich NO, Strouse GF. Nanometal Surface Energy Transfer in Optical Rulers, Breaking the FRET Barrier. J Am Chem Soc. 2005; 127:3115–3119. [PubMed: 15740151]

117. (a) Jennings TL, Singh MP, Strouse GF. Fluorescent Lifetime Quenching near D=1.5 nm Gold Nanoparticles: Probing NSET Validity. J Am Chem Soc. 2006; 128:5462–5467. [PubMed: 16620118] (b) Singh MP, Strouse GF. Involvement of the LSPR Spectral Overlap for Energy Transfer between a Dye and Au Nanoparticle. J Am Chem Soc. 2010; 132:9383–9391. [PubMed: 20560666] (c) Li M, Cushing SK, Wang Q, Shi X, Hornak LA, Hong Z, Wu N. Size-Dependent Energy Transfer between Cdse/Zns Quantum Dots and Gold Nanoparticles. J Phys Chem Lett. 2011; 2:2125–2129.

118. Zhang P, Wang J, Huang H, Chen H, Guan R, Chen Y, Ji L, Chao H. $RuNH_2$@AuNPs as Two-Photon Luminescent Probes for Thiols in Living Cells and Tissues. Biomaterials. 2014; 35:9003–9011. [PubMed: 25103232]

119. Xu J-P, Jia L, Fang Y, Lv L-P, Song Z-G, Ji J. Highly Soluble PEGylated Pyrene-Gold Nanoparticles Dyads for Sensitive Turn-on Fluorescent Detection of Biothiols. Analyst. 2010; 135:2323–2327. [PubMed: 20603668]

120. Tang B, Cao L, Xu K, Zhuo L, Ge J, Li Q, Yu L. A New Nanobiosensor for Glucose with High Sensitivity and Selectivity in Serum Based on Fluorescence Resonance Energy Transfer (FRET) between Cdte Quantum Dots and an Nanoparticles. Chem—Eur J. 2008; 14:3637–3644. [PubMed: 18318025]

121. Li L, Gao F, Ye J, Chen Z, Li Q, Gao W, Ji L, Zhang R, Tang B. FRET-Based Biofriendly Apo-GOx-Modified Gold Nanoprobe for Specific and Sensitive Glucose Sensing and Cellular Imaging. Anal Chem. 2013; 85:9721–9727. [PubMed: 24032474]

122. (a) Cordes DB, Gamsey S, Singaram B. Fluorescent Quantum Dots with Boronic Acid Substituted Viologens to Sense Glucose in Aqueous Solution. Angew Chem, Int Ed. 2006; 45:3829–3832.(b) Fang H, Kaur G, Wang BH. Progress in Boronic Acid-Based Fluorescent Glucose Sensors. J Fluoresc. 2004; 14:481–489. [PubMed: 15617256]

123. Wang L-L, Qiao J, Liu H-H, Hao J, Qi L, Zhou X-P, Li D, Nie Z-X, Mao L-Q. Ratiometric Fluorescent Probe Based on Gold Nanoclusters and Alizarin Red-Boronic Acid for Monitoring Glucose in Brain Microdialysate. Anal Chem. 2014; 86:9758–9764. [PubMed: 25157796]

124. Liu J-M, Chen J-T, Yan X-P. Near Infrared Fluorescent Trypsin Stabilized Gold Nanoclusters as Surface Plasmon Enhanced Energy Transfer Biosensor and *in Vivo* Cancer Imaging Bioprobe. Anal Chem. 2013; 85:3238–3245. [PubMed: 23413985]

125. Huang CC, Chiang CK, Lin ZH, Lee KH, Chang HT. Bioconjugated Gold Nanodots and Nanoparticles for Protein Assays Based on Photoluminescence Quenching. Anal Chem. 2008; 80:1497–1504. [PubMed: 18237154]

126. (a) Tan WH, Wang KM, Drake TJ. Molecular Beacons. Curr Opin Chem Biol. 2004; 8:547–553. [PubMed: 15450499] (b) Tyagi S, Kramer FR. Molecular Beacons: Probes That Fluoresce Upon Hybridization. Nat Biotechnol. 1996; 14:303–308. [PubMed: 9630890] (c) Wang K, Tang Z, Yang CJ, Kim Y, Fang X, Li W, Wu Y, Medley CD, Cao Z, Li J, Colon P, Lin H, Tan W. Molecular Engineering of DNA: Molecular Beacons. Angew Chem, Int Ed. 2009; 48:856–870.

127. Dubertret B, Calame M, Libchaber AJ. Single-Mismatch Detection Using Gold-Quenched Fluorescent Oligonucleotides. Nat Biotechnol. 2001; 19:365–370. [PubMed: 11283596]

128. Maxwell DJ, Taylor JR, Nie SM. Self-Assembled Nanoparticle Probes for Recognition and Detection of Biomolecules. J Am Chem Soc. 2002; 124:9606–9612. [PubMed: 12167056]

129. Fan CH, Wang S, Hong JW, Bazan GC, Plaxco KW, Heeger AJ. Beyond Superquenching: Hyper-Efficient Energy Transfer from Conjugated Polymers to Gold Nanoparticles. Proc Natl Acad Sci USA. 2003; 100:6297–6301. [PubMed: 12750470]

130. Seferos DS, Giljohann DA, Hill HD, Prigodich AE, Mirkin CA. NanoFlares: Probes for Transfection and mRNA Detection in Living Cells. J Am Chem Soc. 2007; 129:15477–15479. [PubMed: 18034495]

131. Prigodich AE, Seferos DS, Massich MD, Giljohann DA, Lane BC, Mirkin CA. Nano-Flares for mRNA Regulation and Detection. ACS Nano. 2009; 3:2147–2152. [PubMed: 19702321]

132. Prigodich AE, Randeria PS, Briley WE, Kim NJ, Daniel WL, Giljohann DA, Mirkin CA. Multiplexed Nanoflares: mRNA Detection in Live Cells. Anal Chem. 2012; 84:2062–2066. [PubMed: 22288418]

133. Zheng D, Seferos DS, Giljohann DA, Patel PC, Mirkin CA. Aptamer Nano-Flares for Molecular Detection in Living Cells. Nano Lett. 2009; 9:3258–3261. [PubMed: 19645478]

134. Li N, Chang C, Pan W, Tang B. A Multicolor Nanoprobe for Detection and Imaging of Tumor-Related mRNAs in Living Cells. Angew Chem, Int Ed. 2012; 51:7426–7430.

135. Foekens JA, Romain S, Look MP, Martin PM, Klijn JGM. Thymidine Kinase and Thymidylate Synthase in Advanced Breast Cancer: Response to Tamoxifen and Chemotherapy. Cancer Res. 2001; 61:1421–1425. [PubMed: 11245445]

136. Pan W, Zhang T, Yang H, Diao W, Li N, Tang B. Multiplexed Detection and Imaging of Intracellular mRNAs Using a Four-Color Nanoprobe. Anal Chem. 2013; 85:10581–10588. [PubMed: 24088027]

137. Song S, Liang Z, Zhang J, Wang L, Li G, Fan C. Gold-Nanoparticle-Based Multicolor Nanobeacons for Sequence-Specific DNA Analysis. Angew Chem, Int Ed. 2009; 48:8670–8674.

138. Zhang J, Wang L, Zhang H, Boey F, Song S, Fan C. Aptamer-Based Multicolor Fluorescent Gold Nanoprobes for Multiplex Detection in Homogeneous Solution. Small. 2010; 6:201–204. [PubMed: 19957283]

139. Bartel DP. MicroRNAs: Genomics, Biogenesis, Mechanism, and Function. Cell. 2004; 116:281–297. [PubMed: 14744438]

140. (a) Mitchell PS, Parkin RK, Kroh EM, Fritz BR, Wyman SK, Pogosova-Agadjanyan EL, Peterson A, Noteboom J, O'Briant KC, Allen A, Lin DW, Urban N, Drescher CW, Knudsen BS, Stirewalt DL, Gentleman R, Vessella RL, Nelson PS, Martin DB, Tewari M. Circulating MicroRNAs as Stable Blood-Based Markers for Cancer Detection. Proc Natl Acad Sci USA. 2008; 105:10513–10518. [PubMed: 18663219] (b) Resnick KE, Alder H, Hagan JP, Richardson DL, Croce CM, Cohn DE. The Detection of Differentially Expressed MicroRNAs from the Serum of Ovarian Cancer Patients Using a Novel Real-Time PCR Platform. Gynecol Oncol. 2009; 112:55–59. [PubMed: 18954897]

141. (a) Dong H, Lei J, Ding L, Wen Y, Ju H, Zhang X. MicroRNA: Function, Detection, and Bioanalysis. Chem Rev. 2013; 113:6207–6233. [PubMed: 23697835] (b) Li J, Tan S, Kooger R, Zhang C, Zhang Y. MicroRNAs as Novel Biological Targets for Detection and Regulation. Chem Soc Rev. 2014; 43:506–517. [PubMed: 24161958]

142. Tu Y, Wu P, Zhang H, Cai C. Fluorescence Quenching of Gold Nanoparticles Integrating with a Conformation-Switched Hairpin Oligonucleotide Probe for MicroRNA Detection. Chem Commun. 2012; 48:10718–10720.

143. Degliangeli F, Kshirsagar P, Brunetti V, Pompa PP, Fiammengo R. Absolute and Direct MicroRNA Quantification Using DNA-Gold Nanoparticle Probes. J Am Chem Soc. 2014; 136:2264–2267. [PubMed: 24491135]

144. You C-C, Miranda OR, Gider B, Ghosh PS, Kim I-B, Erdogan B, Krovi SA, Bunz UHF, Rotello VM. Detection and Identification of Proteins Using Nanoparticle-Fluorescent Polymer 'Chemical Nose' Sensors. Nat Nanotechnol. 2007; 2:318–323. [PubMed: 18654291]

145. Phillips RL, Miranda OR, You C-C, Rotello VM, Bunz UHF. Rapid and Efficient Identification of Bacteria Using Gold-Nanoparticle-Poly(Para-Phenyleneethynylene) Constructs. Angew Chem, Int Ed. 2008; 47:2590–2594.

146. Bajaj A, Miranda OR, Kim IB, Phillips RL, Jerry DJ, Bunz UHF, Rotello VM. Detection and Differentiation of Normal, Cancerous, and Metastatic Cells Using Nanoparticle-Polymer Sensor Arrays. Proc Natl Acad Sci USA. 2009; 106:10912–10916. [PubMed: 19549846]

147. De M, Rana S, Akpinar H, Miranda OR, Arvizo RR, Bunz UHF, Rotello VM. Sensing of Proteins in Human Serum Using Conjugates of Nanoparticles and Green Fluorescent Protein. Nat Chem. 2009; 1:461–465. [PubMed: 20161380]

148. Rana S, Le NDB, Mout R, Saha K, Tonga GY, Bain RES, Miranda OR, Rotello CM, Rotello VM. A Multichannel Nanosensor for Instantaneous Readout of Cancer Drug Mechanisms. Nat Nanotechnol. 2015; 10:65–69. [PubMed: 25502312]

149. Lee S, Cha E-J, Park K, Lee S-Y, Hong J-K, Sun I-C, Kim SY, Choi K, Kwon IC, Kim K, Ahn C-H. A Near-Infrared-Fluorescence-Quenched Gold-Nanoparticle Imaging Probe for *in Vivo* Drug Screening and Protease Activity Determination. Angew Chem, Int Ed. 2008; 47:2804–2807.

150. (a) Susumu K, Oh E, Delehanty JB, Blanco-Canosa JB, Johnson BJ, Jain V, Hervey WJ, Algar WR, Boeneman K, Dawson PE, Medintz IL. Multifunctional Compact Zwitterionic Ligands for Preparing Robust Biocompatible Semiconductor Quantum Dots and Gold Nanoparticles. J Am Chem Soc. 2011; 133:9480–9496. [PubMed: 21612225] (b) Pons T, Medintz IL, Sapsford KE, Higashiya S, Grimes AF, English DS, Mattoussi H. On the Quenching of Semiconductor Quantum Dot Photoluminescence by Proximal Gold Nanoparticles. Nano Lett. 2007; 7:3157–3164. [PubMed: 17845066]

151. Oh E, Hong MY, Lee D, Nam SH, Yoon HC, Kim HS. Inhibition Assay of Biomolecules Based on Fluorescence Resonance Energy Transfer (FRET) between Quantum Dots and Gold Nanoparticles. J Am Chem Soc. 2005; 127:3270–3271. [PubMed: 15755131]

152. Kim YP, Oh YH, Oh E, Ko S, Han MK, Kim HS. Energy Transfer-Based Multiplexed Assay of Proteases by Using Gold Nanoparticle and Quantum Dot Conjugates on a Surface. Anal Chem. 2008; 80:4634–4641. [PubMed: 18457412]

153. (a) Oh E, Lee D, Kim YP, Cha SY, Oh DB, Kang HA, Kim J, Kim HS. Nanoparticle-Based Energy Transfer for Rapid and Simple Detection of Protein Glycosylation. Angew Chem, Int Ed. 2006; 45:7959–7963.(b) Wang C, Ouyang J, Wang YY, Ye DK, Xia XH. Sensitive Assay of Protease Activity on a Micro/Nanofluidics Preconcentrator Fused with the Fluorescence Resonance Energy Transfer Detection Technique. Anal Chem. 2014; 86:3216–3221. [PubMed: 24568176]

154. Lowe SB, Dick JAG, Cohen BE, Stevens MM. Multiplex Sensing of Protease and Kinase Enzyme Activity Via Orthogonal Coupling of Quantum Dot Peptide Conjugates. ACS Nano. 2012; 6:851–857. [PubMed: 22148227]

155. Draz MS, Fang BA, Li L, Chen Z, Wang Y, Xu Y, Yang J, Killeen K, Chen FF. Hybrid Nanocluster Plasmonic Resonator for Immunological Detection of Hepatitis B Virus. ACS Nano. 2012; 6:7634–7643. [PubMed: 22934963]

156. Shi J, Chan C, Pang Y, Ye W, Tian F, Lyu J, Zhang Y, Yang M. A Fluorescence Resonance Energy Transfer (FRET) Biosensor Based on Graphene Quantum Dots (GQDs) and Gold Nanoparticles (AuNPs) for the Detection of mecA Gene Sequence of *Staphylococcus Aureus*. Biosens Bioelectron. 2014; 53:187–192. [PubMed: 24140835]

157. Liu DB, Huang XL, Wang ZT, Jin A, Sun XL, Zhu L, Wang F, Ma Y, Niu G, Walker ARH, Chen XY. Gold Nanoparticle-Based Activatable Probe for Sensing Ultra Low Levels of Prostate-Specific Antigen. ACS Nano. 2013; 7:5568–5576. [PubMed: 23683064]

158. (a) Das J, Aziz MA, Yang H. A Nanocatalyst-Based Assay for Proteins: DNA-Free Ultrasensitive Electrochemical Detection Using Catalytic Reduction of P-Nitrophenol by Gold-Nanoparticle Labels. J Am Chem Soc. 2006; 128:16022–16023. [PubMed: 17165740] (b) Kim SN, Rusling JF, Papadimitrakopoulos F. Carbon Nanotubes for Electronic and Electrochemical Detection of Biomolecules. Adv Mater. 2007; 19:3214–3228. [PubMed: 18846263] (c) Zuo X, Song S, Zhang J, Pan D, Wang L, Fan C. A Target-Responsive Electrochemical Aptamer Switch (TREAS) for Reagentless Detection of Nanomolar ATP. J Am Chem Soc. 2007; 129:1042–1043. [PubMed: 17263380]

159. (a) Xia N, Deng D, Zhang L, Yuan B, Jing M, Du J, Liu L. Sandwich-Type Electrochemical Biosensor for Glycoproteins Detection Based on Dual-Amplification of Boronic Acid-Gold Nanoparticles and Dopamine-Gold Nanoparticles. Biosens Bioelectron. 2013; 43:155–159. [PubMed: 23298627] (b) Yang G, Li L, Rana RK, Zhu J-J. Assembled Gold Nanoparticles on Nitrogen-Doped Graphene for Ultrasensitive Electrochemical Detection of Matrix Metalloproteinase- 2. Carbon. 2013; 61:357–366.

160. Xiao Y, Patolsky F, Katz E, Hainfeld JF, Willner I. "Plugging into Enzymes": Nanowiring of Redox Enzymes by a Gold Nanoparticle. Science. 2003; 299:1877–1881. [PubMed: 12649477]

161. Zayats M, Katz E, Baron R, Willner I. Reconstitution of Apo-Glucose Dehydrogenase on Pyrroloquinoline Quinone-Functionalized Au Nanoparticles Yields an Electrically Contacted Biocatalyst. J Am Chem Soc. 2005; 127:12400–12406. [PubMed: 16131222]

162. Zhang S, Wang N, Yu H, Niu Y, Sun C. Covalent Attachment of Glucose Oxidase to an Au Electrode Modified with Gold Nanoparticles for Use as Glucose Biosensor. Bioelectrochemistry. 2005; 67:15–22. [PubMed: 15967397]

163. Yang W, Wang J, Zhao S, Sun Y, Sun C. Multilayered Construction of Glucose Oxidase and Gold Nanoparticles on Au Electrodes Based on Layer-by-Layer Covalent Attachment. Electrochem Commun. 2006; 8:665–672.

164. (a) Yehezkeli O, Tel-Vered R, Reichlin S, Willner I. Nano-Engineered Flavin-Dependent Glucose Dehydrogenase/Gold Nanoparticle-Modified Electrodes for Glucose Sensing and Biofuel Cell Applications. ACS Nano. 2011; 5:2385–2391. [PubMed: 21355610] (b) Yehezkeli O, Ovits O, Tel-Vered R, Raichlin S, Willner I. Reconstituted Enzymes on Electropolymerizable FAD-Modified Metallic Nanoparticles: Functional Units for the Assembly of Effectively "Wired" Enzyme Electrodes. Electroanalysis. 2010; 22:1817–1823.

165. Andreescu S, Luck LA. Studies of the Binding and Signaling of Surface-Immobilized Periplasmic Glucose Receptors on Gold Nanoparticles: A Glucose Biosensor Application. Anal Biochem. 2008; 375:282–290. [PubMed: 18211816]

166. Holland JT, Lau C, Brozik S, Atanassov P, Banta S. Engineering of Glucose Oxidase for Direct Electron Transfer Via Site-Specific Gold Nanoparticle Conjugation. J Am Chem Soc. 2011; 133:19262–19265. [PubMed: 22050076]

167. Chen J, Tang J, Yan F, Ju H. A Gold Nanoparticles/Sol-Gel Composite Architecture for Encapsulation of Immunoconjugate for Reagentless Electrochemical Immunoassay. Biomaterials. 2006; 27:2313–2321. [PubMed: 16313956]

168. Wu J, Tang J, Dai Z, Yan F, Ju H, Murr NE. A Disposable Electrochemical Immunosensor for Flow Injection Immunoassay of Carcinoembryonic Antigen. Biosens Bioelectron. 2006; 22:102–108. [PubMed: 16427775]

169. Xu Q, Mao C, Liu N-N, Zhu J-J, Sheng J. Direct Electrochemistry of Horseradish Peroxidase Based on Biocompatible Carboxymethyl Chitosan-Gold Nanoparticle Nanocomposite. Biosens Bioelectron. 2006; 22:768–773. [PubMed: 16600589]

170. Liu S, Peng L, Yang X, Wu Y, He L. Electrochemistry of Cytochrome P450 Enzyme on Nanoparticle-Containing Membrane-Coated Electrode and Its Applications for Drug Sensing. Anal Biochem. 2008; 375:209–216. [PubMed: 18164676]

171. Wu J, Yan Y, Yan F, Ju H. Electric Field-Driven Strategy for Multiplexed Detection of Protein Biomarkers Using a Disposable Reagentless Electrochemical Immunosensor Array. Anal Chem. 2008; 80:6072–6077. [PubMed: 18593191]

172. (a) Yan F, Chen J, Ju H. Immobilization and Electrochemical Behavior of Gold Nanoparticles Modified Leukemia K562 Cells and Application in Drug Sensitivity Test. Electrochem Commun. 2007; 9:293–298.(b) Du D, Liu S, Chen J, Ju H, Lian H, Li J. Colloidal Gold Nanoparticle Modified Carbon Paste Interface for Studies of Tumor Cell Adhesion and Viability. Biomaterials. 2005; 26:6487–6495. [PubMed: 15951013] (c) Ding L, Hao C, Xue Y, Ju H. A Bio-Inspired Support of Gold Nanoparticles-Chitosan Nanocomposites Gel for Immobilization and Electrochemical Study of K562 Leukemia Cells. Biomacromolecules. 2007; 8:1341–1346. [PubMed: 17375952]

173. Mahmoud KA, Hrapovic S, Luong JHT. Picomolar Detection of Protease Using Peptide/Single Walled Carbon Nanotube/Gold Nanoparticle-Modified Electrode. ACS Nano. 2008; 2:1051–1057. [PubMed: 19206503]

174. Mahmoud KA, Luong JHT. Impedance Method for Detecting HIV-1 Protease and Screening for Its Inhibitors Using Ferrocene-Peptide Conjugate/Au Nanoparticle/Single-Walled Carbon Nanotube Modified Electrode. Anal Chem. 2008; 80:7056–7062. [PubMed: 18707132]

175. Deng K, Xiang Y, Zhang L, Chen Q, Fu W. An Aptamer-Based Biosensing Platform for Highly Sensitive Detection of Platelet-Derived Growth Factor Via Enzyme-Mediated Direct Electrochemistry. Anal Chim Acta. 2013; 759:61–65. [PubMed: 23260677]

176. Cao X, Ye Y, Li Y, Xu X, Yu J, Liu S. Self-Assembled Glucose Oxidase/Graphene/Gold Ternary Nanocomposites for Direct Electrochemistry and Electrocatalysis. J Electroanal Chem. 2013; 697:10–14.

177. Adams KL, Jena BK, Percival SJ, Zhang B. Highly Sensitive Detection of Exocytotic Dopamine Release Using a Gold-Nanoparticle-Network Microelectrode. Anal Chem. 2011; 83:920–927. [PubMed: 21175175]

178. Liu G, Sun C, Li D, Song S, Mao B, Fan C, Tian Z. Gating of Redox Currents at Gold Nanoelectrodes Via DNA Hybridization. Adv Mater. 2010; 22:2148–2150. [PubMed: 20376817]

179. Chandra P, Noh H-B, Shim Y-B. Cancer Cell Detection Based on the Interaction between an Anticancer Drug and Cell Membrane Components. Chem Commun. 2013; 49:1900–1902.

180. de la Escosura-Muniz A, Sanchez-Espinel C, Diaz-Freitas B, Gonzalez-Fernandez A, Maltez-da Costa M, Merkoci A. Rapid Identification and Quantification of Tumor Cells Using an Electrocatalytic Method Based on Gold Nanoparticles. Anal Chem. 2009; 81:10268–10274. [PubMed: 19911778]

181. Rahman MA, Son JI, Won M-S, Shim Y-B. Gold Nanoparticles Doped Conducting Polymer Nanorod Electrodes: Ferrocene Catalyzed Aptamer-Based Thrombin Immunosensor. Anal Chem. 2009; 81:6604–6611. [PubMed: 20337374]

182. Du D, Ju HX, Zhang XJ, Chen J, Cai J, Chen HY. Electrochemical Immunoassay of Membrane P-Glycoprotein by Immobilization of Cells on Gold Nanoparticles Modified on a Methoxysilyl-Terminated Butyrylchitosan Matrix. Biochemistry. 2005; 44:11539–11545. [PubMed: 16114890]

183. Cui R, Pan H-C, Zhu J-J, Chen H-Y. Versatile Immunosensor Using CdTe Quantum Dots as Electrochemical and Fluorescent Labels. Anal Chem. 2007; 79:8494–8501. [PubMed: 17927140]

184. Liu H, Malhotra R, Peczuh MW, Rusling JF. Electrochemical Immunosensors for Antibodies to Peanut Allergen Ara h2 Using Gold Nanoparticle-Peptide Films. Anal Chem. 2010; 82:5865–5871. [PubMed: 20540504]

185. Labib M, Khan N, Ghobadloo SM, Cheng J, Pezacki JP, Berezovski MV. Three-Mode Electrochemical Sensing of Ultralow MicroRNA Levels. J Am Chem Soc. 2013; 135:3027–3038. [PubMed: 23362834]

186. (a) Liu L, Xia N, Liu H, Kang X, Liu X, Xue C, He X. Highly Sensitive and Label-Free Electrochemical Detection of MicroRNAs Based on Triple Signal Amplification of Multifunctional Gold Nanoparticles, Enzymes and Redox-Cycling Reaction. Biosens Bioelectron. 2014; 53:399–405. [PubMed: 24201003] (b) Xia N, Zhang L, Wang G, Feng Q, Liu L. Label-Free and Sensitive Strategy for MicroRNAs Detection Based on the Formation of Boronate Ester Bonds and the Dual-Amplification of Gold Nanoparticles. Biosens Bioelectron. 2013; 47:461–466. [PubMed: 23624014] (c) Peng Y, Jiang J, Yu R. A Sensitive Electrochemical Biosensor for MicroRNA Detection Based on Streptavidin-Gold Nanoparticles and Enzymatic Amplification. Anal Methods. 2014; 6:2889–2893.

187. Zhou X, Xing D, Zhu D, Jia L. Magnetic Bead and Nanoparticle Based Electrochemiluminescence Amplification Assay for Direct and Sensitive Measuring of Telomerase Activity. Anal Chem. 2009; 81:255–261. [PubMed: 19055424]

188. Duan R, Zhou X, Da X. Electrochemiluminescence Biobarcode Method Based on Cysteamine-Gold Nanoparticle Conjugates. Anal Chem. 2010; 82:3099–3103. [PubMed: 20297795]

189. Yin XB, Qi B, Sun XP, Yang XR, Wang EK. 4-(Dimethylamino)Butyric Acid Labeling for Electrochemiluminescence Detection of Biological Substances by Increasing Sensitivity with Gold Nanoparticle Amplification. Anal Chem. 2005; 77:3525–3530. [PubMed: 15924384]

190. Singh K, Rahman MA, Son JI, Kim KC, Shim Y-B. An Amperometric Immunosensor for Osteoproteogerin Based on Gold Nanoparticles Deposited Conducting Polymer. Biosens Bioelectron. 2008; 23:1595–1601. [PubMed: 18304799]

191. Munge BS, Krause CE, Malhotra R, Patel V, Silvio Gutkind J, Rusling JF. Electrochemical Immunosensors for Interleukin-6. Comparison of Carbon Nanotube Forest and Gold Nanoparticle Platforms. Electrochem Commun. 2009; 11:1009–1012. [PubMed: 20046945]

192. Jensen GC, Krause CE, Sotzing GA, Rusling JF. Inkjet-Printed Gold Nanoparticle Electrochemical Arrays on Plastic. Application to Immunodetection of a Cancer Biomarker Protein. Phys Chem Chem Phys. 2011; 13:4888–4894. [PubMed: 21212889]

193. Mani V, Chikkaveeraiah BV, Patel V, Gutkind JS, Rusling JF. Ultrasensitive Immunosensor for Cancer Biomarker Proteins Using Gold Nanoparticle Film Electrodes and Multienzyme-Particle Amplification. ACS Nano. 2009; 3:585–594. [PubMed: 19216571]

194. Munge BS, Coffey AL, Doucette JM, Somba BK, Malhotra R, Patel V, Gutkind JS, Rusling JF. Nanostructured Immunosensor for Attomolar Detection of Cancer Biomarker Interleukin-8 Using Massively Labeled Superparamagnetic Particles. Angew Chem, Int Ed. 2011; 50:7915–7918.

195. (a) Malhotra R, Patel V, Chikkaveeraiah BV, Munge BS, Cheong SC, Zain RB, Abraham MT, Dey DK, Gutkind JS, Rusling JF. Ultrasensitive Detection of Cancer Biomarkers in the Clinic by Use of a Nanostructured Microfluidic Array. Anal Chem. 2012; 84:6249–6255. [PubMed: 22697359] (b) Chikkaveeraiah BV, Mani V, Patel V, Gutkind JS, Rusling JF. Microfluidic Electrochemical Immunoarray for Ultrasensitive Detection of Two Cancer Biomarker Proteins in Serum. Biosens Bioelectron. 2011; 26:4477–4483. [PubMed: 21632234] (c) Otieno BA, Krause CE, Latus A, Chikkaveeraiah BV, Faria RC, Rusling JF. On-Line Protein Capture on Magnetic Beads for Ultrasensitive Microfluidic Immunoassays of Cancer Biomarkers. Biosens Bioelectron. 2014; 53:268–274. [PubMed: 24144557] (d) Krause CE, Otieno BA, Latus A, Faria RC, Patel V, Gutkind JS, Rusling JF. Rapid Microfluidic Immunoassays of Cancer Biomarker Proteins Using Disposable Inkjet-Printed Gold Nanoparticle Arrays. ChemistryOpen. 2013; 2:141–145. [PubMed: 24482763]

196. Dequaire M, Degrand C, Limoges B. An Electrochemical Metalloimmunoassay Based on a Colloidal Gold Label. Anal Chem. 2000; 72:5521–5528. [PubMed: 11101226]

197. Velev OD, Kaler EW. In Situ Assembly of Colloidal Particles into Miniaturized Biosensors. Langmuir. 1999; 15:3693–3698.

198. Chu X, Fu X, Chen K, Shen G-L, Yu R-Q. An Electrochemical Stripping Metalloimmunoassay Based on Silver-Enhanced Gold Nanoparticle Label. Biosens Bioelectron. 2005; 20:1805–1812. [PubMed: 15681197]

199. Chumbimuni-Torres KY, Dai Z, Rubinova N, Xiang Y, Pretsch E, Wang J, Bakker E. Potentiometric Biosensing of Proteins with Ultrasensitive Ion-Selective Microelectrodes and Nanoparticle Labels. J Am Chem Soc. 2006; 128:13676–13677. [PubMed: 17044681]

200. Ambrosi A, Castaneda MT, Killard AJ, Smyth MR, Alegret S, Merkoci A. Double-Codified Gold Nanolabels for Enhanced Immunoanalysis. Anal Chem. 2007; 79:5232–5240. [PubMed: 17579481]

201. Tang D, Yuan R, Chal Y. Ultrasensitive Electrochemical Immunosensor for Clinical Immunoassay Using Thionine-Doped Magnetic Gold Nanospheres as Labels and Horseradish Peroxidase as Enhancer. Anal Chem. 2008; 80:1582–1588. [PubMed: 18220412]

202. Tang D, Ren J. In Situ Amplified Electrochemical Immunoassay for Carcinoembryonic Antigen Using Horseradish Peroxidase-Encapsulated Nanogold Hollow Microspheres as Labels. Anal Chem. 2008; 80:8064–8070. [PubMed: 18816067]

203. Ho, J-aA; Chang, H-C.; Shih, N-Y.; Wu, L-C.; Chang, Y-F.; Chen, C-C.; Chou, C. Diagnostic Detection of Human Lung Cancer-Associated Antigen Using a Gold Nanoparticle-Based Electrochemical Immunosensor. Anal Chem. 2010; 82:5944–5950. [PubMed: 20557064]

204. Taton TA. Scanometric DNA Array Detection with Nanoparticle Probes. Science. 2000; 289:1757–1760. [PubMed: 10976070]

205. Park SJ, Taton TA, Mirkin CA. Array-Based Electrical Detection of DNA with Nanoparticle Probes. Science. 2002; 295:1503–1506. [PubMed: 11859188]

206. Russell C, Welch K, Jarvius J, Cai Y, Brucas R, Nikolajeff F, Svedlindh P, Nilsson M. Gold Nanowire Based Electrical DNA Detection Using Rolling Circle Amplification. ACS Nano. 2014; 8:1147–1153. [PubMed: 24433087]

207. Wang J, Xu DK, Polsky R. Magnetically-Induced Solid-State Electrochemical Detection of DNA Hybridization. J Am Chem Soc. 2002; 124:4208–4209. [PubMed: 11960439]

208. Zhang J, Song S, Zhang L, Wang L, Wu H, Pan D, Fan C. Sequence-Specific Detection of Femtomolar DNA Via a Chronocoulometric DNA Sensor (Cds): Effects of Nanoparticle-Mediated Amplification and Nanoscale Control of DNA Assembly at Electrodes. J Am Chem Soc. 2006; 128:8575–8580. [PubMed: 16802824]

209. Authier L, Grossiord C, Brossier P, Limoges B. Gold Nanoparticle-Based Quantitative Electrochemical Detection of Amplified Human Cytomegalovirus DNA Using Disposable Microband Electrodes. Anal Chem. 2001; 73:4450–4456. [PubMed: 11575792]

210. Pinijsuwan S, Rijiravanich P, Somasundrum M, Surareungchai W. Sub-Femtomolar Electrochemical Detection of DNA Hybridization Based on Latex/Gold Nanoparticle-Assisted Signal Amplification. Anal Chem. 2008; 80:6779–6784. [PubMed: 18665605]

211. Kerman K, Chikae M, Yamamura S, Tamiya E. Gold Nanoparticle-Based Electrochemical Detection of Protein Phosphorylation. Anal Chim Acta. 2007; 588:26–33. [PubMed: 17386790]

212. Omidfar K, Zarei H, Gholizadeh F, Larijani B. A High-Sensitivity Electrochemical Immunosensor Based on Mobile Crystalline Material-41-Polyvinyl Alcohol Nanocomposite and Colloidal Gold Nanoparticles. Anal Biochem. 2012; 421:649–656. [PubMed: 22209737]

213. (a) Li N, Yuan R, Chai Y, Chen S, An H, Li W. New Antibody Immobilization Strategy Based on Gold Nanoparticles and Azure I/Multi-Walled Carbon Nanotube Composite Membranes for an Amperometric Enzyme Immunosensor. J Phys Chem C. 2007; 111:8443–8450.(b) Che X, Yuan R, Chai Y, Li J, Song Z, Wang J. Amperometric Immunosensor for the Determination of α-1-Fetoprotein Based on Multiwalled Carbon Nanotube-Silver Nanoparticle Composite. J Colloid Interface Sci. 2010; 345:174–180. [PubMed: 20227086]

214. (a) Song Z, Yuan R, Chai Y, Yin B, Fu P, Wang J. Multilayer Structured Amperometric Immunosensor Based on Gold Nanoparticles and Prussian Blue Nanoparticles/Nanocomposite Functionalized Interface. Electrochim Acta. 2010; 55:1778–1784.(b) Ou C, Yuan R, Chai Y, Tang M, Chai R, He X. A Novel Amperometric Immunosensor Based on Layer-by-Layer Assembly of Gold Nanoparticles-Multi-Walled Carbon Nanotubes-Thionine Multilayer Films on Polyelectrolyte Surface. Anal Chim Acta. 2007; 603:205–213. [PubMed: 17963841] (c) Gao X, Zhang Y, Chen H, Chen Z, Lin X. Amperometric Immunosensor for Carcinoembryonic Antigen Detection with Carbon Nanotube-Based Film Decorated with Gold Nanoclusters. Anal Biochem. 2011; 414:70–76. [PubMed: 21396907]

215. Gopalan AI, Lee K-P, Ragupathy D. Development of a Stable Cholesterol Biosensor Based on Multi-Walled Carbon Nanotubes-Gold Nanoparticles Composite Covered with a Layer of Chitosan-Room-Temperature Ionic Liquid Network. Biosens Bioelectron. 2009; 24:2211–2217. [PubMed: 19167880]

216. (a) Mao S, Lu G, Yu K, Bo Z, Chen J. Specific Protein Detection Using Thermally Reduced Graphene Oxide Sheet Decorated with Gold Nanoparticle-Antibody Conjugates. Adv Mater. 2010; 22:3521–3526. [PubMed: 20665564] (b) Du Y, Guo S, Qin H, Dong S, Wang E. Target-Induced Conjunction of Split Aptamer as New Chiral Selector for Oligopeptide on Graphene-Mesoporous Silica-Gold Nanoparticle Hybrids Modified Sensing Platform. Chem Commun. 2012; 48:799–801.(c) Liu K, Zhang JJ, Wang C, Zhu JJ. Graphene-Assisted Dual Amplification Strategy for the Fabrication of Sensitive Amperometric Immunosensor. Biosens Bioelectron. 2011; 26:3627–3632. [PubMed: 21388800] (d) Han J, Zhuo Y, Chai Y, Yuan R, Zhang W, Zhu Q. Simultaneous Electrochemical Detection of Multiple Tumor Markers Based on Dual Catalysis Amplification of Multi-Functionalized Onion-Like Mesoporous Graphene Sheets. Anal Chim Acta. 2012; 746:70–76. [PubMed: 22975182]

217. Liang J, Chen Z, Guo L, Li L. Electrochemical Sensing of L-Histidine Based on Structure-Switching DNAzymes and Gold Nanoparticle-Graphene Nanosheet Composites. Chem Commun. 2011; 47:5476–5478.

218. Liu A-L, Zhong G-X, Chen J-Y, Weng S-H, Huang H-N, Chen W, Lin L-Q, Lei Y, Fu F-H, Sun Z-l, Lin X-H, Lin J-H, Yang S-Y. A Sandwich-Type DNA Biosensor Based on Electrochemical Co-Reduction Synthesis of Graphene-Three Dimensional Nanostructure Gold Nanocomposite Films. Anal Chim Acta. 2013; 767:50–58. [PubMed: 23452786]

219. Kim D-M, Noh H-B, Park DS, Ryu S-H, Koo JS, Shim Y-B. Immunosensors for Detection of Annexin II and MUC5AC for Early Diagnosis of Lung Cancer. Biosens Bioelectron. 2009; 25:456–462. [PubMed: 19717294]

220. Jeong B, Akter R, Han OH, Rhee CK, Rahman MA. Increased Electrocatalyzed Performance through Dendrimer-Encapsulated Gold Nanoparticles and Carbon Nanotube-Assisted Multiple Bienzymatic Labels: Highly Sensitive Electrochemical Immunosensor for Protein Detection. Anal Chem. 2013; 85:1784–1791. [PubMed: 23289608]

221. (a) Wei Y, Li Y, Zhang N, Shi G, Jin L. Ultrasound-Radiated Synthesis of Pamam-Au Nanocomposites and Its Application on Glucose Biosensor. Ultrason Sonochem. 2010; 17:17–20. [PubMed: 19695942] (b) Crespilho FN, Emilia Ghica M, Florescu M, Nart FC, Oliveira ON, Brett CMA. A Strategy for Enzyme Immobilization on Layer-by-Layer Dendrimer-Gold Nanoparticle Electrocatalytic Membrane Incorporating Redox Mediator. Electrochem Commun. 2006; 8:1665–1670.

222. Kavosi B, Hallaj R, Teymourian H, Salimi A. Au Nanoparticles/Pamam Dendrimer Functionalized Wired Ethylene-amine-Viologen as Highly Efficient Interface for Ultra-Sensitive α-Fetoprotein Electrochemical Immunosensor. Biosens Bioelectron. 2014; 59:389–396. [PubMed: 24755256]

223. Arotiba O, Owino J, Songa E, Hendricks N, Waryo T, Jahed N, Baker P, Iwuoha E. An Electrochemical DNA Biosensor Developed on a Nanocomposite Platform of Gold and Poly-(Propyleneimine) Dendrimer. Sensors. 2008; 8:6791–6809. [PubMed: 27873900]

224. Du D, Ding J, Cai J, Zhang A. One-Step Electrochemically Deposited Interface of Chitosan-Gold Nanoparticles for Acetylcholinesterase Biosensor Design. J Electroanal Chem. 2007; 605:53–60.

225. (a) Qiu JD, Liang RP, Wang R, Fan LX, Chen YW, Xia XH. A Label-Free Amperometric Immunosensor Based on Biocompatible Conductive Redox Chitosan-Ferrocene/Gold Nanoparticles Matrix. Biosens Bioelectron. 2009; 25:852–857. [PubMed: 19767192] (b) He X, Yuan R, Chai Y, Shi Y. A Sensitive Amperometric Immunosensor for Carcinoembryonic Antigen Detection with Porous Nanogold Film and Nano-Au/Chitosan Composite as Immobilization Matrix. J Biochem Biophys Methods. 2008; 70:823–829. [PubMed: 17669503] (c) Liu Y, Yuan R, Chai Y, Hong C, Liu K, Guan S. Ultrasensitive Amperometric Immunosensor for the Determination of Carcinoembryonic Antigen Based on a Porous Chitosan and Gold Nanoparticles Functionalized Interface. Microchim Acta. 2009; 167:217–224.

226. (a) Tang DP, Yuan R, Chai YQ, Zhong X, Liu Y, Dai JY, Zhang LY. Novel Potentiometric Immunosensor for Hepatitis B Surface Antigen Using a Gold Nanoparticle-Based Biomolecular Immobilization Method. Anal Biochem. 2004; 333:345–350. [PubMed: 15450811] (b) Tang D, Yuan R, Chai Y, Dai J, Zhong X, Liu Y. A Novel Immunosensor Based on Immobilization of Hepatitis B Surface Antibody on Platinum Electrode Modified Colloidal Gold and Polyvinyl Butyral as Matrices Via Electrochemical Impedance Spectroscopy. Bioelectrochemistry. 2004; 65:15–22. [PubMed: 15522687]

227. (a) Wang J, Li JH, Baca AJ, Hu JB, Zhou FM, Yan W, Pang DW. Amplified Voltammetric Detection of DNA Hybridization Via Oxidation of Ferrocene Caps on Gold Nanoparticle/Streptavidin Conjugates. Anal Chem. 2003; 75:3941–3945. [PubMed: 14572067] (b) Wang J, Zhu X, Tu Q, Guo Q, Zarui CS, Momand J, Sun XZ, Zhou F. Capture of P53 by Electrodes Modified with Consensus DNA Duplexes and Amplified Voltammetric Detection Using Ferrocene-Capped Gold Nanoparticle/Streptavidin Conjugates. Anal Chem. 2008; 80:769–774. [PubMed: 18179182] (c) Wang J, Yi X, Tang H, Han H, Wu M, Zhou F. Direct Quantification of MicroRNA at Low Picomolar Level in Sera of Glioma Patients Using a Competitive Hybridization Followed by Amplified Voltammetric Detection. Anal Chem. 2012; 84:6400–6406. [PubMed: 22788545]

228. Jie G-F, Liu P, Zhang S-S. Highly Enhanced Electro-chemiluminescence of Novel Gold/Silica/CdSe-Cds Nanostructures for Ultrasensitive Immunoassay of Protein Tumor Marker. Chem Commun. 2010; 46:1323–1325.

229. Li J, Gao H, Chen Z, Wei X, Yang CF. An Electrochemical Immunosensor for Carcinoembryonic Antigen Enhanced by Self-Assembled Nanogold Coatings on Magnetic Particles. Anal Chim Acta. 2010; 665:98–104. [PubMed: 20381697]

230. (a) Zhuo Y, Yuan R, Chai Y, Zhang Y, Li Xl, Zhu Q, Wang N. An Amperometric Immunosensor Based on Immobilization of Hepatitis B Surface Antibody on Gold Electrode Modified Gold Nanoparticles and Horseradish Peroxidase. Anal Chim Acta. 2005; 548:205–210.(b) Zhuo Y, Yu R, Yuan R, Chai Y, Hong C. Enhancement of Carcinoembryonic Antibody Immobilization on Gold Electrode Modified by Gold Nanoparticles and Sio2/Thionine Nanocomposite. J Electroanal Chem. 2009; 628:90–96.(c) Li X, Yuan R, Chai Y, Zhang L, Zhuo Y, Zhang Y. Amperometric Immunosensor Based on Toluidine Blue/Nano-Au through Electrostatic Interaction for Determination of Carcinoembryonic Antigen. J Biotechnol. 2006; 123:356–366. [PubMed: 16522340] (d) Li N, Zhao H, Yuan R, Peng K, Chai Y. An Amperometric Immunosensor with a DNA Polyion Complex Membrane/Gold Nanoparticles-Backbone for Antibody Immobilisation. Electrochim Acta. 2008; 54:235–241.(e) Liao Y, Yuan R, Chai Y, Zhuo Y, Yang X. Study on an Amperometric Immunosensor Based on Nafion-Cysteine Composite Membrane for Detection of Carcinoembryonic Antigen. Anal Biochem. 2010; 402:47–53. [PubMed: 20230773] (f) Yuan Y, Yuan R, Chai Y, Zhuo Y, Mao L, Yuan S. A Novel Label-Free Electrochemical Immunosensor for Carcinoembryonic Antigen Detection Based on the [Ag-Ag_2O]/SiO_2 Nanocomposite Material as a Redox Probe. J Electroanal Chem. 2010; 643:15–19. (g) Liu Z, Yuan R, Chai Y, Zhuo Y, Hong C, Yang X. Highly Sensitive, Reagentless Amperometric Immunosensor Based on a Novel Redox-Active Organic-Inorganic Composite Film. Sens Actuators, B. 2008; 134:625–631.(h) Zhuo Y, Yuan R, Chai Y, Sun A, Zhang Y, Yang J. A Tris(2,2′-Bipyridyl)Cobalt(III)-Bovine Serum Albumin Composite Membrane for Biosensors. Biomaterials. 2006; 27:5420–5429. [PubMed: 16843525]

231. Zhou F, Lu M, Wang W, Bian Z-P, Zhang J-R, Zhu J-J. Electrochemical Immunosensor for Simultaneous Detection of Dual Cardiac Markers Based on a Poly(Dimethylsiloxane)-Gold Nanoparticles Composite Microfluidic Chip: A Proof of Principle. Clin Chem. 2010; 56:1701–1707. [PubMed: 20852134]

232. Jeanmaire DL, Van Duyne RP. Surface Raman Spectroelectrochemistry: Part I. Heterocyclic, Aromatic, and Aliphatic Amines Adsorbed on the Anodized Silver Electrode. J Electroanal Chem. 1977; 84:1.

233. Braun G, Lee SJ, Dante M, Nguyen T-Q, Moskovits M, Reich N. Surface-Enhanced Raman Spectroscopy for DNA Detection by Nanoparticle Assembly onto Smooth Metal Films. J Am Chem Soc. 2007; 129:6378–6379. [PubMed: 17469825]

234. (a) Kneipp J, Kneipp H, Kneipp K. SERS-a Single-Molecule and Nanoscale Tool for Bioanalytics. Chem Soc Rev. 2008; 37:1052–1060. [PubMed: 18443689] (b) Le Ru EC, Grand J, Sow I, Somerville WRC, Etchegoin PG, Treguer-Delapierre M, Charron G, Felidj N, Levi G, Aubard J. A Scheme for Detecting Every Single Target Molecule with Surface-Enhanced Raman Spectroscopy. Nano Lett. 2011; 11:5013–5019. [PubMed: 21985399] (c) Li JF, Huang YF, Ding Y, Yang ZL, Li SB, Zhou XS, Fan FR, Zhang W, Zhou ZY, Wu DY, Ren B, Wang ZL, Tian ZQ. Shell-Isolated Nanoparticle-Enhanced Raman Spectroscopy. Nature. 2010; 464:392–395. [PubMed: 20237566] (d) Ryder AG. Surface Enhanced Raman Scattering for Narcotic Detection and Applications to Chemical Biology. Curr Opin Chem Biol. 2005; 9:489–493. [PubMed: 16055368]

235. (a) Howes PD, Rana S, Stevens MM. Plasmonic Nanomaterials for Biodiagnostics. Chem Soc Rev. 2014; 43:3835–3853. [PubMed: 24323079] (b) Wang Y, Yan B, Chen L. SERS Tags: Novel Optical Nanoprobes for Bioanalysis. Chem Rev. 2013; 113:1391–1428. [PubMed: 23273312]

236. Barhoumi A, Zhang D, Tam F, Halas NJ. Surface-Enhanced Raman Spectroscopy of DNA. J Am Chem Soc. 2008; 130:5523–5529. [PubMed: 18373341]

237. Li M-D, Cui Y, Gao M-X, Luo J, Ren B, Tian Z-Q. Clean Substrates Prepared by Chemical Adsorption of Iodide Followed by Electrochemical Oxidation for Surface-Enhanced Raman Spectroscopic Study of Cell Membrane. Anal Chem. 2008; 80:5118–5125. [PubMed: 18489182]

238. Liu X, Huan S, Bu Y, Shen G, Yu R. Liposome-Mediated Enhancement of the Sensitivity in Immunoassay Based on Surface-Enhanced Raman Scattering at Gold Nanosphere Array Substrate. Talanta. 2008; 75:797–803. [PubMed: 18585149]

239. Hu J, Zheng P-C, Jiang J-H, Shen G-L, Yu R-Q, Liu G-K. Electrostatic Interaction Based Approach to Thrombin Detection by Surface-Enhanced Raman Spectroscopy. Anal Chem. 2009; 81:87–93. [PubMed: 19117446]

240. Cheng H-W, Luo W-Q, Wen G-L, Huan S-Y, Shen G-L, Yu R-Q. Surface-Enhanced Raman Scattering Based Detection of Bacterial Biomarker and Potential Surface Reaction Species. Analyst. 2010; 135:2993–3001. [PubMed: 20877832]

241. Premasiri WR, Lee JC, Ziegler LD. Surface-Enhanced Raman Scattering of Whole Human Blood, Blood Plasma, and Red Blood Cells: Cellular Processes and Bioanalytical Sensing. J Phys Chem B. 2012; 116:9376–9386. [PubMed: 22780445]

242. Kong KV, Dinish US, Lau WKO, Olivo M. Sensitive SERS-pH Sensing in Biological Media Using Metal Carbonyl Functionalized Planar Substrates. Biosens Bioelectron. 2014; 54:135–140. [PubMed: 24269755]

243. Yan B, Thubagere A, Premasiri WR, Ziegler LD, Dal Negro L, Reinhard BM. Engineered SERS Substrates with Multiscale Signal Enhancement: Nanoplarticle Cluster Arrays. ACS Nano. 2009; 3:1190–1202. [PubMed: 19354266]

244. Yang L, Yan B, Premasiri WR, Ziegler LD, Dal Negro L, Reinhard BM. Engineering Nanoparticle Cluster Arrays for Bacterial Biosensing: The Role of the Building Block in Multiscale SERS Substrates. Adv Funct Mater. 2010; 20:2619–2628.

245. Yan B, Hong Y, Chen T, Reinhard BM. Monitoring Enzymatic Degradation of Pericellular Matrices through SERS Stamping. Nanoscale. 2012; 4:3917–3925. [PubMed: 22659641]

246. Thacker VV, Herrmann LO, Sigle DO, Zhang T, Liedl T, Baumberg JJ, Keyser UF. DNA Origami Based Assembly of Gold Nanoparticle Dimers for Surface-Enhanced Raman Scattering. Nat Commun. 2014; 5:3448. [PubMed: 24622339]

247. He S, Liu K-K, Su S, Yan J, Mao X, Wang D, He Y, Li L-J, Song S, Fan C. Graphene-Based High-Efficiency Surface-Enhanced Raman Scattering-Active Platform for Sensitive and Multiplex DNA Detection. Anal Chem. 2012; 84:4622–4627. [PubMed: 22497579]

248. Lin C-C, Yang Y-M, Liao P-H, Chen D-W, Lin H-P, Chang H-C. A Filter-Like AuNPs@MS SERS Substrate for *Staphylococcus Aureus* Detection. Biosens Bioelectron. 2014; 53:519–527. [PubMed: 24220346]

249. Hu J, Wang Z, Li J. Gold Nanoparticles with Special Shapes: Controlled Synthesis, Surface-Enhanced Raman Scattering, and the Application in Biodetection. Sensors. 2007; 7:3299–3311.

250. El-Said WA, Kim T-H, Kim H, Choi J-W. Detection of Effect of Chemotherapeutic Agents to Cancer Cells on Gold Nanoflower Patterned Substrate Using Surface-Enhanced Raman Scattering and Cyclic Voltammetry. Biosens Bioelectron. 2010; 26:1486–1492. [PubMed: 20728335]

251. (a) Bi L, Dong J, Xie W, Lu W, Tong W, Tao L, Qian W. Bimetallic Gold-Silver Nanoplate Array as a Highly Active SERS Substrate for Detection of Streptavidin/Biotin Assemblies. Anal Chim Acta. 2013; 805:95–100. [PubMed: 24296148] (b) Bi L, Rao Y, Tao Q, Dong J, Su T, Liu F, Qian W. Fabrication of Large-Scale Gold Nanoplate Films as Highly Active SERS Substrates for Label-Free DNA Detection. Biosens Bioelectron. 2013; 43:193–199. [PubMed: 23306075]

252. Rodriguez-Lorenzo L, Alvarez-Puebla RA, Pastoriza-Santos I, Mazzucco S, Stephan O, Kociak M, Liz-Marzan LM, Javier Garcia de Abajo F. Zeptomol Detection through Controlled Ultrasensitive Surface-Enhanced Raman Scattering. J Am Chem Soc. 2009; 131:4616–4618. [PubMed: 19292448]

253. Li L, Hutter T, Steiner U, Mahajan S. Single Molecule SERS and Detection of Biomolecules with a Single Gold Nanoparticle on a Mirror Junction. Analyst. 2013; 138:4574–4578. [PubMed: 23748709]

254. Kang T, Yoon I, Kim J, Hee H, Kim B. An Nanowire-Au Nanoparticles Conjugated System Which Provides Micrometer Size Molecular Sensors. Chem—Eur J. 2010; 16:1351–1355. [PubMed: 19967728]

255. Ni J, Lipert RJ, Dawson GB, Porter MD. Immunoassay Readout Method Using Extrinsic Raman Labels Adsorbed on Immunogold Colloids. Anal Chem. 1999; 71:4903–4908. [PubMed: 10565281]

256. Grubisha DS, Lipert RJ, Park HY, Driskell J, Porter MD. Femtomolar Detection of Prostate-Specific Antigen: An Immunoassay Based on Surface-Enhanced Raman Scattering and Immunogold Labels. Anal Chem. 2003; 75:5936–5943. [PubMed: 14588035]

257. Driskell JD, Kwarta KM, Lipert RJ, Porter MD, Neill JD, Ridpath JF. Low-Level Detection of Viral Pathogens by a Surface-Enhanced Raman Scattering Based Immunoassay. Anal Chem. 2005; 77:6147–6154. [PubMed: 16194072]

258. Driskell JD, Uhlenkamp JM, Lipert RJ, Porter MD. Surface-Enhanced Raman Scattering Immunoassays Using a Rotated Capture Substrate. Anal Chem. 2007; 79:4141–4148. [PubMed: 17487976]

259. Narayanan R, Lipert RJ, Porter MD. Cetyltrimethy-lammonium Bromide-Modified Spherical and Cube-Like Gold Nanoparticles as Extrinsic Raman Labels in Surface-Enhanced Raman Spectroscopy Based Heterogeneous Immunoassays. Anal Chem. 2008; 80:2265–2271. [PubMed: 18290676]

260. (a) Wang G, Park HY, Lipert RJ. Mixed Monolayers on Gold Nanoparticle Labels for Multiplexed Surface-Enhanced Raman Scattering Based Immunoassays. Anal Chem. 2009; 81:9643–9650. [PubMed: 19874000] (b) Wang G, Lipert RJ, Jain M, Kaur S, Chakraboty S, Torres MP, Batra SK, Brand RE, Porter MD. Detection of the Potential Pancreatic Cancer Marker Muc4 in Serum Using Surface-Enhanced Raman Scattering. Anal Chem. 2011; 83:2554–2561. [PubMed: 21391573]

261. Lin C-C, Yang Y-M, Chen Y-F, Yang T-S, Chang H-C. A New Protein a Assay Based on Raman Reporter Labeled Immunogold Nanoparticles. Biosens Bioelectron. 2008; 24:178–183. [PubMed: 18468881]

262. (a) Lee M, Lee S, Lee JH, Lim HW, Seong GH, Lee EK, Chang SI, Oh CH, Choo J. Highly Reproducible Immunoassay of Cancer Markers on a Gold-Patterned Microarray Chip Using Surface-Enhanced Raman Scattering Imaging. Biosens Bioelectron. 2011; 26:2135–2141. [PubMed: 20926277] (b) Lee M, Lee K, Kim KH, Oh KW, Choo J. SERS-Based Immunoassay Using a Gold Array-Embedded Gradient Microfluidic Chip. Lab Chip. 2012; 12:3720–3727. [PubMed: 22797080]

263. (a) Song C, Wang Z, Zhang R, Yang J, Tan X, Cui Y. Highly Sensitive Immunoassay Based on Raman Reporter-Labeled Immuno-Au Aggregates and SERS-Active Immune Substrate. Biosens Bioelectron. 2009; 25:826–831. [PubMed: 19765972] (b) Wang Z, Zong S, Chen H, Wu H, Cui Y. Silica Coated Gold Nanoaggregates Prepared by Reverse Microemulsion Method: Dual Mode Probes for Multiplex Immunoassay Using SERS and Fluorescence. Talanta. 2011; 86:170–177. [PubMed: 22063527] (c) Wang Z, Zong S, Li W, Wang C, Xu S, Chen H, Cui Y. SERS-Fluorescence Joint Spectral Encoding Using Organic-Metal-QD Hybrid Nanoparticles with a Huge Encoding Capacity for High-Throughput Biodetection: Putting Theory into Practice. J Am Chem Soc. 2012; 134:2993–3000. [PubMed: 22239121]

264. Cao YC, Jin RC, Nam JM, Thaxton CS, Mirkin CA. Raman Dye-Labeled Nanoparticle Probes for Proteins. J Am Chem Soc. 2003; 125:14676–14677. [PubMed: 14640621]

265. Xu SP, Ji XH, Xu WQ, Li XL, Wang LY, Bai YB, Zhao B, Ozaki Y. Immunoassay Using Probe-Labelling Immunogold Nanoparticles with Silver Staining Enhancement Via Surface-Enhanced Raman Scattering. Analyst. 2004; 129:63–68. [PubMed: 14737585]

266. Cui Y, Ren B, Yao JL, Gu RA, Tian ZQ. Synthesis of Agcoreaushell Bimetallic Nanoparticles for Immunoassay Based on Surface-Enhanced Raman Spectroscopy. J Phys Chem B. 2006; 110:4002–4006. [PubMed: 16509689]

267. Shen A, Chen L, Xie W, Hu J, Zeng A, Richards R, Hu J. Triplex Au-Ag-C Core Shell Nanoparticles as a Novel Raman Label. Adv Funct Mater. 2010; 20:969–975.

268. Cao YWC, Jin RC, Mirkin CA. Nanoparticles with Raman Spectroscopic Fingerprints for DNA and RNA Detection. Science. 2002; 297:1536–1540. [PubMed: 12202825]

269. Kang T, Yoo SM, Yoon I, Lee SY, Kim B. Patterned Multiplex Pathogen DNA Detection by Au Particle-on-Wire SERS Sensor. Nano Lett. 2010; 10:1189–1193. [PubMed: 20222740]

270. Sun L, Yu C, Irudayaraj J. Raman Multiplexers for Alternative Gene Splicing. Anal Chem. 2008; 80:3342–3349. [PubMed: 18341356]

271. Sun L, Irudayaraj J. PCR-Free Quantification of Multiple Splice Variants in a Cancer Gene by Surface-Enhanced Raman Spectroscopy. J Phys Chem B. 2009; 113:14021–14025. [PubMed: 19780515]

272. Hu J, Zheng P-C, Jiang J-H, Shen G-L, Yu R-Q, Liu G-K. Sub-Attomolar HIV-1 DNA Detection Using Surface-Enhanced Raman Spectroscopy. Analyst. 2010; 135:1084–1089. [PubMed: 20419260]

273. Hu J, Zhang C-y. Sensitive Detection of Nucleic Acids with Rolling Circle Amplification and Surface-Enhanced Raman Scattering Spectroscopy. Anal Chem. 2010; 82:8991–8997. [PubMed: 20919697]

274. Li M, Zhang J, Suri S, Sooter LJ, Ma D, Wu N. Detection of Adenosine Triphosphate with an Aptamer Biosensor Based on Surface-Enhanced Raman Scattering. Anal Chem. 2012; 84:2837–2842. [PubMed: 22380526]

275. (a) Wang Y, Wei H, Li B, Ren W, Guo S, Dong S, Wang E. SERS Opens a New Way in Aptasensor for Protein Recognition with High Sensitivity and Selectivity. Chem Commun. 2007:5220–5222.(b) Chen X, Liu H, Zhou X, Hu J. Core-Shell Nanostructures for Ultrasensitive Detection of Alpha-Thrombin. Nanoscale. 2010; 2:2841–2846. [PubMed: 20877894]

276. Hu Y, Liao J, Wang D, Li G. Fabrication of Gold Nanoparticle-Embedded Metal-Organic Framework for Highly Sensitive Surface-Enhanced Raman Scattering Detection. Anal Chem. 2014; 86:3955–3963. [PubMed: 24646316]

277. Ruan C, Wang W, Gu B. Detection of Alkaline Phosphatase Using Surface-Enhanced Raman Spectroscopy. Anal Chem. 2006; 78:3379–3384. [PubMed: 16689540]

278. Al-Ogaidi I, Gou H, Al-Kazaz AKA, Aguilar ZP, Melconian AK, Zheng P, Wu N. A Gold@ Silica Core-Shell Nanoparticle-Based Surface-Enhanced Raman Scattering Biosensor for Label-Free Glucose Detection. Anal Chim Acta. 2014; 811:76–80. [PubMed: 24456597]

279. (a) Lin D, Feng S, Pan J, Chen Y, Lin J, Chen G, Xie S, Zeng H, Chen R. Colorectal Cancer Detection by Gold Nanoparticle Based Surface-Enhanced Raman Spectroscopy of Blood Serum and Statistical Analysis. Opt Express. 2011; 19:13565–13577. [PubMed: 21747512] (b) Kahraman M, Zamaleeva AI, Fakhrullin RF, Culha M. Layer-by-Layer Coating of Bacteria with Noble Metal Nanoparticles for Surface-Enhanced Raman Scattering. Anal Bioanal Chem. 2009; 395:2559–2567. [PubMed: 19795108] (c) Harpster MH, Zhang H, Sankara-Warrier AK, Ray BH, Ward TR, Kollmar JP, Carron KT, Mecham JO, Corcoran RC, Wilson WC. SERS Detection of Indirect Viral DNA Capture Using Colloidal Gold and Methylene Blue as a Raman Label. Biosens Bioelectron. 2009; 25:674–681. [PubMed: 19740646]

280. Kneipp J, Li X, Sherwood M, Panne U, Kneipp H, Stockman MI, Kneipp K. Gold Nanolenses Generated by Laser Ablation-Efficient Enhancing Structure for Surface Enhanced Raman Scattering Analytics and Sensing. Anal Chem. 2008; 80:4247–4251. [PubMed: 18439029]

281. Hu J, Zhang C-y. Single Base Extension Reaction-Based Surface Enhanced Raman Spectroscopy for DNA Methylation Assay. Biosens Bioelectron. 2012; 31:451–457. [PubMed: 22129682]

282. Ye S, Yang Y, Xiao J, Zhang S. Surface-Enhanced Raman Scattering Assay Combined with Autonomous DNA Machine for Detection of Specific DNA and Cancer Cells. Chem Commun. 2012; 48:8535–8537.

283. Zheng J, Hu Y, Bai J, Ma C, Li J, Li Y, Shi M, Tan W, Yang R. Universal Surface-Enhanced Raman Scattering Amplification Detector for Ultrasensitive Detection of Multiple Target Analytes. Anal Chem. 2014; 86:2205–2212. [PubMed: 24437937]

284. (a) Huang PJ, Chau LK, Yang TS, Tay LL, Lin TT. Nanoaggregate-Embedded Beads as Novel Raman Labels for Biodetection. Adv Funct Mater. 2009; 19:242–248.(b) Huang PJ, Tay LL, Tanha J, Ryan S, Chau LK. Single-Domain Antibody-Conjugated Nanoaggregate-Embedded Beads for Targeted Detection of Pathogenic Bacteria. Chem—Eur J. 2009; 15:9330–9334. [PubMed: 19655352]

285. Manikas AC, Causa F, Della Moglie R, Netti PA. Tuning Gold Nanoparticles Interfaces by Specific Peptide Interaction for Surface Enhanced Raman Spectroscopy (SERS) and Separation Applications. ACS Appl Mater Interfaces. 2013; 5:7915–7922. [PubMed: 23862632]

286. Yi Z, Li X-Y, Liu F-J, Jin P-Y, Chu X, Yu R-Q. Design of Label-Free, Homogeneous Biosensing Platform Based on Plasmonic Coupling and Surface-Enhanced Raman Scattering Using Unmodified Gold Nanoparticles. Biosens Bioelectron. 2013; 43:308–314. [PubMed: 23353007]

287. Chen J-W, Lei Y, Liu X-J, Jiang J-H, Shen G-L, Yu R-Q. Immunoassay Using Surface-Enhanced Raman Scattering Based on Aggregation of Reporter-Labeled Immunogold Nanoparticles. Anal Bioanal Chem. 2008; 392:187–193. [PubMed: 18597080]

288. Sun L, Yu C, Irudayaraj J. Surface-Enhanced Raman Scattering Based Nonfluorescent Probe for Multiplex DNA Detection. Anal Chem. 2007; 79:3981–3988. [PubMed: 17465531]
289. Wang Y, Lee K, Irudayaraj J. SERS Aptasensor from Nanorod-Nanoparticle Junction for Protein Detection. Chem Commun. 2010; 46:613–615.
290. Qian X, Zhou X, Nie S. Surface-Enhanced Raman Nanoparticle Beacons Based on Bioconjugated Gold Nanocrystals and Long Range Plasmonic Coupling. J Am Chem Soc. 2008; 130:14934–14935. [PubMed: 18937463]
291. Quyen TTB, Su WN, Chen KJ, Pan CJ, Rick J, Chang CC, Hwang BJ. Au@SiO_2 Core/Shell Nanoparticle Assemblage Used for Highly Sensitive SERS-Based Determination of Glucose and Uric Acid. J Raman Spectrosc. 2013; 44:1671–1677.
292. Maher R, Maier S, Cohen L, Koh L, Laromaine A, Dick J, Stevens M. Exploiting SERS Hot Spots for Disease-Specific Enzyme Detection. J Phys Chem C. 2009; 114:7231–7235.
293. Lim D-K, Jeon K-S, Kim HM, Nam J-M, Suh YD. Nanogap-Engineerable Raman-Active Nanodumbbells for Single-Molecule Detection. Nat Mater. 2009; 9:60–67. [PubMed: 20010829]
294. Lim D-K, Jeon K-S, Hwang J-H, Kim H, Kwon S, Suh YD, Nam J-M. Highly Uniform and Reproducible Surface-Enhanced Raman Scattering from DNA-Tailorable Nanoparticles with 1-nm Interior Gap. Nat Nanotechnol. 2011; 6:452–460. [PubMed: 21623360]
295. Lee K, Irudayaraj J. Correct Spectral Conversion between Surface-Enhanced Raman and Plasmon Resonance Scattering from Nanoparticle Dimers for Single-Molecule Detection. Small. 2013; 9:1106–1115. [PubMed: 23281179]
296. Chon H, Lee S, Son SW, Oh CH, Choo J. Highly Sensitive Immunoassay of Lung Cancer Marker Carcinoembryonic Antigen Using Surface-Enhanced Raman Scattering of Hallow Gold Nanospheres. Anal Chem. 2009; 81:3029–3034. [PubMed: 19301845]
297. Chon H, Lee S, Yoon S-Y, Chang S-I, Lim DW, Choo J. Simultaneous Immunoassay for the Detection of Two Lung Cancer Markers Using Functionalized SERS Nanoprobes. Chem Commun. 2011; 47:12515–12517.
298. Zhang H, Harpster MH, Park HJ, Johnson PA. Surface-Enhanced Raman Scattering Detection of DNA Derived from the West Nile Virus Genome Using Magnetic Capture of Raman-Active Gold Nanoparticles. Anal Chem. 2011; 83:254–260. [PubMed: 21121693]
299. Temur E, Zengin A, Boyaci IH, Dudak FC, Torul H, Tamer U. Attomole Sensitivity of Staphylococcal Enterotoxin B Detection Using an Aptamer-Modified Surface-Enhanced Raman Scattering Probe. Anal Chem. 2012; 84:10600–10606. [PubMed: 23140575]
300. Zong S, Wang Z, Chen H, Hu G, Liu M, Chen P, Cui Y. Colorimetry and SERS Dual-Mode Detection of Telomerase Activity: Combining Rapid Screening with High Sensitivity. Nanoscale. 2014; 6:1808–1816. [PubMed: 24356868]
301. Li Y, Zeng Y, Mao Y, Lei C, Zhang S. Proximity-Dependent Isothermal Cycle Amplification for Small-Molecule Detection Based on Surface Enhanced Raman Scattering. Biosens Bioelectron. 2014; 51:304–309. [PubMed: 23994277]
302. Sha MY, Xu H, Natan MJ, Cromer R. Surface-Enhanced Raman Scattering Tags for Rapid and Homogeneous Detection of Circulating Tumor Cells in the Presence of Human Whole Blood. J Am Chem Soc. 2008; 130:17214–17215. [PubMed: 19053187]
303. Wang X, Qian X, Beitler JJ, Chen ZG, Khuri FR, Lewis MM, Shin HJC, Nie S, Shin DM. Detection of Circulating Tumor Cells in Human Peripheral Blood Using Surface-Enhanced Raman Scattering Nanoparticles. Cancer Res. 2011; 71:1526–1532. [PubMed: 21212408]
304. (a) Lee S, Chon H, Lee M, Choo J, Shin SY, Lee YH, Rhyu IJ, Son SW, Oh CH. Surface-Enhanced Raman Scattering Imaging of HER2 Cancer Markers Overexpressed in Single MCF7 Cells Using Antibody Conjugated Hollow Gold Nanospheres. Biosens Bioelectron. 2009; 24:2260–2263. [PubMed: 19056254] (b) Kyu-Lee E, Young-Shin S, Wook-Son S, Hwan-Oh C, Myong-Song J, Ho-Kang S. SERS Imaging of HER2-Overexpressed MCF7 Cells Using Antibody-Conjugated Gold Nanorods. Phys Chem Chem Phys. 2009; 11:7444–7449. [PubMed: 19690717]
305. (a) Maiti KK, Dinish U, Fu CY, Lee JJ, Soh KS, Yun SW, Bhuvaneswari R, Olivo M, Chang YT. Development of Biocompatible SERS Nanotag with Increased Stability by Chemisorption of Reporter Molecule for *in Vivo* Cancer Detection. Biosens Bioelectron. 2010; 26:398–403.

[PubMed: 20801634] (b) Samanta A, Maiti KK, Soh KS, Liao X, Vendrell M, Dinish U, Yun SW, Bhuvaneswari R, Kim H, Rautela S. Ultrasensitive Near-Infrared Raman Reporters for SERS-Based in Vivo Cancer Detection. Angew Chem, Int Ed. 2011; 50:6089–6092.(c) KumaráMaiti K. Multiplex Cancer Cell Detection by SERS Nanotags with Cyanine and Triphenylmethine Raman Reporters. Chem Commun. 2011; 47:3514–3516.

306. Lee K, Drachev VP, Irudayaraj J. DNA-Gold Nanoparticle Reversible Networks Grown on Cell Surface Marker Sites: Application in Diagnostics. ACS Nano. 2011; 5:2109–2117. [PubMed: 21314177]
307. (a) Lu W, Singh AK, Khan SA, Senapati D, Yu H, Ray PC. Gold Nano-Popcorn-Based Targeted Diagnosis, Nanotherapy Treatment, and in Situ Monitoring of Photothermal Therapy Response of Prostate Cancer Cells Using Surface-Enhanced Raman Spectroscopy. J Am Chem Soc. 2010; 132:18103–18114. [PubMed: 21128627] (b) Beqa L, Fan Z, Singh AK, Senapati D, Ray PC. Gold Nano-Popcorn Attached Swcnt Hybrid Nanomaterial for Targeted Diagnosis and Photothermal Therapy of Human Breast Cancer Cells. ACS Appl Mater Interfaces. 2011; 3:3316–3324. [PubMed: 21842867]
308. (a) Khan SA, Singh AK, Senapati D, Fan Z, Ray PC. Targeted Highly Sensitive Detection of Multi-Drug Resistant Salmonella DT104 Using Gold Nanoparticles. Chem Commun. 2011; 47:9444–9446.(b) Fan Z, Senapati D, Khan SA, Singh AK, Hamme A, Yust B, Sardar D, Ray PC. Popcorn-Shaped Magnetic Coreplasmonic Shell Multifunctional Nanoparticles for the Targeted Magnetic Separation and Enrichment, Label-Free SERS Imaging, and Photothermal Destruction of Multidrug-Resistant Bacteria. Chem—Eur J. 2013; 19:2839–2847. [PubMed: 23296491] (c) Fan Z, Kanchanapally R, Ray PC. Hybrid Graphene Oxide Based Ultrasensitive SERS Probe for Label-Free Biosensing. J Phys Chem Lett. 2013; 4:3813–3818.
309. Kneipp K, Haka AS, Kneipp H, Badizadegan K, Yoshizawa N, Boone C, Shafer-Pektier KE, Motz JT, Dasari RR, Feld MS. Surface-Enhanced Raman Spectroscopy in Single Living Cells Using Gold Nanoparticles. Appl Spectrosc. 2002; 56:150–154.
310. Kneipp J, Kneipp H, Rice WL, Kneipp K. Optical Probes for Biological Applications Based on Surface-Enhanced Raman Scattering from Indocyanine Green on Gold Nanoparticles. Anal Chem. 2005; 77:2381–2385. [PubMed: 15828770]
311. Kneipp J, Kneipp H, McLaughlin M, Brown D, Kneipp K. *In Vivo* Molecular Probing of Cellular Compartments with Gold Nanoparticles and Nanoaggregates. Nano Lett. 2006; 6:2225–2231. [PubMed: 17034088]
312. Drescher D, Büchner T, McNaughton D, Kneipp J. SERS Reveals the Specific Interaction of Silver and Gold Nanoparticles with Hemoglobin and Red Blood Cell Components. Phys Chem Chem Phys. 2013; 15:5364–5373. [PubMed: 23426381]
313. Xie W, Wang L, Zhang Y, Su L, Shen A, Tan J, Hu J. Nuclear Targeted Nanoprobe for Single Living Cell Detection by Surface-Enhanced Raman Scattering. Bioconjugate Chem. 2009; 20:768–773.
314. Sathuluri RR, Yoshikawa H, Shimizu E, Saito M, Tamiya E. Gold Nanoparticle-Based Surface-Enhanced Raman Scattering for Noninvasive Molecular Probing of Embryonic Stem Cell Differentiation. PLoS One. 2011; 6:e22802. [PubMed: 21829653]
315. Smith NI, Taguchi A, Inouye Y, Kawata S, Fujita K, Ishitobi S, Hamada K. Time-Resolved Observation of Surface-Enhanced Raman Scattering from Gold Nanoparticles During Transport through a Living Cell. J Biomed Opt. 2009; 14:024038. [PubMed: 19405766]
316. Ando J, Fujita K, Smith NI, Kawata S. Dynamic SERS Imaging of Cellular Transport Pathways with Endocytosed Gold Nanoparticles. Nano Lett. 2011; 11:5344–5348. [PubMed: 22059676]
317. (a) Kneipp J, Kneipp H, Wittig B, Kneipp K. One-and Two-Photon Excited Optical pH Probing for Cells Using Surface-Enhanced Raman and Hyper-Raman Nanosensors. Nano Lett. 2007; 7:2819–2823. [PubMed: 17696561] (b) Kneipp J, Kneipp H, Wittig B, Kneipp K. Following the Dynamics of pH in Endosomes of Live Cells with SERS Nanosensors. J Phys Chem C. 2010; 114:7421–7426.(c) Ochsen-kuhn MA, Jess PR, Stoquert H, Dholakia K, Campbell CJ. Nanoshells for Surface-Enhanced Raman Spectroscopy in Eukaryotic Cells: Cellular Response and Sensor Development. ACS Nano. 2009; 3:3613–3621. [PubMed: 19807067]

318. Lawson L, Huser T. Synthesis and Characterization of a Disulfide Reporter Molecule for Enhancing pH Measurements Based on Surface-Enhanced Raman Scattering. Anal Chem. 2012; 84:3574–3580. [PubMed: 22455337]

319. Cong VT, Ganbold E-O, Saha JK, Jang J, Min J, Choo J, Kim S, Song NW, Son SJ, Lee SB. Gold Nanoparticle Silica Nanopeapods. J Am Chem Soc. 2014; 136:3833–3841. [PubMed: 24517321]

320. Ock K, Jeon WI, Ganbold EO, Kim M, Park J, Seo JH, Cho K, Joo S-W, Lee SY. Real-Time Monitoring of Glutathione-Triggered Thiopurine Anticancer Drug Release in Live Cells Investigated by Surface-Enhanced Raman Scattering. Anal Chem. 2012; 84:2172–2178. [PubMed: 22280519]

321. Tang H-W, Yang XB, Kirkham J, Smith DA. Probing Intrinsic and Extrinsic Components in Single Osteosarcoma Cells by Near-Infrared Surface-Enhanced Raman Scattering. Anal Chem. 2007; 79:3646–3653. [PubMed: 17441678]

322. Kang B, Afifi MM, Austin LA, El-Sayed MA. Exploiting the Nanoparticle Plasmon Effect: Observing Drug Delivery Dynamics in Single Cells Via Raman/Fluorescence Imaging Spectroscopy. ACS Nano. 2013; 7:7420–7427. [PubMed: 23909658]

323. (a) Yuan H, Fales AM, Khoury CG, Liu J, Vo-Dinh T. Spectral Characterization and Intracellular Detection of Surface-Enhanced Raman Scattering (SERS)-Encoded Plasmonic Gold Nanostars. J Raman Spectrosc. 2013; 44:234–239. [PubMed: 24839346] (b) Rodriguez-Lorenzo L, Krpetic Z, Barbosa S, Alvarez-Puebla RA, Liz-Marzan LM, Prior IA, Brust M. Intracellular Mapping with SERS-Encoded Gold Nanostars. Integr Biol. 2011; 3:922–926.

324. Li Q, Jiang Y, Han R, Zhong X, Liu S, Li ZY, Sha Y, Xu D. High Surface-Enhanced Raman Scattering Performance of Individual Gold Nanoflowers and Their Application in Live Cell Imaging. Small. 2013; 9:927–932. [PubMed: 23180641]

325. Xie J, Zhang Q, Lee JY, Wang DI. The Synthesis of SERS-Active Gold Nanoflower Tags for *in Vivo* Applications. ACS Nano. 2008; 2:2473–2480. [PubMed: 19206281]

326. Lee S, Kim S, Choo J, Shin SY, Lee YH, Choi HY, Ha S, Kang K, Oh CH. Biological Imaging of Hek293 Cells Expressing Plcγ1 Using Surface-Enhanced Raman Microscopy. Anal Chem. 2007; 79:916–922. [PubMed: 17263316]

327. Wu P, Gao Y, Zhang H, Cai C. Aptamer-Guided Silver-Gold Bimetallic Nanostructures with Highly Active Surface-Enhanced Raman Scattering for Specific Detection and Near-Infrared Photothermal Therapy of Human Breast Cancer Cells. Anal Chem. 2012; 84:7692–7699. [PubMed: 22925013]

328. Song J, Duan B, Wang C, Zhou J, Pu L, Fang Z, Wang P, Lim TT, Duan H. SERS-Encoded Nanogapped Plasmonic Nanoparticles: Growth of Metallic Nanoshell by Templating Redox-Active Polymer Brushes. J Am Chem Soc. 2014; 136:6838–6841. [PubMed: 24773367]

329. Gandra N, Singamaneni S. Bilayered Raman-Intense Gold Nanostructures with Hidden Tags (Brights) for High-Resolution Bioimaging. Adv Mater. 2013; 25:1022–1027. [PubMed: 23161698]

330. Palonpon AF, Ando J, Yamakoshi H, Dodo K, Sodeoka M, Kawata S, Fujita K. Raman and SERS Microscopy for Molecular Imaging of Live Cells. Nat Protoc. 2013; 8:677–692. [PubMed: 23471112]

331. Kneipp J, Kneipp H, Rajadurai A, Redmond RW, Kneipp K. Optical Probing and Imaging of Live Cells Using SERS Labels. J Raman Spectrosc. 2009; 40:1–5.

332. Tam NC, McVeigh PZ, MacDonald TD, Farhadi A, Wilson BC, Zheng G. Porphyrin-Lipid Stabilized Gold Nanoparticles for Surface Enhanced Raman Scattering Based Imaging. Bioconjugate Chem. 2012; 23:1726–1730.

333. (a) Kong KV, Lam Z, Goh WD, Leong WK, Olivo M. Metal Carbonyl-Gold Nanoparticle Conjugates for Live-Cell SERS Imaging. Angew Chem, Int Ed. 2012; 51:9796–9799.(b) Kong KV, Lam Z, Lau WKO, Leong WK, Oivo M. A Transition Metal Carbonyl Probe for Use in a Highly Specific and Sensitive SERS-Based Assay for Glucose. J Am Chem Soc. 2013; 135:18028–18031. [PubMed: 24168766]

334. (a) Kong KV, Ho CJH, Gong T, Lau WKO, Olivo M. Sensitive SERS Glucose Sensing in Biological Media Using Alkyne Functionalized Boronic Acid on Planar Substrates. Biosens Bioelectron. 2014; 56:186–191. [PubMed: 24487255] (b) Lin L, Tian X, Hong S, Dai P, You Q,

Wang R, Feng L, Xie C, Tian ZQ, Chen X. A Bioorthogonal Raman Reporter Strategy for SERS Detection of Glycans on Live Cells. Angew Chem, Int Ed. 2013; 52:7266–7271.(c) Yamakoshi H, Dodo K, Okada M, Ando J, Palonpon A, Fujita K, Kawata S, Sodeoka M. Imaging of Edu, an Alkyne-Tagged Cell Proliferation Probe, by Raman Microscopy. J Am Chem Soc. 2011; 133:6102–6105. [PubMed: 21443184] (d) Yamakoshi H, Dodo K, Palonpon A, Ando J, Fujita K, Kawata S, Sodeoka M. Alkyne-Tag Raman Imaging for Visualization of Mobile Small Molecules in Live Cells. J Am Chem Soc. 2012; 134:20681–20689. [PubMed: 23198907]

335. Huang Y, Swarup VP, Bishnoi SW. Rapid Raman Imaging of Stable, Functionalized Nanoshells in Mammalian Cell Cultures. Nano Lett. 2009; 9:2914–2920. [PubMed: 19572746]
336. Liu X, Knauer M, Ivleva NP, Niessner R, Haisch C. Synthesis of Core-Shell Surface-Enhanced Raman Tags for Bioimag-ing. Anal Chem. 2010; 82:441–446. [PubMed: 19957963]
337. Lee S, Chon H, Yoon S, Lee E, Chang S, Lim D, Choo J. Fabrication of SERS-Fluorescence Dual Modal Nanoprobes and Application to Multiplex Cancer Cell Imaging. Nanoscale. 2012; 4:124–129. [PubMed: 22080302]
338. Wang Z, Zong S, Yang J, Li J, Cui Y. Dual-Mode Probe Based on Mesoporous Silica Coated Gold Nanorods for Targeting Cancer Cells. Biosens Bioelectron. 2011; 26:2883–2889. [PubMed: 21177092]
339. Wang Z, Wu H, Wang C, Xu S, Cui Y. Gold Aggregates-and Quantum Dots-Embedded Nanospheres: Switchable Dual-Mode Image Probes for Living Cells. J Mater Chem. 2011; 21:4307–4313.
340. Cui Y, Zheng X-S, Ren B, Wang R, Zhang J, Xia N-S, Tian Z-Q. Au@ Organosilica Multifunctional Nanoparticles for the Multimodal Imaging. Chem Sci. 2011; 2:1463–1469.
341. Martinez AW, Phillips ST, Butte MJ, Whitesides GM. Patterned Paper as a Platform for Inexpensive, Low-Volume, Portable Bioassays. Angew Chem, Int Ed. 2007; 46:1318–1320.
342. Martinez AW, Phillips ST, Carrilho E, Thomas SW, Sindi H, Whitesides GM. Simple Telemedicine for Developing Regions: Camera Phones and Paper-Based Microfluidic Devices for Real-Time, Off-Site Diagnosis. Anal Chem. 2008; 80:3699–3707. [PubMed: 18407617]
343. Martinez AW, Phillips ST, Whitesides GM, Carrilho E. Diagnostics for the Developing World: Microfluidic Paper-Based Analytical Devices. Anal Chem. 2010; 82:3–10. [PubMed: 20000334]
344. (a) Lee DS, Jeon BG, Ihm C, Park JK, Jung MY. A Simple and Smart Telemedicine Device for Developing Regions: A Pocket-Sized Colorimetric Reader. Lab Chip. 2011; 11:120–126. [PubMed: 21109898] (b) Delaney JL, Doeven EH, Harsant AJ, Hogan CF. Use of a Mobile Phone for Potentiostatic Control with Low Cost Paper-Based Microfluidic Sensors. Anal Chim Acta. 2013; 790:56–60. [PubMed: 23870409] (c) Nemiroski A, Christodouleas DC, Hennek JW, Kumar AA, Maxwell EJ, Teresa Fernandez-Abedul M, Whitesides GM. Universal Mobile Electrochemical Detector Designed for Use in Resource-Limited Applications. Proc Natl Acad Sci USA. 2014; 111:11984–11989. [PubMed: 25092346]
345. Zhao W, Ali MM, Aguirre SD, Brook MA, Li Y. Paper-Based Bioassays Using Gold Nanoparticle Colorimetric Probes. Anal Chem. 2008; 80:8431–8437. [PubMed: 18847216]
346. (a) Cheng CM, Martinez AW, Gong J, Mace CR, Phillips ST, Carrilho E, Mirica KA, Whitesides GM. Paper-Based ELISA. Angew Chem, Int Ed. 2010; 49:4771–4774.(b) Hsu CK, Huang HY, Chen WR, Nishie W, Ujiie H, Natsuga K, Fan ST, Wang HK, Lee JYY, Tsai WL, Shimizu H, Cheng CM. Paper-Based ELISA for the Detection of Autoimmune Antibodies in Body Fluid-the Case of Bullous Pemphigoid. Anal Chem. 2014; 86:4605–4610. [PubMed: 24708084]
347. Murdock RC, Shen L, Griffin DK, Kelley-Loughnane N, Papautsky I, Hagen JA. Optimization of a Paper-Based ELISA for a Human Performance Biomarker. Anal Chem. 2013; 85:11634–11642. [PubMed: 24206087]
348. Nie J, Zhang Y, Lin L, Zhou C, Li S, Zhang L, Li J. Low-Cost Fabrication of Paper-Based Microfluidic Devices by OneStep Plotting. Anal Chem. 2012; 84:6331–6335. [PubMed: 22881397]
349. Choi DH, Lee SK, Oh YK, Bae BW, Lee SD, Kim S, Shin Y-B, Kim M-G. A Dual Gold Nanoparticle Conjugate-Based Lateral Flow Assay (LFA) Method for the Analysis of Troponin I. Biosens Bioelectron. 2010; 25:1999–2002. [PubMed: 20167468]

350. Lu J, Ge S, Ge L, Yan M, Yu J. Electrochemical DNA Sensor Based on Three-Dimensional Folding Paper Device for Specific and Sensitive Point-of-Care Testing. Electrochim Acta. 2012; 80:334–341.

351. Ge L, Wang S, Yu J, Li N, Ge S, Yan M. Molecularly Imprinted Polymer Grafted Porous Au-Paper Electrode for an Microfluidic Electro-Analytical Origami Device. Adv Funct Mater. 2013; 23:3115–3123.

352. (a) Kong FY, Gu SX, Li WW, Chen TT, Xu Q, Wang W. A Paper Disk Equipped with Graphene/Polyaniline/Au Nanoparticles/Glucose Oxidase Biocomposite Modified Screen-Printed Electrode: Toward Whole Blood Glucose Determination. Biosens Bioelectron. 2014; 56:77–82. [PubMed: 24469540] (b) Wang Y, Xu J, Ma C, Li S, Yu J, Ge S, Yan M. A Chemiluminescence Excited Photo-electrochemistry Aptamer-Device Equipped with a Tin Dioxide Quantum Dot/Reduced Graphene Oxide Nanocomposite Modified Porous Au-Paper Electrode. J Mater Chem B. 2014; 2:3462–3468.(c) Li L, Xu J, Zheng X, Ma C, Song X, Ge S, Yu J, Yan M. Growth of Gold-Manganese Oxide Nanostructures on a 3D Origami Device for Glucose-Oxidase Label Based Electrochemical Immunosensor. Biosens Bioelectron. 2014; 61:76–82. [PubMed: 24858676] (d) Wang Y, Ge L, Ma C, Kong Q, Yan M, Ge S, Yu J. Self-Powered and Sensitive DNA Detection in a Three-Dimensional Origami-Based Biofuel Cell Based on a Porous Pt-Paper Cathode. Chem—Eur J. 2014; 20:12453–12462. [PubMed: 25111016] (e) Li L, Li W, Yang H, Ma C, Yu J, Yan M, Song X. Sensitive Origami Dual-Analyte Electrochemical Immunodevice Based on Polyaniline/Au-Paper Electrode and Multi-Labeled 3d Graphene Sheets. Electrochim Acta. 2014; 120:102–109.

353. (a) Myers FB, Lee LP. Innovations in Optical Microfluidic Technologies for Point-of-Care Diagnostics. Lab Chip. 2008; 8:2015. [PubMed: 19023464] (b) Yetisen AK, Akram MS, Lowe CR. Paper-Based Microfluidic Point-of-Care Diagnostic Devices. Lab Chip. 2013; 13:2210–2251. [PubMed: 23652632]

354. (a) Mark D, Haeberle S, Roth G, von Stetten F, Zengerle R. Microfluidic Lab-on-a-Chip Platforms: Requirements, Characteristics and Applications. Chem Soc Rev. 2010; 39:1153–1182. [PubMed: 20179830] (b) Gubala V, Harris LF, Ricco AJ, Tan MX, Williams DE. Point of Care Diagnostics: Status and Future. Anal Chem. 2012; 84:487–515. [PubMed: 22221172]

355. Mao X, Ma Y, Zhang A, Zhang L, Zeng L, Liu G. Disposable Nucleic Acid Biosensors Based on Gold Nanoparticle Probes and Lateral Flow Strip. Anal Chem. 2009; 81:1660–1668. [PubMed: 19159221]

356. He Y, Zhang S, Zhang X, Baloda M, Gurung AS, Xu H, Zhang X, Liu G. Ultrasensitive Nucleic Acid Biosensor Based on Enzyme-Gold Nanoparticle Dual Label and Lateral Flow Strip Biosensor. Biosens Bioelectron. 2011; 26:2018–2024. [PubMed: 20875950]

357. Gao X, Xu H, Baloda M, Gurung AS, Xu L-P, Wang T, Zhang X, Liu G. Visual Detection of MicroRNA with Lateral Flow Nucleic Acid Biosensor. Biosens Bioelectron. 2014; 54:578–584. [PubMed: 24333569]

358. Li J, Zou M, Chen Y, Xue Q, Zhang F, Li B, Wang Y, Qi X, Yang Y. Gold Immunochromatographic Strips for Enhanced Detection of Avian Influenza and Newcastle Disease Viruses. Anal Chim Acta. 2013; 782:54–58. [PubMed: 23708284]

359. Choi DH, Lee SK, Oh YK, Bae BW, Lee SD, Kim S, Shin Y-B, Kim M-G. A Dual Gold Nanoparticle Conjugate-Based Lateral Flow Assay (LFA) Method for the Analysis of Troponin I. Biosens Bioelectron. 2010; 25:1999–2002. [PubMed: 20167468]

360. Hu J, Wang L, Li F, Han YL, Lin M, Lu TJ, Xu F. Oligonucleotide-Linked Gold Nanoparticle Aggregates for Enhanced Sensitivity in Lateral Flow Assays. Lab Chip. 2013; 13:4352–4357. [PubMed: 24056409]

361. Ge C, Yu L, Fang Z, Zeng L. An Enhanced Strip Biosensor for Rapid and Sensitive Detection of Histone Methylation. Anal Chem. 2013; 85:9343–9349. [PubMed: 23978305]

362. (a) Qin Z, Chan WCW, Boulware DR, Akkin T, Butler EK, Bischof JC. Significantly Improved Analytical Sensitivity of Lateral Flow Immunoassays by Using Thermal Contrast. Angew Chem, Int Ed. 2012; 51:4358–4361.(b) Fu E, Liang T, Houghtaling J, Ramachandran S, Ramsey SA, Lutz B, Yager P. Enhanced Sensitivity of Lateral Flow Tests Using a Two-Dimensional Paper Network Format. Anal Chem. 2011; 83:7941–7946. [PubMed: 21936486] (c) Kim YT, Chen Y, Choi JY, Kim WJ, Dae HM, Jung J, Seo TS. Integrated Microdevice of Reverse Transcription-

Polymerase Chain Reaction with Colorimetric Immunochromatographic Detection for Rapid Gene Expression Analysis of Influenza a H1n1 Virus. Biosens Bioelectron. 2012; 33:88–94. [PubMed: 22265877] (d) Lie P, Liu J, Fang Z, Dun B, Zeng L. A Lateral Flow Biosensor for Detection of Nucleic Acids with High Sensitivity and Selectivity. Chem Commun. 2012; 48:236–238.

363. Nam JM, Thaxton CS, Mirkin CA. Nanoparticle-Based Bio-Bar Codes for the Ultrasensitive Detection of Proteins. Science. 2003; 301:1884–1886. [PubMed: 14512622]
364. Thaxton CS, Elghanian R, Thomas AD, Stoeva SI, Lee J-S, Smith ND, Schaeffer AJ, Klocker H, Horninger W, Bartsch G, Mirkin CA. Nanoparticle-Based Bio-Barcode Assay Redefines "Undetectable" Psa and Biochemical Recurrence after Radical Prostatectomy. Proc Natl Acad Sci USA. 2009; 106:18437–18442. [PubMed: 19841273]
365. Georganopoulou DG, Chang L, Nam JM, Thaxton CS, Mufson EJ, Klein WL, Mirkin CA. Nanoparticle-Based Detection in Cerebral Spinal Fluid of a Soluble Pathogenic Biomarker for Alzheimer's Disease. Proc Natl Acad Sci USA. 2005; 102:2273–2276. [PubMed: 15695586]
366. Zheng G, Daniel WL, Mirkin CA. A New Approach to Amplified Telomerase Detection with Polyvalent Oligonucleotide Nanoparticle Conjugates. J Am Chem Soc. 2008; 130:9644–9645. [PubMed: 18597453]
367. Stoeva SI, Lee JS, Smith JE, Rosen ST, Mirkin CA. Multiplexed Detection of Protein Cancer Markers with Biobarcoded Nanoparticle Probes. J Am Chem Soc. 2006; 128:8378–8379. [PubMed: 16802785]
368. Nam JM, Stoeva SI, Mirkin CA. Bio-Bar-Code-Based DNA Detection with PCR-Like Sensitivity. J Am Chem Soc. 2004; 126:5932–5933. [PubMed: 15137735]
369. Stoeva SI, Lee JS, Thaxton CS, Mirkin CA. Multiplexed DNA Detection with Biobarcoded Nanoparticle Probes. Angew Chem, Int Ed. 2006; 45:3303–3306.
370. (a) Oh BK, Nam JM, Lee SW, Mirkin CA. A Fluorophore-Based Bio-Barcode Amplification Assay for Proteins. Small. 2006; 2:103–108. [PubMed: 17193564] (b) Liu Z, Zhou B, Wang H, Lu F, Liu T, Song C, Leng X. Highly Sensitive Detection of Human Igg Using a Novel Bio-Barcode Assay Combined with DNA Chip Technology. J Nanopart Res. 2013; 15:1964.(c) Zhang D, Carr DJ, Alocilja EC. Fluorescent Bio-Barcode DNA Assay for the Detection of Salmonella Enterica Serovar Enteritidis. Biosens Bioelectron. 2009; 24:1377–1381. [PubMed: 18835708]
371. (a) Nam JM, Wise AR, Groves JT. Colorimetric Bio-Barcode Amplification Assay for Cytokines. Anal Chem. 2005; 77:6985–6988. [PubMed: 16255599] (b) Nam JM, Jang KJ, Groves JT. Detection of Proteins Using a Colorimetric Bio-Barcode Assay. Nat Protoc. 2007; 2:1438–1444. [PubMed: 17545980]
372. (a) Zhang X, Qi B, Li Y, Zhang S. Amplified Electrochemical Aptasensor for Thrombin Based on Bio-Barcode Method. Biosens Bioelectron. 2009; 25:259–262. [PubMed: 19608403] (b) Zhang X, Su H, Bi S, Li S, Zhang S. DNA-Based Amplified Electrical Bio-Barcode Assay for One-Pot Detection of Two Target DNAs. Biosens Bioelectron. 2009; 24:2730–2734. [PubMed: 19188057] (c) Zhou J, Zhuang J, Tang J, Li Q, Tang D, Chen G. Dual-Nanogold-Linked Bio-Barcodes with Superstructures for in Situ Amplified Electronic Detection of Low-Abundance Proteins. Mol BioSyst. 2013; 9:622–625. [PubMed: 23361043]
373. Lee H, Park J-E, Nam J-M. Bio-Barcode Gel Assay for MicroRNA. Nat Commun. 2014; 5:3367. [PubMed: 24569571]
374. Timurdogan E, Alaca BE, Kavakli IH, Urey H. MEMS Biosensor for Detection of Hepatitis a and C Viruses in Serum. Biosens Bioelectron. 2011; 28:189–194. [PubMed: 21803562]
375. (a) Lee WG, Kim YG, Chung BG, Demirci U, Khademhosseini A. Nano/Microfluidics for Diagnosis of Infectious Diseases in Developing Countries. Adv Drug Delivery Rev. 2010; 62:449–457.(b) Whitesides GM. The Origins and the Future of Microfluidics. Nature. 2006; 442:368–373. [PubMed: 16871203]

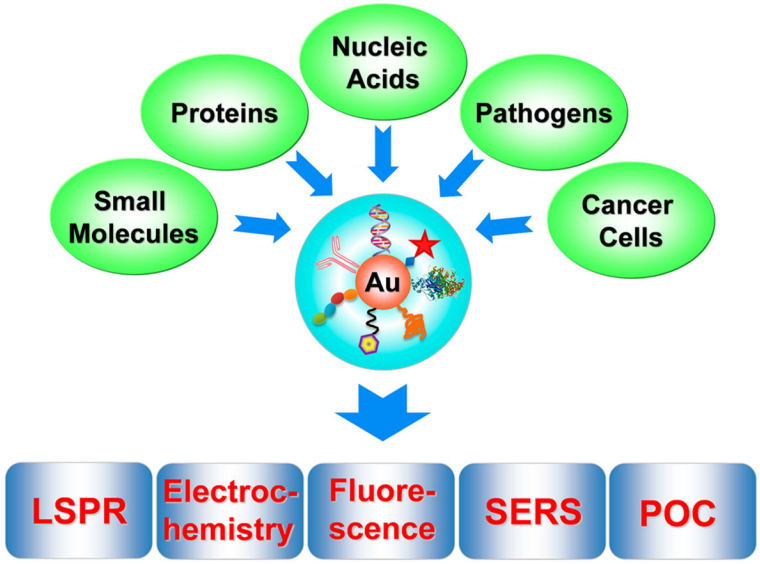

Figure 1.
Schematic illustration of AuNP-based assays for various detection targets in the applications of IVDs.

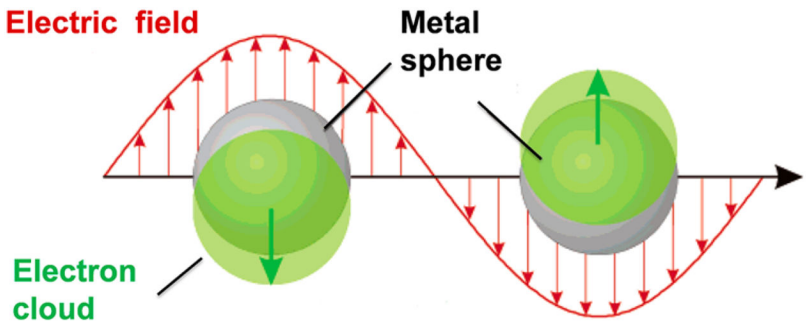

Figure 2.

Schematic illustration of a localized surface plasmon. The electric field induces polarization of the free electrons on the surface of the metal sphere. Reprinted with permission from ref 25. Copyright 2003 American Chemical Society.

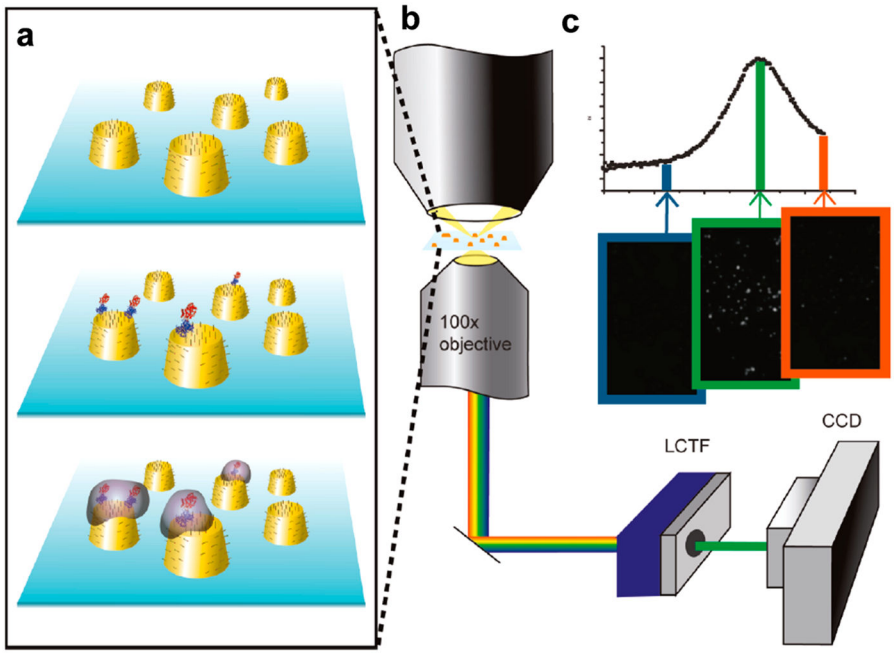

Figure 3.

Schematic representation of the enzymatically amplified LSPR detection of target proteins. (a) Streptavidin-HRP conjugates can bind the biotinylated AuNPs, thus catalyzing a precipitation reaction on the particle surfaces. The precipitate in turn leads to a detectable shift in the LSPR λ_{max}. (b) A great number of AuNPs are measured simultaneously using dark-field imaging and a tunable narrow band-pass liquid crystal filter. (c) Images recorded at discrete wavelengths are combined so as to obtain scattering spectra for each individual AuNP. Reprinted with permission from ref 45. Copyright 2011 American Chemical Society.

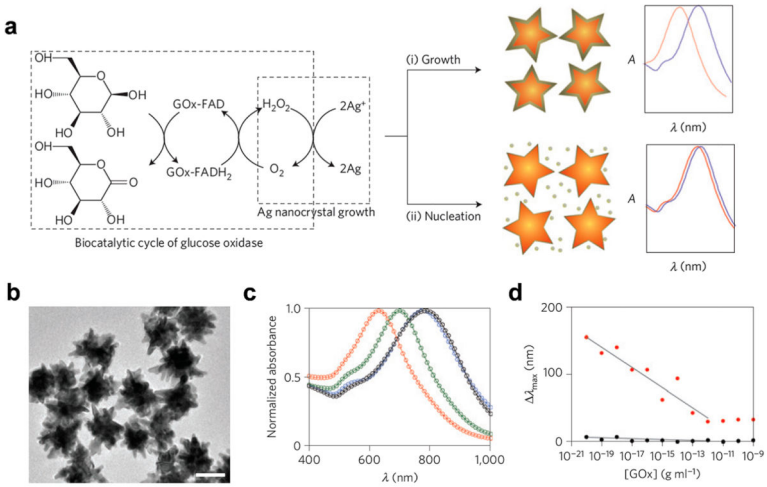

Figure 4.

LSPR detection of protein biomarkers by means of enzyme-guided nanocrystal growth. (a) Scheme of detection mechanism. GOx catalyzes the generation of H_2O_2, which reduces silver ions to grow a silver coating around Au nanostars. The concentration-dependent nanocrystal growth favors either the nucleation of AgNPs in solutions (at high concentrations) or the epitaxial growth of Ag around the Au nanostars (at low concentrations). (b) TEM image of Au nanostars (scale bar, 50 nm). (c) Visible/near-infrared spectra of the Au nanostar probe (black), and those treated with 10^{-14} g mL^{-1} GOx (green), 10^{-20} g mL^{-1} GOx (red), and without GOx (blue). (d) Blueshift of the LSPR λ_{max} of the Au nanostar probes treated with various concentrations of GOx in the absence (black) or in the presence (red) of the enzyme substrate glucose. Reprinted with permission from ref 56. Copyright 2012 Nature Publishing Group.

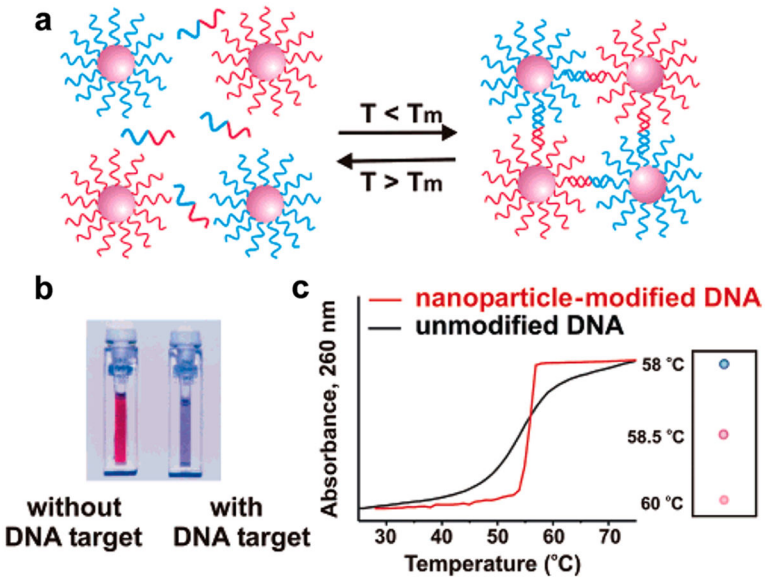

Figure 5.

Complementary target DNA can induce the aggregation of AuNPs (a), leading to color change of the solution from red to blue (b). The aggregation process can also be monitored by using UV–vis spectroscopy. Reprinted with permission from ref 63. Copyrights 2005 American Chemical Society.

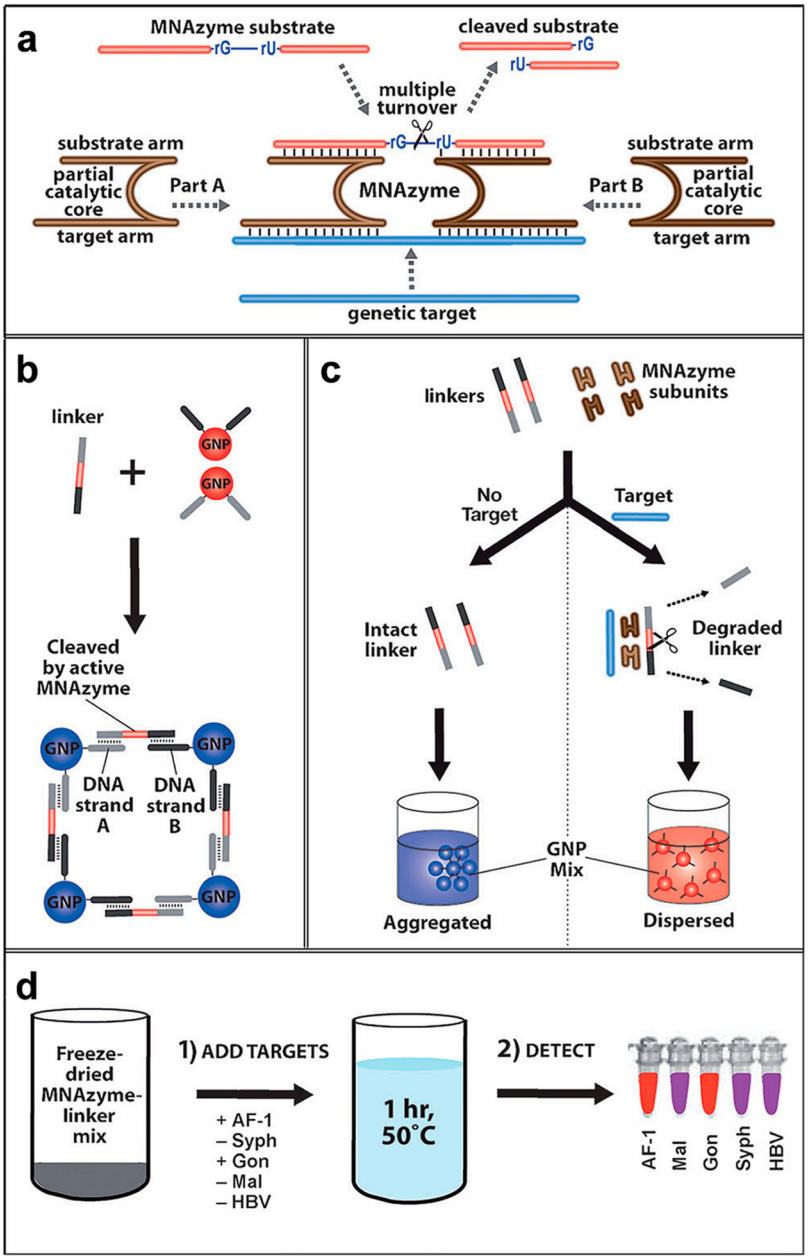

Figure 6.

Plasmonic DNAzyme strategy for genetic detection of infectious pathogens. (a) Mechanism of MNAzyme catalysis. (b) The linker hybridizes to the DNA strands A and B to cause the cross-linking of AuNPs, turning the solution purple. (c) The target-activated MNAzyme can degrade the linker DNA, allowing the dispersion of AuNPs. In the absence of the target, the linker remains intact and induces the aggregation of AuNPs. (d) Scheme outlining the detection procedures of the multiplexed assay in real samples. Reprinted with permission from ref 68. Copyright 2013 Wiley-VCH Verlag & Co. KGaA.

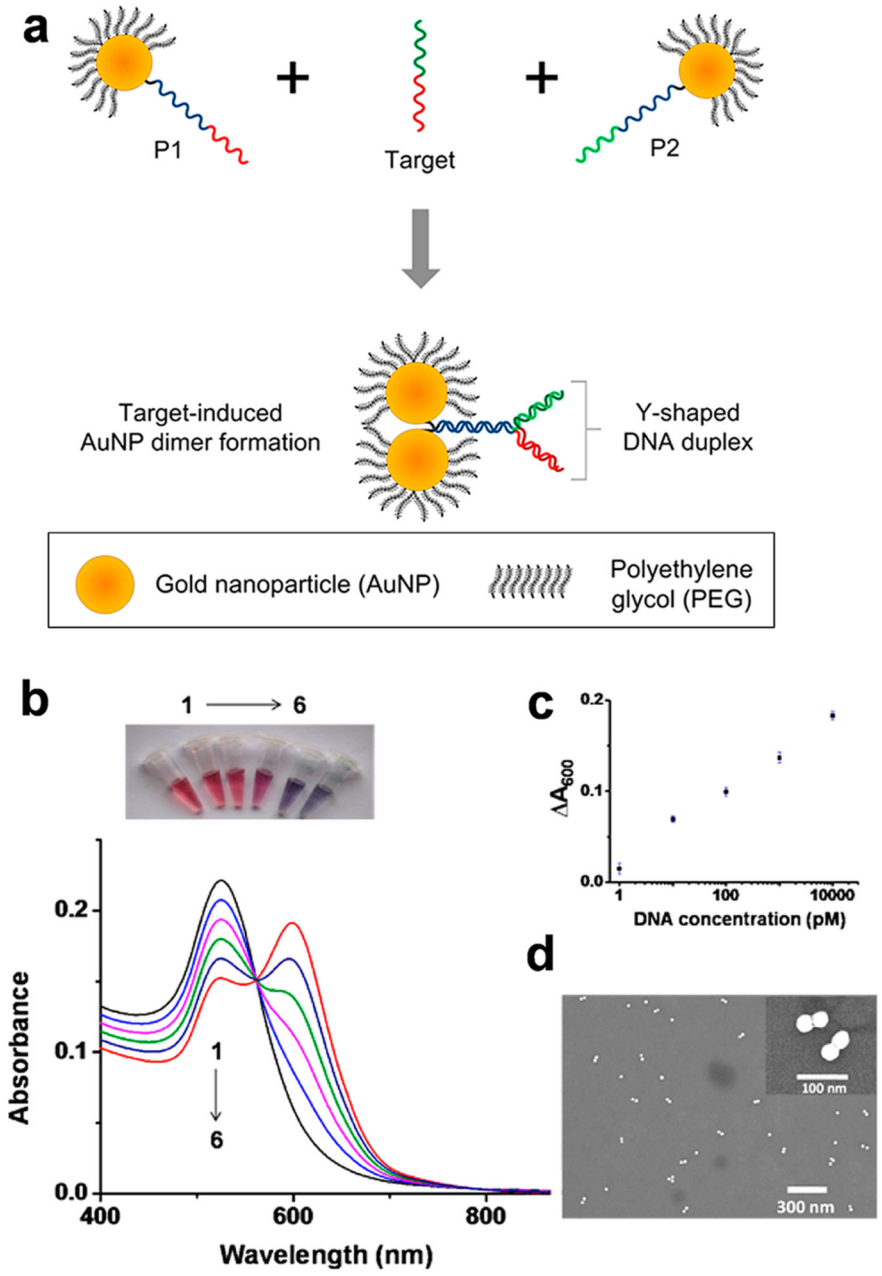

Figure 7.

(a) Schematic representation of the colorimetric assay based on asymmetrically functionalized AuNPs. (b) Photographs and corresponding UV–vis spectroscopy of the asymmetrically functionalized AuNP solutions added with various concentrations of target DNA (samples 1–6 are 0, 1 pM, 10 pM, 100 pM, 1 nM, and 10 nM, respectively). (c) The dose–response curve for (b). (d) A representative SEM image of the dimeric AuNPs treated with 10 nM target DNA. Reprinted with permission from ref 71. Copyright 2013 American Chemical Society.

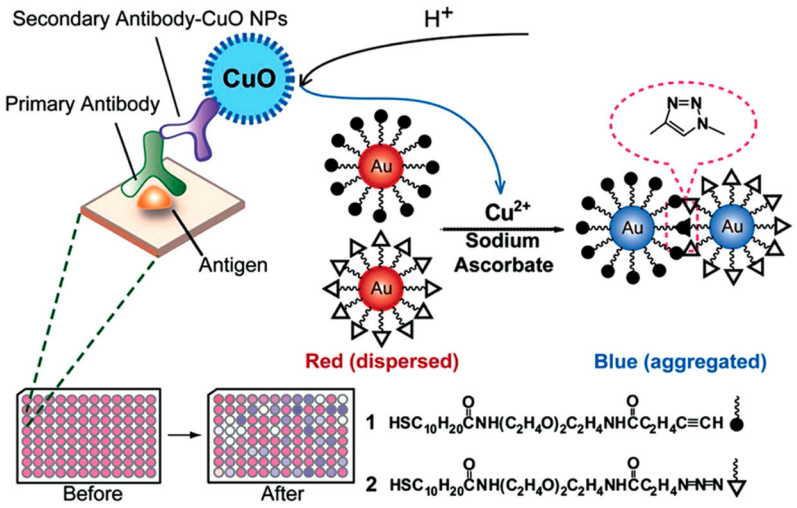

Figure 8.

AuNP-based immunoassay with the combination of CuO-labeled antibody and click chemistry. The CuO label was dissolved by acid to liberate copper ions, which act as a catalyst of click chemistry, thereby inducing aggregation of AuNPs functionalized with azide and alkyne groups. The resulted red-to-blue color change in turn reflects the presence of the target antigen. Reprinted with permission from ref 78. Copyright 2011 Wiley-VCH Verlag & Co. KGaA.

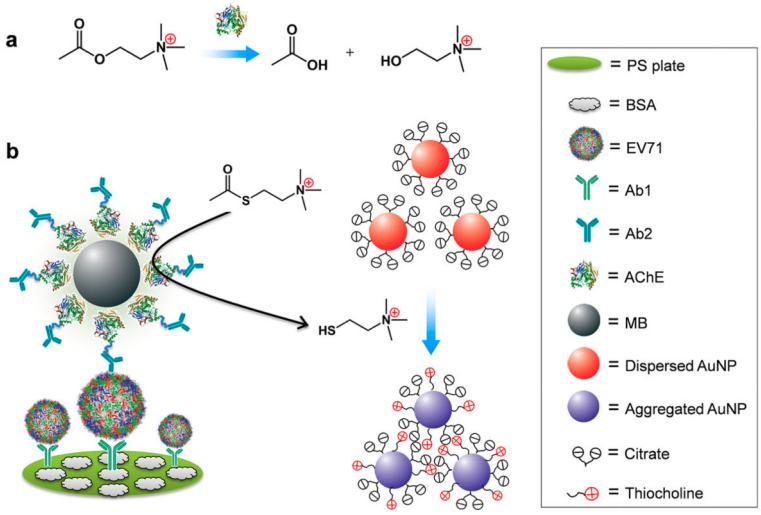

Figure 9.

(a) AChE catalyzes the hydrolysis of acetylcholine to generate acetate and choline. (b) Colorimetric detection of EV71 based on two rounds of signal amplification. In the first round, the labeled AChE can catalyze the generation of thiocholine, which is able to induce aggregation of citrate-AuNPs through electrostatic interactions. This aggregation event can be transformed into a red-to-purple change of the AuNP solutions. In the second round, many thousands of AChE and Ab2 were loaded onto a magnetic bead to further enhance detection signals. Reprinted with permission from ref 80. Copyright 2013 Wiley-VCH Verlag & Co. KGaA.

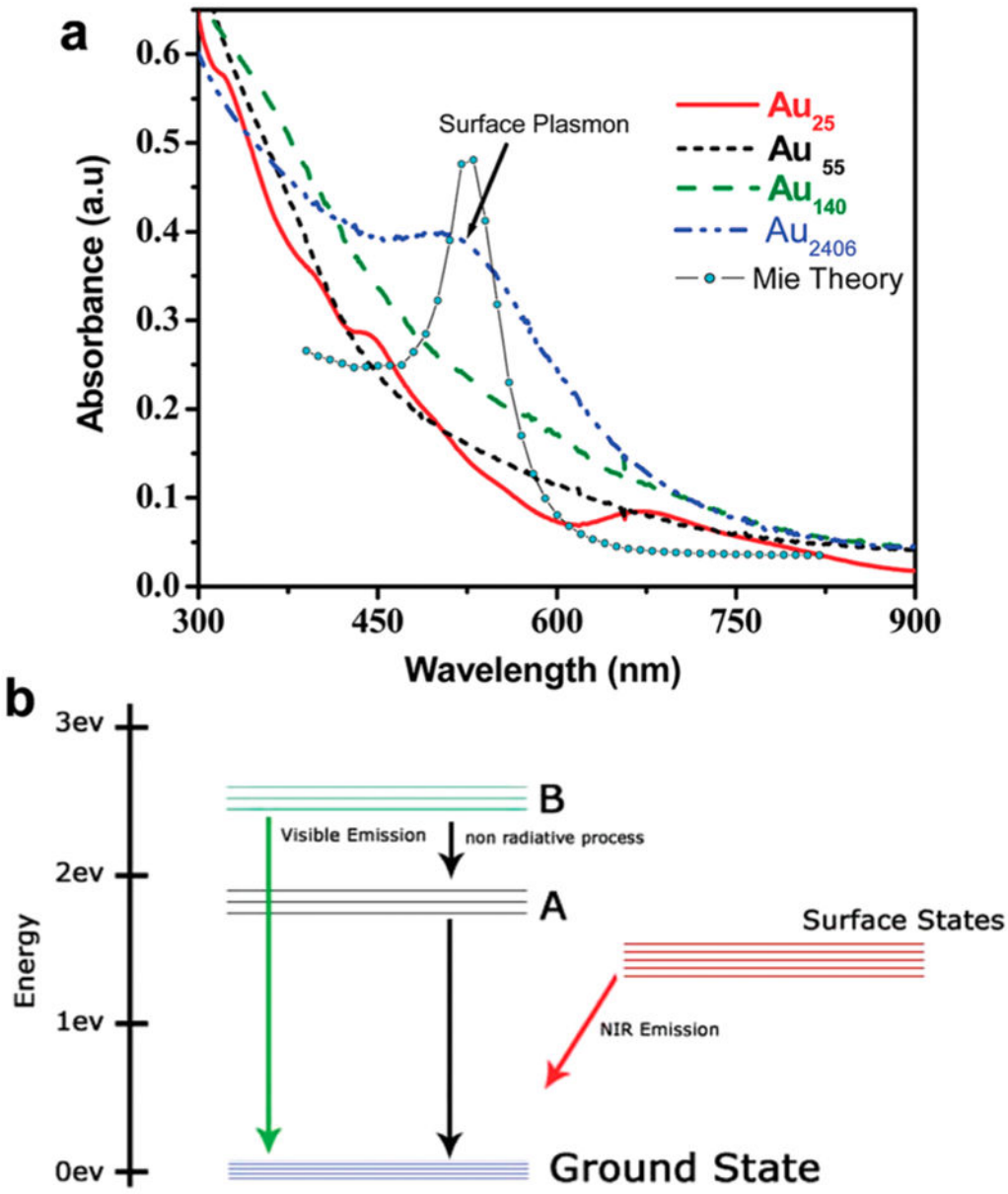

Figure 10.

(a) Steady-state absorption for Au_{25}, Au_{55}, Au_{140}, and Au_{2406} clusters and Mie theory calculation using parameters similar to those of Au_{25}. (b) Transition-energy diagram for the emissions for MPCs using data from steady-state emission, fluorescence upconver-sion, and transient absorption. Reprinted with permission from ref 94b. Copyright 2010 American Chemical Society.

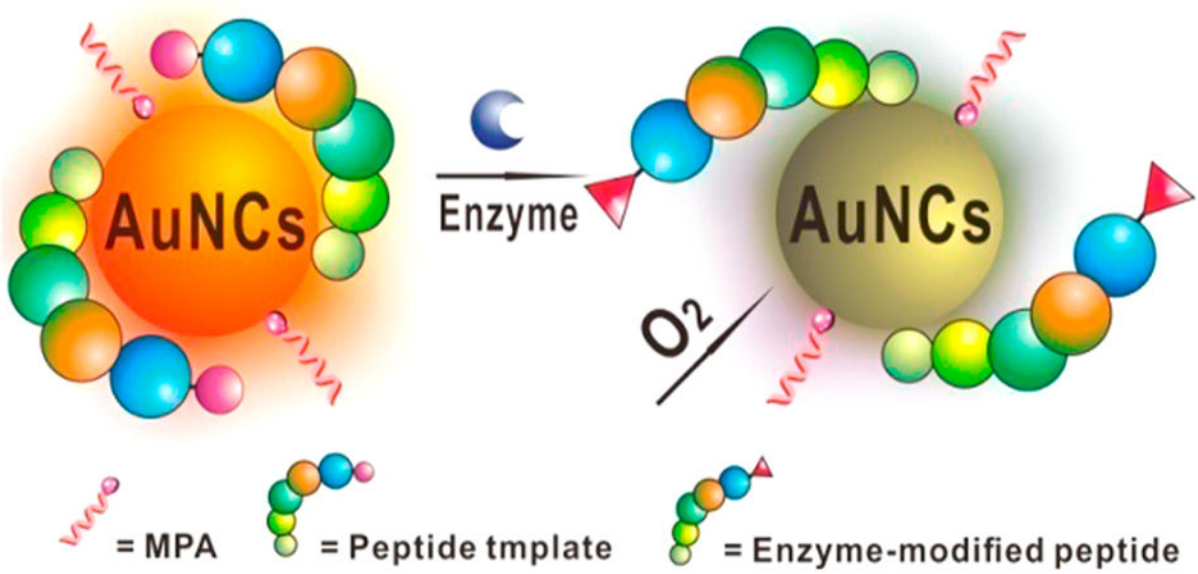

Figure 11.

Illustration of the mechanism for the peptide-templated AuNCs as a label-free sensor for PTM enzyme. The peptides act as a compacting coating to protect the AuNCs from contacting with O_2, thus diminishing O_2-mediated fluorescence quenching. In the presence of target enzyme, the deacetylation of the substrate peptides destroys the interactions between the peptides and the AuNC core, thus allowing the diffusion of O_2 into the peptide layer to contact with the AuNC cores. As a result, the fluorescence of AuNCs was quenched. Reprinted with permission from ref 109. Copyright 2013 American Chemical Society.

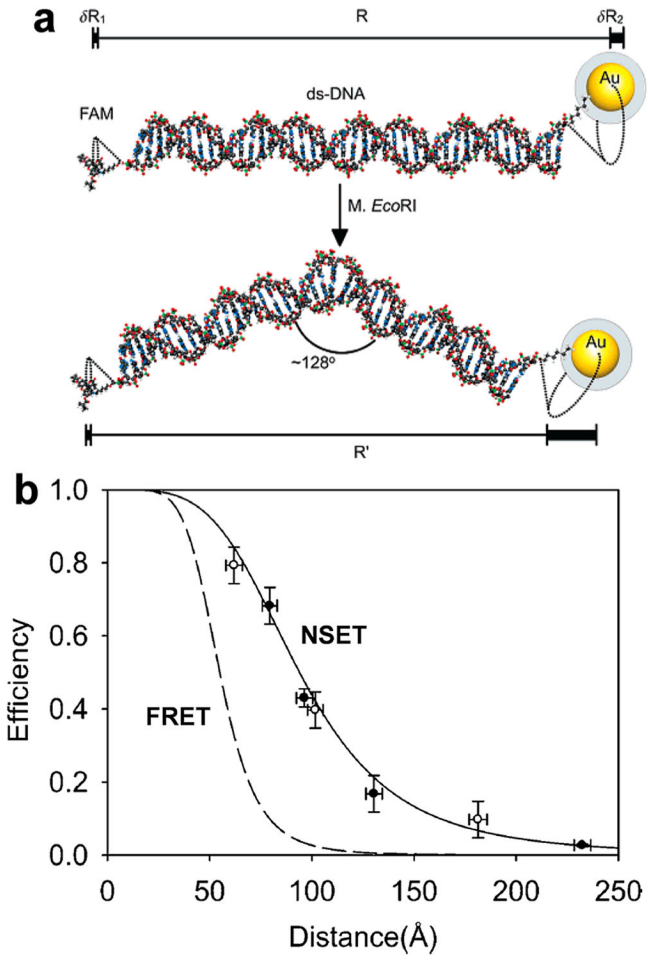

Figure 12.

(a) A fluorescein moiety (FAM) and AuNC (d = 1.4 nm) were tethered by a ds-DNA of length R varying from 15bp to 60bp. Addition of *M. Eco*RI bends the ds-DNA to produce a new distance R'. (b) Energy transfer efficiency plotted versus separation distance between FAM and AuNC. Filled circles (●) represent DNA lengths of 15bp, 20bp, 30bp, and 60bp. The measured efficiencies of these strands with the addition of *M. Eco*RI are represented by the open circles (○). The error bars reflect the standard error in repeated measurements of the fluorescence as well as the systematic error related to the flexibility of the C6 linker as illustrated in (a). The dashed line is the theoretical FRET efficiency, while the solid line is the theoretical NSET efficiency. Reprinted with permission from ref 116. Copyright 2005 American Chemical Society.

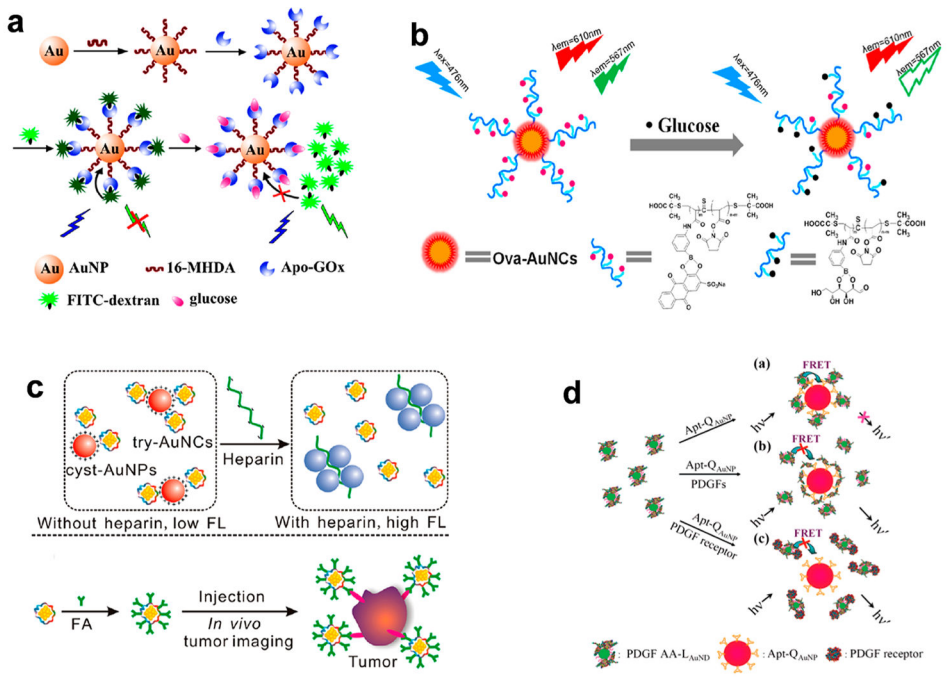

Figure 13.

Several representative AuNP-based activatable assays. (a) Glucose sensing principle based on the assembled AuNPs-apo-GOx-dextran-FITC nanoprobe. Reprinted with permission from ref 121. Copyright 2013 American Chemical Society. (b) Principle of the fluorescent probe based on AuNCs and ARS-boronic acid for monitoring glucose. The glucose can displace the ARS in the fluorescent probe PNAS-APBA-ARS. Reprinted with permission from ref 123. Copyright 2014 American Chemical Society. (c) Schematic illustration of the selective detection of heparin based on try-AuNCs and cyst-AuNPs. Reprinted with permission from ref 124. Copyright 2013 American Chemical Society. (d) Schematic representations of PDGF and PDGF receptor sensors based on the modulation of the quenching process. Reprinted with permission from ref 125. Copyright 2008 American Chemical Society.

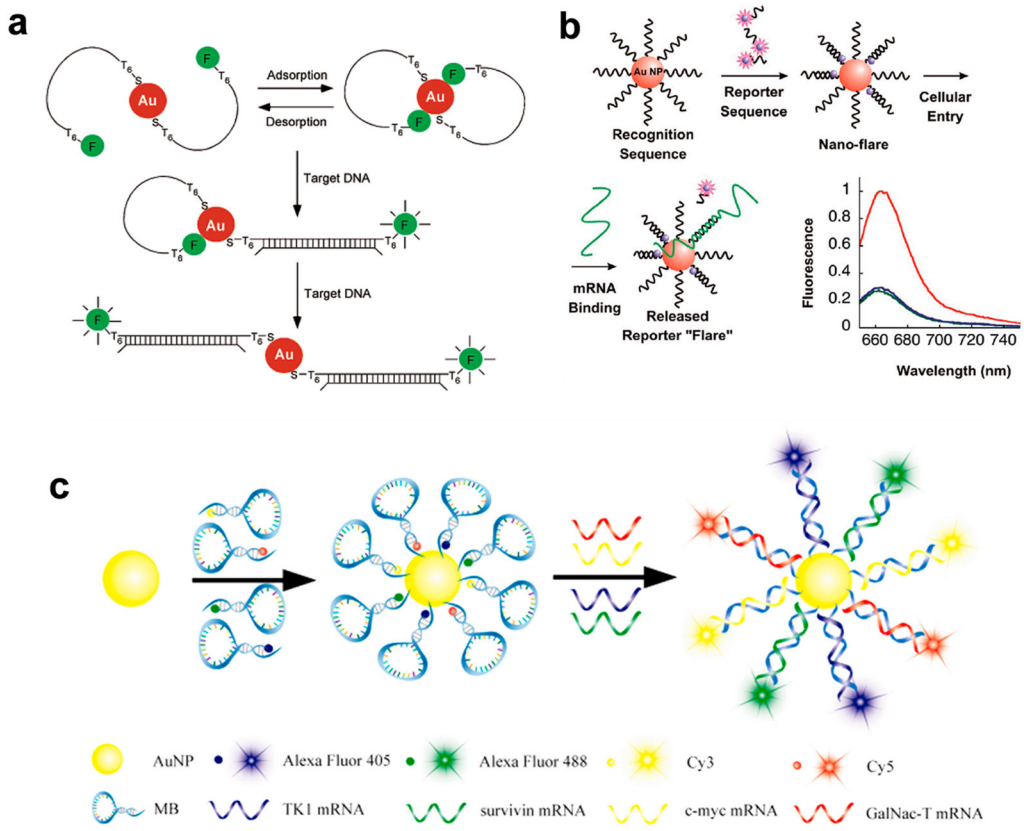

Figure 14.

Several representative AuNP-based activatable assays for DNA detection. (a) Target DNA induces the opening of the constrained conformation of the fluorophore-labeled DNA on AuNPs, allowing the fluorescence to be restored. Reprinted with permission from ref 128. Copyright 2002 American Chemical Society. (b) Target mRNA is capable of displacing the short Cy5 labeled reporter strand from the hybridized sequence on AuNPs, inducing the fluorescence recovery. Reprinted with permission from ref 130. Copyright 2007 American Chemical Society. (c) The principle of the four-color nanoprobe for detection of multiple intracellular mRNAs. Reprinted with permission from ref 136. Copyright 2013 American Chemical Society.

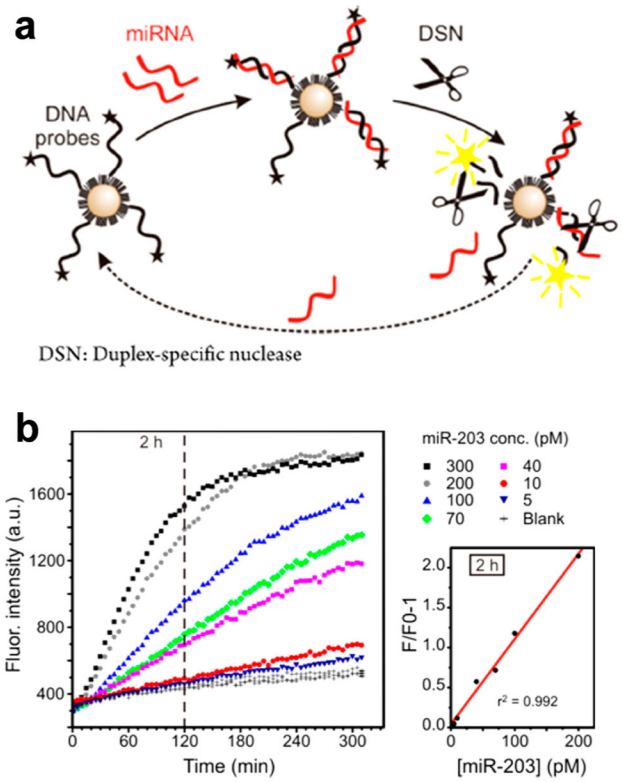

Figure 15.

(a) The principle of DSN-catalyzed hydrolysis for direct and absolute quantification of miRNAs. (b) Real-time monitoring of assay mixtures containing different concentrations of miRNA. Reprinted with permission from ref 143. Copyright 2014 American Chemical Society.

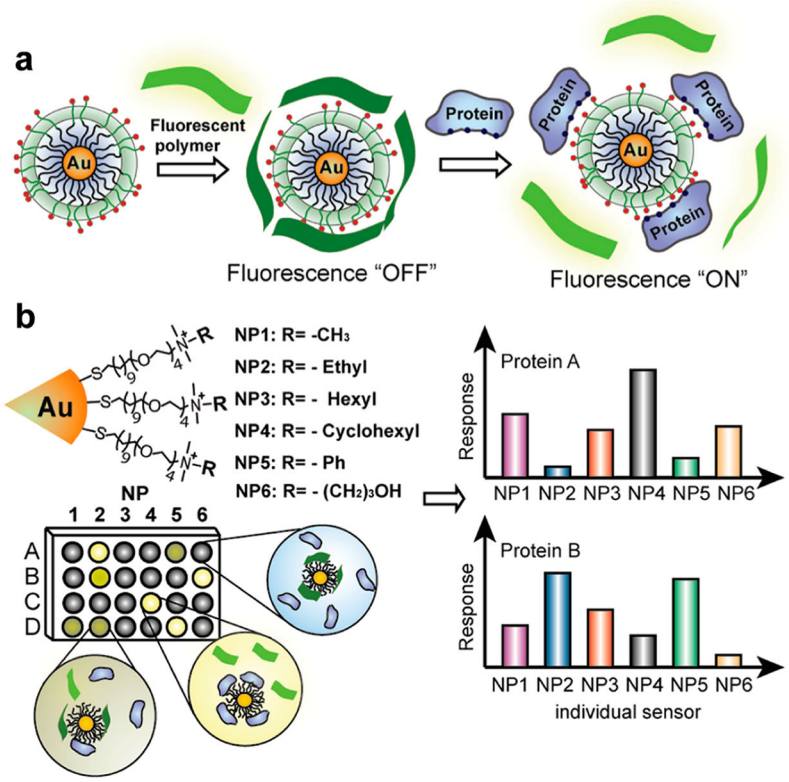

Figure 16.

(a) Schematic illustration of the displacement reaction between protein and quenched polymer-AuNP complexes, which leads to unquenching of the fluorescent polymer. (b) The combination of an array of sensors generates fingerprint response patterns for individual proteins. Reprinted with permission from ref 144. Copyright 2007 Nature Publishing Group.

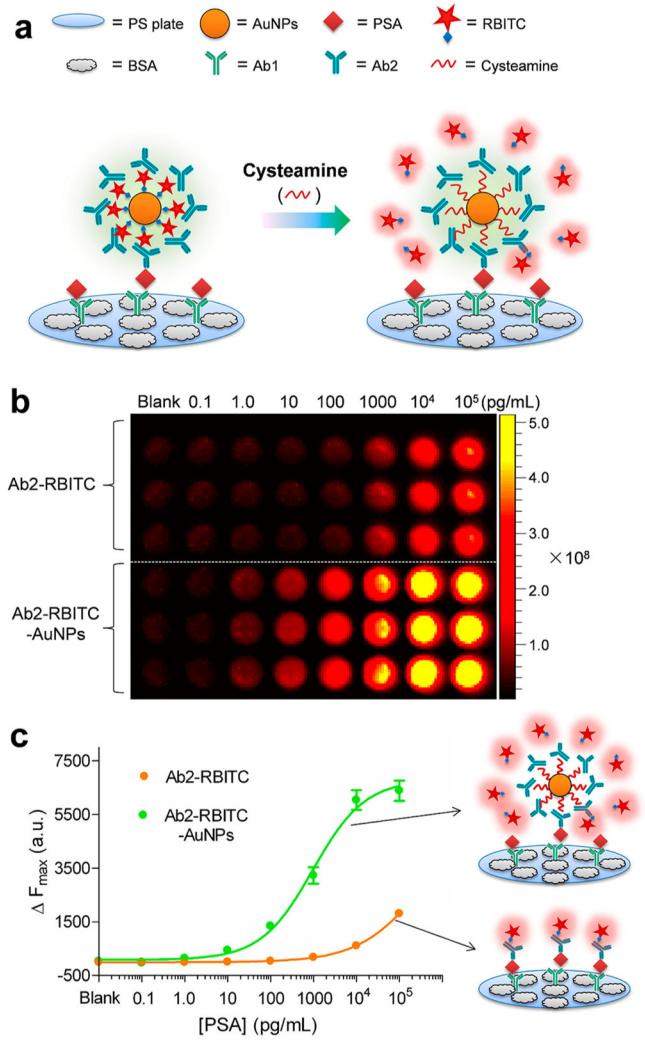

Figure 17.

(a) Schematic illustration of the fluorescence-activatable immunoassay for PSA performed in a 96-well microplate. (b) Comparison of conventional fluorescent immunoassay and the activatable immunoassay for sensing various concentrations of PSA. (c) Plotted ΔF_{max} versus the same concentrations of PSA in (b). $\Delta F_{max} = F - F_0$, where F is the emission fluorescence intensity at 590 nm and F_0 is the background fluorescence. Reprinted with permission from ref 157. Copyright 2013 American Chemical Society.

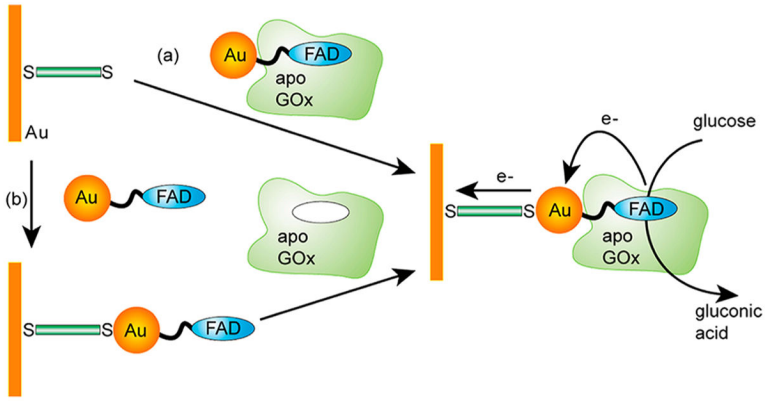

Figure 18.

Fabrication of GOx electrode by assembling the reconstituted GOx on a FAD-functionalized AuNP: (a) The adsorption of AuNP-reconstituted apo-GOx on a dithiol monolayer-modified gold electrode and (b) the adsorption of FAD-AuNPs on a dithiol-assembled Au electrode followed by reconstitution of apo-GOx on AuNPs. Reprinted with permission from ref 160. Copyright 2003 American Association for the Advancement of Science.

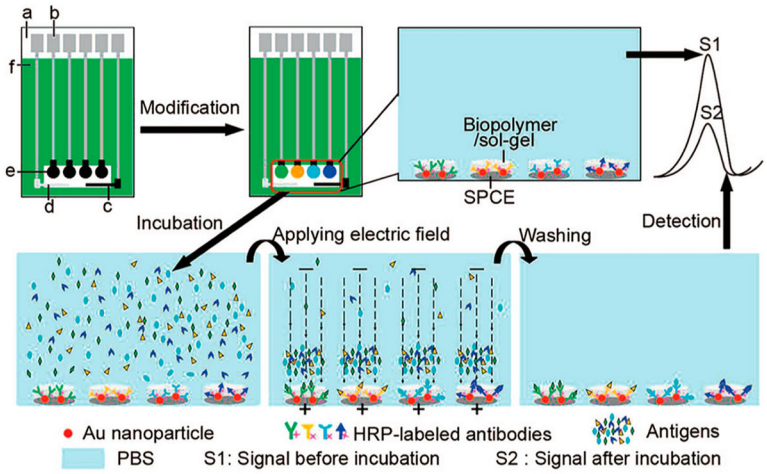

Figure 19.

Schematic representation of electrochemical multiplexed immunosensor based on HRP-labeled antibody-modified AuNPs with an electric field-driven incubation process. (a) Nylon sheet, (b) silver ink, (c) graphite auxiliary electrode, (d) Ag/AgCl reference electrode, (e) graphite working electrode, and (f) insulating dielectric. Reprinted with permission from ref 171. Copyright 2008 American Chemical Society.

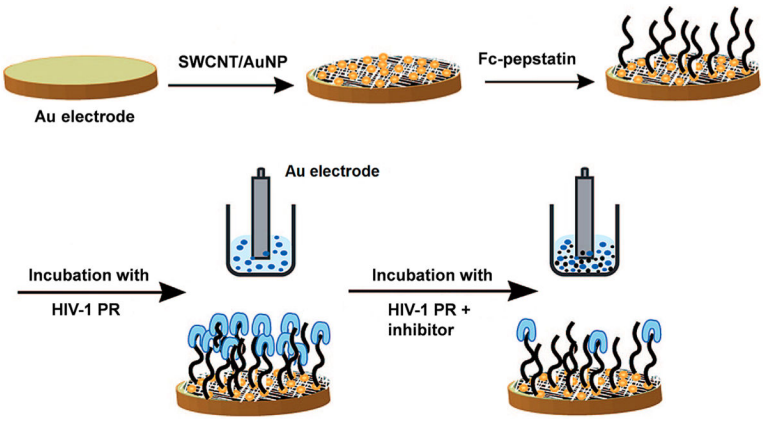

Figure 20.

Schematic illustration for the preparation of SWCNT/AuNP-modified electrodes coating with Fc-pepstatin conjugates and their use for detecting HIV-1 PR and the subsequent assay of HIV-1 PR inhibitors. The prethiolated SWCNTs were coated on the electrode surface, and AuNPs were subsequently immobilized on the SWCNTs by electrochemical deposition. A monolayer of Fc-pepstatin conjugate was formed on the SWCNT/AuNP modified electrode surface through Au–S bonds. The obtained electrode was incubated in a buffer containing HIV-1 PR in the absence or presence of its inhibitors. Reprinted with permission from ref 174. Copyright 2008 American Chemical Society.

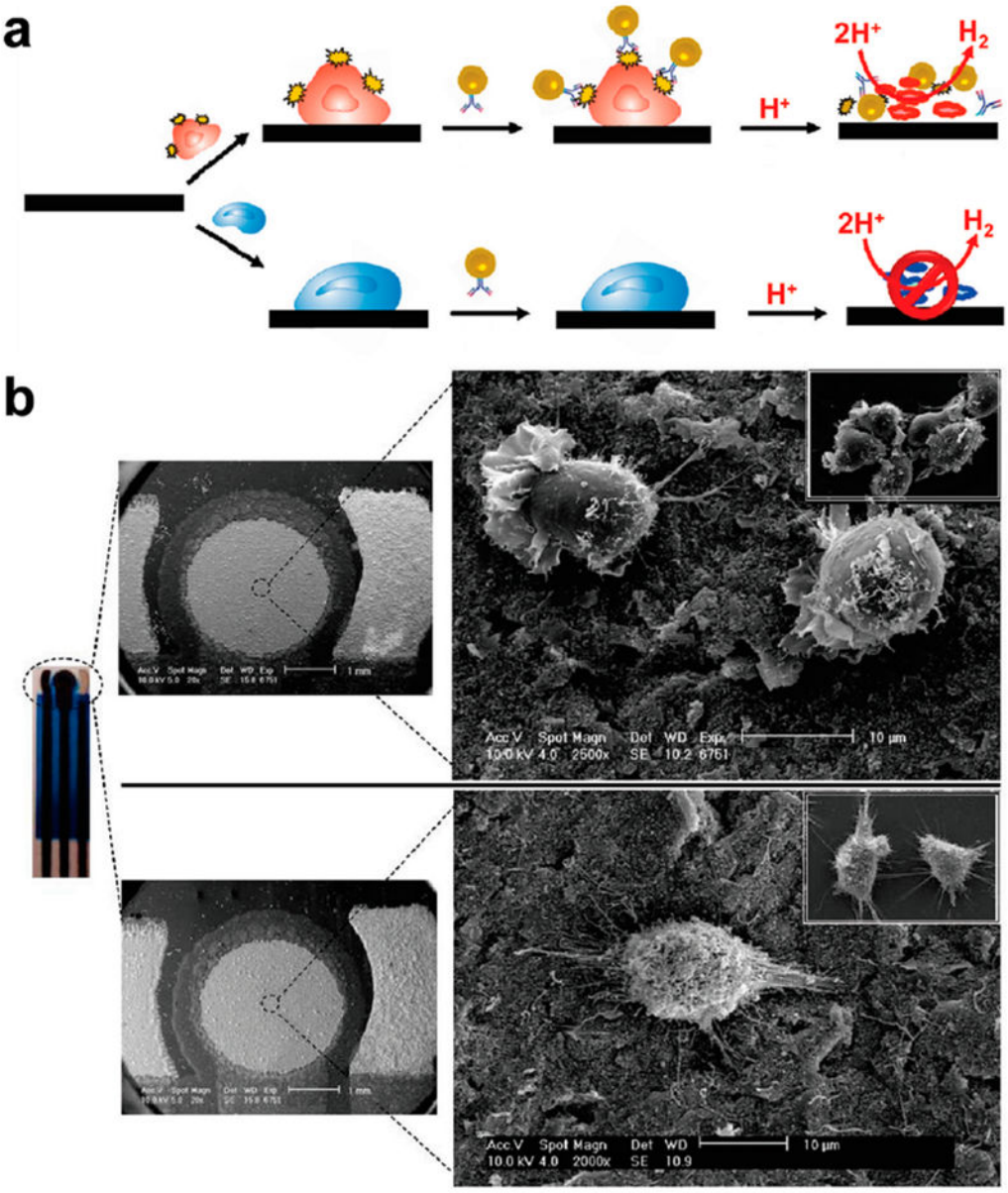

Figure 21.

(a) An AuNP-based electrochemical sensor for identification of HMy2 cell line expressing surface HLA-DR markers (top) and a PC-3 cell line that is negative to this marker (bottom). The specific binding of AuNPs with cells catalyzes hydrogen evolution in the acidic environment, generating electrochemical responses. (b) The corresponding SEM details of the HMy2 (top) and PC-3 cells (bottom) on the carbon working electrode. Inset images correspond to cell growth on the plastic area of the electrode. Reprinted with permission from ref 180. Copyright 2009 American Chemical Society.

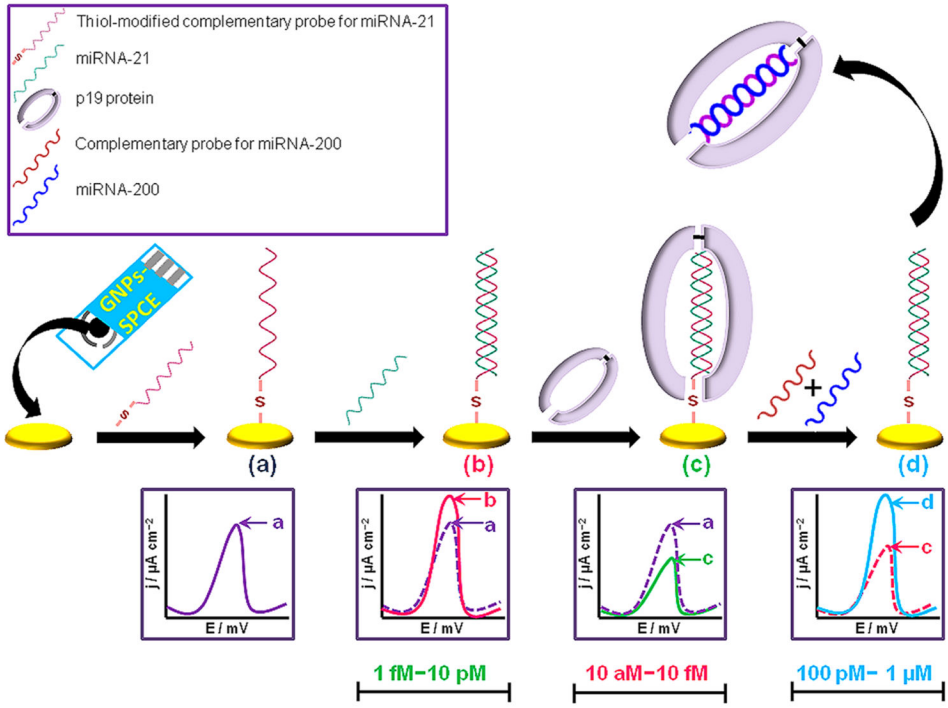

Figure 22.

Schematic representation of the three-mode electrochemical sensor for miRNA detection. (a) A thiol-modified complementary probe for miR-21 was self-assembled onto an AuNP-modified screen-printed carbon electrode (SPCE). (b) The binding of the target miR-21 caused an increase in the current intensity, with a linear detection range from 1 fM to 10 pM. (c) The binding of the p19 protein caused a large decrease in current density, with a linear detection range from 10 aM to 10 fM. (d) The hybridization product of miR-200 and its complementary probe forced the p19 protein to dissociate from the previously immobilized hybrid, causing a shift-back in the signal with a linear detection range from 100 pM to 1 μM. Reprinted with permission from ref 185. Copyright 2013 American Chemical Society.

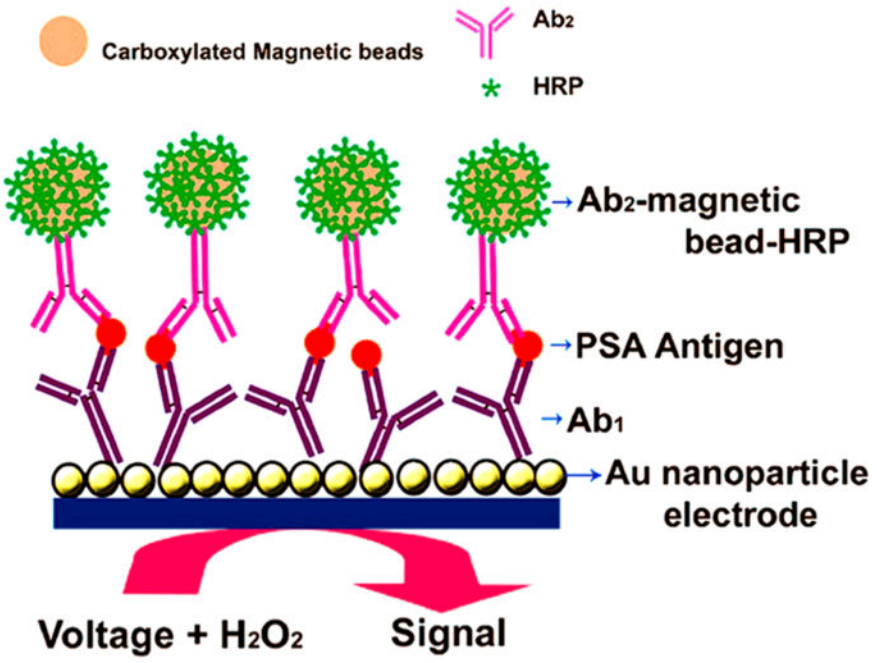

Figure 23.

Electrochemical immunosensor based on Ab2-magnetic bead-HRP conjugates performed on AuNP electrode, allowing detection of PSA with a detection limit of 0.5 pg/mL. Reprinted with permission from ref 193. Copyright 2009 American Chemical Society.

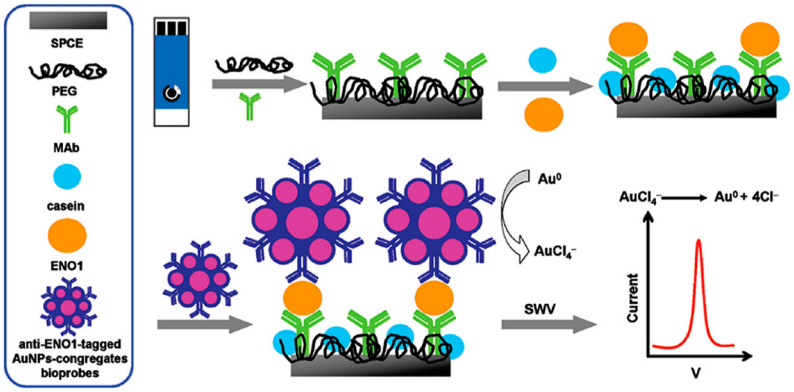

Figure 24.

Schematic illustration of the operation of the electrochemical immunosensor for the detection of ENO1 by means of anti-ENO1-tagged AuNP congregates. Reprinted with permission from ref 203. Copyright 2010 American Chemical Society.

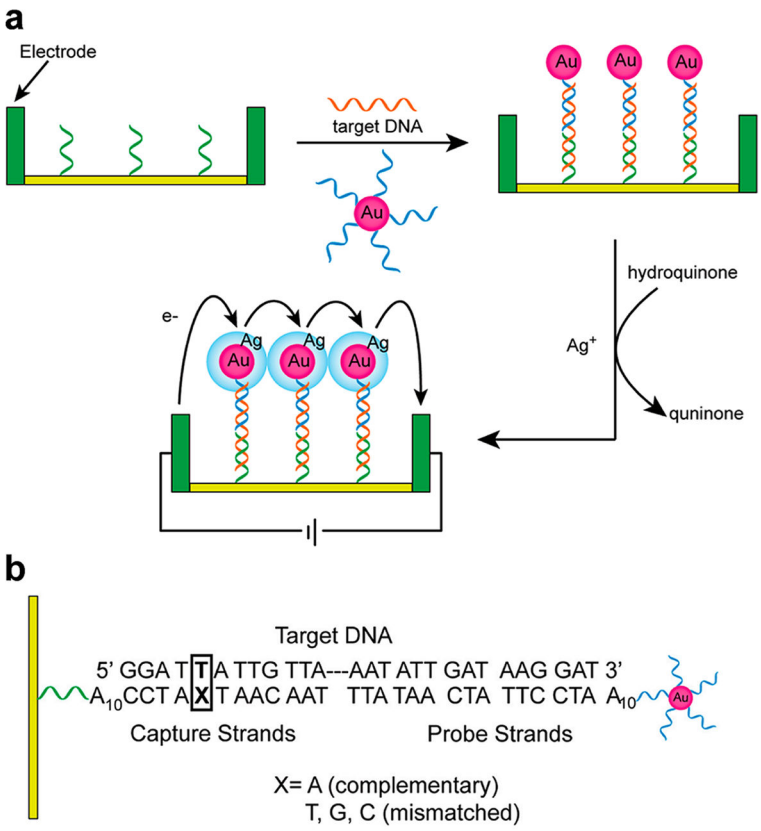

Figure 25.

(a) Schematic illustration of the electrical detection of DNA based on the target-induced sandwiched hybridization, followed by silver enhancement. (b) Sequences of capture, target, and probe DNA strands. Reprinted with permission from refs 205 and 16f. Copyright 2002 American Association for the Advancement of Science and 2012 American Chemical Society.

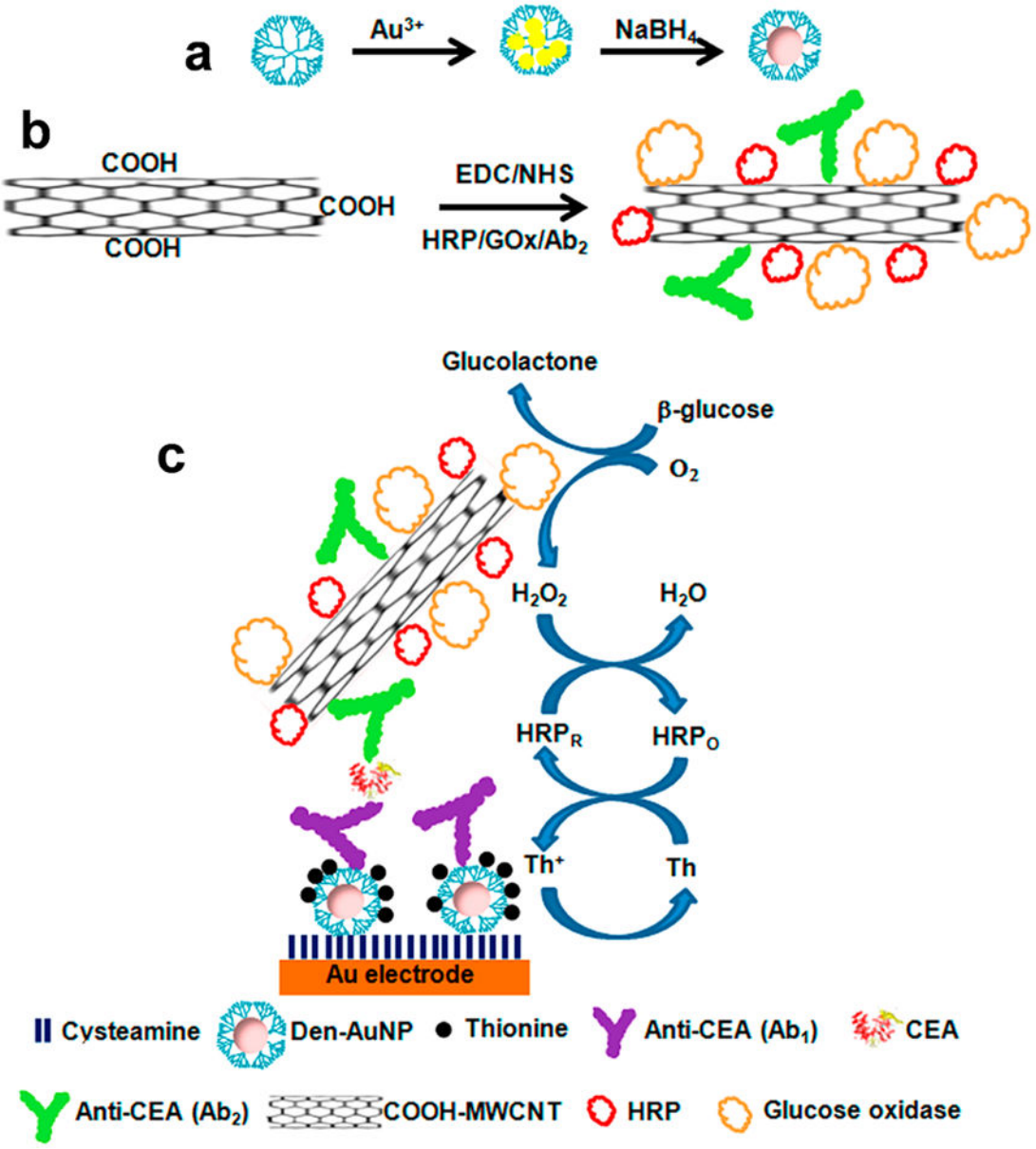

Figure 26.

(a) Preparation of AuNP-encapsulated dendrimer. (b) Modification of MWCNT with HRP, GOx, and anti-CEA (Ab2). (c) Detection principle of the electrochemical assays. In brief, the labeled GOx catalyzes its substrate glucose to generate H_2O_2, which is measured by the multiple HRP labels through the mediating ability of the loaded multiple thionine (Th). The ultimately generated electrochemical signals reflect the presence of CEA. Reprinted with permission from ref 220. Copyright 2013 American Chemical Society.

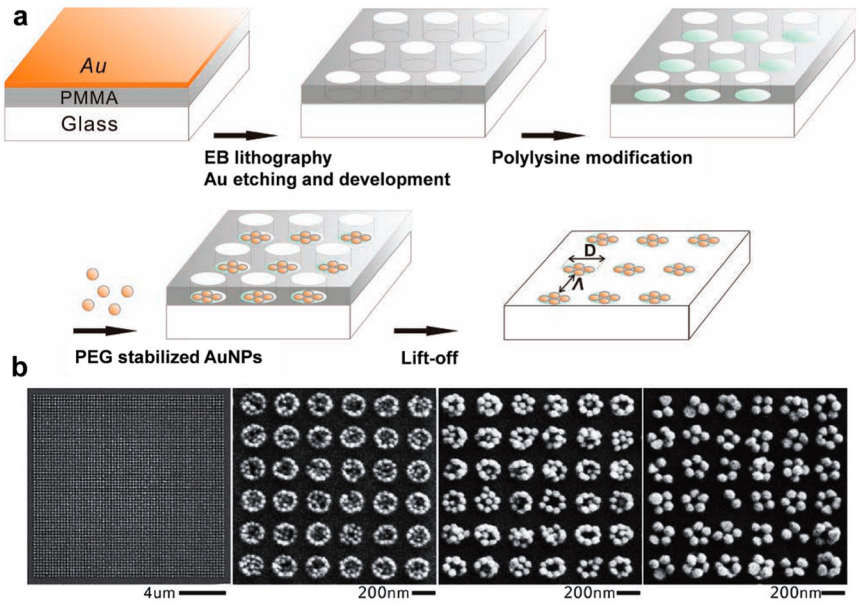

Figure 27.

(a) Fabrication procedure of NCAs using template-assisted assembly on glass substrate. E-beam lithography is used to create binding sites in a PMMA mask. These binding sites are functionalized with polylysine. Negatively charged AuNPs are then bound to these cluster binding sites. In a final process step, PMMA is removed and the NCA is obtained. (b) SEM images of the fabricated NCAs with various AuNP diameters (d = 40, 60, and 80 nm). Reprinted with permission from ref 244. Copyright 2010 Wiley-VCH Verlag & Co. KGaA.

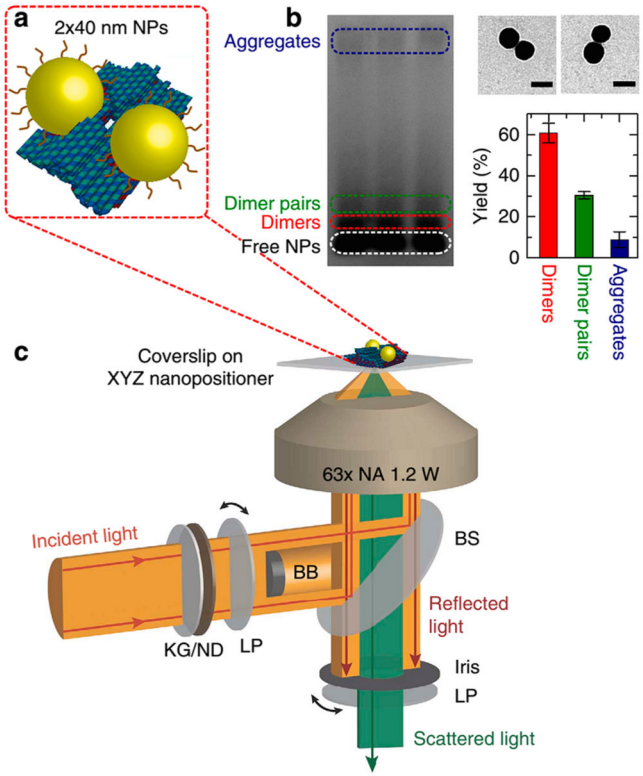

Figure 28.

(a) Schematic of AuNP dimer assembled on the DNA origami platform. (b) Gel electrophoresis of the AuNP dimers in the presence of other free AuNPs or aggregates. The dimer structures were imaged by TEM (scale bar, 50 nm). (c) Schematic of the custom built setup for measuring the scattering spectra of single dimer nanostructures. KG, heat absorbing filter; ND, neutral density filter; LP, linear polarizer; BB, beam block; and BS, beam splitter. Reprinted with permission from ref 246. Copyright 2014 Nature Publishing Group.

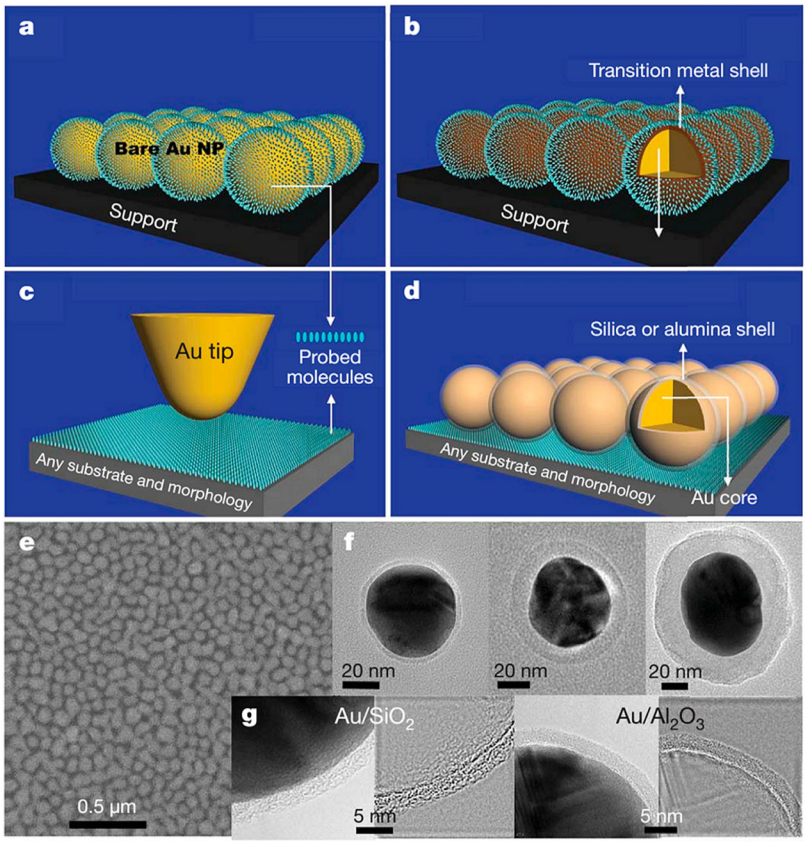

Figure 29.

Working principles of SHINERS as compared to other modes. Schematic of the contact mode. (a) Bare AuNPs: contact mode. (b) Au core-transition metal shell NPs adsorbed by probed molecules: contact mode. (c) Tip-enhanced Raman spectroscopy: noncontact mode. (d) SHINERS: shell-isolated mode. (e) SEM image of a monolayer of Au/SiO_2 NPs on a smooth Au surface. (f) HRTEM images of Au/SiO_2 core–shell NPs with Different shell thicknesses. (g) HRTEM images of Au/SiO_2 NP and Au/Al_2O_3 NP with a continuous and completely packed shell about 2 nm thick. Reprinted with permission from ref 234c. Copyright 2010 Nature Publishing Group.

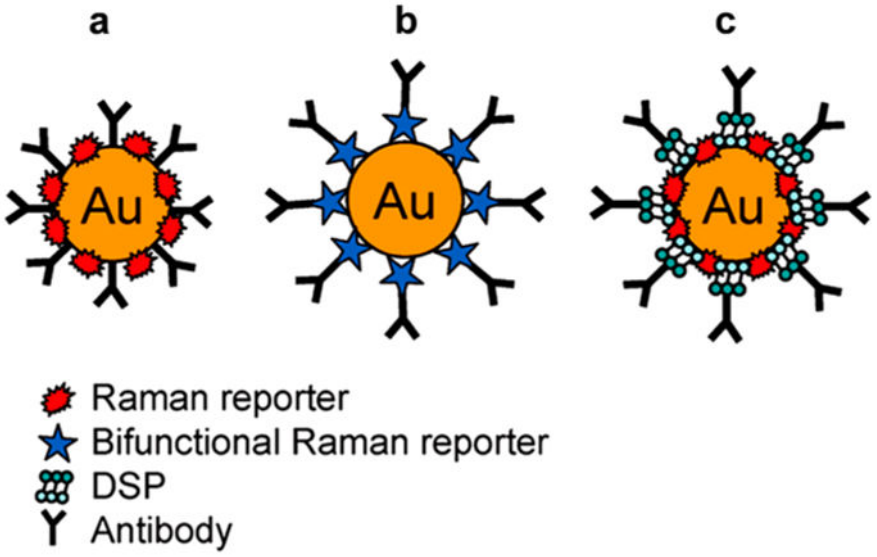

Figure 30.

Representation of ERLs prepared with (a) coimmobilization, where the antibody and Raman label are immobilized directly onto the surface of the AuNPs; (b) bifunctional reporter, where a bifunctional Raman reporter molecule is used to covalently conjugate the antibody to the AuNPs and thus prevent antibody exchange between ERLs; and (c) mixed monolayer, where the surface of AuNPs is modified with two Different thiolates. One thiolate is derived from the bifunctional compound dithiobis (succinimidyl propionate) (DSP), which can tether the antibodies onto AuNP surfaces. The other thiolate consists of molecules that have large Raman cross sections and serve as the Raman reporter. Reprinted with permission from ref 260a. Copyright 2009 American Chemical Society.

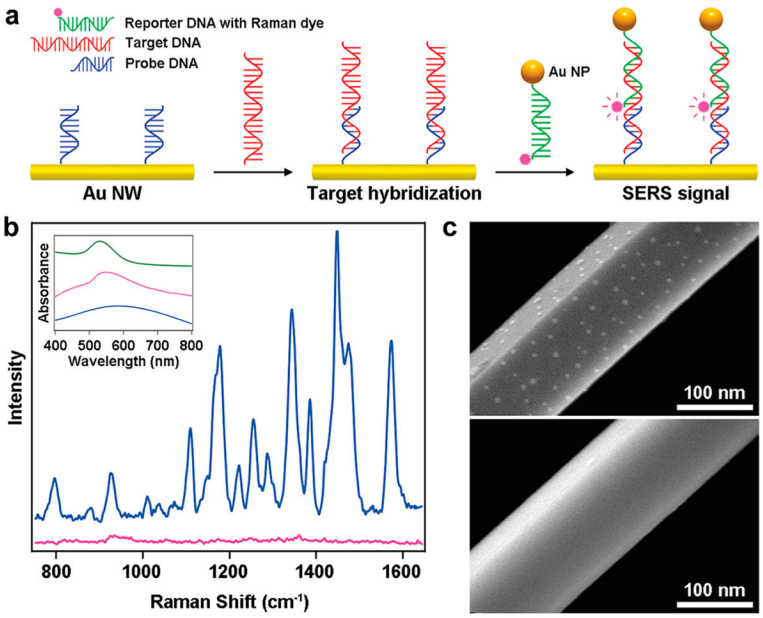

Figure 31.

(a) Working principle of Au particle-on-wire system. (b) SERS spectra of Au particle-on-wire system in the presence (blue) and absence (magenta) of complementary target DNAs. (c) SEM image of a typical Au particle-on-wire system by adding complementary target DNAs (top) and that of a clean nano wire (bottom). Reprinted with permission from ref 269. Copyright 2010 American Chemical Society.

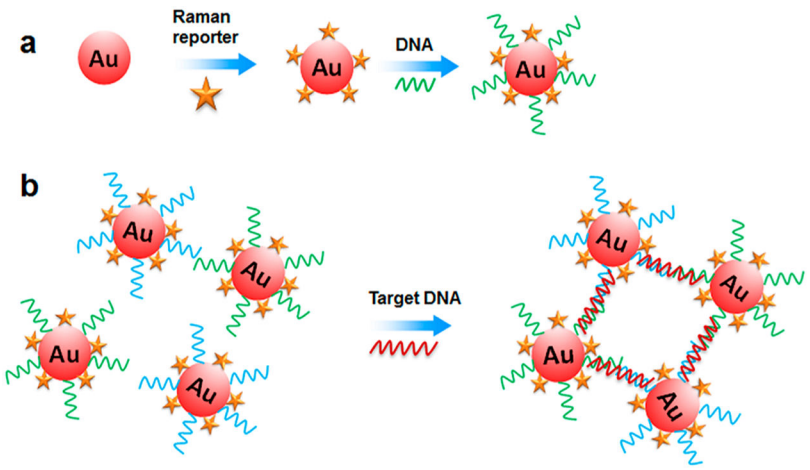

Figure 32.

(a) AuNPs were encoded with Raman reporter molecules (e.g., malachite green) and functionalized with thiolated DNA probes. Each AuNP contains ~500–1000 Raman reporter molecules and 2500–7000 thiol-DNA molecules, depending on the particle sizes. (b) Schematic representation of target-induced aggregation of AuNPs, leading to significant enhancement of Raman signals.

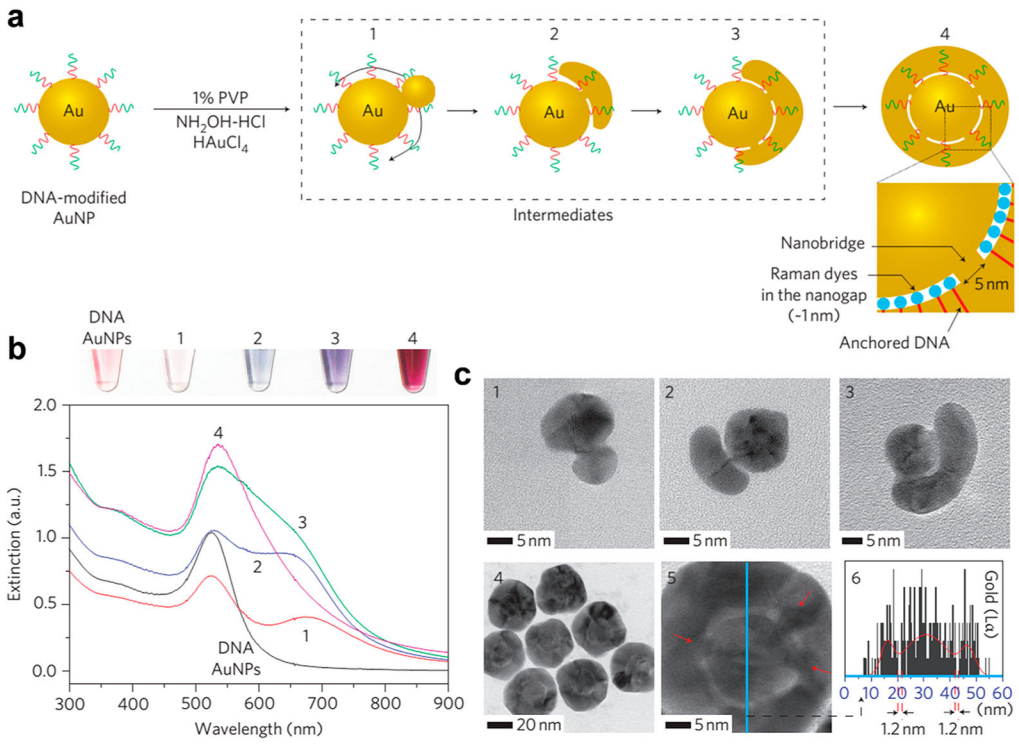

Figure 33.

(a) Fabrication of Au nanogapped particles (Au-NNPs) using DNA-modified AuNPs as templates. (b) Photograph and corresponding UV–vis absorption spectra of DNA-AuNPs, intermediate (panels 1–3), and Au-NNPs (panel 4) in the process of the Au growth in (a). (c) HRTEM images of intermediate (panels 1–3) and Au-NNPs (panels 4 and 5). Nanobridges within the Au-NNP are indicated by red arrows in panel 5, and elemental line mapping and the 1.2 nm gap in the Au-NNP structure are shown in panel 6. Reprinted with permission from ref 294. Copyright 2011 Nature Publishing Group.

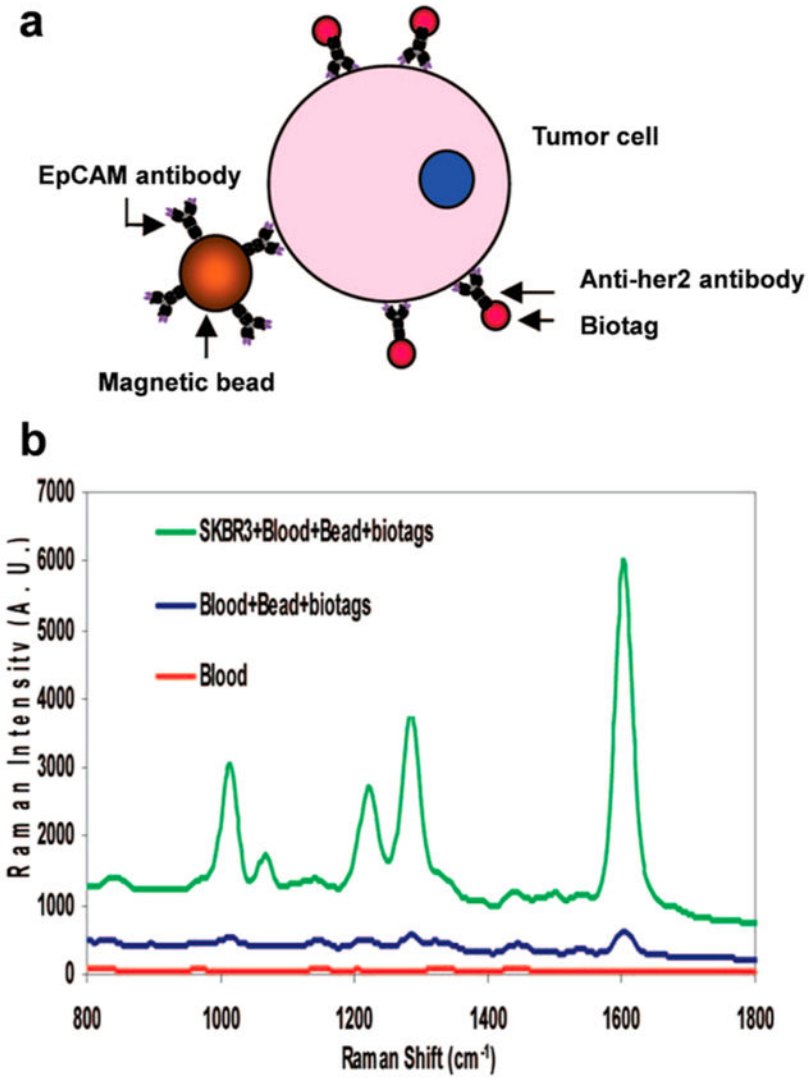

Figure 34.

(a) Schematic of the complex formed by nanoplex biotags and magnetic bead conjugates binding to the model tumor cell. (b) Raman detection of SKBR3 spiked into whole blood. Raman spectra of whole blood (red) and of beads and biotag reagents in blood without a cell spike (blue) and with SKBR3 cells spike (green). Reprinted with permission from ref 302. Copyright 2008 American Chemical Society.

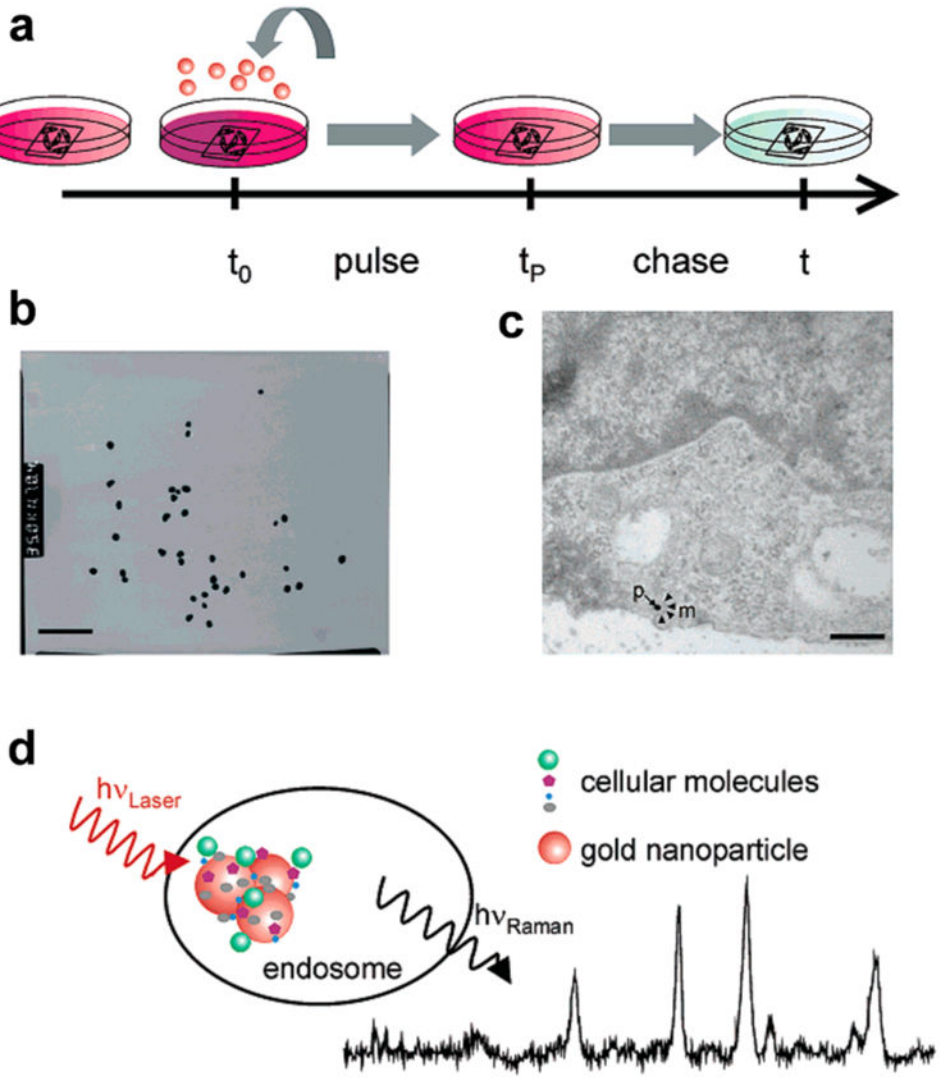

Figure 35.

(a) Procedure of SERS imaging by incubating SERS tags into cell culture medium for Different times. (b) TEM image of AuNPs immersed in cell culture medium (scale bar, 500 nm). (c) TEM image showing the endocytotic uptake of an individual AuNPs by an IRPT cell (scale bar, 500 nm). (d) Schematic of the SERS measurements inside the endosomal compartment. Reprinted with permission from ref 311. Copyright 2006 American Chemical Society.

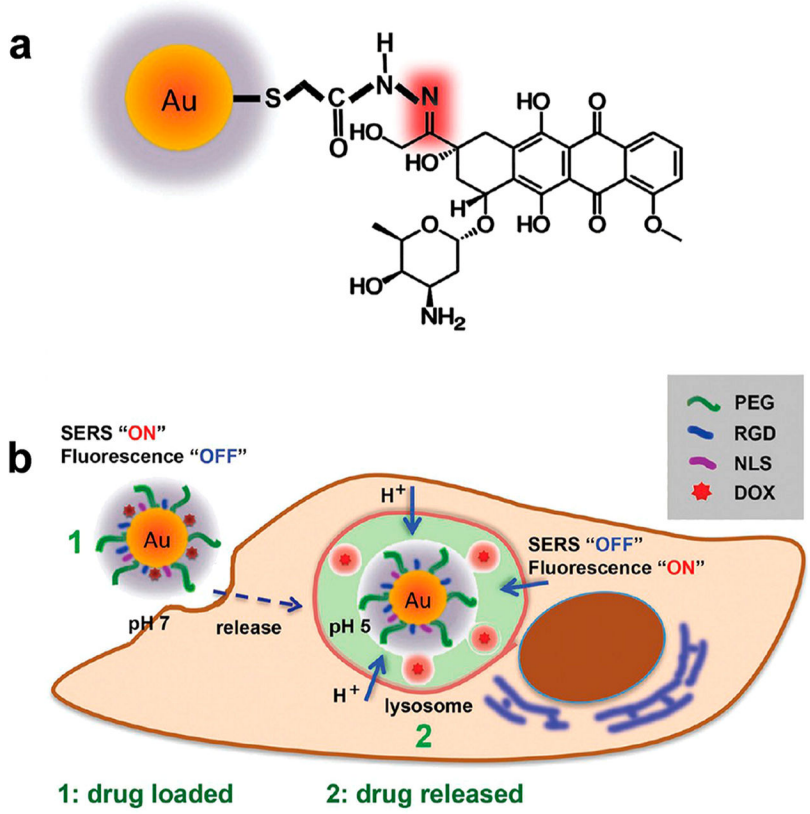

Figure 36.

(a) DOX-functionalized AuNPs tethered by a pH-sensitive hydrazine linkage. (b) Schematic of pH-triggered drug release tracking in acidic lysosomes by monitoring both the SERS spectra and the fluorescence signal from the DOX molecules. Reprinted with permission from ref 322. Copyright 2013 American Chemical Society.

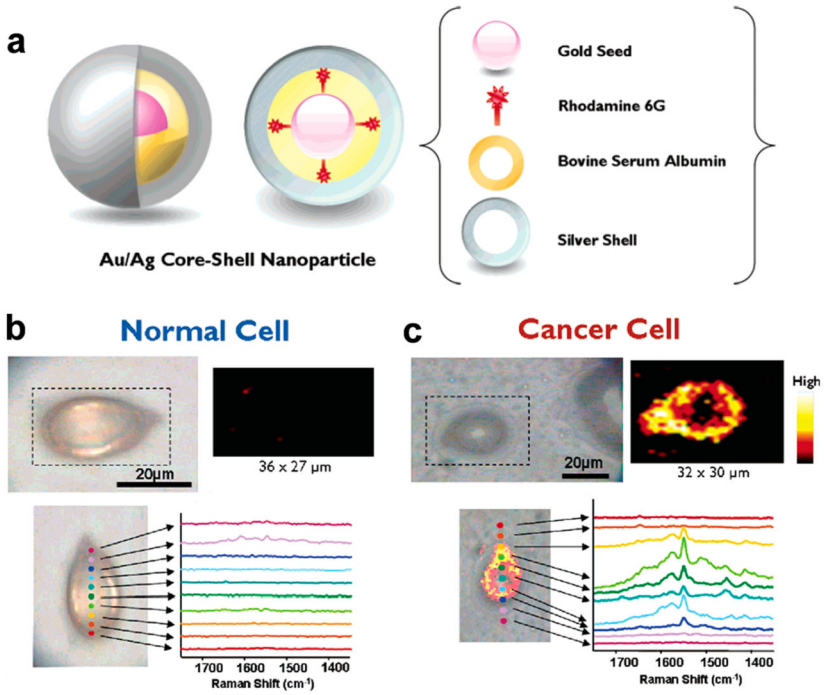

Figure 37.

(a) Au/Ag core–shell nanoparticle with Rhodamine 6G sandwiched in the gap. SERS images and corresponding spectra of single normal cell (b) and cancer cell (c). Reprinted with permission from ref 326. Copyright 2007 American Chemical Society.

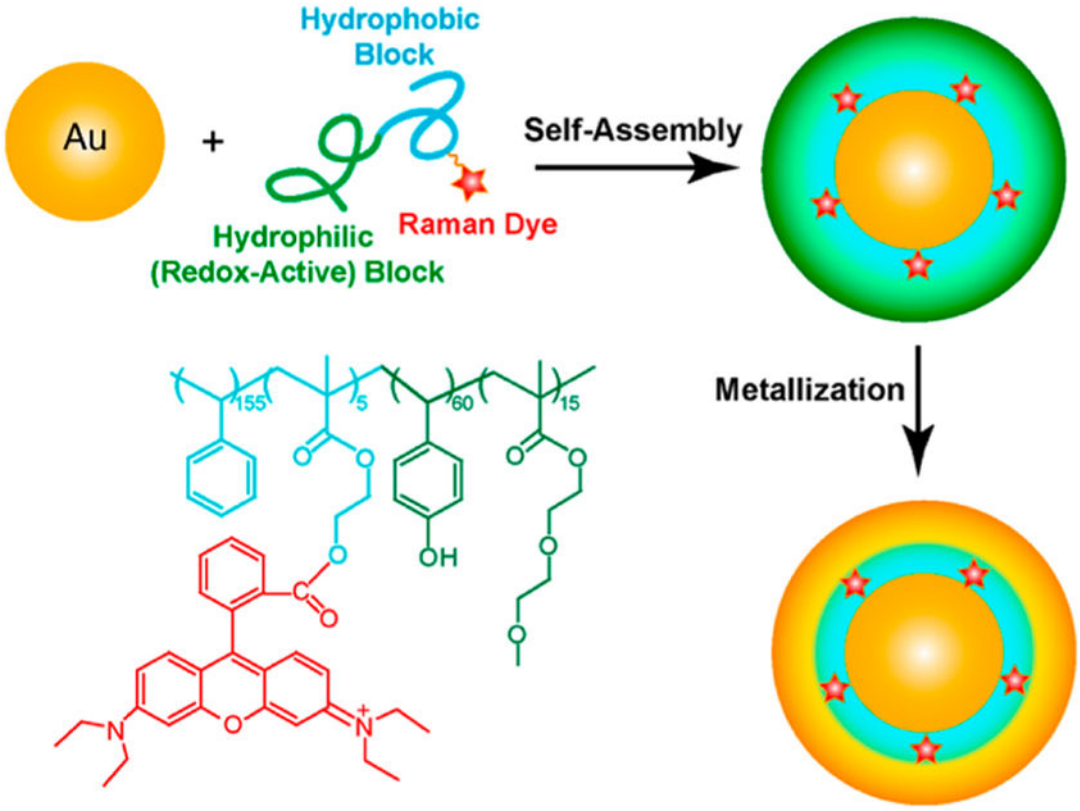

Figure 38.

(a) The preparation of nanogapped AuNPs, based on AuNP-templated self-assembly of amphiphilic block copolymers and the subsequently localized reduction of Au precursor by phenol group-containing polymer brushes. Reprinted with permission from ref 328. Copyright 2014 American Chemical Society.

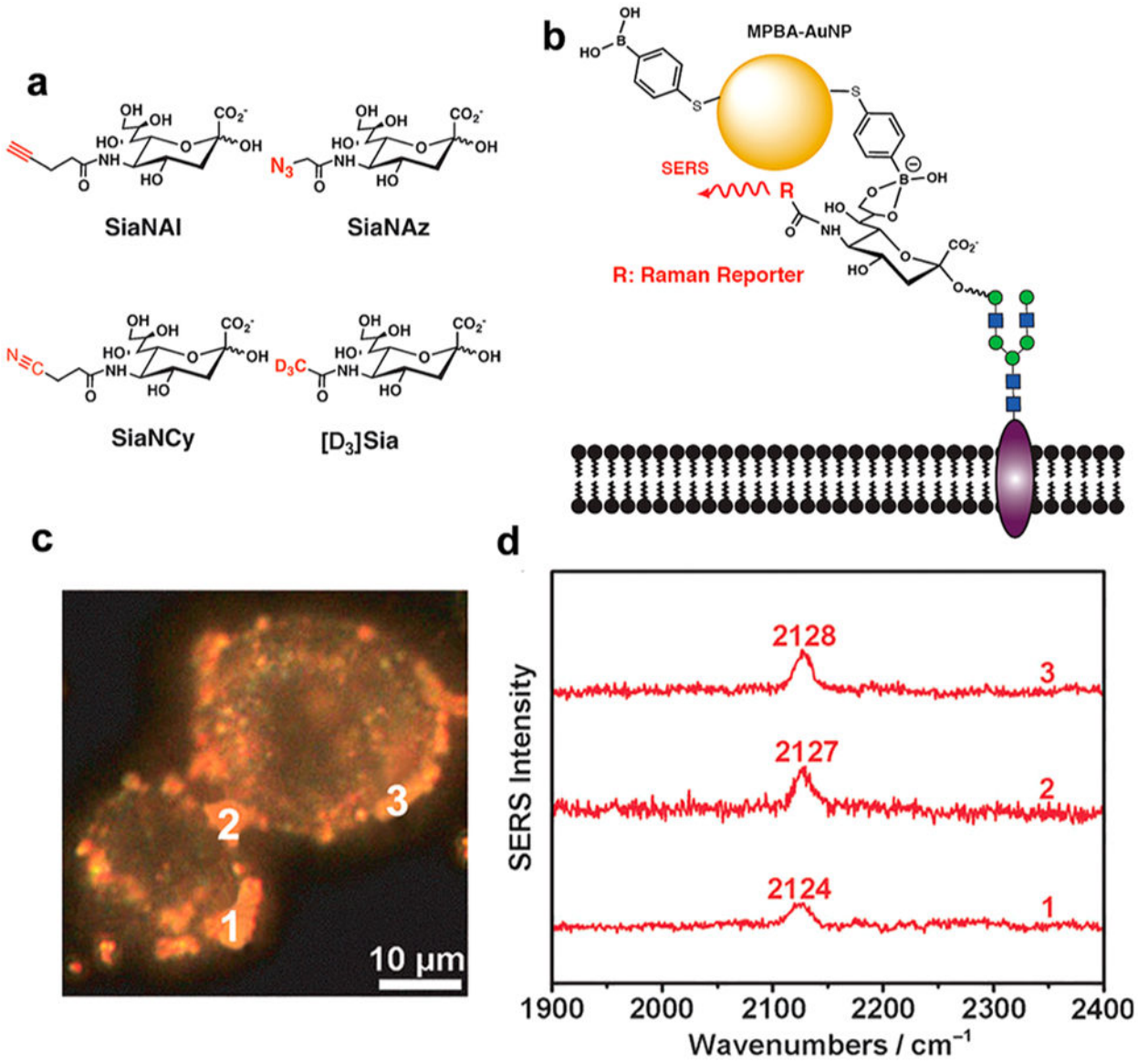

Figure 39.

(a) Monosaccharide analogues containing a Raman reporter highlighted in red. (b) Schematic illustration of SERS detection of cell-surface sialylated glycans using MPBA-AuNPs as the Raman signal amplifier. (c) Dark-field image of HeLa cells treated with the Raman reporter-labeled monosaccharide analogues, followed by incubation with MPBA-AuNPs. (d) Representative SERS spectra of the HeLa cells taken at three locations as indicated in (c). Reprinted with permission from ref 334b. Copyright 2013 Wiley-VCH Verlag & Co. KGaA.

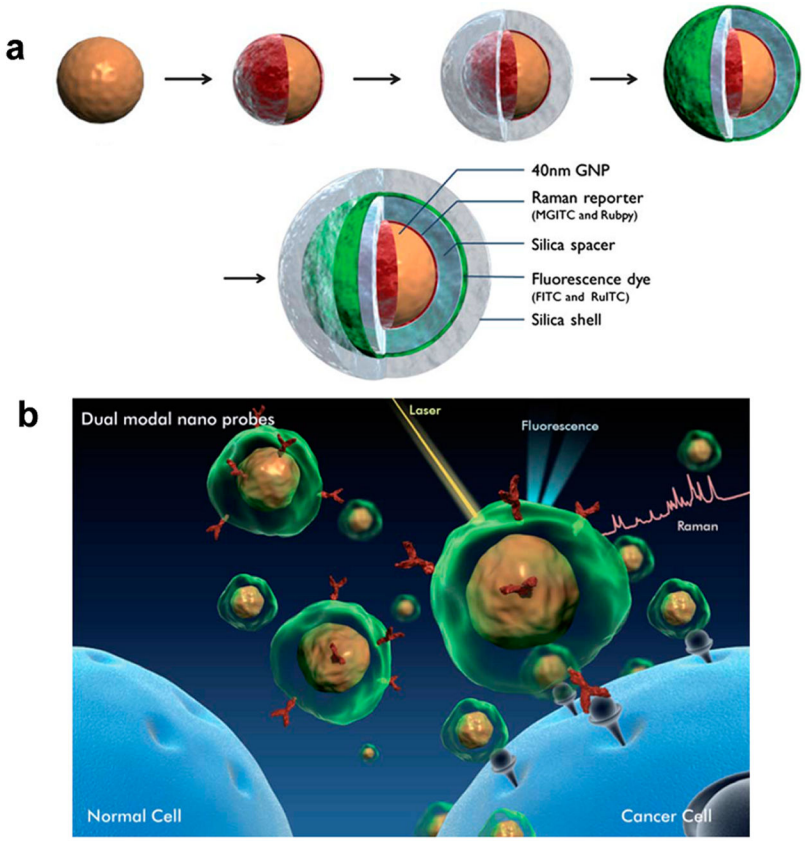

Figure 40.

(a) Step-by-step fabrication of SERS-fluorescence DMNP. The 40 nm sized AuNPs are first functionalized with Raman reporters, and a layer of silica is then coated on the AuNPs. The silica encapsulated SERS tags are labeled with fluorescent dyes. The resulted SERS-fluorescence probes are further coated with an outer silica shell. (b) Illustration of cancer marker detection using fluorescence-SERS DMNPs. The functional DMNPs are selectively targeted onto cancer markers expressed in live cells. Fluorescence and Raman signals are emitted simultaneously. Reprinted with permission from ref 337. Copyright 2012 Royal Society of Chemistry.

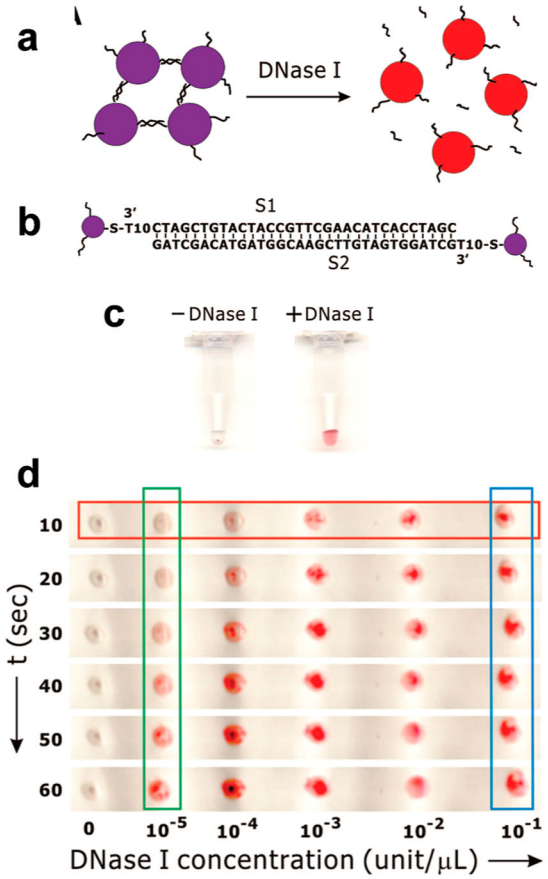

Figure 41.

(a) Schematic representation of the DNase I-sensing system based on the redispersion of AuNPs. AuNPs modified with S1 and S2 (b) tend to aggregate via DNA hybridization. The aggregates can be redispersed by the addition of DNase I that is able to cleave DNA cross-linkers, resulting in a red color (c). Left tube: a clump of AuNP aggregates. Right tube: DNase I (0.1 unit/μL) was added to the left tube. The right tube was scanned at 20 s after the addition of DNase I. (d) DNase I-sensing assays on hydrophobic paper as functions of assay time and DNase I concentration. As expected, more red color is observed when more target analyte is added (red box) or longer assay time was utilized (green box). Reprinted with permission from ref 345. Copyright 2008 American Chemical Society.

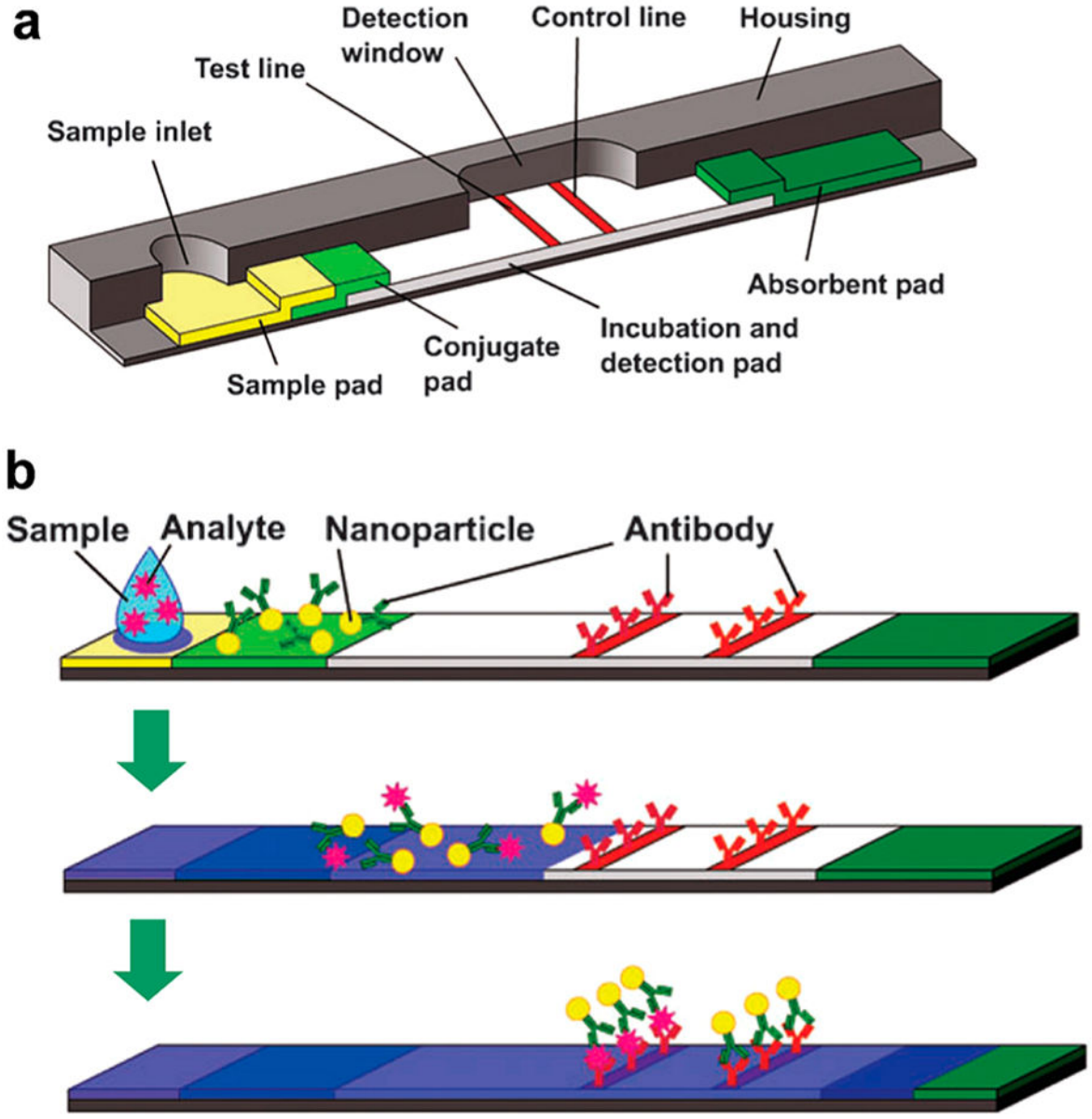

Figure 42.

(a) Schematic illustration of a lateral flow test. (b) Start of assay by adding liquid sample, in which analytes bind the antibody-conjugated AuNPs. With the flow of sample, the analyte-bound particles are captured by antibodies in test line (positive result) and control line (proof of validity), respectively. Reprinted with permission from ref 354a. Copyright 2010 Royal Society of Chemistry.

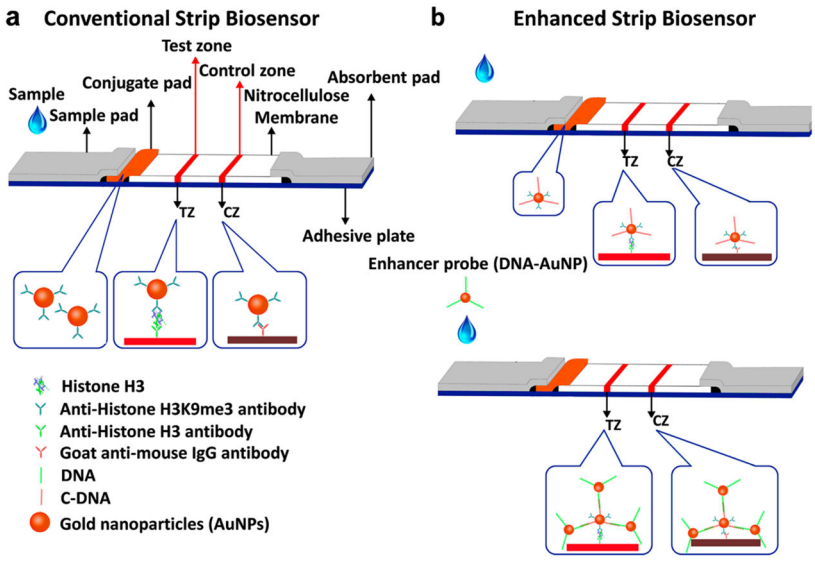

Figure 43.

Schematic of the LFA using DNA-AuNPs cross-linking networks to further enhance the detection sensitivity. (a) In the conventional strip biosensor for H3K9me3 detection, the AuNPs on the conjugate pad are only labeled with an anti-histone H3K9me3 monoclonal antibody. (b) In the enhanced strip biosensor, the AuNPs are labeled with anti-histone H3K9me3 antibodies and c-DNAs simultaneously. Mouse monoclonal antibody against histone H3 and goat antimouse IgG antibody are immobilized on the membrane to form the test zone and control zone, respectively. In the presence of histone extract, the dual-labeled AuNPs are immobilized on the test zone and control zone to form two red bands. Ten minutes later, AuNP-DNA solution is loaded onto the strip to hybridize with the c-DNA on the dual-labeled AuNPs. The enhanced signals can be observed within 15 min by the naked eye. Reprinted with permission from ref 361. Copyright 2013 American Chemical Society.

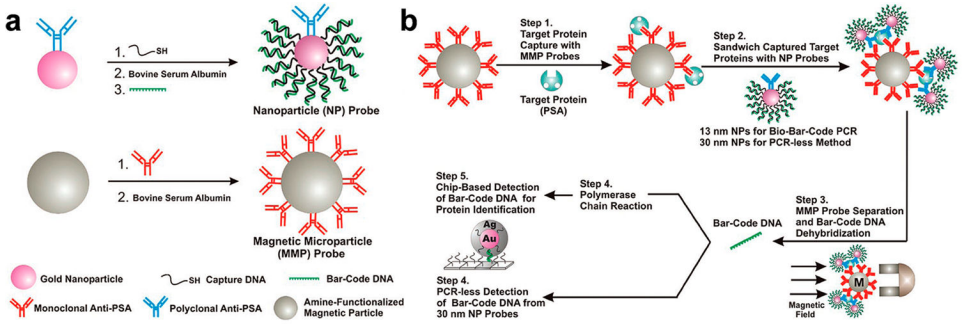

Figure 44.

Biobarcode assay technique. (a) The preparation of AuNP barcode and antibody-modified magnetic microparticle. (b) The detection procedures of the biobarcode assay for target protein. The antibody-modified magnetic microparticle probes capture the target protein (step 1). The probes are magnetically separated from the buffer and resuspended in a fresh buffer where the AuNP barcodes are introduced. These probes sandwich the protein target (step 2). The hybrid particles are separated by magnet again and the barcode DNA is dehybridized (step 3). The isolated barcode DNA can then be amplified by PCR (step 4, top), or the probes undergo scanometric DNA detection (step 5). Reprinted with permission from ref 363. Copyright 2003 American Association for the Advancement of Science.

Table 1

Summary of AuNP-Based LSPR Assays for Various Detection Targets

target	nanomaterial	linear range	detection limit	real sample	ref
DNA	AuNP-conjugated polyelectrolyte	N/A	1.25 pM	N/A	17b
thrombin			10 nM		
cocaine			10 μM		
DNA	AuNPs	N/A	100 fM	SARS virus	35
HIV viral	AuNPs	(1.3 ± 0.7)–(4.3 ± 1.2) $\log_{10}$ copies/mL	98 ± 39 copies/mL	whole blood	39
anti-IgG	Au-patterning nanostructures	N/A	66.7 pM	N/A	42
HRP	AuNPs-glass substrate	N/A	350 fM	N/A	45
PSA	AuNRs	1.11×10^3–1.11×10^7 aM	111 aM	N/A	47a
PSA	AuNRs	10–10^7 aM	1 aM	N/A	47b
cTnI	AuNRs	0–20 ng/mL	30 pM	plasma	51
IgG	Au nanoplates	N/A	10 pg/mL	N/A	52b
prA	AuNPs	100–500 ng/mL	100 ng/mL	N/A	53
MCF-7	AuNPs	8.56×10^3–1.09×10^6cells/mL	N/A	N/A	54
RPE-1		2.28×10^4–8.20×10^5 cells/mL			
PSA	Au nanostars	10^{-18}–10^{-13}g/mL	10^{-18} g/mL	whole serum	56
CRP	AuNPs	N/A	50 ng/mL	serum	57
ATP	AuNPs	4.4–132.7uM	0.6 μM	N/A	67
DNA	AuNPs	0–7.5 nM	50 zM	cell lysate	70
RNA	MBs				
DNA	AuNPs	1 pM–10 nM	1.0 pM	*Vibrio cholerae*	71
cathepsin B	AuNPs	N/A	5 nM	N/A	72b
AChE	AuNPs	N/A	0.1 mU/mL	CFS	75
enterovirus 71	AuNPs	N/A	10^4 copies/mL	human throat swab	80
PSA	AuNPs	10–10^5 fg/mL	3.1 fg/mL	serum	82
PSA HIV-1 p24	AuNPs	N/A	10^{-18} g/mL	whole serum	83

Table 2

Summary of AuNP-Based Fluorescent Assays for Various Detection Targets

target	nanomaterial	linear range	detection limit	real sample	ref
urea	AuNCs	N/A	1 mM	serum whole blood milk	101
ATP	AuNCs	50–500 μM	43 μM	cell lysate	102
pyrophosphate		50–100 μM	28 μM	human plasma	
human IgG	AuQD-PAMAM	0.5–7 mg/mL	N/A	N/A	105
NSE	$CaCO_3$/AuNCs	0.005–1.0 ng/mL 0.0005–2.0 ng/mL	2.0 pg/mL 0.1 pg/mL	serum	106
IL-6	PDDA-BN-AuNCs	5 pg/mL–1.0 ng/mL	0.03 ng/mL	N/A	107
HDAC1	AuNCs	15 pM–30 nM	5 pM	N/A	109
PKA		15 pM–60 nM	6 pM		
GST/GST-tagged proteins	AuNCs	N/A	25 μM	cell lysate	110
glucose	apo-GOx@AuNPs	20–200 nM	5 nM	cell lysate	121
glucose	ova-AuNCs	0.50–10.0 mM	0.10 mM	rat brain microdialysate	123
heparin	try-AuNCs	0.1–4.0 μg/mL	0.05 μg/mL	serum	124
miRNA-122	AuNPs	0.05–50 pM	0.01 pM	cell lysate	142
MMP	AuNPs	1–14 nM	1 nM	tumor tissue	149
MMP-7	AuNP-QD	10–5000 ng/mL	126 ng/mL	malignant tissues	152
caspase-3		20–500 ng/mL	20 ng/mL		
thrombin		1–50 U/mL	1U/mL	serum	
uPA	AuNP-QD	N/A	50 ng/mL	N/A	154
HER2			7.5 nM		
HBV	AuNP-QD	1–100 viral particles/μL	1 virus particle/μL	HepG2	155
HBsAg		N/A	0.1 pg/mL	serum	
PSA	AuNPs	0.5–2 pg/mL	0.032 pg/mL	serum	157

Table 3

Summary of AuNP-Based Electrochemical Assays for Various Detection Targets

target	nanomaterial	linear range	detection limit	real sample	ref
hCG	HRP-anti-hCG/AuNP	0.5–5 mIU/mL, 5–30 mIU/mL	0.3 mIU/mL	serum	167
CA 153	HRP-antibody/AuNP	0.084–16 U/mL	0.06 U/mL	serum	171
CA 125		0.11–13 U/mL	0.03 U/mL		
CA 199		0.16–15 U/mL	0.1 U/mL		
CEA		0.16–9.2 ng/mL	0.04 ng/mL		
PDGF	P-Gra-AuNPs composite	0.005–60 nM	1.7 pM	N/A	175
cancer cell	antibody labeled AuNP	10 000–200 000 cells	4000 cells	N/A	180
miRNA	AuNP	10 aM–1 μM	5 aM	serum	185
DNA	cysteamine-AuNP	N/A	100 fM	serum	188
IL-6	inkjet-printed AuNP	20–400 pg/mL	20 pg/mL	serum	190
PSA	AuNP film	N/A	0.5 pg/mL	serum	193
IL-8	GSH-AuNP	1–500 fg/mL	1 fg/mL	serum	194
Il-6	AuNP	5–1000 fg/mL	5 fg/mL	serum	195a
IL-8		10–1000 fg/mL	10 fg/mL		
VEGF		5–1000 fg/mL	5 fg/mL		
VEGF-c		50–2000 fg/mL	50 fg/mL		
IgG	anti-IgG-AuNP	0.5–7.5 μg/mL	12.5 pmol	N/A	199
ENO1	anti-ENO1-tagged AuNP	1 pg/mL–10 ng/mL	11.9 fg	N/A	203
DNA	DNA-AuNP	500 fM–50 nM	500 fM	N/A	205
AFP	AuNP/azure I/MWNT	0.1–8.0 ng/mL 8.0–250.0 ng/mL	0.04 ng/mL	N/A	213a
CEA	den/AuNP	10.0 pg/mL–50.0 ng/mL	4.4 ± 0.1 pg/mL	serum	220
miRNA	Fc-capped AuNP/streptavidin conjugates	10 fM–2.0 pM	10 fM	serum	227c
CEA	gold/silica/CdSe-CdS nanostructures	0.32 pg/mL–10 ng/mL	0.064 pg/mL	serum	228
CEA	AuNP/BSA/[Ag–Ag_2O]/SiO_2	0.5–160 ng/mL	0.14 ng/mL	serum	230f

Table 4

Summary of AuNP-Based SERS Assays for Various Detection Targets

target	nanomaterial	linear range	detection limit	real sample	ref
thrombin	AuNPs	0.1–10 nM	20 pM	serum	239
DNA	AuNP-graphene	N/A	10 pM	N/A	247
MUC4	ERLs	0.01–10 μg/mL	33 ng/mL	serum	260
hepatitis B virus surface antigen	probe-labeling AuNP	1–40 μg/mL	0.5 μg/mL	N/A	265
DNA	Au particle-on-wire	10 pM–10 nM	10 pM	N/A	269
BRCA1	DNA-AuP-RTag	N/A	1 fM	N/A	270
HIV-1 DNA	oligonucleotide-AuNPs	0–0.1 pM	0.1 aM	N/A	272
DNA	AuNPs	10 pM–100 nM	10 pM	N/A	273
ATP	Au nanostar@MGITC@SiO_2	12.4 pM–2 nM	12.4 pM	N/A	274
ALP	AuNPs	4.1 fM–41 pM	4 fM	N/A	277
DNA	DNA-AuNPs	0.5–1000 fM	0.2 fM	cell	282
thrombin	AuNR-AuNPs	N/A	220 pM	serum	289
CTCs	antibody-AuNPs	N/A	10 cells/mL	blood	302
CTCs	EGF-functionalized AuNPs	1–720 cell/mL	5 cells/mL	blood	303
prostate cancer Cell	Au nanopopcorn	N/A	50 cells	N/A	307

Table 5

Summary of AuNP-Based POC Assays for Various Detection Targets

readout	target	nanomaterials	linear range	detection limit	real sample	ref
electrochemical	DNA	AuNPs/graphene	$8\times 10^{-}{}_{16}$–5×10^{-10} mM	2×10^{-16} mM	serum	350
electrochemical	D-glutamic acid	AuNPs	1.2–125 nM	0.2 nM	serum	351
colorimetric	DNA	AuNPs	5–100 μg/mL	2.5 μg/mL	human genomic DNA	355
colorimetric	nucleic acid sequence of HIV-1	AuNPs	0.5–2.5 nM	0.1 nM	N/A	360
colorimetric	hCG	AuNPs	N/A	0.3 ± 0.2 mIU/L	N/A	362b
colorimetric	DNA	AuNPs	1 fM–1 pM	0.01 fM	blood	362d
scanometric	PSA	AuNPs	N/A	330 fg/mL	serum	364
scanometric	ADDLs	AuNPs	100 aM–100 fM	100 aM	cerebral spinal fluid	365
scanometric	telomerase	AuNPs	10^3–10^5 cells	10 cells	HeLa cells	366
scanometric	DNA	AuNPs	500 zM–5 fM	500 zM	N/A	368
scanometric	multiple DNA	AuNPs	N/A	N/A	N/A	369
fluorescence	PSA	AuNPs/MBs	300 aM–3 pM	300 aM	serum	370a
colorimetric	IL-2	AuNPs/MBs/silica bead	30 aM–300 fM	30 aM	serum	371a